ASSESSMENT OF UNCERTAINTIES OF SOIL EROSION AND SEDIMENT YIELD ESTIMATES AT TWO SPATIAL SCALES IN THE UPPER LLOBREGAT BASIN (SE PYRENEES, SPAIN)

GUSMAN CATARI YUJRA

Ph.D. DISSERTATION

Institute of Environmental Assessment and Water Research - IDAEA, CSIC

Institute of Environmental Sciences and Technology - ICTA, UAB

January 2010

Barcelona, Spain

INSTITUTE OF ENVIRONMENTAL ASSESSMENT AND WATER RESEARCH (IDAEA-CSIC)

INSTITUTE OF ENVIRONMENTAL SCIENCES AND TECHNOLOGY (ICTA, UAB)

ASSESSMENT OF UNCERTAINTIES OF SOIL EROSION AND SEDIMENT YIELD ESTIMATES AT TWO SPATIAL SCALES IN THE UPPER LLOBREGAT BASIN (SE PYRENEES, SPAIN)

BY:

GUSMAN CATARI YUJRA

Submitted for the degree of Ph.D. in Environmental Sciences to the Institute of Environmental Sciences and Technology, Autonomous University of Barcelona

SUPERVISED BY: **DR. FRANCESC GALLART AND DR. DAVID SAURI**

"Be it deep or shallow, red or black, sand or clay, the soil is the link between the rock core of the earth and the living things on its surface. It is the foothold for the plants we grow. Therein lies the main reason for our interest in soils."- Roy W. Simonson, USDA Yearbook of Agriculture, 1957.

"Each soil has had its own history. Like a river, a mountain, a forest, or any natural thing, its present condition is due to the influences of many things and events of the past."- Charles Kellogg, The Soils That Support Us, 1956.

Acknowledgements

While a completed Ph.D. thesis bears the single name of the student, it is always accomplished with the help of other people. I wish to express my acknowledgment to certain people who helped get to this stage.

First and foremost I want to thank Dr. Francesc Gallart, supervisor of this dissertation. I appreciate all of his contributions in time and ideas, which made my Ph.D. experience productive and meaningful. He has been very helpful to me during the entire period of my studies. The enthusiasm he has for his research was motivational for me, even when the pursuit of my Ph.D. became daunting. I believe that without his help this dissertation would have been a wish.

I would like to thank Dr. David Sauri who spent time helping me refine my thoughts and providing insights on the workings of academic research.

Many thanks go to the members of the Surface Hydrology and Erosion Research Group at the Institute of Environmental Assessment and Water Research (IDAEA, CSIC). The Group has been a good source of advice and collaboration. I am especially grateful to Dr. Montserrat Soler and Dr. Guillaume Nord who provided excellent and timely advice. I would also like to acknowledge Juliana Delgado for her advice and willingness to share both her bright thoughts and her abilities with GIS, which were formative in the use of GIS in my research.

I gratefully acknowledge the Catalan Government through the *Agència de Gestió d'Ajuts Universitaris i de Recerca* (AGAUR) for funding this research.

I would like to thank Dr. Ramon Josa, for helping me with analyses of soil samples, sharing his expertise on soil erodibility, advice and for reading drafts of this dissertation.

I would like to acknowledge professors and staff from the Pan-American School of Agriculture (Zamorano), particularly Dr. George Pilz and Dr. Martin Schwarz for their encouragement.

Thanks also are due to the staff from the Institute of Environmental Sciences and Technology (ICTA-UAB) for providing administrative assistance.

I want to thank Miquel Angel González and Bernat Tòmas for helping me with computer problems. To the administrative staff at Institute of Earth Sciences Jaume Almera particularly to Xavi and Leo for the steady help provided.

Librarians at UB provided steady support with many inter-library loans, also support from librarians at UAB, UPC and UPF is appreciated.

My time in Barcelona was made enjoyable to a large extent by the many friends that became a part

of my life. I am grateful for the time I spent with them. It is a pleasure to express my gratitude wholeheartedly to John Wylie, Roser Casas and their family for their hospitality in Manresa. Thanks to Akgün Ilhan, Thomas Dite, Romy Büchner and Matthias Pope for the time we spent together. To Burke Green and his wife Beth Reid, Ayana Ishii, Raffaele Mancini, Juliet Mullins, Stephan Harjes, Stig Torp, Joan Corrigan, Edwin Agudelo, Grant Buffet and his wife Anna for their friendship, fun moments and advice. I would also like to thank the rest of my friends, housemates and officemates for their support, as well express my apology that I could not mention them one by one.

Last but not least, my family deserves special mention for their love and support. My father, Juan Francisco, and my mother Antonia are the persons who raised me with a love of learning and working hard. To both of you thank you very much for grooming me to be what I am now. Lastly, I want to thank my brothers and sisters Felipa, Bosco, Hernán, Raúl, Ana and Max Raúl for their unconditional support throughout my life. To my niece Mary-Luz for being a source of inspiration.

Gusman,

Contents

List of Tables

List of Figures

ABSTRACT

Sediment yield in mountain areas is a matter of concern not only because of the loss of the fertile topsoil, but also due to its off-site effects such as sediment deposition in reservoirs and damage to aquatic life. Therefore, a better understanding of sediment yield at different spatial and temporal scales is necessary, for management purposes and to envisage uncertainties when developing soil erosion models. In this work, sediment yield was studied at two spatial scales, a small catchment and a relatively large river basin in the SE Pyrenees, Spain. The small catchment is Cal Rodó (4.2 km^2) (it is one of the Vallcebre catchments), and the river basin is the Upper Llobregat Basin (504 km^2) where at its outlet is located the La Baells Reservoir (an important water supplier of Barcelona City), the former is nested within the latter. The temporal scales studied were diverse within each. The study area is a mountain range, where land cover has shifted from being primarily agricultural before the 1950s to being mostly forested. This affects soil erosion rates and sediment yield. Additionally, as a transition zone this area is highly susceptible to Global Change. The problems addressed within each spatial scale studied are somehow different, mainly because of the existence of prior research and the available resolution of input data.

In the Cal Rodó catchment, hydrological variables such as sediment concentration and water discharge have been monitored since the 1990s. As a consequence of different interacting factors, daily suspended sediment concentration and sediment yield can present large variations in time and space. The reliability of methods to calculate sediment load need to be assessed as sediment load is the product of water discharge and sediment concentration. Whilst water discharge can be continuously measured, concentration can not be, instead discharge sampling and turbidity measurements are used as surrogates. Otherwise, load calculations are based on mathematical interpolations and extrapolation techniques from samples, such as sediment rating curves (SRC) (which is the relationship between concentration and discharge), however the accuracy of outcomes using rating curves in mountain event based streams is unknown. The purpose of this research is to examine, compare and estimate the confidence intervals of suspended sediment load estimations at the event and annual scales. Data used spanned 10 years (1996-2005) and 27 of the biggest storm events ($\approx$ 80th percentile of sediment transport) during that period were selected. Dataset includes discrete water samples collected by an automatic water sampler (ISCO 2700), turbidity readings provided by (1) an infra-red backscattering turbidity sensor (OBS-1), and (2) an ultrasonic beam attenuation suspended sediment sensor (Bestobell Mobrey MSM 40), water stage measurements connected to a data logger, which records readings every 20 or 2 minutes depending on water level. Data recorded by sensors were transformed on suspended sediment concentration by linear calibrations and thereafter instantaneous concentration is multiplied by instantaneous discharge and time step in order to calculate instantaneous suspended sediment load, which then is integrated to attain the sediment load or transport for each episode.

Uncertainty of load (event scale) and sediment yield (one decade) were assessed with Monte

Carlo simulation of the distribution function of sediment load obtained by (1) sediment rating curves (logarithmic scale) prior to bias correction (this correction is not needed when Monte Carlo simulations are used), and by (2) calibrations of turbidity sensors.

The total sediment yield for 10 years estimated through sensor calibrations was 17,217.0 Mg (4.1 Mg $ha^{-1}yr^{-1}$) and its 90% confidence interval is between 16,311.4 Mg and 18,395.8 Mg (6% difference). On the other hand, sediment yield estimated by annual sediment rating curves for the same period was 103,441.0 Mg (24.6 Mg $ha^{-1}yr^{-1}$), and its confidence interval is between 49,107.0 Mg and 254,803.0 Mg (99.4% difference); similarly by seasonal rating curves the total yield was 88,302.0 Mg (21.0 Mg $ha^{-1}yr^{-1}$), and its 90% confidence interval is between 49,099.0 Mg and 197,038.0 Mg (83.8% difference). Since the sediment yield from the annual and seasonal rating curves are 6.0 and 5.1 times larger than the estimated by sensor calibrations, rating curves were developed by splitting the hydrograph into its rising and decreasing limb, thus averages values were 97,718 Mg (90% confidence interval was between 46,767.3 Mg and 253,748.7 Mg) and 87,645 Mg (90% confidence interval was between 45,300 Mg and 193,395 Mg) for annual and seasonal rating curves respectively. These values represent a slight improvement over the values obtained from previous rating curves. The sediment load at event scale varied largely, values obtained by rating curves (MCS) were larger than the load obtained by sensor calibration in 23 episodes, and in three episodes were smaller, there is no clear pattern of over or underestimation in regards to event size. Given the large differences, a test using a good distribution of samples (hourly "virtual sampling") along the hydrograph was conducted, sediment yield results have shown that the average values obtained from sensor calibration and rating curves are very similar 10,400 Mg and 11,952 Mg respectively, although the 90% confidence interval for rating curves remained very large in this test the error term was split into errors between episodes and error within episodes, since residual analysis has shown that different events have different discharge-concentration relationships. Moreover, as sediment concentration and load can not be measured first-hand, other easy-to-measure hydrological variables were studied, e.g. bivariate correlations where the dependent variable is sediment load. It was found that total kinetic energy of rainfall and peak of discharge of a flood episode are good predictors at the annual scale. Similarly, at the seasonal scale it was found that runoff and peak of discharge correlated well to sediment load. In both cases sediment yield was underestimated in 26% and 28% respectively in relation to sediment yield estimated by sensor calibrations. The overall conclusions of the study conducted in Cal Rodó are that uncertainty of sediment load by sediment rating curves are very wide ($> 300\%$) and sediment yield was overestimated in one order of magnitude. A good distribution of samples throughout the hydrograph needs to be ascertained in order to develop reliable rating curves which then can be used to extrapolate alongside a recalibration of sensors according to existing particle sizes are also needed.

The second phase of this study was conducted in the Upper Llobregat River Basin at the headwaters of the La Baells Reservoir. The basin (504 km^2) is located in the SE Pre-Pyrenees; land cover is mainly coniferous forest and pastures, and some intensely eroded areas (badlands) exist, which, in many cases are connected directly to streams. Annual average soil erosion was quantitatively estimated with an integration of GIS (IDRISI) and the Revised Universal Soil Loss Equation (RUSLE). Rainfall dataset from eight weather stations spanning 14 years (1991-2004), soil properties, land cover inventory, land management features and a digital elevation model were used as resource datasets to generate each of the RUSLE's factors images (20 m resolution). Sediment yield was computed by applying a sediment delivery ratio to the results obtained by RUSLE. Sensitivity analyses for each of the RUSLE factors were undertaken and an overall uncertainty assessment of soil erosion and sediment yield was also performed. Soil erosion scenarios under Global Change conditions were also developed. Results showed that the annual average sediment

yield was 3.35 Mg $ha^{-1}yr^{-1}$ and its 90% confidence intervals laid between 0.95 and 13.7 Mg $ha^{-1}yr^{-1}$. These results are similar with those from a pre-existing reservoir bathymetric survey which was 4.54 Mg $ha^{-1}yr^{-1}$, and for which its 90% confidence interval was determined to be between 4.29 Mg $ha^{-1}yr^{-1}$ and 4.79 Mg $ha^{-1}yr^{-1}$. Sediment yield estimates obtained by other semi-quantitative methods such as the Pacific Southwest Interagency Committee (PSIAC), Factorial Scoring Model (FSM) and a regression between drainage area - sediment yield, were within the confidence interval estimated for results obtained by combined the RUSLE-SDR. The erosion risk map showed that there are a few hotspots ($\approx$ 5% of the river basin) that produce 50% of the sediment. These areas are located in steep slopes and coincide in many cases with badlands which, as mentioned before, are near streams. Finally, sediment yield changes under climate conditions for the late 21st century were not relevant, whilst spreading agricultural activity as in the 1950's had a relevant increase in sediment yield.

It is highlighted our understanding of factors affecting erosion dynamics and performance of empirical and semi-quantitative erosion models. Uncertainty analyses are given throughout the study, as the are crucial for application and research purposes.

Keywords: Soil Erosion, Suspended Sediment Yield, Sediment Rating Curve, Uncertainty Analysis, RUSLE, Upper Llobregat Basin, La Baells Reservoir, Vallcebre.

Chapter 1

GENERAL INTRODUCTION

1.1 Background

Soil erosion by water is one form of soil degradation and has become an important environmental problem. It is beginning to be recognized for being, not simply a farming problem but one with implications for wider civil society (Boardman & Poesen, 2006). In the European Union (2009), an estimated 115 million hectares (12% land area) are subject to water erosion (EEA, 2008). Unlike other regions of the world, where extensive agriculture is still significant, during the last half century agricultural areas in the Mediterranean Region has suffered an important decrease. Erosion rates vary a great deal spatially, and land use is one of the driving forces that can accelerate erosion.

Land use change, is the difference of state of the land use between two or more moments in time, and these changes can be positive or negative for soil protection from erosive agents. This depends on the climatic, features of the terrain, and land cover type of the land after change has ocurred. In the Spanish mountains, farmers modified the terrain by constructing terraces and ditches in order to increase yields and protect the valuable topsoil. However, land abandonment has resulted in subsequent and progressive degradation of the terraces and ditches (Gallart & Latron, 1994). In the Pyrenees abandonment of agricultural areas is widely spread (MacDonald & Wiesinger, 2000; Geeson & Thornes, 2002). It has shifted from intensively farmed areas to a increasingly forested areas, because on many of the abandoned hillslopes an extensive policy of reforestation in order to control the hydrologic and geomorphic processes of slope erosion was encouraged (Garcia-Ruiz *et al.*, 1996). These changes in land cover are likely to continue due to Global Climate Change, policies at the EU level and urbanisation, and one way or another, they will have effects on sediment yield and surface runoff.

Understanding the sediment production cycle and the processes involved are important, in order to provide sound elements for land use planning and management. Assessment of sediment production is neccesary not only because of its on-site effects (where agriculture is little), but also because of its off-site effects. In Europe, in the short term the costs related to off-farm impacts seem to be more important than those related to on-farm impacts (Boardman & Poesen, 2006). Soil erosion may occur at slow rates that can go unnoticed or may it occur at an alarming rates causing serious problems, such as reservoir siltation. Reservoir siltation has become a contemporary problem and it can not be put off until the future (Morris, 1997).

It is estimated that the annual loss in storage capacity of the world's reservoir due to sediment deposition is around 0.5-1%, and for individual reservoirs these values can be as high as 4-5% (WCD, 2000), therefore, the long-term loss of storage capacity is a serious concern. A bathymetry survey of La Baells Reservoir performed 25 years after its construction (1976) has shown that its storage capacity suffered an annual reduction of 0.19% (CEDEX, 2002). Hence, quantifying the rates of sediment delivered downslope is critical and need a better assessment in order to reduce negative impacts on the hydroelectrical energy, and water supply in the growing urban areas, especially in the Mediterranean coast.

Climate change predictions for the Mediterranean area during the 21st century is expected to disturb the hydrological cycle. The stress conditions are predicted to be harsher in these areas because of increase in temperature and reduction of precipitation (EEA, 2004; Giorgi & Lionello, 2007; López-Moreno *et al.*, 2008); consequently, the off-site effects of soil erosion will increase with climate change and related changes in rainfall patterns and intensity (EEA, 2008). The impact of climate change on soil erosion by water is complex, involving disruption of the precipitation pattern and duration, lengthening of summertime, land cover changes among others. Soil erosion is one of the environmental concerns that requires to be evaluated under current climate, and land management patterns, to develop appropriate measures to be used in conservation planning programs.

1.2 Problem statement

The general statement of problem, under, which this research has been conducted, are divided in two parts. The first part deals with assessing the accuracy of sediment yield estimations in a small gauged catchment. The second part has to do, with sediment yield assessment in a large ungauged drainage basin.

1.2.1 Sediment yield assessment in a gauged basin

Hydrological and geomorphological research in gauged basins have been conducted worldwide; the understanding of erosion processes and sediment transport at small gauged catchments is relatively high. Some reasons for this, are that at small catchment scale there is little heterogeneity of the landscape and climatic conditions, and the measurement techniques characterize fairly well those processes and the outcome data often has a high resolution. As for sediment yield, common studies include determination of temporal variability of suspended sediment, relationships among precipitation, discharge and suspended sediment. There is an increasing awareness of the environmental significance of suspended sediment in regards to, its role as a vector for the transfer of nutrients and contaminants in fluvial systems (Ballantine *et al.*, 2008), hence techniques and procedures to estimate sediment transport, need to be reliable and they must account for uncertainties involved.

Since 1986, there has been interest in monitoring the erosion and fluvial transport of suspended sediment in the Upper Llobregat basin, especifically in the Vallcebre catchments (19.6 km^2) (Clotet *et al.*, 1983; Clotet, 1984; Clotet & Gallart, 1986; Pardini, 1996; Regüés *et al.*, 2000; Regüés & Gallart, 2004; Gallart *et al.*, 2005; Catari, 2007). The Vallcebre catchments includes several small gauged catchments, namely Cal Rodó, Cal Isard, and Can Vila, where discharge and suspended

sediment concentration are measured at low temporal resolutions (minutes), and instruments are set up by performing calibrations. As yet, large data as regards to discharge, discrete suspended sediment concentration collected by automatic samplers, and suspended sediment concentration derived from continuous measurement of turbidity exist. Often suspended sediment load is obtained in function of discharge, since it can not be measured directly. The most common relationship between concentration and discharge are the sediment rating curves, which can be used for episodes without samples.

Nonetheless, the use of sediment rating curves raises issues related to the accuracy of the estimations. When a non-linear rating curve is used, sediment concentration is obtained by transforming discharge and discrete concentration data, into the logarithmic scale, and then back-transformed into the arithmetic scale, and then, a bias correction based on residual analysis (in logarithm domain) is applied, but it is reported that it underestimates the sediment loads (Ferguson, 1986). Morever, the computation of the confidence interval of the mean sediment concentration is rarely performed. Currently, the uncertainty evaluation for streams with continuous flow regime is conducted by using Monte-Carlo approaches, nevertheless its reliability in streams with ephemeral flow might be subjected to errors, and it needs to be evaluated.

Additional sources of uncertainty when estimating sediment yield, can also be, due to calibration of the instruments used to measure suspended sediment concentration and discharge, and these, also need to be accounted for, in sediment yield assessments. Overall, sediment yield estimations at small gauged basins is site specific and needs to be evaluated as such. Understanding the magnitude of uncertainties related to procedure issues is important, and it can help to understand how these small catchments are nested within larger drainage basins in terms of the processes occurring within them.

1.2.2 Sediment yield predictions in an ungauged basin

Soil erosion and sediment yield predictions in ungauged drainage basins is challenging, because of spatial heterogeneity and the complex arrangement of the components of the drainage basin. It is important to understand the physics of ungauged drainage basins to develop a science-based capability for estimating soil erosion and sediment yield. Most of the drainage basins in the world are ungauged. It is inadequate to extrapolate results from gauged to ungauged basins (Sivapalan, 2003), because the spatial scale dependency is still unknown. The understanding of how hydrology and earth surface processes work in small individual research areas is substantial (Douglas, 1999), yet, at larger scales it is still limited.

Research progress has been made over the last half century in understanding erosion and sediment transport, and their impact on the environment. This understanding has led to the development of soil erosion technology and adoption of a variety of erosion control practices. Soil erosion and sediment yield research has followed several approaches. One of the them is the evaluation of Cs 137 to trace sediment as it moves along the drainage basin (Walling & Quine, 1991). Bathymetry surveys and studies of sediment deposited in lakes are another, and they are important tools for assessing sediment yield especially in basins where monitoring is unexistent; and the third approach is modelling.

Modelling approach is increasingly important with the advent of GIS and Remote Sensing, parameterization of the erosional processes at the basin scale. One advantage of GIS framework is that it brings together much of the useful data that is dispersed. This approach, includes

the integration of topography, land cover, land use, climate and soil characteristics of the basin. There are three types of erosion models namely, empirical, conceptual and physically-based models (Lane & Singh, 1988). Their scope, rationale, structural framework, computational procedures and data requirements vary. However, prediction in ungauged basins without calibration remains a difficult, unsolved problem, demanding urgent resolution and improvements in data collection, process knowledge and understanding (Sivapalan, 2003). The abscence of data of high resolution precludes calibration of predictive models, hence, predictions at the current stage of technology are done by understanding the hydrological functioning.

Currently several models to estimate sediment production at large basins exist, such as the physically based SHETRAN (Ewen, et al., 2000), RHINEFLOW (Asselman, et al. 2003) which was calibrated for Rhine River, SEMMED (De Jong, et al. 1999) designed for Mediterranean regions and RUSLE (Renard, et al. 1997). Among these models, RUSLE is the most widely used and accepted empirical model, because its data inputs are relatively easy to obtain and it is not computationally intensive. Simple empirical models are usually more successful in predicting soil erosion than a complex physically based one, which is difficult to operate and has been only partially evaluated (Morgan, 1995).

Although there have been a few studies to assess the sediment production in the Upper Llobregat area (Clotet & Gallart, 1986), such as from a bathymetry survey of the La Baells Reservoir (CEDEX, 2002), at the plot scale (Regüés *et al.*, 1995), and at a few small sub-basin scales by measuring the suspended sediment concentration (Catari, 2007), there is no sediment yield assessment at the drainage basin scale. Hence, a more comprehensive and integrated assessment of the amount of sediment yield that has occurred in the basin is needed.

Accurate sediment yield assessment in any given drainage basin is difficult, because, only part of the soil eroded on the hillslopes or supplied to the stream ends up reaching the outlet of the basin. The remainder is stored on valley slopes, deppressions or on floodplains. In order to account for deposition, sediment yield is quantified by using sediment delivery ratios (SDR), expressed as the percent of gross soil erosion by water that is delivered to the outlet of the basin. SDR is of spatially lumped nature and problems arise when estimating a single SDR for a basin, to solve this problem a relationship between drainage area and SDR is commonly used, often SDR decreases with increasing drainage area. The hydrological and geomorphological processes that regulate the sediment delivery are highly scale-dependent (Walling, 1983; Cammeraat, 2004; de Vente & Poesen, 2005).

Prediction of probable future rates of soil erosion and sediment yield is needed under Global Change predictions. Such assessment should be based upon a detailed evaluation of the geomorphic, vegetation and hydrologic processes of the drainage basin.

Little progress has been made in establishing reliable predictors of erosion risk due to forest disturbance at a scale which is relevant and usable to forest managers.

Uncertainties need to be recognized, understood and accounted for in any soil erosion assessment. Successfully addressing these issues, will result in a greater understanding of erosion, sediment transport processes, and their potential consequences, leading to improved erosion control practices and better tools for land-use planners.

1.3 Objectives and research questions

The overall objective of this thesis was to contribute to the understanding of the magnitude of inherent uncertainties attached to sediment yield estimations in a small gauged catchment and in a relatively large ungauged drainage basin. The specific objectives addressed and a few guiding research questions for each are as follows:

1. To review existing approaches to predict soil erosion and sediment yield.

- What progress has been made in recent years concerning soil erosion and sediment yield research?

- What are the implications of scale for which soil erosion models were developed?. Can results from different working spatial scales be linked?

2. To compute the suspended sediment load (single flood events) and assess the uncertainty of the mean value in a gauged catchment.

- What is the degree of reliability of the discrete suspended sediment concentrations samples, and the ones derived from calibration, of an infra-red backscattering turbidity sensor and an ultrasonic beam attenuation suspended sediment sensor?

- How accurately can the suspended sediment load for single streamflow episodes be calculated by sediment rating curves?

- What is the magnitude of error associated to each method?

3. To compute the sediment yield and assess the uncertainty of the mean value in a gauged catchment.

- What is the role of small and large streamflow episodes in the computed sediment yield?

- To what extent are the sediment yield computed from both methods different?

4. To evaluate which and to what extent might other hydrological variables be used as surrogates to estimate sediment yield in a gauged catchment.

- Is there any hydrological variable besides discharge, that can be used to estimate sediment yield? since measurement of suspended sediment concentration is expensive and laborious?

5. To evaluate the performance of two semi-quantitative methods, and an existing relationship between sediment yield and drainage area to predict sediment yield in an ungauged basin.

- How accurately can sediment yield be predicted using a few relevant descriptors of the drainage basin?. The degree of accuracy will be determined by comparing with existing results from a bathymetry survey.

6. To estimate soil erosion by an empirical model (RUSLE) in an ungauged basin.

- Can the mean soil erosion be accurately predicted using RUSLE at the drainage basin scale?.

- What is the spatial distribution of erosion rates?

- What is the sensitivity of soil erosion to each of the RUSLE's factors?

- What is the confidence interval for the mean erosion value?

7. To determine the sediment delivery ratio for an ungauged basin.

- What are the potentialites and drawbacks of using existing sediment delivery functions, which where developed elsewhere?

8. To estimate sediment yield by combining RUSLE with sediment delivery ratio in an ungauged basin.

- What is the accuracy of the predicted mean sediment yield?. The mean sediment yield value is compared to results from existing bathymetry survey results.

- What is the degree of uncertainty associated to estimated sediment yield?

9. To assess the soil erosion and sediment yield by the end of this century under Global Change in an ungauged basin.

- Are the climate predictions for a transition zone like the Pyrenees congruent to each other?

- What changes in land cover, land use, and rainfall are most likely to occur?

- What is the magnitude of impact of predicted climate change on sediment yield?

1.4 Relevance of this Thesis

The relevance of this thesis can be traced in two directions:

Applicability side:

The work in this thesis will contribute to the understanding of the magnitude of uncertainties involved in sediment transport assessment at small catchment scale, if suspended sediment rating curves (common technique on gauged cacthments) are to be used, the land manager will know the magnitude of errors associated to them. On the other hand, at the medium basin scale, since there is no universally accepted method for determination of sediment yield, this thesis tests the performance of a few erosion methods in the study area. The GIS technology has helped to incorporate land surface characteristics such as land cover, topography and geology which has allowed to use them within RUSLE. The results are compared with factorial scoring methods which also use readily available information and its costs are not prohibitive, in addition, these results are compared against the results from a bathymetry therefore the magnitude of accuracy of each method can be obtained. RUSLE allows to identify hot-spots of erosion within the river basin and it can be used by water or soil conservation agencies to conduct soil conservation measures.

It also provides an insight to the extent of uncertainty involved in each of the components of RUSLE, which are also important when it comes to make a soil conservation or planning decisions.

Theoretical side:

Provides the understanding of the magnitude of uncertainty associated to sediment rating curves to estimate sediment discharge in Mediterranean mountain areas where episodes of high magnitude are infrequent but important. It also provides some hints of the existing uncertainty and its distributiion when applying the widely used RUSLE model at river basin scale.

1.5 Thesis outline

This thesis is organized into seven chapters. Most of the Chapters are organized in a stand-alone manner.

Chapter 1 gives a brief background to the work in this thesis, introduces the problems in a gauged catchment and in an ungauged drainage basin both addressed in this work, provides the objectives and research questions in chronological order, the relevance of this research, and a detailed chapter plan.

Chapter 2 presents a background to soil erosion and sediment yield approaches, and discusses the advantages and drawbacks of these approaches, with emphasis on the spatial and temporal scales issues. This Chapter is kept relatively brief as focused and detailed reviews of available literature are made in appropriate sections throughout the thesis.

Chapter 3 outlines the geomorphological, hydrological, land cover and land uses of the study area. Emphasis is given to characteristics of the ungauged basin, since the gauged catchment is nested within the ungauged. A more detailed information regarding the characteristics of the gauged catchment is given in Chapter 4.

Chapter 4 is devoted to the assessment of uncertainties of suspended sediment load estimates in a small gauged catchment. A combination of procedures and methods are presented, this includes measurement of discharge using a pressure transducer, collection of discrete water samples by automatic samplers and the use of an infra-red backscattering turbidity sensor and an ultrasonic beam attenuation suspended sediment sensor which are used to determine sediment concentration. In addition, an extensive application of sediment rating curves to individual streamflow episodes is presented. Then, sediment yield for the set of episodes is presented. Uncertainty assessment is provided throughout the Chapter, as it helps to understand the role of small versus large episodes in the sediment yield.

Chapter 5 deals with the assessment of sediment yield at the catchment scale by means of semi-quantitative methods such as the Factorial Scoring Model (FSM) and the Pacific Southwest Inter-Agency Committee (PSIAC) models, and a drainage area-sediment yield relationship. These methods allow the assessment of the total sediment yield (including gully erosion, not only erosion from rills and interrill areas).

Chapter 6 highlights the use of the Revised Universal Soil Loss Equation (RUSLE) in an medium-sized ungauged rangeland basin. In addition, it presents a calculation of sediment delivery ratio in order to obtain the sediment yield from the entire basin. Sensitivity analysis for each of RUSLE's factors are illustrated, furthermore uncertainty assessment of soil erosion and sediment yield are provided. The overall results are benchmarked against an existing bathymetry survey for which its confidence interval was estimated.

Chapter 7 has a focus on soil erosion and sediment yield assessment under predicted Global Change. At first, a review of the predicted rainfall and temperature conditions by the end of this century for the Mediterranean is given, and then a few scenarios of land cover and rainfall pattern changes, and their effect on erosion rates calculated using RUSLE are illustrated.

Chapter 8 is devoted to a brief evaluation of the methods and approaches used, and obtained results; in addition, it is also highlights the main conclusions reached in the thesis, and a summary

of suggested further research are presented.

In the appendices section, additional information can be found regarding detailed calculations or information that might be unknown to the reader.

Chapter 2

STATE OF THE ART IN SOIL EROSION AND SEDIMENT YIELD

2.1 Introduction

Soil erosion is a recognized environmental problem of modern times. Scientists devoted considerable efforts to understand and predict soil erosion since the 1920's in the USA, following the mid-western dust bowl erosion problems, as a consequence of the modernization of agriculture. Soil erosion is a debatable issue, because of the scarcity of quantitative and reliable data on the magnitude of problem (Lal, 1988).

Most of the soil erosion studies are site-specific, and as a result they can not be extrapolated, in part because of the use of unstandarized equipment and methodologies, and the issue of working scale. Soil erosion results from the operation of the laws of physics and chemistry, and since these laws are presumed to be applicable throughout the universe, it can be expected that all soil erosion models attempt to describe the erosional processes and there is little difference among them, however this is not always true (Jetten & Favis-Mortlock, 2006).

2.2 Objectives

This Chapter attempts to provide an overview of the current knowledge of soil erosion and sediment yield.

- First, a brief description of the detachment, transport and deposition processes of soil particles is given.
- Next, a short review of sediment yield and sediment transfer concepts are presented.
- Finally, a brief review of relevant issues related to scale and scaling problems is provided, and types of erosion models are also briefly discussed.

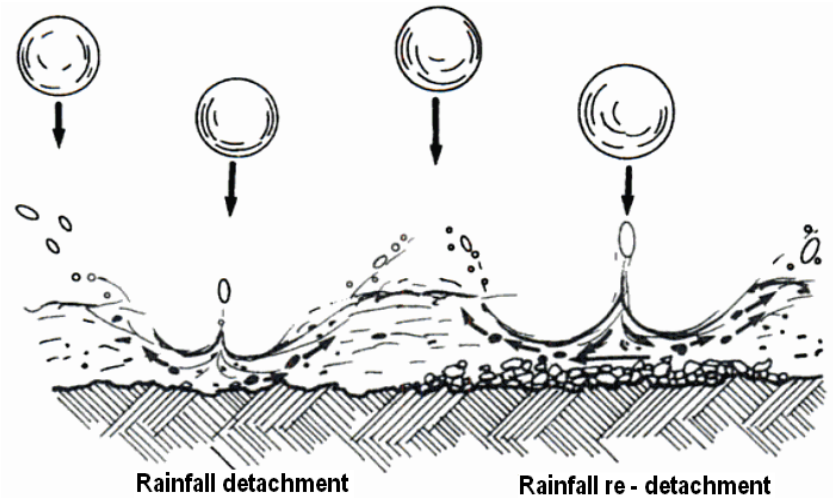

Figure 2.1: Schematic illustration of the distinction between rainfall detachment of the original soil matrix, and re-detachment of the previously eroded and deposited sediment. Source: Marshall (1996) after Rose (1993).

2.3 Soil erosion processes by water

Soil erosion by water occurs in a two-phase process, consisting of the detachment of individual particles from the soil mass and their transport by erosive agents, and when sufficient energy is no longer available to transport the particles, a third phase, deposition occurs (Morgan, 1995).

Detachment of soil particles from the soil surface is result of rainfall impact and overland flow (runoff) strain. Rainfall detachment is caused by the locally intense shear stresses at the soil surface by raindrop impact (Loch & Silburn, 1996), breaking down the interstitial forces holding the soil particles together.

When the rainfall rate exceeds the infiltration rate of the ground's surface and depression storage capacity, overland flow occurs, which consists of a thin film of water. Overland flow, causes a shear stress to the soil surface, which if it exceeds the cohesive strength of the soil, results in sediment detachment (Merritt *et al.*, 2003).

The amount of eroded and transported soil particle is controlled by the capacity of the splash and flowing water, to detach and move soil particles downslope. Therefore, deposition of eroded soil particles may occur depending on spatial organization of the surface, and transport capacity of the flow. If the velocity of water decreases, deposition of suspended soil particles may occur.

Ellison & Ellison (1947) proposed four processes: detachment by raindrop impact, transport by rainsplash, detachment by surface flow and transport by surface flow. There are two concepts commonly used to explain the magnitude of sediment flux: the transport capacity and detachment capacity. The transport capacity is defined as the maximum amount of sediment that a flow can carry without net deposition occurring (Nearing *et al.*, 1994). On the other hand, the detachment capacity is the maximum detachment rate that is assumed to occur when there is no sediment in the water. Both concepts are linked, and erosion conditions can be either transport limiting or detachment limiting, depending on which one is the limiting factor. In detachment-limited regime

(or detachment-limited erosion), the detachment capacity of the soil is lower than the transport capacity (Van Rompaey *et al.*, 2003), in this case it is possible that no soil is detached when the shear stress of flowing water (at the given location) is lower than the critical shear stress of the soil. On the contrary, the transport-limited regime occurs if the detachment capacity is greater than the transport capacity (Harmon & Doe, 2001), in this case the supply of soil particles is abundant and the transport of sediment is controlled by the strength of flowing water, deposition occurs where the transport flux slows down.

Five main types of soil erosion are commonly identified, depending on the stage in the erosion cycle: splash, interrill, rill, gully and in-stream erosion (bank erosion and stream bed erosion). Splash erosion is the first stage of erosion, and it is caused by raindrop impact on bare soil, the individual particles are splashed onto the soil surface. Interrill erosion is the detachment or removal of soil particles by raindrop impact (and very shallow flow), and deliver the detached material to nearby channels called rills. Interrill erosion can occur without rill incision, and that flow concentration caused by microtopographic depressions does not necessarily lead to rill initiation, even if threshold conditions for particle entrainment are exceeded (Bryan, 1987).

Rill erosion is viewed as a small channel that receives only interrill material, and have been defined by Hutchinson & Pritchard (1976) as flow channels that can be obliterated by tillage. Gully erosion occurs when the erosive power increases and more than one rill converge to form a large surface channel, called gully (Poesen & Valentin, 2003). Gullies are watercourses cut into the subsoil and they can have different shapes (V, U, T-inverted shaped bottoms) and depth is > 0.15 m (Planchon *et al.*, 1987), which makes difficult to cross with a farm equipment. Govers (1987) has found that gully erosion, only occurs where the subsoil consists of loose or unconsolitated materials and has its own dynamics. The regression of the gully headcut and the deepening of the depth are limited to major runoff events (Govers, 1987).

As will be discussed in later sections, most erosion models tend to predict soil erosion only for one of these erosion types, and it therefore the processes occurring in the basin are not fully represented.

The main characteristics of the drainage basin that affect soil erosion rates are: soil type, rainfall, topography, land cover and human influence. The susceptibility of soil to erosive forces varies, mainly related to texture and structure. Fine sand and silt are the most susceptible to erosion (Wischmeier & Smith, 1978). Clay particles are difficult to detach, but they can be easily transported, sand particles are easy to detach but difficult to transport. As for structure, fine granular are more susceptible to erosion than coarser structures (USDA, 1983).

Erosion is greater in longer, steeper and convex areas than in short length, flat, and concave areas. This is because of velocity and depth of runoff is larger in the former situation (Hudson, 1995). As it relates to shape, convex areas produce more sediment than concave and uniform areas, due to the higher velocity of runoff in the latter. The shape also influences the degree of sediment sink along the hillside, deposition is greater in concave areas than in convex areas.

The amount of sediment leaving a plot, hillslope or river basin, is a function of the erosional and depositional processes ocurring upstream of the measurement point. The amount of sediment leaving (mass) per unit of time is known as the sediment load, and it can be calculated by multiplying concentration by discharge.

2.4 Sediment yield

Sediment yield, is the amount of particulated solid matter that is delivered to the outlet of the basin. Sediment yield is the portion of the gross erosion within a basin, that is not deposited before being transported from the basin; sediment sources include upland interrill-rill erosion, gullies, streambansk, channels, construction sites, spoil banks and roadsides, and the relative magnitude of these potential sources depends on factors that include slope steepness and length, slope shape, soil type, land use and rainfall characteristics (Onstad, 1984). In Fig. 2.2 a general scheme of the interaction and linkages between sediment mobilization, storage and yield is illustrated.

Sediment yield at a point (e.g. mouth of the basin), is traditionally calculated by multiplying gross erosion above that point by a delivery ratio. Sediment delivery ratio is the fraction of upland gross erosion that is transported out of a defined area (e.g. basin), it is a measure of sediment transport efficiency. It is a lumped parameter and it is used to compensate for sediment deposited along the runoff pathway, and it is the sum of all types of erosion by water. It has been reported negative (e.g. Avendaño, 1997) and positive (e.g. Slaymaker, 2003b) relationships between drainage area and sediment yield, depending on the dominant erosion processes occurring in a given river basin. A detailed overview of these opposing trends and the scale dependance of erosion and sediment deposition (sediment delivery problem) can be found in de Vente *et al.* (2007).

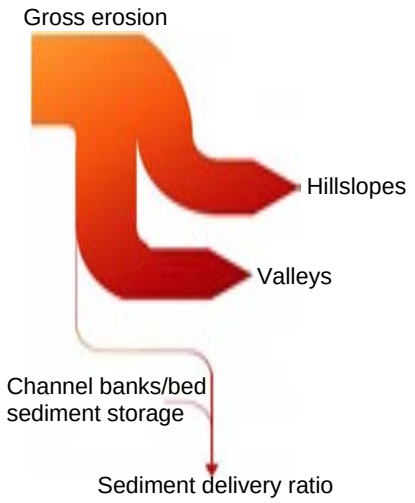

Figure 2.2: Scheme of sediment mobilization within a river basin.

The processes involved in sediment supply, transport and deposition are generally not linearly dependent on the causal factors, nor do they relate to one another in a linear manner (White, 2005). The failure to achieve reasonable estimates of annual sediment yield can be associated to the extrapolation of relationships, derived from field data with no consideration of their appropriateness for future conditions (White, 2005). A lack of ability of fully describing the system, adds more uncertainty. There is a random variability, which can be reduced by increasing the dataset and developing more efficient models.

Uncertainties are dealt with different approaches, such as the stochastic, which are often solved discretely by Monte Carlo modelling, which simulates a set of pre-calculated simulation results. Also are possible by performing scenarios based on assumptions. The uncertainty analysis can be presented by probability curves, confidence intervals, by fuzzy sets, or by other qualitative descriptions (Merz, 2006).

2.5 Sediment transfer

The soil eroded (from primary erosion) that has been delivered downslope and deposited on or at the base of slopes is called colluvium. There is an important linkage between the eroded soil from hillslopes, and its transfer to channels and valley floors; the effectiveness of this transfer is dependent on the degree of hillslope-channel coupling (Charlton, 2007). In Fig. 2.2 a scheme of sediment mobilization is illustrated.

The term coupling describes the linkage between components of a landscape, Brunsden (1993) identified three types of coupling: coupled, decoupled and not coupled. Coupled system occurs where there is active (direct) transfer of mass between hillslopes and channels at all timescales. This is typically the case in headwater regions, where narrow valleys are bordered by steep hillslopes (Charlton, 2007), this type is more sensitive to perturbation (Brunsden, 1993). Decoupled systems were once coupled, but have become inactive temporarily; and not coupled means a complete discontinuity between the hillslope and channel elements.

The size of soil particles delivered to channels varies largely, there are different mechanisms involved in the transport of these particles, as illustrated in Fig. 2.3, particle size is important on how are transferred through the system. The coarsest particles are found in the bedload, rolling and bouncing (saltating) along the river bottom; finer sediment are lifted well above the bed by the turbulence of flow and comprises the suspended load, usually called wash load and which is transported at rates close to the flow of the water itself (Komar, 1988).

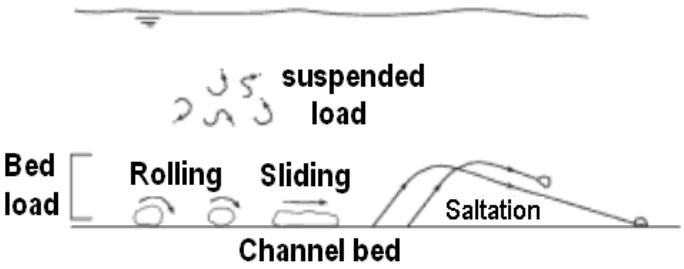

Figure 2.3: Modes of sediment transport. Source: Charlton, 2007.

In a dynamic flow and sediment routing simulation, Wainwright (2006) stated that the basin configuration has a very strong effect producing a complex system response based on the output of sediment from the catchment, and that there are no simple relationships between climate and catchment output, and furthermore that the complex response itself also evolves through time as the basin dynamically reorganizes.

2.6 A review of soil erosion models

From the applicability point of view, erosion studies attempt to estimate how much soil has been lost and where the sources in a basin are; and from a more broad perspective, the major aims for erosion studies can be summarized as stated by Boardman & Favis-Mortlock (1998) as: (1) to control erosion and preserve the soil resource, and (2) to contribute to the understanding of the long-term evolution of landscape. To be able to achieve these objectives it is neccesary to have some knowledge of the processes, and to be able to predict the rate, extent and frequency of erosion in the field (Boardman & Favis-Mortlock, 1998). There is still much to be done in research, because soil erosion has proven to be a highly complex process with rates varying in response to highly complex factors, such as weather, soil, vegetation, and land management (Toy *et al.*, 2002).

Soil erosion research is conducted at various temporal and spatial scales. Temporal scales range from changes in erosion processes during a precipitation event, to the potential influence of long-term climate change on erosion processes; on the other hand, spatial scales range from erosion on areas no larger than a square meter on ridges and hillslopes to the sediment discharged from entire river basins (Toy *et al.*, 2002). Erosion models are, by nature, abstractions of reality used to simulate. All of them have their strengths and limitations, the scale (temporal and spatial) issue is an important element defining their applicability, in addition and on the side of limitations, there are issues related to input data availability, data agregations and error propagation of the input

factors and errors associated to the model itself, that must be considered while using these models.

Extensive efforts have been made in the past to model the processes of erosion and sediment transport, the understanding on the subject is still less than complete (Mishra & Singh, 2003), therefore there exist lack of a universally accepted formula for determination of the sediment yield from a river basin (Shen & Julien, 1992).

Soil erosion models differ from one to another, in terms of complexity of the processes included and the data required for model calibration and use. Some considerations for model selection may include: characteristics of the study area, the purpose of use, input data requirements, model accuracy and validity of underlying assumptions, computer characteristics required to use the model.

These models are commonly grouped in three categories: empirical, conceptual and physically based models. Nonetheless, most models do not fall strictly into one category, as even the physics-based models still retain some empirism in the model algorithms (de Vente & Poesen, 2005).

Another way of classifying soil erosion models is, if they take into account the spatial distribution of the characteristics of the basin (modelled area), these can be: (a) distributed, and (b) lumped. Distributed models consider the spatial distribution of the important features of the basin, they provide information of the processes from the bottom up, example of this type is the WEPP model. On the other hand, lumped models do not account for details of the space unit's characteristics, in other words are non-spatial predicting the overall sediment production, an example of this type is the PSIAC model. In the case of RUSLE, it becomes a distributed model if it is applied to a basin. Their use depends on the objectives of the research, lumped models may be useful for some quite large basins and detailed distributed models may be more suitable for small catchments.

2.6.1 Empirical "black-box" models

Empirical soil erosion models do not reveal specific features of the erosion processes, but they can estimate erosion quite effectively. The use of these models might have a great advantage of conceptual and mathematical simplicity. These type of models are based on data collected in field experiments, and they use statistical techniques to provide a general feature of the basin.

Empirical models combine all soil erosion governing processes into one equation (spatial and temporal aggregation), which utilize empirical coefficients or factors for rainfall characteristics, soil properties, and ground cover conditions (Mishra & Singh, 2003). Parameter values in these type of models may be obtained by calibration, but are more often transferred from calibration at experimental sites (Merritt *et al.*, 2003).

Most empirical models do not attempt to represent the physical processes involved in sediment generation, and for this reason many empirical models tend to be basin specific, that is, they apply only to the catchment for which they have been developed, and often under the specific land use conditions existing within the catchment at that time (Letcher *et al.*, 1999), and generally do not estimate erosion at the event scale. In addition, these type of models are often critized for employing unrealistic assumptions about the physics of the basin, for ignoring the heterogeneity of basin's inputs and for ignoring the inherent nonlinearities in the response of the drainage system (Letcher *et al.*, 1999).

However, empirical models are frequently used in preference to more complex models as they can be implemented in situations with limited data and parameter inputs, and are especially useful as a first step in identifying sediment sources and nutrient generation (Merritt *et al.*, 2003). A deep review of these type of models is provided by Merritt *et al.* (2003) and Aksoy & Kavvas (2005). An example of this type of models is the RUSLE (Renard, et al., 1994) implemented in a GIS environment, which estimates long-term soil erosion, but nonetheless its main drawbacks are: (1) it does not account for sediment transport and deposition, (2) it only considers rill and interrill water erosion (no gullies nor mass movements).

2.6.2 Conceptual models

Conceptual models represent the river basin (modelled area) as a series of internal storages and pathways. They usually incorporate the underlying physical mechanisms of sediment and runoff generation within their structure, where flow paths are represented as a series of storages (Letcher *et al.*, 1999), thus they describe the transfer mechanisms of sediment and runoff. These models lie between empirical and physics based models.

These models provide an indication of the qualitative and quantitative effects of land use changes, without requiring large amounts of spatially and temporal distributed input data (Merritt *et al.*, 2003). They are capable of continuous long term predictions. Input parameter values for these models are normally obtained via calibration against observed data such as stream discharge and sediment concentration measurements (Abbott *et al.*, 1986; de Jong *et al.*, 1999), nevertheless, identifying the parameter values can be a problem (Merritt *et al.*, 2003). An example of these type of models is the LASCAM (Large Scale Catchment Model), that operates on a continuous basis, and it is capable of forecasting long-term estimates of daily stream loads of water, salt, sediment and nutrients, and it is of distributed type. A review of model outputs, input data, model structure, advantages and limitations of these type of models is given by Merritt *et al.* (2003).

2.6.3 Physically based models

Process based models have an explicit physical basis, and are the most complex erosion models. Represent the essential mechanisms controlling soil erosion, based on the solution of fundamental physical equations. These models incorporate the laws of conservation of mass, momentum and energy; most of them use a particular differential equation known as the continuity equation, which is a statement of the conservation of matter as it moves through space over time (Morgan, 1995). Current thinking on soil erosion modelling recognises the importance of runoff simulation as a critical control on erosion loss (Gobin *et al.*, 2006).

Within these models the modelled area is divided into regular grid cells, where the output fluxes from one spatial element, is transferred to the next spatial element as an input. In other words, they compute the inputs of material to a specific segment from the segment upslope and outputs of material to the segment downslope. However, these type of models are of limited application at the regional scale, in part because of their high data demand, and in many cases, by a focus on individual events rather than long-term cumulative impacts (Gobin *et al.*, 2006). These models, while having other merits, are not particularly appropriate for estimating basin sediment exports, since many of these models focus only on a limited number of erosion and sediment transporting processes (Merritt *et al.*, 2003).

Uncertainty in the parameter values of these models is a major issue, because the large number of parameters and heterogeneity of important characteristics affecting erosion, means that these parameters must be calibrated against observed data; and the finer the spatial scale of a model discretisation, the more the errors in such transfers will tend to grow (Merritt *et al.*, 2003).

Examples of these type of models are the ANSWERS (Aerial Non-point Source Watershed Environment Responses) model (Beasley *et al.*, 1980), which forecasts runoff and erosion, and requires four main categories of landform (soil, land uses, elevation based slope and aspect, and channel description), although runoff process is empirical, and the erosion and sediment transport processes are modelled via physics-based continuity equations, it is a temporally and spatially distributed model. Other examples of these type of models are the WEPP (Water Erosion Prediction Project) model (Nearing *et al.*, 1989), AGNPS (Agricultural Non-Point Source) Pollution Model (Young *et al.*, 1987), KINEROS (Kinematic Runoff and Erosion Model) (Smith *et al.*, 1995). A detailed analysis of the characteristics of these models can be found in Merritt *et al.* (2003) and Aksoy & Kavvas (2005).

2.7 Scaling and scale facts

The term *scale* refers to a characteristic time (or length) of a process, observation or model; similarly, the transfer of information across scales, is called *scaling*, and the problems associated with it are *scale issues* (Blöschl & Sivapalan, 1995).

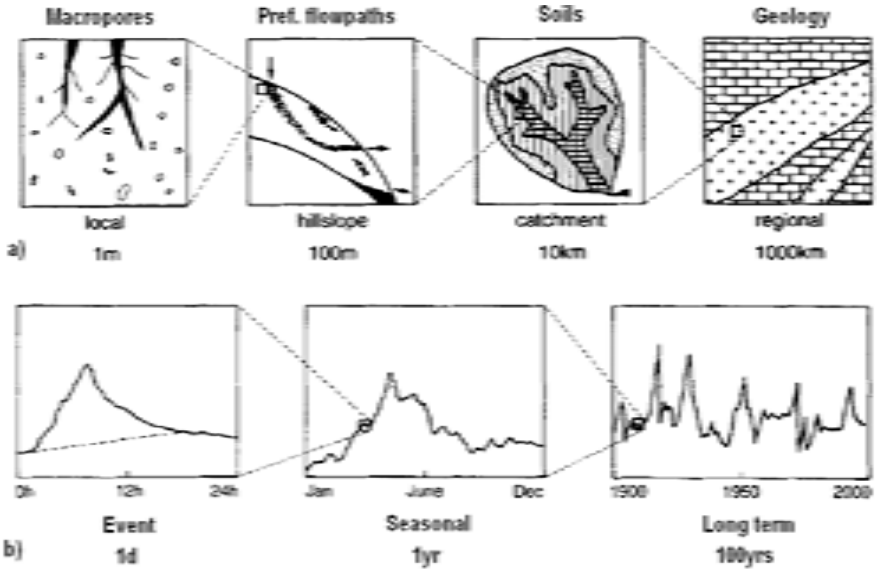

Figure 2.4: Heterogeneity (variability) of catchments and hydrological processes at a range of: (a) spaces scales, and (b) time scales. Source: Blöschl and Sivapalan, 1995.

Fig. 2.4a and Fig. 2.4b illustrate the subsurface spatial and temporal heterogeneity in a basin, and it goes from the local scale to the regional scale. Each scale allows the study of different systems, such as macropores (at the local scale), preferential flowpaths (at the hillslope scale), soils (at the catchment scale), and geology (at the regional scale).

Soil erosion has been studied at various scales, such as plot, hillslope, basin and regional scales; however, scaling problems exists, since soil erosion rates measured at one scale, are not representative for sediment yield at another scale level (de Vente & Poesen, 2005), and the dominant processes and factors influencing sediment movement across scales are different.

Despite efforts to understand the erosion processes at one scale, particularly small scales (plot and hillslope), the understanding of how these processes behave in other scales (basin) is still limited.

The lack of a simple relationship between drainage area and erosion rates demonstrates complex, and scale-dependant process domination (Parsons *et al.*, 2006). Downscaling and upscaling have inherent problems, because the processes being modelled are generally nonlinear.

Parsons *et al.* (2006) has argued that understanding and modelling of sediment flux, will enable geomorphologists to elucidate the links between the various components of the sediment cascade that creates landscape change.

2.8 Conclusions

Soil erosion research has begun as consequence of soil erosion in agricultural areas in the USA. Currently it is also studied to understand landscape evolution. Sediment erosion studies are approached from diverse perspectives, and as result several models were developed over the last decades, such as: empirical, conceptual and physics based models. All of them aim to improve our understanding of the erosion processes. These approaches can be also classified as distributed and lumped.

The understanding of sediment transfer processes at the basin scale is still limited, because of the nonlinearities of these processes and complex relationships among basin's characteristics.

Studies reporting negative and positive relationships between drainage area and sediment yield, indicates a strong site-specificity of the sediment cycle.

Selection of models depends on the trade-offs occurring in a basin. Physics-based models have the advantage that they can be transferred to other areas, and can be used for event and long-term erosion studies. On the other hand, empirical models are useful as a first assessment tool in large areas (e.g. basin), however they do not provide a description of processes ocurring in a basin and they are only valid for long-term assessment since it is based on temporal and spatial aggregation of data.

Chapter 3

STUDY AREA

3.1 Introduction

This Chapter is devoted to the description of the characteristics of the study area, the Upper Llobregat Basin. The study area is part of Pyrenees, a range of mountains, which joins the Iberian Peninsula to the rest of continental Europe. This area has experienced widespread land cover and land use changes since the 1950's, and it has become an important research target, because of its transition characteristics between Mediterranean and Continental Europe, in addition, it is an important water supplier for the increasing city sprawl.

This study was conducted at two spatial scales, as illustrated in Fig. 3.1, these are: (1) a medium ungauged river basin (the Upper Llobregat Basin), and (2) a small gauged catchment (Cal Rodó, Vallcebre) which is nested within the former.

3.2 Objectives

The specific objectives of this Chapter are:

- to describe the physical characteristics of the study area.
- to describe the land cover and land use changes in the last decades.

In this Chapter, emphasis is given to the Upper Llobregat Basin, since the particular characteristics of the Cal Rodó (Vallcebre) catchment are described in Chapter 4.

3.3 The Upper Llobregat Basin

The Upper Llobregat Basin has an area of 504 km^2, and it is located in the Bergueda County, in the NW of Barcelona Province, Catalonia, Spain. This area constitutes the Pre-Pyrennees, a mountanious rangeland, which does not have very high mountains as those in the Pyrenees. Fig. 3.1

illustrates its geographical location, at the mouth of this basin is located the La Baells Reservoir, which is located 95 km NW of Barcelona City.

The Cal Rodó catchment has an area of 4.17 km^2, it is one of the Vallcebre research catchments, which are nested within the Upper Llobregat Basin. Cal Rodó is a gauged catchment, and its hydrological functioning has been studied during the last 20 years, a few relevant characteristics of this catchment such as, the location of badlands, are illustrated in Fig. 3.1.

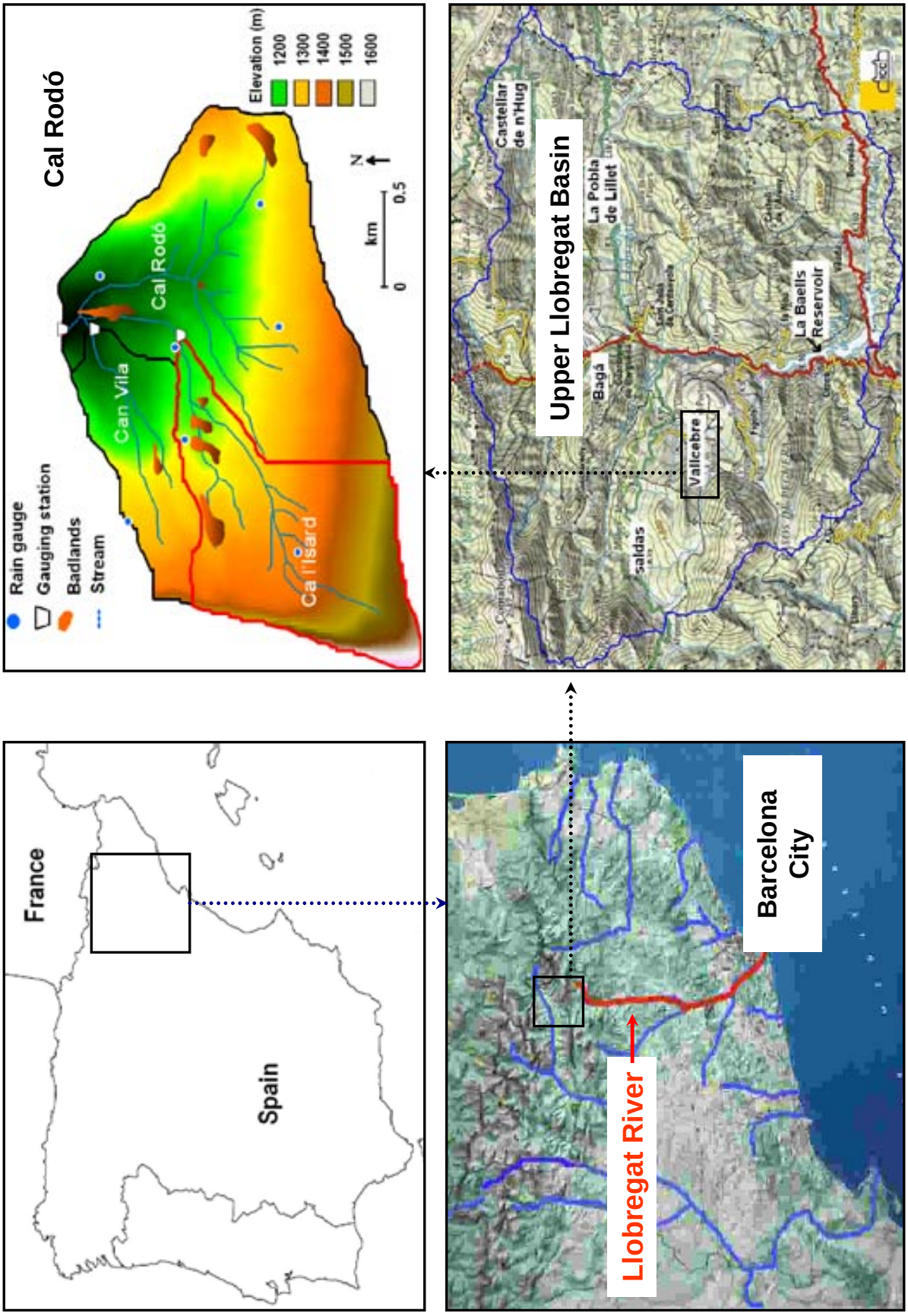

Figure 3.1: Study area: Upper Llobregat Basin (lower left), and Cal Rodó catchment (upper left).

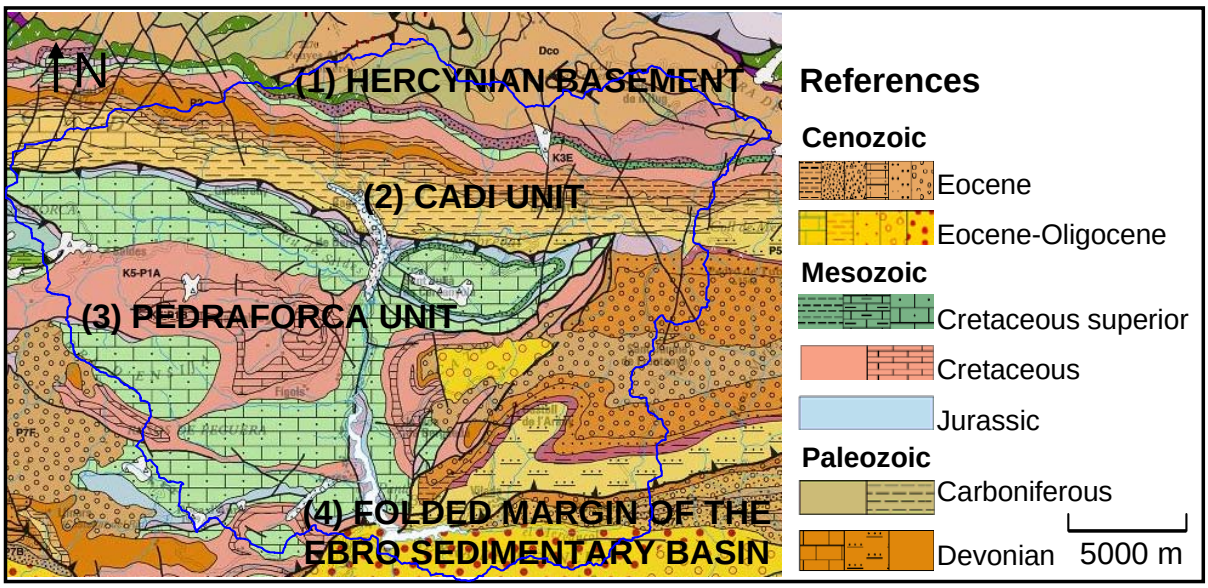

Figure 3.2: Geology of the Upper Llobregat Basin. Source: adapted from ICC (1980) and Clotet, 1984.

3.3.1 Geology

Geologically, the Upper Llobregat Basin lies on the southern edge of the Pyrenees, commonly known as the Pre-Pyrenees mountain ranges. An extract of the geological map (scale 1:250 000) of the study area is shown in Fig. 3.2.

Clotet (1984) mentions four geological units in the study area: (1) Hercynian unit, (2) Cadi unit, (3) Pedraforca Mantle Unit, and (4) Folded margin of the Ebro sedimentary basin Unit. The geological material of the (1) Hercynian basement is comprised of materials from the Devonic and Carboniferous, the dominat lithologies are calcareous-schist, slates and conglomerates; (2) the Cadi Unit, comprises materials from the Cenozoic, mudstones are dominant; (3) Pedraforca Mantle Unit, is comprised of materials from the Mezosoic, dominant materials are clays and marls, and mudstone; finally, (4) the Folded Margin Unit, is comprised of conglomerates, from the Eocene and Oligocene. These units are illustrated in Fig. 3.2.

In summary, the materials are from post-mesozoic rifting stages (in the southern part) and mesozoic sediment in the upper part of the basin (Cerdanya) (Daignieres *et al.*, 1981).

The Pedraforca Massif Unit, which is illustrated in Fig. 3.3, forms the easternmost element of the Pyrenean Rift, its thrust sheet represent almost completely inverted Early Cretaceous extensional basins that was transported southwards by large-displacement low-angle thrusts (Verges & Garcia-Senz, 2001).

The bedrock is folded and multiple vertical faults are present, which has determined the main structure of the drainage network. The geological formation consists of massive conglomerates in the SE side; sedimentary rocks, mainly limestones and calcareous sandstones in the N and W side of the basin; in the central part, can be distinguished presence of sedimentary rocks, for instance nearby Vallcebre, areas of clays and sandstones, similarly nearby Guardiola de Bergueda, Gosol and

Figure 3.3: A view of the Pedraforca massif, located at the south of the Cadi mountain chain. It sours up ≈1300 m to the peak ≈2500 m a.s.l.

around La Baells dam limestones are common, however presence of metamorphic (e.g. slates) and igneous is also noticeable. Superficial deposits are found nearby Pedraforca, Sant Jordi de Cercs and the western side between Guardiola de Bergueda and Baga. A detailed description of geology of some specific areas within Upper Llobregat Basin can be found at diverse sources; for Vallcebre area (Pardini, 1996; Oms *et al.*, 2007), for Pedraforca area (Molina, 2000), and geologic maps developed by Catalan Institute of Cartography (ICC, 2002) for the entire study area. Gypsum-rich substrates can also found as thin layers alternating along the slopes. A number of badlands developed mainly on Upper Cretaceous clays, which are rich in smectite and illite (Solé *et al.*, 1992).

3.3.2 Geomorphology

The geomorphology of the study area is characterized by the existence of contrasted lithological units, the existence of tectonic structures clearly differentiated, and a complex hydrological network (Clotet, 1984).

Altitude within the basin ranges from 627 m to 2540 m a.s.l. with a highly contrasting relief. Outcrops are predominantly limestones, conglomerates, marls, claystones and sandstones, and turbidites.

Badlands are widespread in the foothills of the Pyrenees, although they occupy only small areas, they are the main source of fluvial sediment in their associated river basins (Clotet *et al.*, 1988).

A few number of mass movements have ocurred on steep slopes, nevertheless, these are not often of considerable size and are of the slump type, the ocurrence of these mass movements can probably be related to hydrological conditions at the bedrock boundary.

In the study area, it is evident the construction of an extensive system of agricultural terraces, these were built primarily to make easier agricultural works and to minimize soil erosion. Terraces are earth embankments constructed accross the slope to intercept surface runoff and convey it to a stable outlet at a non-erosive velocity, and to shorten slope length (Morgan, 1995). The length of terraces are about 15 m or narrower, and are closely-spaced, the location of terrace outlets are commonly at the edges, the gradient is about 10%, currently these terraces are covered by pastures and are commonly grazed by sheep and cattle.

3.3.2.1 Drainage network

The hydrological network in the study area is a general adaptation of the movements of the rangeland as a whole in relation to local depressions (Clotet, 1984). The main river is the Llobregat River, which begins in Castellar de N'Hug, and flows first NE, and then SW until Pobla de Lillet, where is joined by L'Arija River, later at Guardiola is joined by Bastanery River and then it flows direction S until reaches the La Baells Reservoir.

The secondary network is comprised by L'Arija, Riufort, Bastanery, Saldes Rivers and Peguera stream.

3.3.3 Soils and erodibility

In the study area soil, supports a wide variety of vegetation, and its depth is variable. Soils in the study area are generally shallow and stony, its depth varies according to the location: less than 15 cm in the hilly and sloped areas and up to 100 cm in areas of low inclination. The organic matter ranges from 3% to 30% owing to the mainly forest areas. A high organic matter content, improves the soil structure aggregation and the water-holding capacity.

Soil texture is mostly loam clay, followed by loam-clayey and these are derived from colluvial deposits. Soil drainage is variable, terraced areas are generally well drained and less susceptible to erosion. Because of the fine texture in most of the basin, runoff is favoured.

3.3.4 Climate

The climate in the area is irregular and can be classified as mountainous Mediterranean, typically semi-humid with two humid periods (autumn and spring) and two arid periods (winter and summer) (Delgado, 2006), and ocassional thunderstorms in summer. Winter Mediterranean climate is mostly dominated by the westward movement of storms originating over the Atlantic and impinging upon the western European coast where it is affected by North Atlantic Oscillation (NAO), in addition, climate is affected by the complex physiography and the Mediterranean Sea (Giorgi & Lionello, 2007).

The mean annual rainfall in the Upper Llobregat Basin between 1985 and 2002 was 887 mm ± 156 mm, and the mean annual temperatures at La Molina (1680 m a.s.l.) and Borreda (845 m a.s.l.) weather stations were 7 and 11°C respectively (Delgado, In preparation). On the other hand, the mean annual rainfall at Vallcebre station between 1982 and 2009 was 863 mm ± 206 mm, most of the rainfall occurs between autumn and spring; whereas the mean annual temperature was 9.1°C.

Over 200 forest fires have occurred between 1968 and 2007. In decreasing order the size of burnt areas and locations were: 1570 ha (La Pobla de Lillet, January 1981), 229 ha (Baga, February 1984), 180 ha (Cercs, November 1978) and 153 ha (Montmajor, July 1994) (Catalan-Government, 2008), these are small areas compared to the size of the river basin (504,000 km^2).

The strong seasonal variability in weather conditions has effects on soil aggregates. In a study to define the physical weathering in badland areas, it was found that the strong and frequent freezing-thawing cycles at high moisture values are the most important physical weathering, thus availability of water (or snow) for freezing and the number of freezing cycles are important factors (Regüés *et al.*, 1995).

During winter, the highest altitudes (>2000 m a.s.l.) of the basin are usually covered by snow, which commonly lasts a month or sometimes more.

3.3.5 Land use and land cover

The study area, and as it is in most of Spain is mountainous, where significant land use change and land cover shifts have occurred particularly since 1960's (Vicente-Serrano *et al.*, 2004a). Land abandonment has effects on land cover, and it may cause degradation, although it may result in increased vegetation cover, and therefore reduced erosion as indicate Conacher & Sala (1998) and EEA (2006); it also means that traditional forms of soil conservation, especially terraces and stones walls, are no longer maintained; the crumbling of these structures may result in serious erosion problems (Conacher & Sala, 1998).

Effects of land use changes on runoff and sediment yield are evident in the study area, nowadays the hillslopes, which were cultivated a few decades ago are characterized by an open submediterranean shrub on a very thin and stony soil, a proof of intense soil loss (Garcia-Ruiz *et al.*, 1995), although the progressive colonization of bench terraces by shrubs and trees, results in a significant decrease of runoff (Llorens, 1994) this annual reduction in runoff can also be due to climatic causes (López-Moreno *et al.*, 2008). These shrublands and pastures areas have become important grazing grounds for cattle and sheep.

The main land cover type is forest (63% of the area), at the intermediate altitudes and the steeper slopes the vegetation is largely forest, mostly *Pinus sylvestris* and some deciduous oak (*Quercus pubescens*), with evergreen oak (*Quercus ilex*) in the warmer locations. Grassland occupies 33% of the basin, large areas of it, are found in the northern portion (La Molina, Clot del Moro), and in the western side of La Baells Reservoir. Agriculture is almost negligible (1.2% of the basin). The remainder areas are comprised of urban areas, bare soil, water bodies, and civil infraestructure (CREAF, 2002).

In areas near badlands, initially are vegetated by a meso-xerophylous pasture with an open tree-layer of *Pinus sylvestris*, and on steeper slopes, which is normally bare may be colonized by a perennial tussock grass (*Achnatherum calamagrostis*) (Guardia & Caswell, 2000). In the less exploited areas remnants of the deciduous oak forest (*Quercetum pubescentis*) exist (Carreras *et al.*, 1994).

In the Pyrenees afforestation at the basin scale results in a change of the hydrological behaviour of the basins, reducing the peak flows and the size of the sediments, and causing plant reestablishment in the channels and on the river banks (Ortigosa & Garcia-Ruiz, 1995).

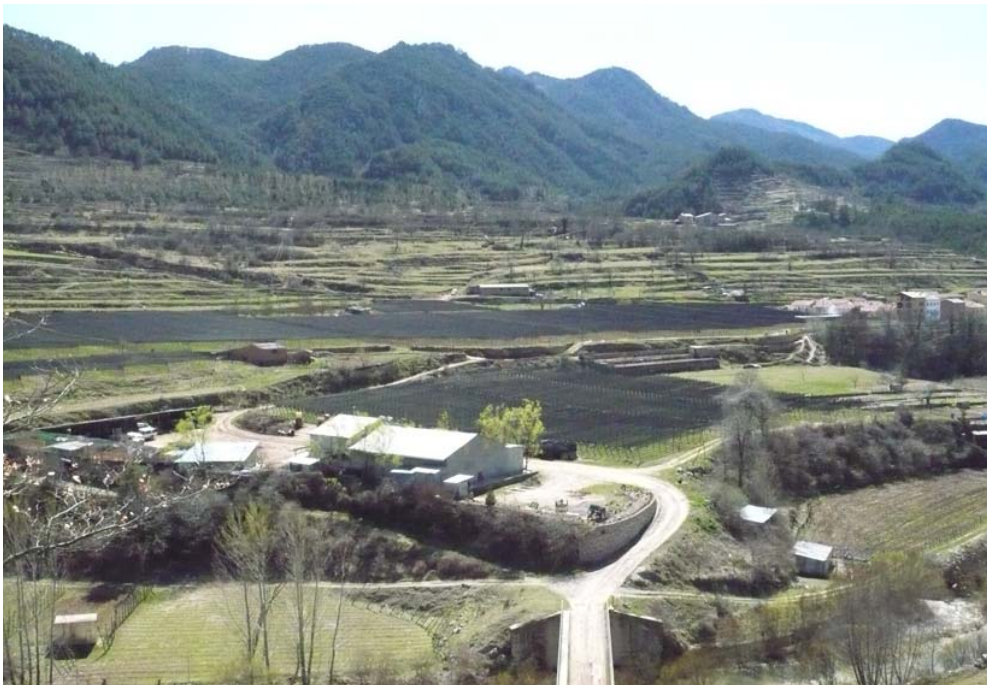

Figure 3.4: A view of a few remainder agricultural areas nearby La Pobla de Lillet. In the background, terraces are visible.

Mining operations in the Upper Llobregat Basin took place about a century ago, and it might have increased erosion rates, considering that mine dumps and spoil banks, often continue to supply sediment by natural rainfall for many years after mining operations have stopped (Clotet *et al.*, 1983).

3.3.5.1 Cultivation

In the study area, as it is in most of the Mediterranean Europe, policies to reduce the number of people employed in agriculture had consequences on landscape, because fewer people remain on the land to maintain traditional terracing which is left to decay (Morgan, 1986). However in general (except some terraced areas) land abandonment has reduced erosion rates (less agricultural areas); but in the case of terraced areas, abandonment and disrepair of them have in a number of cases led to gully erosion and landsliding (Boardman & Poesen, 2006).

In the Upper Llobregat Basin, agricultural areas have decreased from 23% in the 1950's (Delgado, In preparation) to 1.2% in 2002 (CREAF, 2002), same pattern was reported for the Pyrenees as a whole, where the area under cultivation has shifted from 30% (1950's) to 2% of the total area (Vicente-Serrano *et al.*, 2004b; Lasanta *et al.*, 2005). In Fig. 3.4 a view of a very few remainder agricultural areas is illustrated.

Studies conducted by Garcia-Ruiz *et al.* (1995) in the central-western part of the Spanish Pyrenees, which presents similar physiographic characteristics to the study area have shown that, under dense shrubs low soil erosion were measured, and increasing soil erosion was reported for meadows, and the highest rates were reported for cereal crops on steep slopes, especially under low conservation

systems. Given the mentioned similarities with the study area, a similar trend in erosion rates might be expected.

3.3.5.2 Urbanization

The Upper Llobregat Basin is sparsely populated. The important villages are: Baga, Castellar de N'Hug, Cercs, Guardiola de Bergueda, Vallcebre and Pobla de Lillet. In the beginning, this area was merely agriculture, later a few industries were set and mining activities emerged and dissapeared eventually, and most recently (since 1950's) agricultural areas were abandoned.

In general, there the pressure on land is low, except in urban areas and tourism activity, the latter has increased since roads have been improved (e.g. construction of Tunnel of Cadi). Earth movement in urban areas might be important source of sediment, even though it is temporary.

3.3.6 Database for the Upper Llobregat Basin

3.3.6.1 Climate data

Rainfall information was obtained from the Spanish Meteorological Center. Dataset included 15 years (1994 - 2005) of daily and average annual rainfall, these data were available for eight weather stations: Berga, Figols, Borreda, Baga, Pobla, La Molina, Vallcebre and Josa. Four of them located within the study area and four nearby. In addition sub-hourly rainfall database for over 15 years measured at Vallcebre station by the Hydrology and Erosion Research Group from the Institute of Environmental Assessment and Water Research, was also available. In Vallcebre, several precision tipping bucket rainfall gauges connected to a datalogger are used, where 1 tip is equal to 0.2 mm.

Furthermore, at Vallcebre daily temperature records since 1986 are available.

3.3.6.2 Slope data

Slope gradient and slope aspect information were derived from the available DEM. The resolution of the DEM is 20 m. This resolution was achieved by the Geography Faculty of the University of Barcelona, based on the 30 m resolution from the Catalan Institute of Cartography (ICC).

3.3.6.3 Land cover data

A land cover map (20 m resolution) of the study area compiled from aerial photographs taken in 1993 was provided by the Centre for Ecological Research and Forestry Applications (CREAF), this map has 11 land cover classes.

3.3.6.4 Other data

Cartographic and geologic maps at diverse resolution (digital and printed versions at 1:5000, 1:10000, and 1:25000 scales, and printed version at 1:250000) are available at the Catalan Institute of Cartography.

Chapter 4

SEDIMENT YIELD IN CAL RODO CATCHMENT

4.1 Introduction

Long term monitoring of water discharge and suspended sediment load requires considerable investment of time and resources. In order to make more efficient these processes, several techniques and methodologies have been applied in streams throughout the world during the last 60 years; however the accuracy of the accepted ones are still a subject of debate due to the large spatial and temporal variability associated with the transport of suspended sediment (Wren, 2002).

An accurate and compelling estimations of suspended sediment load, including uncertainty assessment (e.g. confidence intervals) is neccesary to underpin land management planning, and adequate allocation of limited resources. Although sediment transport in rivers is a natural process, human activities have accelerated the soil loss; consequently on-site and off-site effects are evident. An example of on-site effect is the loss of productivity, and off-site effects can be related to siltation of reservoirs, pollutant transport, delta and estuaries formation, and other environmental impacts.

Nowadays, efforts in sediment monitoring are addressed to minimize both, the temporal and spatial variability, and error sources. A number of techniques or methods to estimate suspended sediment transport have been used, and an evaluation of the performance of these under diverse conditions is needed.

Procedures to estimate sediment load rely on the sampling process to perform calibrations, which then are used for further calculations. Sampling has considerably importance in sediment concentration researches, because, it has to be representative of the population (ideally from the entire flow cross-section), achieving a representative sample is hindered by the fact that suspended sediment concentration varies on time.

The relationship between suspended sediment concentration and discharge is scarcely predictable, and it may suffer shifts over time (e.g. clockwise hysteresis), however long-term seasonal or annual loads are less variable than individuals, but this may require many years to amass enough data to detect statistically significant changes; therefore discrete storm event loads are more useful, and this should be accurate in order to avoid masking real effects with measurement error (Lewis, 1996).

Because temporal variations of sediment concentration are very high in ephemeral streams which drain small catchments, sampling gaps or mistakes are the main source of errors, which can be of one order of magnitude (Walling, 1988).

Sediment concentration, can be estimated by interpolation or extrapolation of periodic or infrequent concentration data. These may involve use of high discharge frequency records for the period under investigation, and high frequency of sampling. These procedures require development of sediment rating curves (SRC), which is a relationship between sediment concentration and discharge at the time of sampling, which can then be applied to high frequency discharge and covering a much longer period of time. The accuracy of a particular sediment concentration estimation procedure, is commonly assessed in terms of its bias, where it indicates the degree of systematic error inherent to the procedure, and is defined as the difference between the actual and mean load, of the replicate flux estimates (Phillips *et al.*, 1999).

There are some works analyzing annual sediment load errors, nevertheless, there is still lack of knowledge of annual estimations based on the analysis of individual event and even more important how much error these events add to total estimations.

In this Chapter, suspended sediment load assessment for 10 years period was done, based on continuous measurement [1] of discharge, and continuous or discrete estimations of sediment concentration through several instruments, which provide some elements to elucidate the uncertainty involved in the estimations.

First, a description of the theoretical frame of suspended sediment load assessment is provided. Then, it goes into a description of the operating principles of the measuring devices, along with its advantages and disadvantages, and finally a detailed description of variables involved is given.

Second, a detailed analysis of the quality of data and assessment of sediment load for a number of sediment transport episodes (27) are presented. Assessment is made by using several sediment rating curves, and results are benchmarked against results obtained by interpolation of discrete sampling and data provided by turbidity sensors.

Finally, relationships between sediment load and a number of hydrological variables are explored.

4.1.1 Problem statement

Studies of event based suspended sediment transport assessment in mountain streams, is not very common, and even less common is the uncertainty assessment of such studies, in terms of quality of input data and error propagation. Sediment transport in these streams is highly variable and mainly occurs during infrequent high-flow events. Sources of error get little attention in most load estimating projects, but should play a central role to know the reliability of the estimates (Thomas, 1989). Error transmision in such estimations is systematic, because of the use of surrogate variables, such as water discharge and turbidity, making impractical the error analyses, under this scenario Monte Carlo simulations allow uncertainty analyses, especially when non-linear relationship among input variables exist. Again, these type of studies are not common in suspended sediment studies and would be of great interest for resource allocation within sediment transport monitoring programs.

[1] every 2 or 20 minutes time step according to the amount of water discharge.

4.1.2 Research objectives

The general objective of this Chapter is to present an assessment of the uncertainties involved in suspended sediment load and sediment yield in a event based mountain gauging station.

The specific objectives are to:

- verify the quality of discrete suspended sediment sampling dataset, and remove outliers if neccesary.
- analyse the quality of turbidity sensor readings and remove faulty information.
- calculate sediment load for each flood (sediment transport) episode by using data obtained from the integration of discrete sampling and turbidity readings, and sediment rating curves.
- perform an uncertainty assessment of sediment load estimates for each flood episode.
- perform an uncertainty assessment of sediment yield (whole set of flood events).
- find alternative predictors of sediment load by using precipitation or hydrological variables.

4.2 Relevant theory about suspended sediment load

4.2.1 Importance

Sediment monitoring programs are important from the environmental and economical standpoints; although suspended sediment transport is a natural process in streams, when it reaches certain threshold, it can trigger negative consequences in natural systems and civil engineering, thereby, the fact of understanding how much sediment is transported and the accuracy of estimations are necessary to implement control and preventive activities.

Predicting sediment load at the catchment scale, is one of the most important challenges in soil erosion surveys, the application of both physics-based and regression models has until now not provided very satisfying results for calculation of sediment yield, because it is required large data and there is a lack of knowledge to describe all processes and interactions at the catchment scale (de Vente *et al.*, 2006). For example in a study in three gauged sub-catchments of a small coniferous forested upland drainage basin in the Southern Pennines of United Kingdom was obtained suspended sediment load between 7 to 124 Mg $km^{-2}yr^{-1}$, that study has shown that regression models are imprecise, unsuitable in headwater streams because of the high scatter in the relationship between discharge and sediment load (Liam, 2004).

4.2.2 Surrogate variables

Continuous direct measurement of suspended sediment is not possible at the current state of technology. Therefore, substitute variables are used, these consists of, the use of turbidity sensors combined with discrete sampling. Detailed records available from such sensors can compensate for

imperfect relations between the surrogate variables and suspended sediment concentration (Lewis, 1996).

The most common surrogate variables used for sediment concentration estimations are through turbidity sensor calibrations, discharge, and time. If the sensor readings are of good quality, setting calibrations would be enough to estimate concentration; nevertheless, when these readings are of poor quality or even worse, when there are not at all, other surrogates need to be used. Turbidity correlates with concentration, but the relationship is site specific (Lewis, 1996), in addition turbidity depends on grain size that may change in time (Regüés *et al.*, 2002). Discharge is another surrogate to estimate concentration through the well known sediment rating curves. Another option is the time-interpolations of discrete samples, collected for the rising and falling limb of the hydrograph.

4.2.3 Components

4.2.3.1 Discharge

From the environmental perspective, the amount of water generated within a catchment is important to be quantified for several key reasons. First, in order to estimate water resources, flood peaks and drought frequency (extreme events); second, to estimate the evapotranspiration rate using time-series within a water-balance equation (Chappel, 2000); and third, the multiplication of sediment concentration by discharge gives the mass of sediment load moved over time. Because of these multiple and important purposes, water discharge calculation methods, must be selected according to stream characteristics and the purpose of research.

The term runoff is normally used to distinguish surface flows from ground-water, and streamflow refers to the flow, that passes through the control measurement point, for example through a gauging station.

Below a brief description of the most common methods to measure streamflow is presented. The selection of one, or the other, depends on the morphological characteristics of the stream and on the application of the results.

4.2.3.2 Direct discharge measurement methods

Volumetric gauging This method is used in small streams, which consists in collecting water in a recipient which volume is known, during a specified period of time, for example using buckets, etc.

Float gauging This technique consists of measuring the velocity of a floating object transported by a section of the river (useful in steady flows) and multiplied by the river cross-sectional average area.

Current metering By the means of a current meter rotation, at different depths which gives the water velocity. The transverse distribution of river velocity can be characterized by dividing

the channel cross-section into a number of segments, then the *Mean Section Method* (Eq. 4.1) can be used to calculate the discharge for each segment (Hartley & Dingman, 1993).

$$Q_{seg} = 0.5(v_1 + v_2) \times 0.5(d_1 + d_2) \times b \tag{4.1}$$

In Eq. 4.1, Q_s is the water discharge for each segment, v_1 and v_2 are the water velocities at depth d_1 and depth d_2 respectively, and b is the chosen width of channel segment.

4.2.3.3 Indirect discharge measurement methods

Slope-area methods Within this category the most common is the *Manning Equation* (Eq. 4.2 and 4.3), typically used after the passage of a flood peak.

$$v = \frac{R^{2/3} \times S^{1/2}}{n} \tag{4.2}$$

$$Q = \frac{AR^{2/3} \times S^{1/2}}{n} \tag{4.3}$$

Where v is the river velocity, R is the hydraulic radius which is the cross-sectional area of the flow divided by the wetted perimeter, S is the downstream slope on the river surface, and n is Manning's roughness coefficient which varies from 0.025 to 0.07 (Hewlett, 1969).

Stage-discharge rating curves Involves a relationship called *Rating Curve* between the height of water h (*stage*) in the river and several discrete discharge measurements. The river *stage* represents the depth of flow above the river bed. The exact nature of the relationship is not readily known (Mishra & Singh, 2003). Usually a staff gage is used to measure h. Staff gages are usually vertical boards or rods precisely graduated with reference to a datum (Julien, 1998). These sort of rating curve are used especially in permanent gauging stations for long term discharge and sediment load studies. As the discharge-stage relationship changes from *subcritical flow* to *supercritical flow*, it is necessary to build a structure to reduce these hydraulic changes, these structures are called *weirs*. There are many types of weirs from V-notches, rectangular, flumes from trapezoidal to H-flume types (Chappel, 2000).

Once the measurement point is established, the next step is, to define the method of stage measurement, devices such as *pressure transducer* are often used to automatize measurement, these devices measure the pressure p exerted at any point in the water column into an analog electrical signal (measured in mV) which then may be transformed in water height h.

A relationship between stage and pressure is defined, in order to do so, it is neccesary to have previous measurements for both variables. Normally a linear relationship is the best-fit.

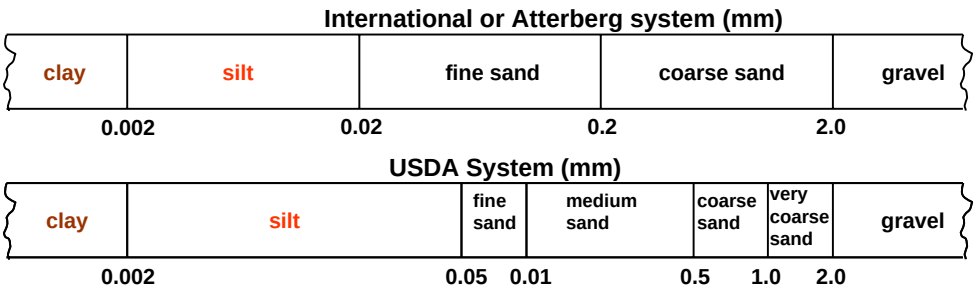

Figure 4.1: Soil particle size classes (diameter).
Source:Adapted from (White, 2006).

When stage is continuously measured from the calibration, discharge can be determined by using a discharge rating curve: $Q = f(h)$ which depends on stream shape and its proportions.

Pressure transducer sensor and its accompanying cables need to be firmly attached to an underwater surface, both, to protect the sensor from damage, and to act as an firm reference point for depth measurement and avoiding situations where the sensor could be eventually obstructed by silt or sand, as this will lead to a slow response and ultimately the sensor may cease to sense changes in pressure when its filter membranes becomes clogged (Scientific-Campbell, 2002). Eventually re-calibration might be necessary to adjust for drifts.

4.2.4 Suspended sediment concentration

Suspended sediment is the amount of sediment or solids in suspension, carried out by a watercourse, and it commonly constitutes between 85% and 90% of the total sediment load (Walling, 1988; Julien, 1998). On the other hand sediment concentration is the amount of particles (weight) in a known amount of water; and sediment load is the amount of sediment transported during a certain period of time and can be calculated by multiplying sediment concentration, by discharge, and a given time step (Walling,1988; Crawford, 1991; Jansson, 1996; Asselman, 2000).

Traditionally studies of suspended sediment transport by streams have emphasized the magnitude of sediment transported, however, it is also important the type of particles being transported in terms of their physical or chemical properties. Erosion by water may preferentially mobilize and transport specific fractions and constituents of the soil that are of particular importance in maintaining fertility (fertile layer).

Suspended sediment is comprised by sand, silt and clay. In Fig. (4.1) two of the most common classification systems of particle sizes are given.

Sediment concentration can be estimated by discrete sampling, or indirectly by turbidity sensors, and sediment rating curves.

4.2.4.1 Discrete sampling

Automatic sampler An automatic sampler is an instrument designed to pump up a discrete sample of water into a series of bottles, either at predetermined time intervals or as triggered by flow conditions. In the market there are available samplers of different capacity.

For instance the model ISCO 2700 is designed to collect up to 24 separate sequential samples (botles of 1000 ml capacity and made of polypropylene) from the river; samples are collected at equal time intervals using the sampler's internal timing circuitry, or at equal flow volume intervals using flow pulse inputs from an external flow meter. Automatic samplers use a peristaltic pump, which is driven by a battery, to convey water through a strainer and flexible sample tube to the collection bottle. Most of them use a computer processor, which allows programming of sampler functions, such as collection intervals, sample volumes and bottle positions (ISCO, 1986).

Advantages of using automatic samplers are that they offer the possibility of taking samples during short-lived floods at any time, fewer trips to the stream and less time spent on-site (less labour hours), safer working conditions, and samples could be retrieved after storms have passed. Some disadvantages are their high cost, however this could be reduced by less labour costs throughout the monitoring program, and it can allow the recovery of the investment, another disadvantages are device failure (there is no foolproof instrument), possible programming errors, flood damage, and even vandalism.

These devices work together with a data logger, which is programmed in this way to maximize the information obtained about the initial streamflood period, and to ensure that samples for the analysis of sediment concentration are collected throughout the entire flood. During large floods, sample bottles are recommended to retrieve, and replace them with another set of empty bottles, in order to obtain a good representativeness. The acompanying data logger also stores additional data such as date, time, water level, sample number, and sampler response everytime a sample is triggered.

In the study area (Cal Rodó) for instance, an automatic sampler (ISCO 2700 model) is connected to the stream by a tubing sampler to 12.7 mm diameter and it automatically switchs on, and starts to collect discrete samples when there is an increase in discharge over the regular predetermined levels, and collect suspended sediment over a range of time steps, such as 2 minutes or 20 minutes depending on discharge, that were established in so far as the monitoring goes on. Its optimal measurement range of concentration is from $\approx$ 10 up to 200 g/L.

Then, water samples are taken to a laboratory in order to determine sediment concentration, which basically consists on weighing the sediment or solids in the sample, through methods such as evaporation, filtration, wet-sieving filtration, or settling down (specific gravity). All of these methods will measure both, the organic and inorganic fractions, unless they are previously separated. Commonly samples are left for at least 24 hours settling down, then, the water is poured and the solids are collected in a recipient in order to dry it out by one of the methods mentioned, but the most usual is to dry out in an oven at 60 °C.

Sediment concentration is generally expressed in mg/L (net weight of the filtered sediment to volume filtered).

Having a good distribution of samples along the hydrograph is extremely important, for example to obtain a reliable sensor calibration, and develop analytical relationships (i.e. sediment rating

curves). In regards to particle size, commonly this is obtained through sieving and using a laser beam scattering for instance a Malvern Mastersizer which can make measurements between 5 up to 600 μm.

Sediment load is the product of sediment concentration (expressed in g/L) and discharge (expressed in L/s), and time step between sensor readings (expressed in s). Therefore, the total sediment load, that passes through a given cross section (expressed in g/s) for any given time step is represented in Eq. 4.4 and Eq. 4.5. Where SSC_i is the suspended sediment concentration, and Q_i is discharge in a given time step, and dt is time step. Eq. 4.4 is valid if continuous measurement of concentration and discharge exist. However, in reality sediment load is obtained by Eq. 4.5 where n is the number of readings, since measurements are not continuous strictly speaking.

$$SSL = \int_0^t SSC_i \times Q_i \times dt \tag{4.4}$$

$$SSL = \sum_{k=1}^{n} SSC_i \times Q_i \times dt \tag{4.5}$$

Time step is usually long and therefore the difference between two succesive sediment concentration measurements are large, which make time integration sediment load difficult. This justifies the need for continuous estimation of sediment concentration by sensors or by interpolation between discrete samples over only discrete sampling.

4.2.4.2 Continuous recording

Infrared turbidity sensor (nephelometers) Measurement of sediment concentration through nephelometers, such as Optical Backscattered Sensing (OBS) consists on a reflection detector, which sends out a beam of infrared light emitted by an Infrared Emitting Diode (IRED) and then, the reflected light is measured by a phototransistor. A portion of beam will be scattered if particles are in suspension, where a high light scattered means high concentration. This is one practical application of optical theory and similarly to the other sensors requires calibration.

For example, considering an incident light beam with an intensity I_{inc} and a wavelength γ striking a spherical particle of diameter d, the intensity I_{sc} of the scattered light is a function of the scatter angle θ, d, γ, and the optical properties of the particle and the medium such as the refractive index n. This functional relationship can then be summarized as:

$$I_{sc} = f(\theta, \gamma, d, n)$$

An advantage of OBS, is that it has a nearly linear response to varying concentration of homogeneous sediments (Black & Rosenberg, 1994), and it allows good spatial and temporal resolution. In Fig. 4.2 a schematic representation of the common operating principle of turbidimeters is illustrated. OBS sensor operate in configuration backscatterance in Fig. 4.2.

Another illustration of what occurs in a water sample containing sediment is presented in Fig. 4.3, where the red-shaded region, is illuminated by a light source, shown by the red light bulb, and one

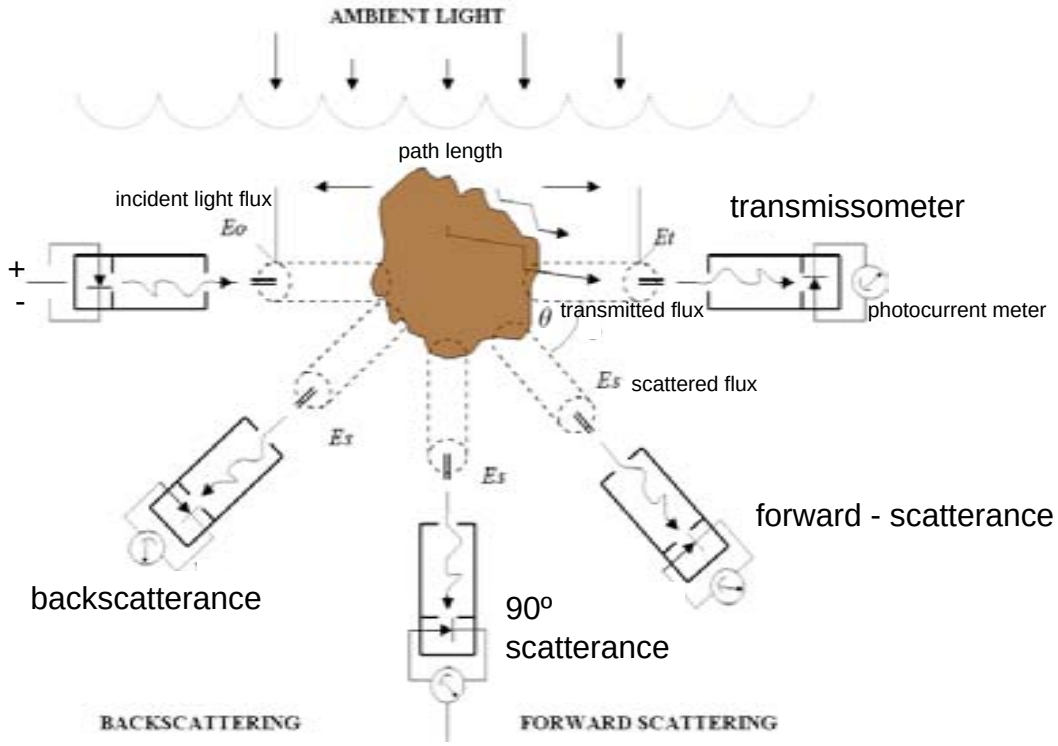

Figure 4.2: Optical particle detectors.
Source:Adapted from D&A Instruments Company (1991).

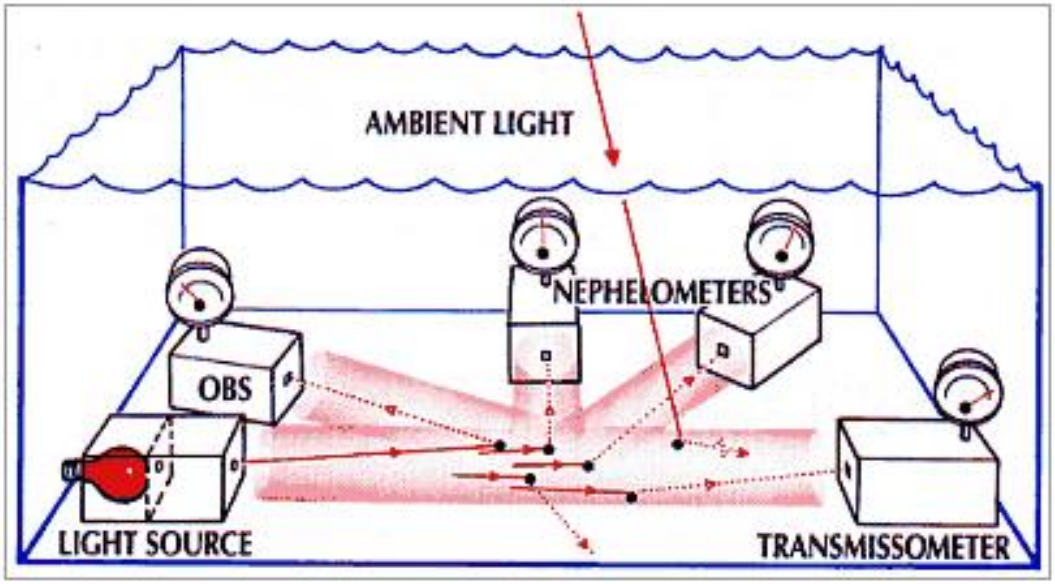

Figure 4.3: Infrared sensor and other optical sensors.
Source:D&A Instruments Company (1991).

or more photodetectors convert the light radiated from the sample to photocurrent. The amount of photocurrent depends mainly on the area of the illuminated particles but also on particle size, shape and reflectivity. OBS sensors detect light scattered over a range of angles that depends on the model and particle concentration in the sample. The OBS-3 detects light scattered between 140 and 160 °, the OBS-4 sensor between 70-160 ° and the OBS-5 between 88-170 ° (D&A Instruments, 2005).

In clear waters (for example in alpine streams and springs) there is little light scattering, most other surface waters contain suspended matter that scatters more light from a beam than is absorbed (D&A Instruments, 2005).

Particle size dependency is the main disadvantage with using OBS (Wren *et al.*, 2000), because its response is determined by the optical properties of the particle and finer sediments give a relatively a larger signal than coarser ones (Van, 2001), or in other words, backscattering from particles is inversely related to particle size (D&A Instruments, 1991). Optical sensors are more responsive to fine sediments than to coarse sediment (Admiraal & Garcia, 2000). In environments with particle size of less that 100 μm results are greatly affected, and OBS performs well for concentrations where particle size is constant or remains between 200 - 400 μm (Conner & de Visser, 1992).

In addtion, water color can alter the relationship between turbidity and concentration (Gippel, 1995).

Ultrasound sensor Ultra sound sensors operate transmitting pressure pulses or short bursts of approximately 10 μs of high frequency sound (1-1.5 MHz) emitted from a transducer to another, where a fraction of each pulse is rejected or backscattered by suspended sediment to the first transducer (Thorne, 1991).

The strength of the transmitted sound signal depends on concentration, particle size, and acoustic frequency. Using typical ultrasonic frequencies, the particle size range is approximately 62-2000 μm and concentrations may range up to 30 g/L, although the available sampling depth will be limited at high concentrations (Thorne, 1991). Fig. 4.4 illustrates the general operating principle of a ultrasonic attenuation sensor.

The way the sensor are mounted are variable, for example the *Mobrey* suspended solids monitoring system, has a sensor mounted in the settlement tank which provides analogue measurement of the settled solids blanket density at the sensor level (Mobrey, 2005).

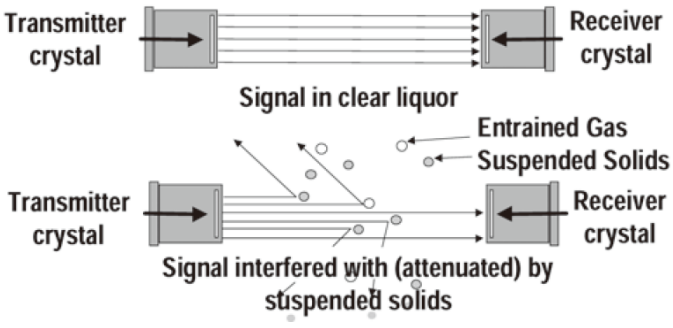

Figure 4.4: Operating principle of Mobrey ultrasonic attenuation sensor. Source: Mobrey (2005).

Advantages of ultra sound sensors are their good spatial and temporal resolution, they measure over a wide vertical range and is non-intrusive; disadvantages are that backscattered signal is difficult to translate, and there is signal attenuation (reduction) at high particle concentration (Wren *et al.*, 2000).

Information generated by these sensors are stored in a data logger, which store other related

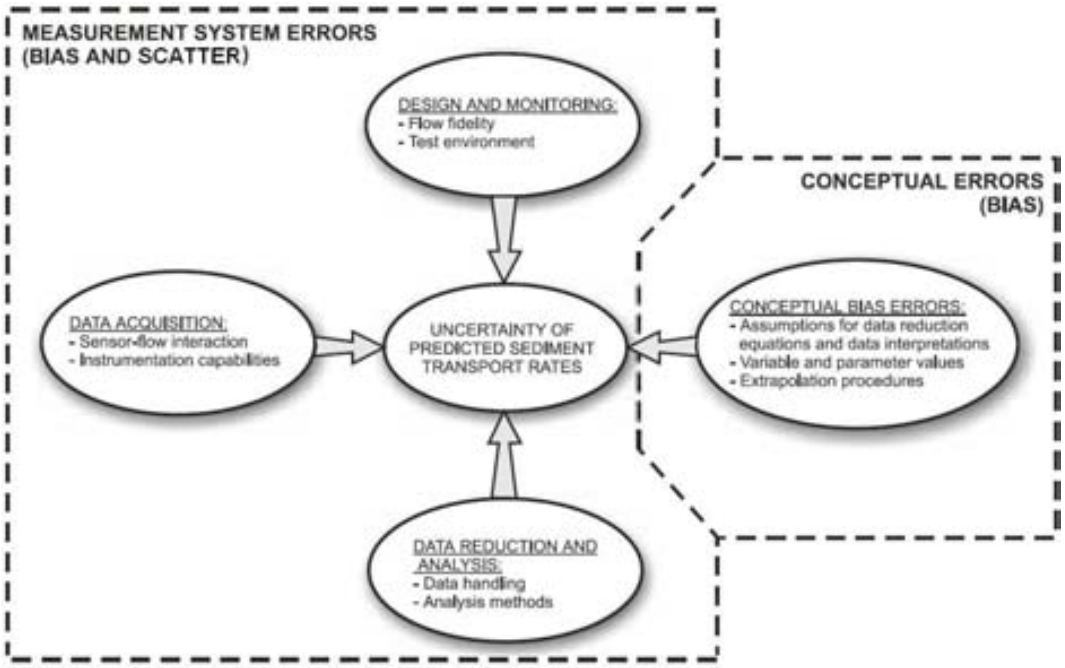

Figure 4.5: Sources of errors on suspended sediment transport.
Source: American Society of Mechanical Engineers (1998) quoted by Muste (2002).

information as well which are necessary for further sediment load calculations.

4.2.5 Uncertainty sources

The error in an empirical result is the difference between the true and the measured value of the result, in most situations, the true value is not known and hence, it is neccesary to estimate the limits that bound the possible error. These limits are called uncertainty or uncertainty intervals, uncertainty defines the interval around the measured value, within which the true value is believed to lie with a pre-established level of confidence (Muste, 2002).

It is important that when reporting an estimate, the uncertainty of that estimate is given, so that those who use it, are able to assess its reliability. The result of a measurement is only an estimate of the value of the measurand and thus, is only complete when accompanied by a statement of uncertainty (Herschy, 1999).

There are different criteria to classify the errors, and its components can be the bias (fixed) and scatter (random), bias errors are systematic, therefore difficult to detect and remove, scatter errors can be estimated by inspection of the measurement dispersion, both are generated through the phases of the experiment (Muste, 2002).

In Fig. 4.5 is shown a classification of the sources of uncertainties made by the American Society of Mechanical Engineers (1998), these are: calibration, data acquisition, data reduction, and conceptual (methodological). These errors also can be classified as instrumental and temporal integration of data.

4.2.5.1 Instrumental

Sediment load estimations can be affected by instrument malfunction or when these are saturated (when their capacity is exceeded).

In the case of pressure transducers accuracy varies according to technology sophistication, ranging from 0.01% for certain vibrating quartz crystal transducers to 1 % for other devices (Stevens, 2005).

All pressure transducers are subject to drift. Drift is tolerable in situations where is needed only a rough idea of how flows vary over time, but it is intolerable in applications where absolute values are needed such as billing calculations, and modeling (Stevens, 2005). Hence, submersible pressure transducers must be re-calibrated periodically.

Similar errors may arise when using automatic samplers. The depth from where samples are collected could influence the sediment concentration if the solids concentration in the sample is similar to the stream concentration, another factor that could influence the concentration is the intake velocity (quality of samples) during the sampling process, sediment particles experience their own dynamics that are not exactly the same as those of the water mass because of fall and uplifting of particles (FAO, 1997).

For example in a study conducted in the Vallcebre catchments, was found that the velocity of intake during sampling affects the size of sediments, thus concentration have decreased with particles diameter larger than 250μm (Soler *et al.*, 2006). On the other hand, physical and electronic faults such as: inlet blockage by bigger debris or other objects conveyed by the river (intakes typically are 9.5 mm and 12.7 mm), and line plugging may occur during the storm, which may cause limited suction, as well an improper installation and programming may derive in errors (Othmer & Berger, 2002).

Additional errors may be derived in laboratory, for example during leaching process (particles retained on the filter paper, weighing, missing drops, etc.), temperature variations during drying out, presence of organic matter, and even how the samples are transported.

Because of these multiple likely error sources, sediment load value obtained by discrete sampling should be used with caution and compared with the results achieved through other methods; therefore, discrete sampling is the reference value to compare results obtained by the means of sensor readings.

In regard to infrared turbidity sensors, errors may arise from drift and dirtiness burial on sensor, the depth where the sensor is located, and diameter of transported solids. Light backscattered from particles is inversely related to particle size, and the sensitivity of OBS sensors may change with particle size by more than one order of magnitude and it can lead to serious difficulties when particle size varies over the time (D&A Instruments, 1991).

In reference to ultrasound sensor, possible error sources may arise from litter burial which may hamper correct device performing.

Combination of information obtained through discrete sampling and continuous reading is a good way to obtain accurate suspended sediment load estimations.

4.2.5.2 Temporal integration of data

When the sediment concentration is obtained using instantaneous samples, it is necessary, to use some interpolation or extrapolation procedures to estimate continuous sediment concentration, which then is multiplied by the discharge to compute sediment load.

The relationship in the arithmetic domain between suspended sediment load and discharge is heteroscedastic (high variability at high discharge) therefore, a linear regression do no fit the data, on the other hand, in the log domain, the relationship is often monoscedastic (Crawford, 1991) this form is commonly used. This temporal irregularity of sediment concentration, and the non-linearity between these two variables can be a major cause of error during temporal integration.

Additional errors may arise when selecting the appropriate equation to estimate discharge. To reduce these errors sources may be necessary to increase the number of stage readings. Studies assessing the magnitude of error when using sediment rating curves, show diverse results, for example in a study at the lower Wollondilly River (Australia) the error of sediment loads using sediment rating curves by applying bootstrap and Monte Carlo resampling techniques was $\approx 85\%$ (Rustomji & Wilkinson, 2008), in another study, for the Mississipi River at Thebes and Rhine River at Maxau the mean annual percentage differences of suspended sediment fluxes were 8 and 27% respectively (Horowitz, 2003).

4.2.5.3 Alternatives to reduce uncertainty

A series of statistics are necessary to assess the accuracy of sediment yield, as no single statistic can fully characterize the match between predicted and observed values (Willmott, 1981). Generally, these statistics include: (a) the slope b and intercept a of the least square log-linear regression fit to the scatterplot of predicted sediment concentration, (b) the coefficient of determination r^2 between the predicted and observed values, (c) the root-mean-square error (RMSE), and (d) the proportion of predicted values that fall within the 90% confidence interval.

Obviously, a suitable sampling design is more than essential and also making the minimum use of interpolation and extrapolation exercises would reduce uncertainty in regard to sampling, its frecuency was recomended to be typically 5 minutes for ephemeral catchments (FAO, 1997).

In reference to sediment rating curves, it has been proved that it is not statistically consistent (Thomas, 1985), because in general it tends to underestimate suspended sediment load (prior to retransformation bias). In studies with field data this bias sometimes exceeded 50% (FAO, 1997). Some others researchers such as Bennett & Sabol (1973) considered several rating-curve-type estimators, and concluded that errors could be as low as 20%.

Direct methods (e.g. sampling and sensor calibrations) have some important advantages over the rating curves, because, they require fewer mathematical steps than rating curves to make load estimations. However, they are economically more expensive. When using turbidity sensors it is neccesary to perform calibrations using local materials (in-situ), because these sensors are sensitive to small changes.

Uncertainty levels for suspended-sediment flux calculations, depend to a large extent on the poorly known temporal and spatial variability (including the unsampled zone) in the transport of suspended sediment (Wren & Kunhle, 2005). Proposal of acceptable levels of uncertainty for

Table 4.1: Range of acceptable uncertainties for individual suspended-sediment samples.

Concentration range (mg/L)	Best-case isokinetic (%)	Gray et al.(2002) (%)	Generalized approach
< 10	± 10	± 50	± 10 to ± 20 % for all concentration ranges
10 to < 100	± 10	± 50 to ± 25	
100 to < 1,000	± 4	± 25 to ± 15	
>1,000	–	± 15	
1000,100	± 3		

Source: Wren and Kuhnle (2005).

individual suspended-sediment samples given by Wren & Kunhle (2005) are presented in Table 4.1, where it can be observed that an increased frequency and improved spatial coverage of suspended-sediment reduces uncertainty.

4.3 Study area

The study area (Cal Rodó) is part of the Vallcebre catchments, which is located in the SE Pre-Perynees (see Fig. 4.6). Vallcebre catchments are experimental catchments where hydrological and erosion processes has been largely studied. Vallcebre catchment has an area of 19.6 km^2, it is located in the headwaters of the Llobregat River, at 1200 m a.s.l. (1 °49'E, 42 °12'N) and it is comprised of small subcatchments namely: Cal Rodó (4.17 km^2), Santa Magdalena and Cal Parisa. Cal Rodó includes: Can Vila (1.32 km^2) and Cal Isard (0.58 km^2). For this research, data from Cal Rodó gauging station has been used. In Table 4.2 are shown some general characteristics of Vallcebre catchments.

Table 4.2: General features of Vallcebre (Cal Rodó) catchments.

Parameter	Description
Area	19.6 km^2
Land cover	Pastures and mostly *Pinus silvestris*
Mean annual temperature	7.3 °C
Mean annual precipitation	863 ± 206 mm, with 91 rainy days per year on average. Spring and autumn have large precipitation; winter presents scarce precipitation and in summer it is possible some scattered short and high intensity rainstorms.
Geology	Bedrock is mainly comprised of red clay mudstones with gypsum and sandstone layers

Source: Gallart, *et al.* (2002)

The land use in Vallcebre includes forested hillslopes, old agricultural terraces which were made in the past for cultivation, and now, are used for cattle and sheep stockbreeding or forestry, also small badland areas exist. The bedrock is dominated by red clayey mudrocks with massive limestone beds (Gallart *et al.*, 2002).

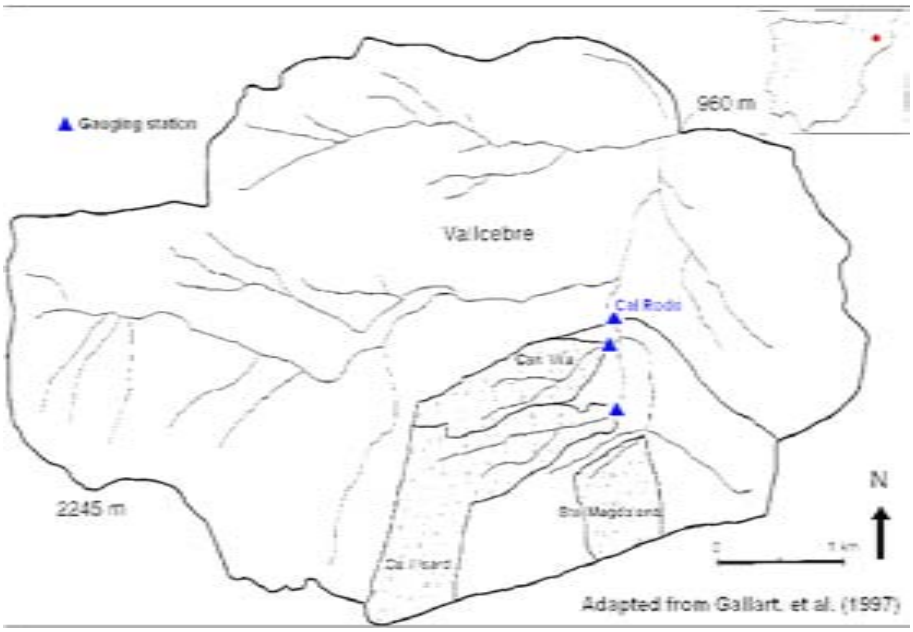

Figure 4.6: Study area.

The characteristics of the bedrock and the steep topography, as well as winter freezing and summer rainstorms, have led to the formation of badland areas (Solé *et al.*, 1992). Some studies in the Pyrenees have demonstrated that badlands are a significant contributor of sediment load (Francke *et al.*, 2007), and in Vallcebre, badland development and its dynamics, such as the seasonal weathering of regolith and erosion are identified as important sediment sources (Regüés *et al.*, 1995).

4.4 Materials and methods

4.4.1 Instrumental set up

Some of the features of the instruments used to collect data is shown in Table 4.3. The instruments are an infrared turbidity and ultrasound beam attenuation sensors, which are shown in Fig. 4.8 and Fig. 4.9. An automatic sampler ISCO model to collect discrete samples and a pressure transducer which is set on the streambed are shown in Fig. 4.7 and Fig. 4.10 respectively.

Table 4.3: Characteristics of the devices used in Cal Rodó gauging station.

Equipment	Optimal concentration
Infrared turbidimeter sensor, OBS-1 (D&A Company)	0 up to $\approx$ 6 g/L
Ultrasound sensor, MSM 40 (KDG Mobrey Ltd.)	$\approx$ 6 g/L up to $\approx$ 200 g/L
Automatic sampler, ISCO Model 2700	Unlimited

Source: (Latron, 2003).

Figure 4.7: Automatic sampler ISCO 2700 model.

Figure 4.8: Infrared turbidimeter sensor.

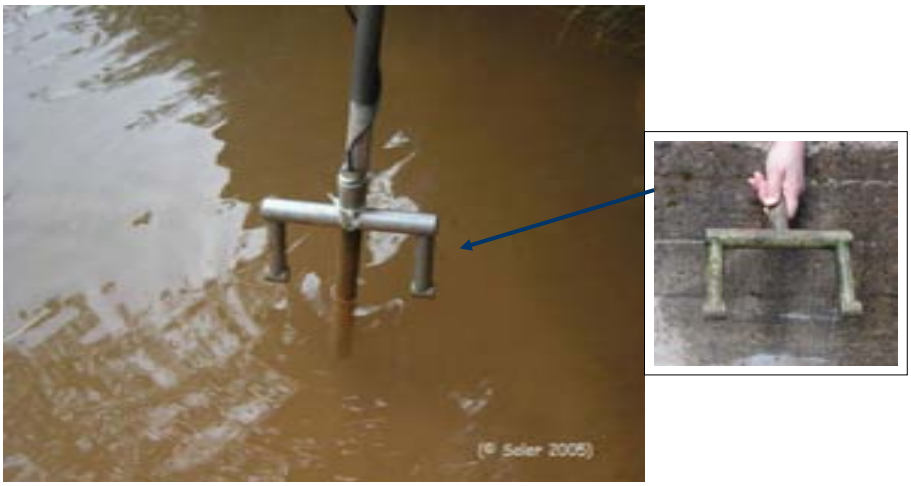

Figure 4.9: Ultrasound beam attenuation sensor.

Figure 4.10: Pressure transducer.

4.4.1.1 Sensor calibrations

Calibration is the process of converting units measured by sensors (mV) to a physical unit of interest, such as measurement of sediment concentration. For example, the infrared turbidity (IR) and ultrasound attenuation (US) sensors provide readings (mV), which then are converted to g/L by the means of a calibration.

Data needed to perform calibrations are: sediment concentration obtained by sampling (in this case through a automatic sampler, henceforth refered as SSC_{AS}) and electrical signals or readings (mV) given by sensors. In Fig. 4.11 relevant steps followed for determination of weight of sediment in laboratory are illustrated.

Normally a linear model is the best fit in this type of calibrations, which is of the form:

$$SSC = a + bR$$

Where:

a = intercept on y axis, b = slope, and R = sensor reading given by sensors (expressed in mV).

The parameters a and b are often estimated using least square models, the mean and standard deviation of these parameters are also estimated and residuals in order to determine if the regression model is unbiased and the errors occur randomly.

There are two options to test if the calibration explains the relationship between observed (obtained by sampling) and predicted data (obtained through calibration). The first test, is to perform an ANOVA for regression, under null hypothesis that H_o: the variance of regression model and the variance of residuals are equals. If they are equals, it is less likely that the independent variable (e.g. R) have a significant effect on the dependent variable (e.g. SSC). F is calculated by Model Mean Square divided by Residual Mean Square. The second option, is to calculate the mean ($\overline{x}$) and standard deviation (s) of the slope b, under the null hypothesis that H_o: $b = 0$. As in any null hypothesis test, the aim is to reject it. Here a may be equal to zero.

A graphical analyses of data is helpful, thus, plotting the SSC_{AS} values on y axis and R on the x

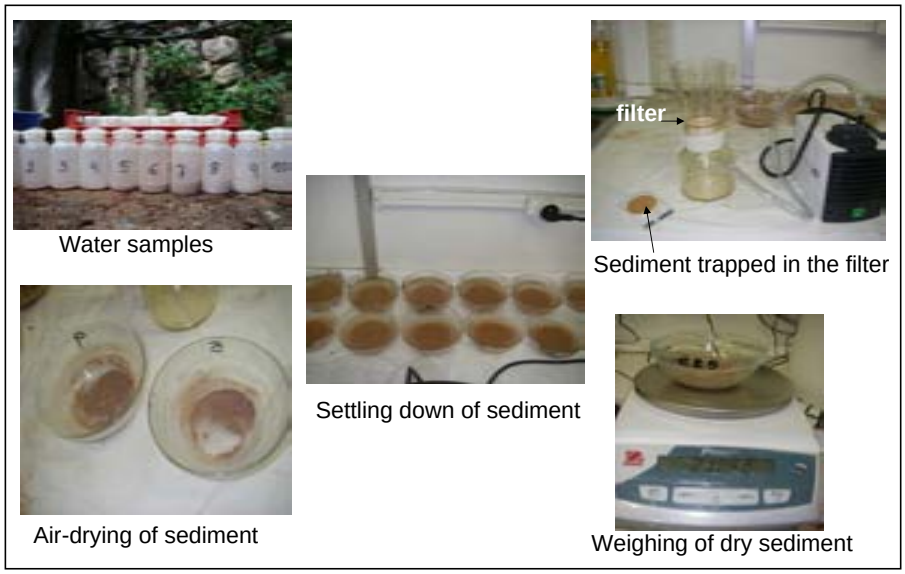

Figure 4.11: Steps for determination of sediment weight.

axis, in order to identify data points that may have large influence on the regression model (outliers or invalid sensor readings) is performed. The data points should lie close to the best fit line.

Pressure transducer Water stage (h) is estimated indirectly converting the electrical signal (mV) given by a pressure transducer (which measures pressure exerted by a water column), into a certain water height expressed in mm by the means of a linear regression. For the study area it was defined Eq. 4.6, which has a $r^2 = 0.99$. The scatter plot and best fit line are illustrated on Fig. 4.12.

$$h = -30.01 + 2.17 \times R \tag{4.6}$$

Finally, dicharge is estimated by combining water stage (h) with other parameters (generally site specific), this relationship commonly known as discharge rating curve: $Q = f(h)$. In the study area, the gauging station has a rectangular shape as shown in Fig. 4.13; partial discharges were calculated for each cross section.

Thus, for Cal Rodó catchment the total discharge Q_T (Eq. 4.7) has been estimated by summing up all the partial discharges values (q_n) passing through the specific cross section area and during a specified period of time.

$$Q_T = q_1 + q_2 + q_3 \tag{4.7}$$

The three empirical equations (Eqs. 4.8, 4.9, 4.10) were used to perform calculations of partial cross section discharges (Latron, 2003). Where: q_1, q_2, and q_3 are the partial discharges expressed in L/s, and h_1, h_2, and h_3 are the water height of each cross section expressed in cm.

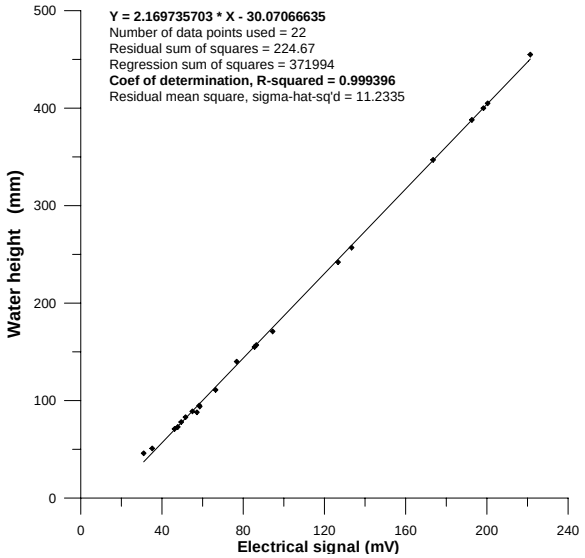

Figure 4.12: Calibration between water height and pressure transducer's readings. Source: Elaborated from data given by Latron (2003).

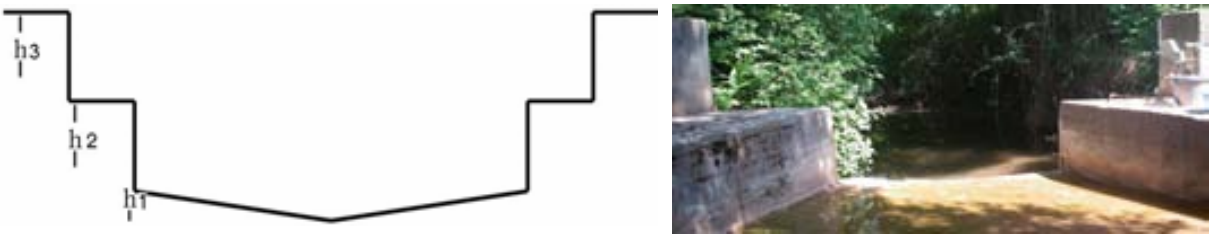

Figure 4.13: Cross section of the Cal Rodó gauging station.

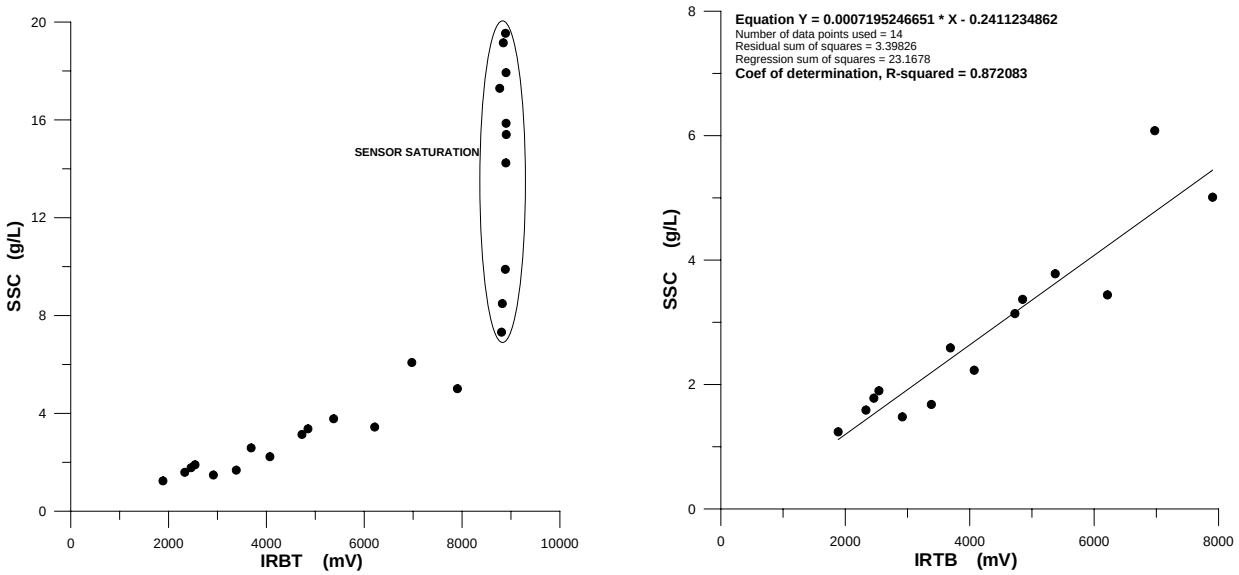

Figure 4.14: Infrared turbidity sensor calibration.

$$q_1 = 0.6 \times \frac{8}{15} \times \sqrt{2 \times 9.8} \times 20.09 \times \sqrt[5]{\frac{h_1}{1000}} \times 1000 \tag{4.8}$$

$$q_2 = 0.49 \times 1.785 \times \frac{h_2}{1000} \times \sqrt{2 \times 9.8 \times \frac{h_2}{1000}} \times 1000 \tag{4.9}$$

$$q_3 = 0.49 \times 3.585 \times \frac{h_3}{1000} \times \sqrt{2 \times 9.8 \times \frac{h_3}{1000}} \times 1000 \tag{4.10}$$

Infrared turbidity sensor Calibration of infrared turbidity (IR) sensor was done using data from a storm event occured on the 3rd of March 2001 (CR010301 where CR stands for Cal Rodó) and the numbers are the day/month/year), which had the best sampling representativeness among the 27 episodes studied. This calibration, was used for episodes without reliable samples or for events without samples, which makes impossible to define a storm-based relationship. The resulting calibration is called reference calibration for IR sensor. The use of the reference calibration it is also justified by the use of same device (sensor) during the studied period (10 years) and it is assumed that no significant changes in land use have during that period of time.

In Fig. 4.14a, it is shown a scatter plot of samples versus IR sensor readings, it was identified 10 data points which are not reliable due to saturation of sensor. Hence, the calibration was done only with 14 data points, the best fit line was obtained by least squares method, which estimates the intercept a and slope b, the deviations around the regression line are assumed to be normally and independently distributed with a mean $\overline{x}$ of 0 and the standard deviation s that does not depend on the independent variable R (sensor readings). The best fit line is illustrated in Fig. 4.14b.

The equation which relates the SSC_{AS} and IR sensor readings was:

$$SSC_{IR} = -0.24112 + 0.000719 \times R \tag{4.11}$$

However, validity tests of the model are neccesary in order to determine if the conditions to apply

a regression are acomplished. For this, first an ANOVA for regression was done under the null hypothesis stated as MSER = MSEM. The ANOVA results have given significant, therefore, the null hypothesis is rejected. The MSER and MSEM were 23,168 and 0.283 respectively, F statistic was 81.8 with a probability of observing this statistic of p < 0.001, at an $\alpha = 0.05$. Therefore, MSER and MSEM are not equals and a significant variation on SSC_{IR} is explained by the regression model (Eq. 4.11) which r^2 was 0.87.

In addition, it was calculated the standard deviation and standard error of the mean $\overline{x}$ of the a and b coefficients. A t test was done (t = coeficient value/std. dev.) under the null hypotheses stated as, $a = 0$ and $b = 0$. The parameters of the test were: for the intercept (a = -0.241), the typical error was 0.366 and std. dev. was 1.369. The t test for intercept has shown that the intercept is not significantly different from zero (p = 0.52, $\alpha = 0.05$); for slope: $b = 0.0007$, typical error = 7.995×10^{-5} and $s = 0.0003$, for slope, the t test has shown that b is significantly different from zero ($p < 0.001$, $\alpha = 0.05$) therefore, the null hypothesis that $b = 0$ is rejected. The intercept might take values of zero, which is not relevant in order to use a linear model is that the slope b can not be zero, therefore Eq. 4.11 can be used to perform sediment load estimations.

Residual analysis of estimates was done, in order to determine whether the residuals follow a Normal Distribution or not, which is another assumption of the model to be accomplished, in order to use it. A Kolmogorov-Smirnov (K-S) test for 1 sample was used, which gave no significant (p = 0.635, $\alpha = 0.05$), then null hypothesis stated as residuals follow a Normal Distribution ($\overline{x} = 0$, $s = 0.511$) is accepted.

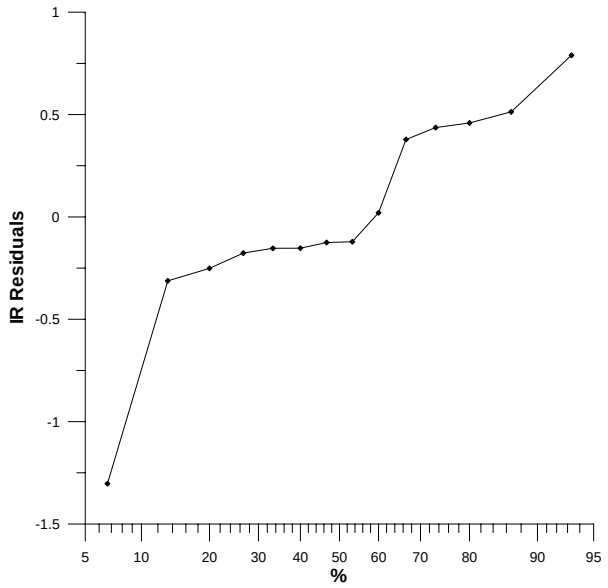

Figure 4.15: Cumulative probability of residuals from IR calibration.

An alternative procedure to conduct a normality test for residuals, is plotting the residuals (on the y axis) sorted in ascending order against its corresponding cumulative frequency expressed in % (on the x axis) in a normal probability scale; the relationship between these two should be linear if it follows a Normal Distribution. As it is shown in Fig. 4.15 the relationship follows a linear pattern, therefore, residuals follow a Normal Distribution (mean = 0, std. dev. = 1).

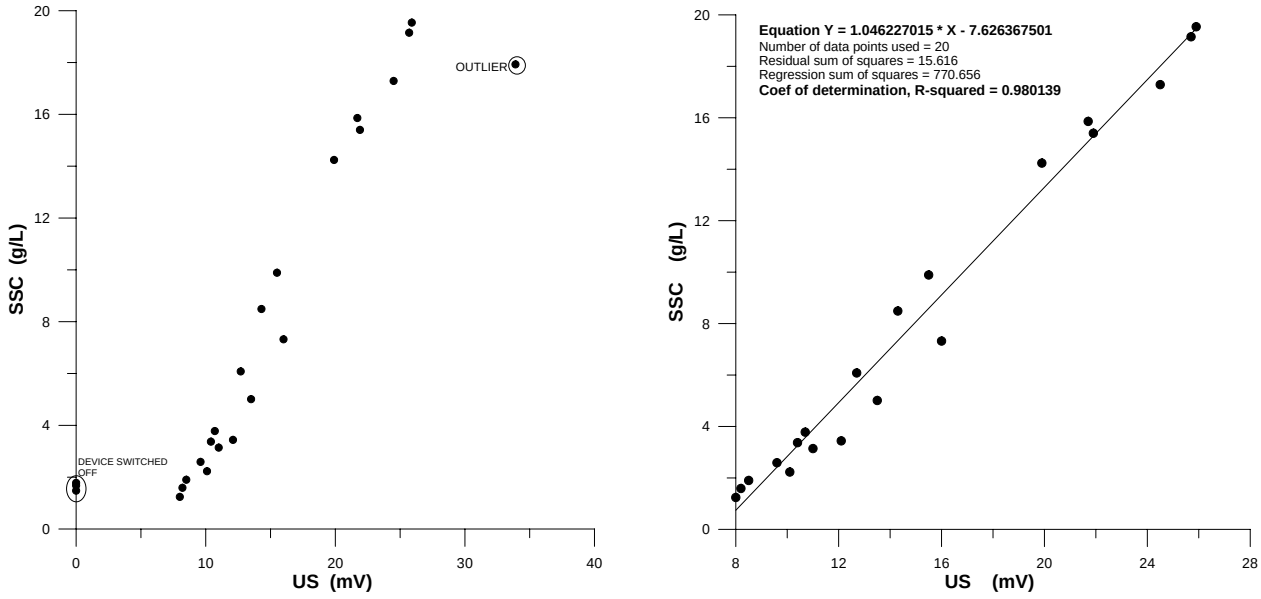

Figure 4.16: Ultrasound sensor calibration

Ultrasound sensor The procedure to set a calibration between ultrasound sensor readings and discrete samples was similar to the calibration procedure followed for infrared sensor, and also data from event CR010301 were used. The scattered plot of samples against US readings allowed to identify 1 outlier and 3 not valid data points, which are located at lower left cluster on Fig. 4.16a.

Linear regression was performed using 20 valid data points (Fig. 4.16b). An ANOVA for regression was done in order to determine if the linear regression model was suitable (null hypothesis: MSEM = MSER); the results were: MSEM = 770.6 and MSER = 0.868, F statistic = 888.3 with a probability of observing this value of $p < 0.001$, $\alpha = 0.05$, this is statistically significant hence, the null hypothesis is rejected. The calibration for ultrasound sensor is shown in Eq. 4.12 and which had a r^2 of 0.98.

$$SSC_{US} = -7.6263 + 1.0462 \times R \tag{4.12}$$

Error analysis of parameters a and b, has shown the following values intercept a = -7.626, typical error of intercept was 0.567, its std. dev. was 2.536; the t test for intercept was statistically significant ($p < 0.001$, $\alpha = 0.05$) thus, null hypothesis was rejected; for slope (b = 1.046), the typical error was 0.035 and std. dev. 0.156, the null hypothesis that $b = 0$, is rejected because $p < 0.001$ at $\alpha = 0.05$. This analysis shows that calibration fits the data and the model is appropriate.

A normality test to analyse errors was done through K-S test for 1 sample in order to verify if the residuals follow a Normal Distribution (Fig. 4.16b). The results have shown that the distribution of residuals are normally distributed, with $\overline{x} = 0$ and $s = 0.906$ (p = 0.532, $\alpha = 0.05$). Moreover the cumulative frequency of residuals suggests, that residuals are also normally distributed, because they follow a linear pattern (Fig. 4.17).

Once regression models or calibrations for both, infrared and ultrasound sensors were established, suspended sediment concentration values were calculated. Then, sediment load was calculated by

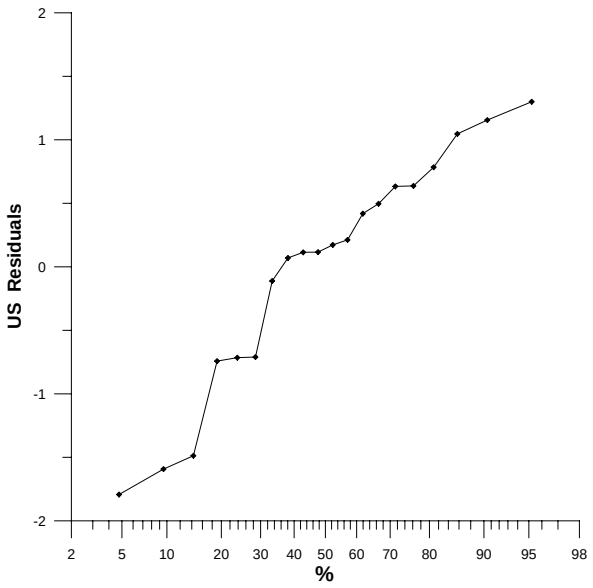

Figure 4.17: Cumulative probability of residuals from US calibration.

applying Eq. 4.5.

Suspended sediment load estimates through calibrations are done based on the assumption that samples are representative of the entire stream cross section area.

4.4.2 Criteria to choose reliable suspended sediment concentration

Sediment concentration for event CR010301 obtained by calibrations (Eq. 4.11 and 4.12) were significantly different for high concentration values. Infrared turbidimeter sensor provides reliable values up to 6 g/L, when it gets saturated. On the other hand, ultrasound sensor provides reliable results for a much wide range of concentration.

The obtained thresholds were used as reference to evaluate the calculated concentration for the remainder flood episodes. Summarizing, this can be expressed as:

$$SSC = \begin{cases} SSC_{IR} & \text{if } SSC \leq 6 \text{ g/L} \\ SSC_{US} & \text{if } SSC > 6 \text{ g/L} \end{cases}$$

4.4.3 Available data set

Suspended sediment dataset and other hydrological information for the study area was available from 1996 to 2005, and they were collected by the Surface Hydrology and Erosion Research Group from the Institute of Environmental Assessment and Water Research (IDAEA, CSIC), Spain.

Available information includes: continuous measurement of water stage in order to estimate discharge, and turbidity measurement and discrete water sampling in order to estimate suspended

sediment concentration. Other data, such as kinetic energy, rainfall intensity, runoff among other hydrological variables also exist and which are explained later. Turbidity sensor readings are available every 2 or 20 minutes (shifts depends on discharge).

Table 4.4: Selected flood events at Cal Rodó gauging station.

Date	Event code	Duration (h)	SSL raw approach (Mg)	Available sediment data
22/01/96	CR220196	144.2	1026.9	none
22/04/96	CR220496	198.0	281.3	samples, IR
14/10/96	CR141096	44.1	315.1	samples, US
11/11/96	CR111196	30.9	551.9	samples, US
04/06/97	CR040697	104.4	2494.3	Samples, US and IR
05/11/97	CR051197	83.8	49.2	US
17/12/97	CR171297	89.5	4534.7	Samples, US and IR
07/05/99	CR070599	80.4	106.8	samples, IR
28/08/99	CR280899	44.2	278.1	Samples, US and IR
14/09/99	CR140999	84.9	152.0	IR
19/09/99	CR190999	102.1	518.6	IR and US
12/11/99	CR121199	4.4	1138.3	IR and US
28/09/00	CR280900	51.6	348.7	IR and US
11/23/00	CR231100	31.7	385.3	Samples, US and IR
12/23/00	CR231200	30.4	1833.5	IR
01/03/01	CR010301	46.3	89.9	Samples, US and IR
18/08/01	CR180801	15.8	264.8	Samples, US and IR
20/10/01	CR201001	66.8	62.4	samples, IR and US
04/07/02	CR070402	71.1	1308.2	Samples, US and IR
10/04/02	CR100402	33.3	20.2	samples, IR and US
09/10/02	CR091002	64.4	133.5	samples, IR
02/28/03	CR280203	117.3	483.0	Samples, US and IR
10/31/03	CR311003	59.7	563.1	Samples, US and IR
04/12/03	CR041203	45.8	144.0	IR and US
31/03/04	CR310304	24.5	62.4	none
08/05/04	CR050804	24.5	737.9	Samples, US and IR
14/10/05	CR141005	25.3	1785.9	samples, IR and US

The twenty seven biggest flood events measured at Cal Rodó station that occurred between 1996 - 2005 were analized. These events constitute approximately 80% (from a very first raw approach) of the total sediment transport during that period. Available data for each flood episode and a first raw approach of sediment transport are presented in Table 4.4. The duration of these storm events varies between less than one day (4.4 h) up to almost four days (198 h).

In Table 4.5 specific hydrological information for the selected events are shown, which will be used later to set correlations with sediment load estimates (last section of this Chapter).

Sediment load can be assessed at the annual, seasonal, monthly basis or other defined period of time. For this study, it was done on the annual and seasonal basis. Annual basis means that all events occured within a given year are treated as one set; seasonal basis refers to seasonal grouping of all episodes. The seasonal classification, was done using the clasification for temperate and polar regions (Northern Himesphere): spring (21st of March - 20th of June), summer (21st of June - 20th

Table 4.5: Hydrological features of selected events in Cal Rodó catchment.

Event name	Precipitation (mm)	Rainfall intensity (mm/h)	Runoff (mm)	Peak of Q (L/s)	Total kinetic energy ($J/m^2/h$)	Max.kinetic energy ($J/m^2/h$)
CR010301	41.9	9.6	6.1	610.4	746.4	196.4
CR220196	115.9	16.9	146.9	9574.3	2135.6	384.2
CR220496	51.5	21.9	16.4	1589.4	975.9	516.4
CR141096	74.7	16.9	14.0	697.8	1393.8	382.8
CR111196	90.9	14.5	27.7	2253.4	1675.2	319.5
CR040697	105.0	65.6	37.6	6994.1	2396.8	1823
CR051197	51.9	29.4	2.9	321.5	894.6	727.2
CR171297	135.1	16.9	113.8	7588.9	2440.5	382.8
CR070599	30.1	30.0	8.3	636.4	604.7	743.2
CR280899	47.5	88.0	6.7	4536.9	1245.6	2542.3
CR140999	57.1	26.8	14.3	1115.8	1115.2	654.4
CR190999	54.6	12.0	32.2	3438.5	1056.9	257.4
CR121199	29.9	26.7	11.5	6804.0	2612.4	2612.4
CR280900	63.4	32.0	7.2	550.6	1335.5	802.4
CR231100	42.3	9.6	8.6	939.0	734.6	196.4
CR231200	89.4	12.0	34.1	3089.9	1577.2	255.8
CR180801	36.5	57.8	1.0	957.9	946.8	1577.9
CR201001	51.6	29.6	4.7	484.0	997.6	731.8
CR070402	58.6	16.9	34.5	2967.5	1099.8	383.8
CR100402	53.9	12.0	19.2	1168.5	938.8	256,8
CR091002	69.5	19.4	17.9	1444.9	1253.3	449,2
CR280203	69.5	9.6	39.2	3491.5	1186.6	196.3
CR311003	44.9	9.5	20.5	1905.7	758.8	196.3
CR041203	54.6	7.2	22.1	2233.5	908.2	139.3
CR310304	82.2	14.1	17.6	1718.3	1373.4	309.7
CR050804	55.5	65.5	11.2	3750.0	1347.0	1819.1
CR141005	59.9	39.6	25.0	5834.4	1304.0	1022.7

of September), autumn (21st of September - 20th of December), and winter (21st of December - 20th of March).

4.4.4 Steps for sediment load and error assessment

In order to estimate the average SSL and its confidence interval the following sequential steps were performed:

- plotting the suspended sediment concentration obtained through calibrations of both sensors and samples on axis y_1 against time (in hours) in axis x; and a second y_2 axis was added for discharge.
- checking the concentration plots in order to identify reliable segments and prune unreliable segments within the curves. Readings given by devices were analyzed in order to detect

abnormal readings (e.g. sensor malfunctions, clogged periods, ephemeral foulings) which are faulty information.

- treatment and estimation of *missing* data by performing linear interpolations between reliable data points or segments (observed on a plot).
- recalibrating sensor readings by using event based samples when necessary.
- making interpolations between valid sections and data points identified previously when necessary.
- assessment the SSL obtained by sensor's calibrations for the whole set of events.
- definition of confidence intervals of estimates by sensor calibrations using Monte Carlo simulations.
- estimation of SSL and its confidence intervals for individual storm events by using annual and seasonal sediment rating curves.
- assessment of confidence intervals of estimates by sediment rating curves using Monte Carlo simulations.

4.4.5 Suspended sediment load from calibration of turbidity sensors

Sediment load calculations, which are made based on empirical data (explained in Section 4.4.1.1) may have large uncertainties associated to measurement and interpretations. These uncertainties should be assessed in order to provide sound results, with a probability that a specific sediment load estimate can be observed within a confidence interval.

4.4.5.1 Confidence intervals for sensors

Since the sediment load is estimated by multipliying the concentration by other variables, such as discharge and time step (dt) which vary unsystematically, the error transmision formulas are impractical to define the range of errors. For this reason, the range of errors can be estimated by modelling the regression residuals within Monte Carlo simulation.

$$e = SSC_{predicted} - SSC_{observed} = a + b \times R - SSC_{observed} \tag{4.13}$$

The first step is the calculation of residuals, or the differences between the SSC observed and simulated (Eq. 4.13). The next step is the analyses of the distribution function of these residuals, specifically, if they are normally distributed and also if they are independent on the independent variable (sensor readings). The final step is the use the calculated concentration with the addition of the error simulated using an suitable random generator, that considers its distribution function (Eq. 4.14), in other words to every sediment concentration value, it is added an random error and this procedure is repeated for a large number of replications. In Eq. 4.14, SSL is sediment load, SSC is suspended sediment concentration, Q is discharge, e is the error term added to every SSC, and i refers to time step between sensor's readings.

$$SSL = \sum_{i=1}^{t} (SSC_i + e_{iSCC}) \times Q_i \times dt \tag{4.14}$$

In order to do faster such replications and define the confidence interval, it has been developed a program (code made in BASIC) named *sederror* (Gallart, 2006).

In Table 4.6 are shown the input variables and parameters required to run *sederror*. In the first row (head of the script) it has been written the following variables: number of observations or rows (NLINS), average discharge (AVG Q), standard deviation in logarithmic scale of residuals of discharge (SDEV Ln Q), standard deviation in logarithmic scale of residuals of infrared turbidity sensor (SDEV Ln TB) and standard deviation in logarithmic scale of residuals of ultrasound turbidity sensor (SDEV Ln US); in the following rows are written: number of row, time step dt (s), discharge Q (L/s), infrared turbidity sensor readings IR (g/L) and ultrasound turbidity sensor readings US (g/L). Once these inputs are fullfilled it was run *sederror*.

In *sederror*, it was assumed as the standard deviation of discharge (SDEV ln Q) 10% of the total variation. However in order to define the extent to which the variability of discharge affects the sediment load for an individual event a test was performed considering two scenarios: (a) (SDEV ln Q as null and (b) as 10%). This test was done only for CR010301, for the rest of the events it was taken as SDEV ln Q equal to 10%, because it would be unrealistic to assume that there is no variability in discharge measurements.

Table 4.6: Input parameters to run *sederror*.

	Q	SSC	Input parameters
variability	yes	yes	Number of rows (NLINS)
			Standard deviation Ln Q (SDEV Ln Q)
			Standard deviation Ln Infrarred Sensor (TB)
			Standard deviation Ln Ultra sound sensor (US)
	no	yes	All the above but SDEV Ln Q = 0

With *sederror*, m replicates are obtained (in this case $m = 1000$), which means having m sediment load estimates. A scheme of the procedure used to run *sederror* is presented in Fig. 4.18. Then, in order to define the confidence interval the m sediment load estimates, these values (1000) are sorted from the lowest to the highest, in order to identify the bounds, such as the 5% and 95% percentiles.

4.4.6 Suspended sediment load from sediment rating curves

The equation which describes the relationship between discharge and sediment concentration are called sediment rating curves. These curves have been used over the last 30 years, because of its usefulness in absence of frequent event-based discrete samples. These relationships are developed for a specific site, and seldom are used in other sites (extrapolation).

The most common type of sediment rating curve is a power function between discharge as the independent variable and concentration as the dependent variable (Walling, 1974). This curve is

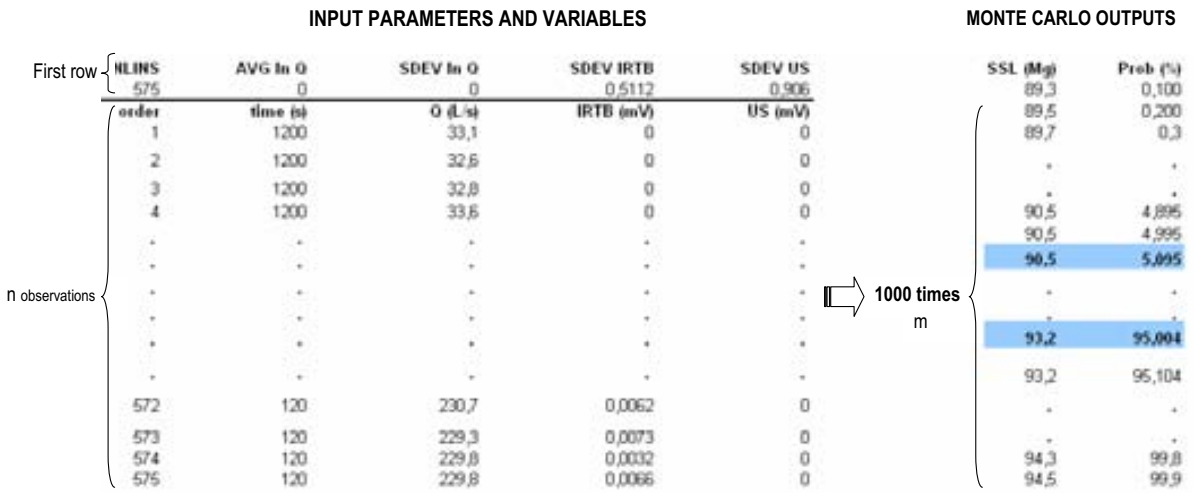

Figure 4.18: Scheme of inputs and outputs to estimate SSL confidence intervals with Monte Carlo procedure.

very useful when turbidity sensors are not available or when there are no samples for the event being studied, in these cases a sediment rating curve developed utilizing data of previous episodes can be used.

The power function can be formulated either as a linear (Eq. 4.15) or non-linear (Eq. 4.16) models. A linear model is the one in which the parameters intercept a and slope b to be estimated, appear linearly in the model and a non-linear model is the one in which at least one of the parameters appear non-linearly in the model (Crawford, 1991) which fit typically in a power function.

$$SSC = a + b \times Q + \epsilon_i \tag{4.15}$$

$$SSC = a \times Q^b \times 10^{\epsilon_i} \tag{4.16}$$

In the non-linear case, there are several methods to determine the parameters a and b (Phillips *et al.*, 1999) the most common is the formulation of the power function as linear model, to do so, it is required a logarithmic transformation (Eq. 4.17), in order to linearize the function and a subsequent correction for transformation bias (Crawford, 1991) is applied. The retransformation bias is well documented e.g. (Ferguson, 1986);(Walling, 1988);(Jansson, 1996), this is due a problem of distributional assumptions of the model. In order to estimate the untransformed "true" estimate some authors e.g. Duan (1983) proposed a method to compensate this bias called *smearing estimator*, which is a non-parametric estimator, this is shown in Eq. 4.18 and where s is the standard deviation of residuals in the logarithimic domain. The *smearing estimator* requires the assumption that residuals are homocedastic (variance is fixed throughout a distribution) and independent.

The linear models (Eq. 4.15) are less common because a and b must be obtained by iterative methods which do not always converge to a solution and its residual errors typically are not identically distributed throughout the range of streamflow values (Crawford, 1991).

$$log\ SSC = log\ a + b \times log\ Q + \epsilon_i \tag{4.17}$$

Generally sediment concentration increases with discharge, where the exponent b (Eq. 4.16) takes usually values higher than the unity. The relation between concentration and discharge in the logarithmic scale, as it is shown in Fig. 4.19b is linear and its residuals (error term ϵ_i in Eq. 4.17) are additive and assumed as log-normally distributed, however in the arithmetic scale residuals are multiplicative (absolute errors are directly proportional to sediment concentration along the rating curve) as are shown in Eq. 4.16.

In the linear model, the use of log transformates of the relationship sediment concentration - discharge, means an underestimation of the sediment load due to the non-linearity of the relationship called a "retransformation bias" (from log scale to arithmetic scale) which is well documented e.g. Duan (1983); Ferguson (1986); Crowder *et al.* (2007) and correction factors were proposed e.g. the smearing estimator m (Duan, 1983) which is estimated through Eq. 4.18 (where s is the standard deviation of the log-transformed residuals); however, correction factors, are not needed when SSL is estimated using simulated residuals (e.g. using Monte Carlo procedure) because the systematic underestimation in the non-linear equation is compensated by a random modelling of residuals.

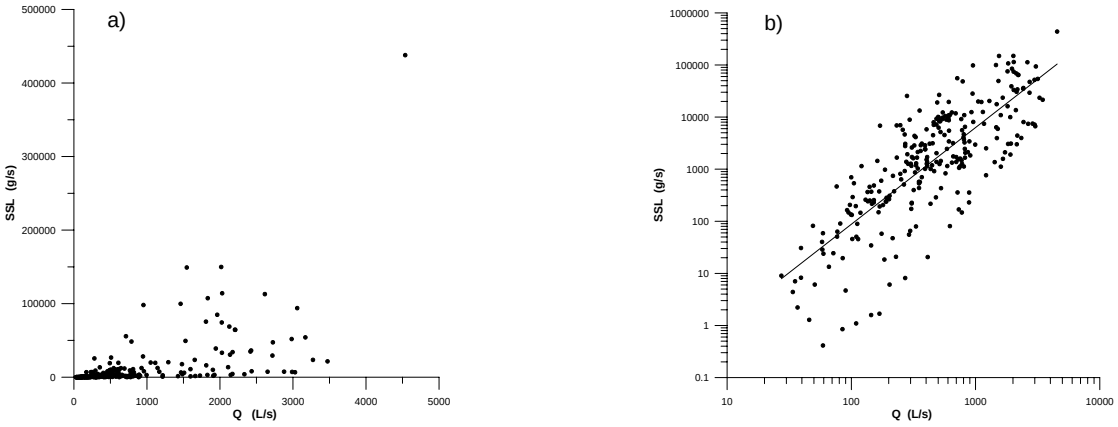

Figure 4.19: Suspended sediment load vs. discharge (annual basis): (a) real units, (b) Log scale.

In order to illustrate and compare the sediment load estimates obtained by log transformates (common SRC) of the concentration - discharge relationship (involving bias correction), a stochastic approach, which consists of modelling the distribution function of the residuals gathered from the common SRC, and data pertaining to 27 storm episodes was used.

Annual and seasonal sediment rating curves were developed using samples collected from 19 flood events, although the total events studied are 27, 8 events did not have samples. The annual basis of the sample set was comprised of 270 samples. For the seasonal basis, two sets were defined: summer and "rest of seasons" (all the seasons but summer).

Hence, three sediment rating curves were defined one for each of the following data sets: annual, summer and for the rest of the seasons". Out of the total 19 events, 16 events (245 samples) belong to the category "rest of seasons" and only 3 events to summer (25 samples).

$$m = e^{s^2/2} \tag{4.18}$$

In principle, annual rating curves were developed using the whole data set. A plot of the relationship between concentration and discharge is presented in Fig. 4.19a, where the majority of the data points are in the lower left and as discharge increases the plot is more scattered, also, at the upper right part of the curve, the largest observed value is not an outlier, since that sample was taken close to the peak of discharge of one the events with high discharge. In the logarithmic scale (Fig. 4.19b), the data points are distributed in a linear relationship. Residuals were tested under the null hypothesis that residuals follow a normal distribution, with the K-S test, results of this test were: Z = 1.22, p = 0.10 and $\alpha = 0.05$ as $p > \alpha$, hence it is failed to rejected the null hypothesis, the mean of residuals and standard deviation were: $\overline{x} = 0.0018$ and $s = 1.55$. Therefore, the logarithmic transformed model obtained using the whole set samples is valid to assess suspended sediment concentrations.

In addition, in order to determine if splitting the whole set of samples according to the season when they have been collected reduces or not the annual variability, a test was performed. The samples were divided into two groups: summer and "rest of seasons". Autumn, winter and spring were grouped in "rest of seasons" because in a previous study using 13 events included in the group of 27 was demonstrated that there was no difference on splitting and setting an equation for each of these seasons. The test was done by performing an ANOVA under the null hypothesis: the standard deviation of the annual regression is not reduced (one equation is better than two). Results of ANOVA test are given in Table 4.7, according to this the null hypothesis is rejected ($p < \alpha$), since F = 4.83, p = 0.04 and $\alpha = 0.05$, which means that performing two equations: one for summer and another for "rest of seasons", explain better the variability.

Table 4.7: ANOVA for annual sediment rating curve.

Source of variation	Degree of freedom	Sum square	Mean square	F_{value}	$F_{0.05}$
Model	1	3.90E+10	3.90E+10	4.83[a]	4.28
Error	23	1.85E+11	8.06E+09		
Total	24	2.24E+11	-		

[a]Significantly different at a 0.05 percent level of significance

In Fig. 4.20a the scattering of samples collected during "rest of seasons" is illustrated. It shows a distribution of data points similar to the annual fit, and in the logarithmic scale (Fig. 4.20b) data points follow a linear trend. Using these samples, a regression was developed. An ANOVA test indicates that the obtained regression is significant (Z = 1.33, p = 0.6 and $\alpha = 0.05$). A summary of regression parameters are given in Table 4.8. In addition a residual analyses using K-S test was performed, and it has demonstrated that residuals are normally distributed, so residuals can be easily simulated (useful for uncertainty analyses).

Finally, an equation was performed using samples from events occurred during summer. The scatter plot (Fig. 4.21b) shows that, most of the data points are located far above or below the regression line, as they are not outliers they can not be removed from the plot. ANOVA test indicated that the regression is significant. Regression parameters are summarized in Table 4.8. K-S test of residuals has shown that residuals are normally distributed (Z = 0.29, p = 0.29 and $\alpha = 0.05$).

The large scatter of data points can be explained in part by the hysteresis between concentration and discharge at a event scale (Walling, 1974), seasonal variation, inaccuracies in flow and sediment measurements, and variability in the washload (Julien, 1998). The events studied presented hysteresis with different shapes, in Fig. 4.22 are shown some of these loops at event scale, the

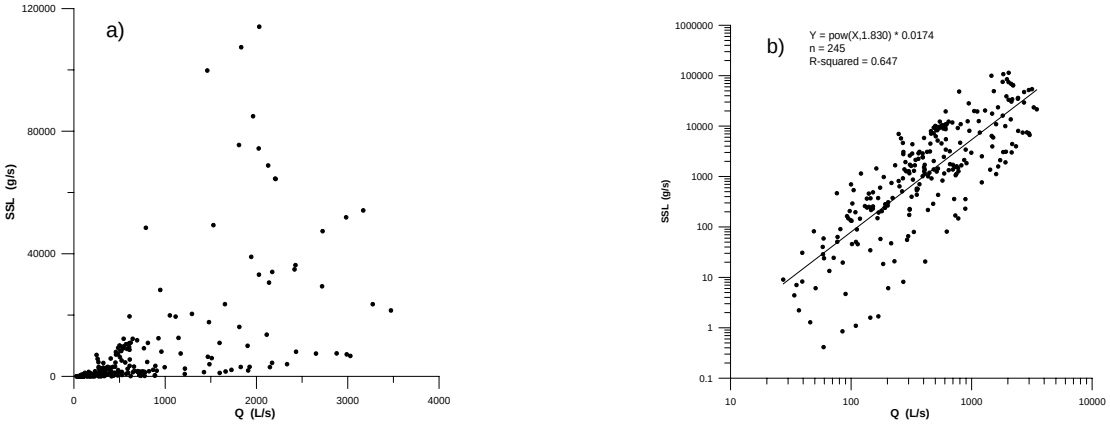

Figure 4.20: Suspended sediment load vs. discharge for rest of seasons : (a) real units, (b) Log scale.

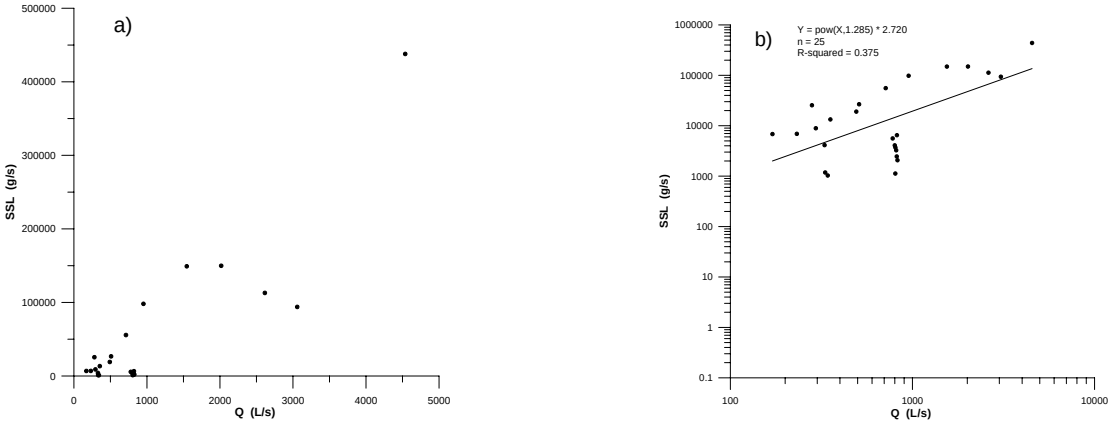

Figure 4.21: Suspended sediment load vs. discharge for summer: (a) real units, (b) Log scale.

majority of the loops are clockwise e.g. (a) to (b), a number of them are anticlockwise, such as (e) and (f), and less common are the ones with an eight loose shape e.g. (g) and (h).

The ratio between concentration and discharge in a clockwise hysteresis is greater in the rising limb of the hydrograph than for the falling limb. The clockwise loops for an individual episode are attributed to sediment depletion before the discharge peak was reached (Williams, 1989). In a previous research in the same study area, it was found that concentration peak, usually preceded discharge and it was reported that the saturation mechanisms are responsible for the main floods, which transport most of the sediments, nevertheless, intense rainstorms during summer which have low discharge can produce an active erosion in the degraded areas (Soler *et al.*, 2005).

Attempts to explain the magnitude of parameters of the power function a and b exist. Despite the intercept and slope do not have any physical meaning, they can be used to make interpretations, such as a high ln a values indicate intensively weathered materials (Asselman, 2000), therefore available to be transported. On the other hand b is interpreted as the erosive power of the river (Asselman, 2000). A progressive reduction in ln a values and increases in b, results in a reduction of sediment load (Yang *et al.*, 2007), according to these findings the pair of parameters (ln a and b) for summer and rest of the seasons (1.00;1.28 and -4.05; 1.83 respectively) indicate, that there is more sediment readily transportable in summer than in the rest of seasons, because of a reduction

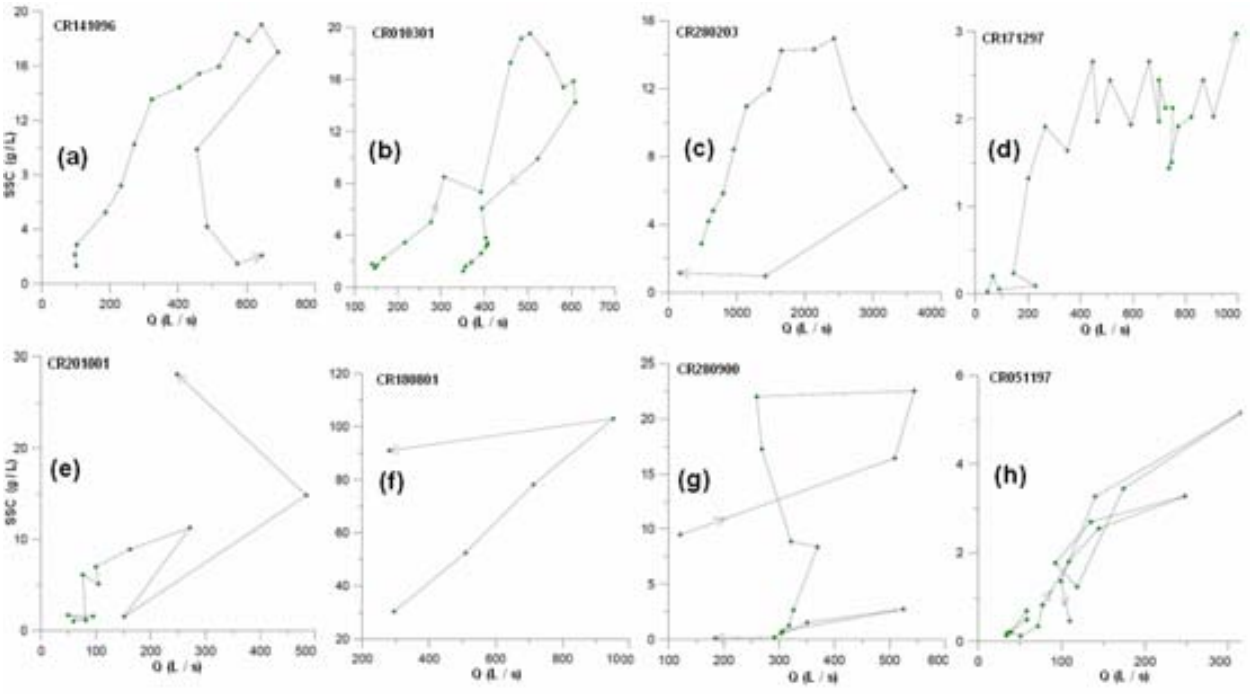

Figure 4.22: Types of hysteresis loops.

of ln a and increases in b. This process can be linked to badlands weathering and flashy discharges occurred during summer.

A summary of statistical parameters for all the three regressions (annual, rest of seasons, and summer) are shown in Table 4.8, also it is presented the r^2 which represents the goodness of fit in logarithmic scale for both variables; in addition, the smearing estimator m for each sediment rating curve is presented and which were estimated through Eq. 4.18.

The conventional sediment rating curve pointed out so far, is developed from the logarithmic transformation of concentration and discharge based on the assumed lognormality of the residuals and the assumed homogeneity of variance under the logarithmic transformation. Despite the bias correction, the load estimates are only a close approximation to the "true" load and considering its assumptions a more detailed analysis of residuals would be necessary.

Table 4.8: Summary of the regression parameters.

Type SRC	a	ln a	b	r^2	$\overline{x}$ residuals	s residuals	smearing estimator
Annual	0.0169	-4.077	1.857	0.63	0.0018	1.551	3.32
Rest of seasons	1.017	0.017	1.830	0.65	0.0000	1.500	3.08
Summer	2.7210	1.001	1.285	0.38	0.0000	1.376	2.57

4.4.6.1 Confidence intervals using sediment rating curves (SRC)

The constituents of a power sediment rating curve are the constant a, exponent b, and discharge; by using these it is aimed to characterize the sediment load for an event, or a series of events.

However, these constituents are subject to sources of uncertainty i.e. errors of measurement, this uncertainty imposes a restrictions; therefore, an evaluation of the confidence in the regression model is necessary. The outputs (e.g. suspended sediment load) given by the model should be bounded by a level of uncertainty with a specified level of confidence.

The confidence intervals can be assessed by modelling the residuals using Monte Carlo procedures; two approaches were studied, in the first attempt (using 13 out of the 27 events) the sediment load confidence intervals have been estimated by modelling a relatively large number of these estimates adding an error (drawn from log-normal distribution) ϵ_i to every sediment concentration estimate (SSC_i) for every time step of Q_i. The sediment load for a given event (SSL_j) is obtained by Eq. 4.19.

$$SSL_j = \sum_{t=1}^{t} Q_i \times (SSC_i \times e^{\epsilon_{ij}}) \times dt \tag{4.19}$$

Nevertheless, results using the first approach (Eq. 4.19) have shown, that the confidence intervals were narrower than expected, because the large errors obtained for every single SSC_i from SRC are considered as random, so they are compensated by the large number of readings (usually 50 to 100 times the number of samples) when the SSL_j or series of events. In addition, the sediment load obtained from Eq. 4.19 were significantly different from the results obtained with sensors (Eq. 4.14), since estimations obtained through sensors are below or above the confidence interval using this first approach.

A second approach was tested making a more detailed analysis of the residuals of the SRC, it was done by computing the residuals for every one of the events (j) and then analyse if the assumption of the independence of the events may be accepted or has to be refuted. This means testing if the residuals taking into account the events are significantly smaller than the residuals, if the events are not taken into account. This relationship is shown in Eq. 4.20, where s_t^2 is the total variance of residuals in logarithmic domain without partitioning into its components, s_j^2 is the variance attributed to events and s_i^2 is the variance related to the effects of samples within events.

$$s_t^2 = s_j^2 + s_i^2 \tag{4.20}$$

Using techniques such as the ordinary least squares, it is assumed that the error term ϵ_i has a constant variance along the best-fit curve and this would be true if the ϵ_i are assumed to be drawn from identical distribution, if this assumption is violated there is a heteroscedasticity case, which means the error term could vary with each event or the events are not independent. To test this hypothesis (H_o: events are independent), a F - test was made using 270 samples (from 19 events), results have shown a highly significant differences between events (F = 15.3, $p < 0.001$). ANOVA results are shown in Table 4.9, and it has indicated that the variability among events has to be the taken into account. This means that when using the SRC for events without or with insufficient number of samples it is necessary to estimate both the variability within each event and among events.

However as an alternative, it was possible to use a unique SRC and to consider that every one of the events have a mean positive or negative deviation (i.e. bigger or smaller than the unity in the

Table 4.9: ANOVA test if diverse (19) events are different.

Source of variation	Degree of freedom	Sum square	Mean square	F_{value}	$F_{0.05}$
Model	18.0	357.8	19.9	15.3[a]	1.65
Error	225.0	291.7	1.3		
Total	243.0	649.5	2.7		

[a]Significantly different at a 0.05 percent level of significance

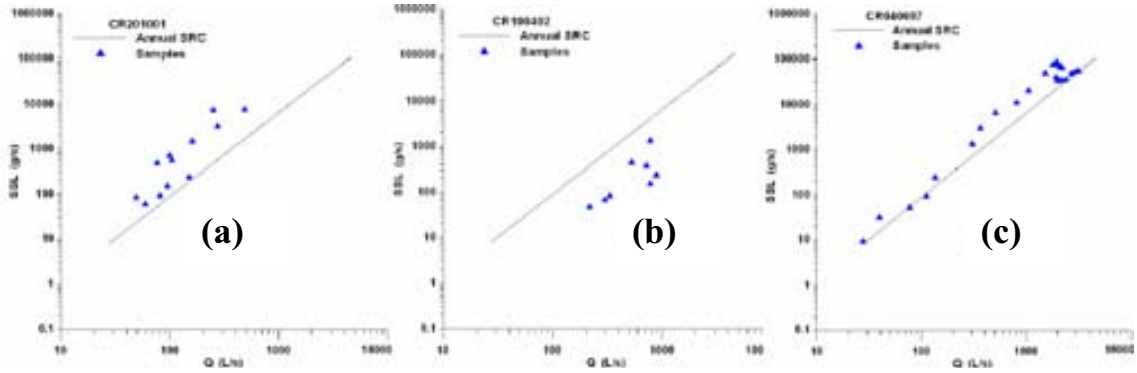

Figure 4.23: Position of samples in regard to best fit line: a) above, b) below, c) close to fit.

physical values) from the common SRC, for example see Fig 4.23, where the data points fan out from the straight line, which suggest heteroscedasticity of the errors. In Table 4.10 are presented the mean and standard deviation of residuals of events (19) with samples, it clearly shows that the distribution of events along the best fit line (most of them) are spread out either above (Fig 4.23a), below (Fig 4.23b) or near the fit line (Fig 4.23c).

Table 4.10: Statistical parameters of residuals (logarithmic scale) for events used in SRC.

Event	Mean	Std. deviation	Event	Mean	Std. deviation
CR220496	3.376	1.743	CR010301	-0.381	0.559
CR141096	-1.026	0.800	CR201001	-1.434	0.794
CR111196	0.422	1.021	CR070402	2.230	0.494
CR040697	-0.639	0.501	CR091002	0.383	0.922
CR051197	-0.114	0.738	CR100402	2.198	0.719
CR171297	1.014	0.789	CR280203	0.144	0.703
CR070599	-0.614	1.270	CR311003	-0.546	0.802
CR280899	-1.194	0.909	CR050804	-0.748	1.419
CR280900	-0.148	1.674	CR180801	-2.984	0.463

In order to find a solution to approach two, a Monte Carlo simulation designed to obtain the distribution function of sediment load estimates is done considering individually, the errors caused by the events ϵ_j and the errors caused by the samples ϵ_i within the events. A large number of events are modelled (1000), for everyone of them, an event error ϵ_j and an error due to samples ϵ_i, and for every time step dt are considered. By doing so, the event errors ϵ_j are directly transmitted to the distribution function, whereas the samples errors ϵ_i are averaged in the cumulating process. Therefore, the confidence intervals depend mainly on the event error (ϵ_j), while on the contrary

the median value is affected by the non-linear averaging effect related to the sample error (ϵ_i).

To perform a Monte Carlo simulation for SSL estimates including ϵ_j and ϵ_i separately, two logic steps were necessary. Firstly, for every SSL_j estimate the mean error for the event ϵ_j is simulated; this mean error is drawn from a log-normal distribution considering all events which have $\overline{x} = 0$ and s_j. Secondly, for every time step it is computed the SSC_i and simulate the sample error ϵ_i as a deviate from the mean of residuals of the event, ϵ_i is drawn from a log-normal distribution of the event with $\overline{x} = 0$ and s_i. The value of the SSL simulated for everyone of the j simulated events are estimated by the means of Eq. 4.21, unlike the results obtained from Eq. 4.19 the errors are taken separately.

$$SSL_j = e^{\epsilon_j} \sum_{t=1}^{t} (Q_i \times SSC_i) \times e^{\epsilon_i}) \times dt \tag{4.21}$$

The SSC_i component of Eq. 4.21 is obtained from the power function (conventional SRC). For consistency, as the number of events is relatively small and its standard deviation might be obtained with some error, it is better to calculate a standard deviation for the whole set of residuals (s_t) from the SRC (logarithmic domain) and the standard deviation of the samples (s_i) from the mean deviation of the events (the standard deviation of samples is a weighted average, which means the standard deviation of residuals of each event is multiplied by the number of samples and then divided by total number of samples of all events), here the unknown parameter is the standard deviation of events s_j and this can be estimated from Eq. 4.22 which is a derivative of Eq. 4.20.

$$s_j = \sqrt{s_t^2 - s_i^2} \tag{4.22}$$

Results of standard deviations of errors for events s_j, and samples s_i, are presented in Table 4.11; these values along with the constant a, exponent b, time step dt, and discharge q_i are used in Monte Carlo simulation to obtain a distribution function of sediment load for every event (SSL_j).

In Fig 4.24, it is shown a diagram of inputs and outputs of Monte Carlo procedure, which consists of a code (made in BASIC and named *sedcuesq*). The uncertainty rises, not only due to SSC term from Eq. 4.14, but also due to Q. To tackle the error due to Q, it was used a 10% of the total variability as its standard deviation. The variables and parameters used to run *sedcuesq* are: in the first row are written the number of observations (number of time steps or NLINS), standard deviation of discharge errors (SDEV%Q), constant a, and exponent b from the SRC, the standard deviation of errors due to the events s_j, and the standard deviation of errors due to the samples within every event s_i. From row two on, the duration dt, discharge q_i are written.

Table 4.11: Standard deviations of error for sediment rating curves.

Scale of SRC	Total (s_t)	Event (s_j)	Samples (s_i)
Annual	1.551	1.148	1.042
Summer	1.500	0.707	1.180
Rest of seasons	1.376	1.093	1.027

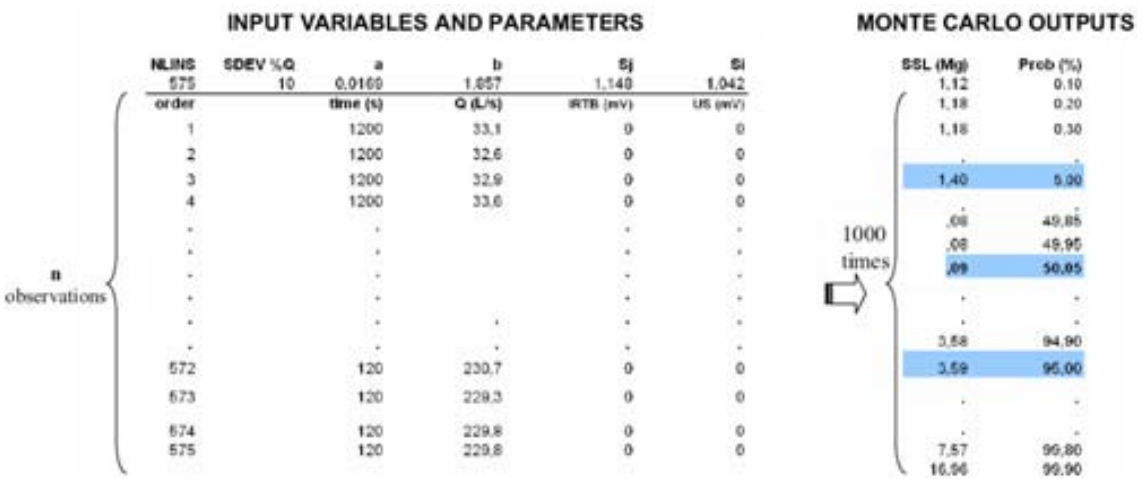

Figure 4.24: Scheme of the inputs and outputs of *sederror*.

In order to find the confidence intervals of the SSL_j estimate for every event, a 90% of confidence level is used; the output (sediment load) given by *sedcuesq* are sorted from the lowest to the highest, the values corresponding to the 5% and 95% percentiles are chosen as the lower and upper bounds of the confidence interval, in addition, the value corresponding to the 50% (the median) is chosen as the average SSL_j.

4.5 Results

4.5.1 Suspended sediment load and error ranges at event scale

In this section a description of suspended load assessment by the means of sensors calibrations and sediment rating curves, are presented for the selected 27 flood events. In an attempt to provide a detailed explanaition of the methodologies and procedures followed in order to estimate the average sediment load for each event and their corresponding confidence intervals, it has been selected one event. The selected event was CR010301, which had the best spanning of samples along the hydrograph. Same procedure was followed for the remaining 26 events.

4.5.1.1 CR010301

Available dataset for this event which occurred between the 1st and 3rd of March 2001 (duration 26.3 h) are, a set of 575 observations (sensors readings) taken every 2 or 20 minutes (shift according to Q) as a time step, and a set comprised of 24 discrete samples.

Sediment load from sensor readings Samples are well distributed along the hydrograph, as it is shown in Fig. (4.25). The IR and US sensors have functioned correctly most of the time. Using calibrations established previously (Eq. 4.11 and 4.12) for both sensors and choosing, and combining their reliable concentrations from the curve (Fig. 4.25), and by the means of Eq. (4.5)

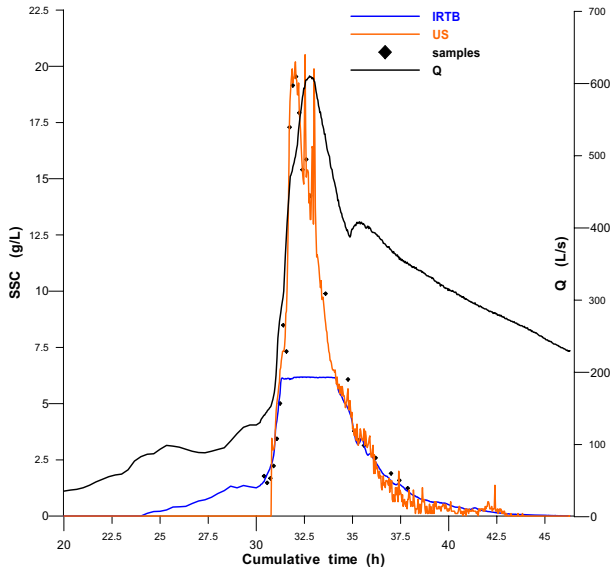

Figure 4.25: Sediment concentration and discharge for event CR010301, plotted as a function of time.

the total sediment load for this event using sensor calibrations was 92 Mg.

Out of the 92 Mg the amount of sediment load estimated by IR was 18 Mg (19.6%) which was obtained through equation (Eq. 4.11), the period of time when concentrations given by infrared sensor are reliable occurred between hours 24.0 and 34.7 after the flood event started, during these points in time, the concentrations were 0.0011 g/L and 34.7 g/L respectively, then the IR sensor was saturated (high SSC) hence, data during that time was not reliable, and when concentration decreased the same sensor collected valid information again, which happened between hours 34.7 and the end of flood, the sediment concentrations at both points were 4.7 g/L and nearly zero respectively.

During the time when IR was saturated, information given by US sensor has been considered as correct, and it allowed to estimate 73.8 Mg (80.4%) out of the total 92 Mg. US sensor performed well between concentrations 7.3 g/L and to 20.2 g/L, and between 20.2 g/L and 5.4 g/L.

Confidence intervals for sensor readings The confidence interval for the sediment load estimate (92 Mg) using calibrations of sensors, was performed using the method described in Section 4.4.5.1. The procedure consists of modelling the distribution function of residuals (Figs. 4.14 and 4.16) and adding random errors to every SSC_i.

The standard deviations of residuals from calibrations of IR and US sensors were $s_{IR} = 0.511$, and $s_{US} = 0.906$ (Kolmogorov-Smirnov test gave non significant; therefore, residuals are normally distributed). These standard deviations jointly, with other parameters and variables shown in Fig. 4.18 were used in Monte Carlo simulation (*sederror*).

In order to quantify the uncertainty caused or added by using sensor calibrations, and to assess the wideness of the confidence interval, three likely conditions were tested. These tests were performed assuming whether each sensor has or not variability (s). These three tests were: (1) $s_{IR} = 0.511$

and $s_{US} = 0$ assuming no variation added by US sensor; (2) $s_{IR} = 0$ and $s_{US} = 0$ under the assumption that none of the sensor added variation; (3) finally the most likely scenario is that both sensors added uncertainty $s_{IR} = 0.5112$ and $s_{US} = 0.906$.

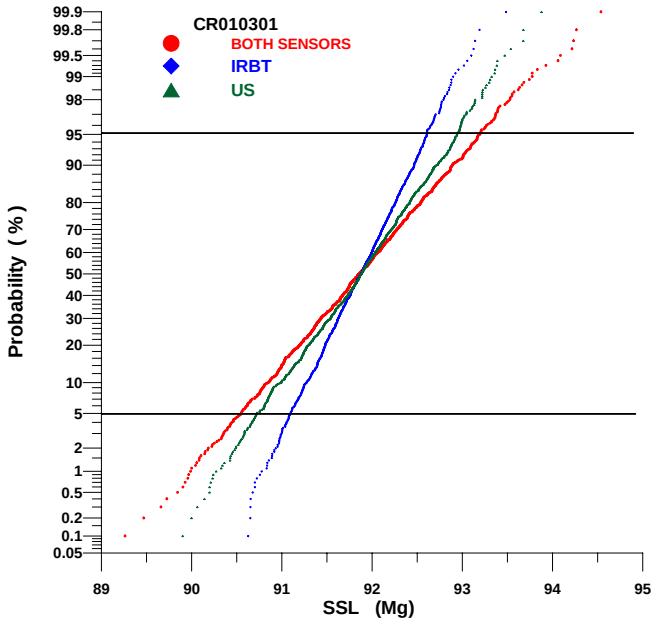

Figure 4.26: Confidence interval of sediment load for event CR010301.

In the first alternative, assuming the $s_{US} = 0$, the likely true SSL estimate is between 91.5 Mg and 92.6 Mg, where the difference is 1.2% (1.1 Mg); with the second alternative, if s_{IR} is zero the difference between both bounds is 2.2% (2 Mg), which means the variability added by IR sensor is lower than the variability added by US sensor. Finally, if both sensors added uncertainty, the range of confidence interval is wider than the assessed for the previous alternatives, this was 3% (2.7 Mg) with 90% of confidence. After verifying that both sensors added uncertainty the confidence interval estimated by using both standard deviations are assumed correct, and now it is known the range where the true SSL value lies. The range of confidence intervals for all of the three alternatives are show in Fig. 4.26 and a summary of lower and upper limits are presented in Table 4.12.

In addition, there is an error due to discharge, so far only the SSC term (from Eq. 4.5) was studied. It was assumed as standard deviation of discharge errors 10% of the discharge value. The confidence interval adding the variability of discharge was defined between 90.0 Mg and 93.7 Mg, with a difference of 4.1% (3.7 Mg). The average SSL (92 Mg) still falls within the new bounds.

Sediment rating curves For this event (CR010301), several sediment rating curves were performed using different sets of data, in order to find the one which assesses the SSL estimate more closely to the SSL estimates obtained by sensors calibrations. The sediment load assessed by sensors is considered as a reference estimate around which the SSL estimates through SRC should be found.

SRC in function of all samples Taking into account the whole set of samples (n = 24) distributed along the hydrograph, a SRC was constructed (Eq. 4.23) based on suspended sediment

Table 4.12: Confidence intervals of SSL obtained by calibration of sensors.

Set	s_{IRTB}	s_{US}	90% Confidence interval (Mg)		Reference value (Mg)	Difference %
			Lower bound	Upper bound		
1	0.511	0.001	91.5	92.6	92.0	1.2
2	0.001	0.906	90.7	92.7	92.0	2.2
3	0.511	0.906	90.5	93.2	92.0	3.0
4^a	0.511	0.906	90.0	93.7	92.0	4.1

[a]Assuming the standard deviation of discharge 10% of the total.

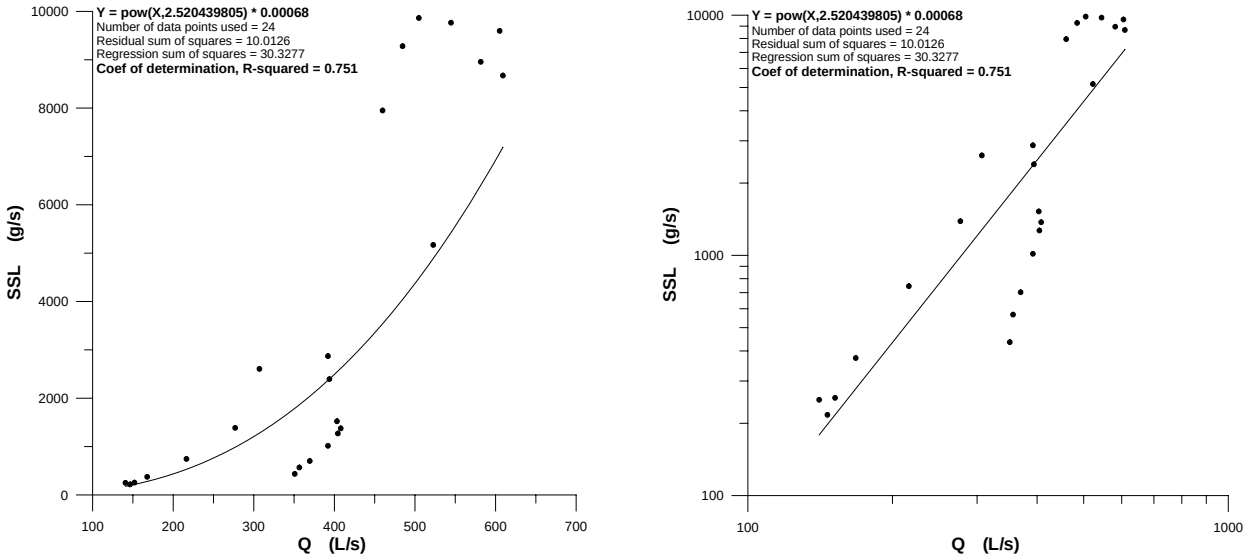

Figure 4.27: Log-log sediment rating curve between load and discharge.

load SSL_i (from concentration of samples and discharge). In Fig. 4.27 scatter plots in the arithmetic and logarithmic scales are shown, although the few number of samples, these have a good spanning throughout the hydrograph (rising, peak and falling limbs of discharge). A clockwise hysteresis for this event is notorious.

An ANOVA on the logarithmic scale has shown, that the regression model is highly significant. It is very unlikely that slope b is equal to zero. The statistical parameters of the ANOVA test were: MSEM = 3589 and the MSER = 0.054, F statistical = 66.6 with $p < 0.001$, $\alpha = 0.05$; the r^2 on logarithmic scale was 0.75. The best fit line is shown in Fig. 4.27b.

$$SSL_i = 0.00068 \times Q^{2.52} \tag{4.23}$$

Finally, a normality test of residuals (H_o: residuals follow a log normal distribution) done with $K - S$ test for 1 sample, concluded that residuals are normally distributed (p = 0.249, $\alpha = 0.05$) therefore the null hypothesis is accepted.

The total sediment load is estimated by summing up all the SSL_i for every time step multiplied by its time interval which is every 2 or 20 minutes. The total sediment transport for this event

Table 4.13: ANOVA for residuals by splitting data in function of discharge.

Source	Degree of freedom	Sum of Squares	Variance	F_{value}	$F_{0.05}$
Model	1	8.56	8.56	118.2	4.3
Residuals	20	1.44	0.072		
Total	21	10.01	0.48		

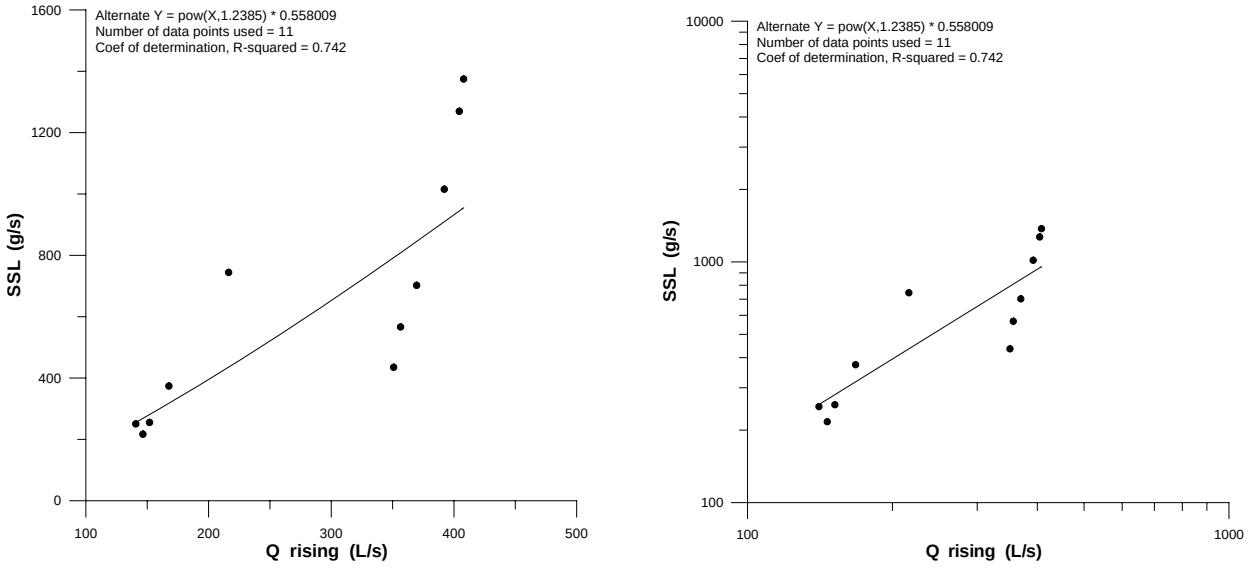

Figure 4.28: Relation between suspended sediment load and rising limb of discharge.

estimated by developing one sediment rating curve based on all samples, was 117.7 which is 28% greater than the estimate through sensors calibrations.

SRC's by splitting the event hydrograph into the rising and falling limbs Decomposing the hydrograph into its rising and falling segments is another alternative to obtain suspended sediment load.

In order to determine, if splitting the hydrograph into, two groups decreases variability, an ANOVA test has been done (Table 4.13) under the hypothesis that: one equation (using all samples from the hydrograph) explains the same fraction of the variability in the independent variable (load) as two equations. According to the ANOVA results the hypothesis is rejected ($p < 0.001$, $\alpha = 0.05$), because the probability is too low, therefore setting one equation for each limb of the hydrograph, is necessary since the variability in load estimates decreases.

The equation used to estimate the transport on the rising limb of the hydrograph was performed through the relationship (Fig. 4.28) between sediment load (samples on the rising limb) and rising water discharge values (Q_r) and setting a SRC with them (Eq. 4.24). Although the samples (Fig. 4.28) are largely scattered especially in the right side of the plot, the r^2 of the model was 0.74. An ANOVA for regression, to test the hypothesis that: $b = 0$, was also done, according to the results of this test this hypothesis is rejected, hence the equation is suitable, the parameters were: MSEM = 22.5, MSER = 0.035, F = 648.2, $p < 0.001$ and $\alpha = 0.05$.

A residual test for 1 sample done through the K-S test for the rising limb of the hydrograph has indicated, that residuals may be assumed to follow a log normal distribution (p = 0.269, $\alpha = 0.05$), therefore the hypothesis which states that residuals follow a log normal distribution is accepted.

$$SSL_i(r) = (3.30 \times 10^{-04}) \times {Q_r}^{2.72} \tag{4.24}$$

Similar procedure was performed for the falling limb. The SRC (Eq. 4.25) was done with samples collected on the falling limb of the hydrograph (Fig. 4.29). An ANOVA for regression has shown that the SRC is suitable, the statistical parameters were MSEM = 14.95, MSER = 0.095, F = 157.2 and $p < 0.001$ and $\alpha = 0.05$.

Finally, a K-S normality test for residuals (Fig. 4.29b) has determined that residuals follow a Log Normal Distribution (p = 0.323, $\alpha = 0.05$).

$$SSL_i(d) = (3.80 \times 10^{-13}) \times {Q_d}^{5.96} \tag{4.25}$$

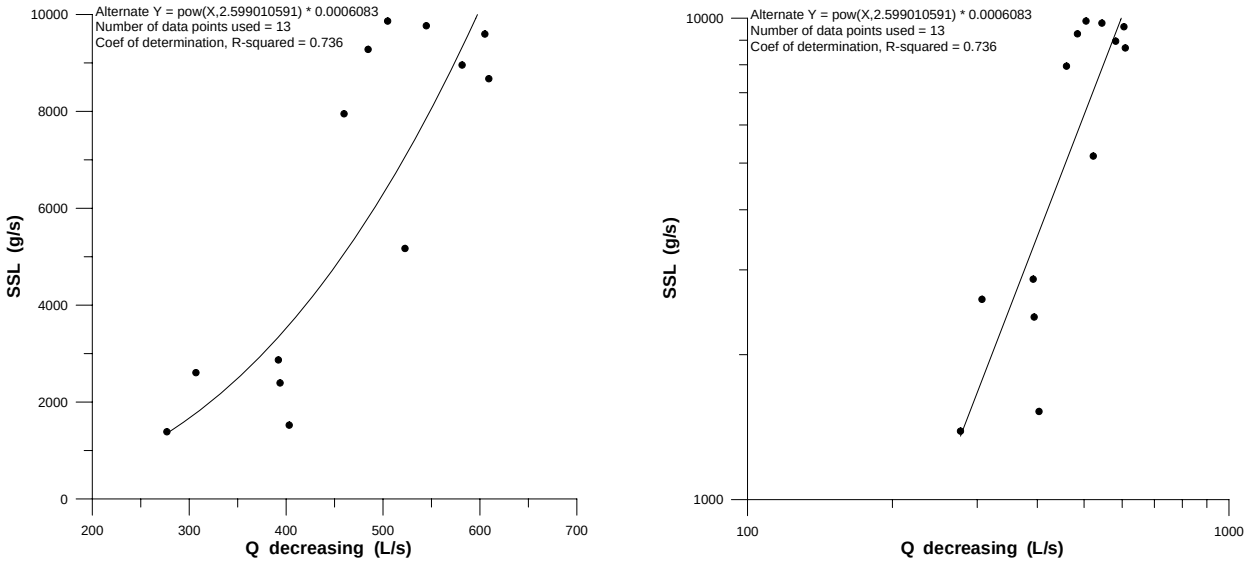

Figure 4.29: Relation between suspended sediment load and decreasing limb of discharge.

The total sediment load -by splitting the hydrograph into its two segments- is the addition of partial load estimates for each limb of the hydrograph.

The following results were obtained, the sediment load transported during the rising limb hydrograph was 48.0 Mg (after applying a smearing correction of $m = 1.005$). For the falling limb the amount of suspended sediment load was 64.5 Mg (smearing correction $m = 1.09$). Then, the total transport was 112.7 Mg, which is 22.5% greater than the value (92 Mg) assessed through sensor calibrations alone.

A summary plot of the methods studied to perform sediment load estimations for this event CR010301 is illustrated in Fig. 4.30. Clearly, the sediment rating curve obtained by least squares

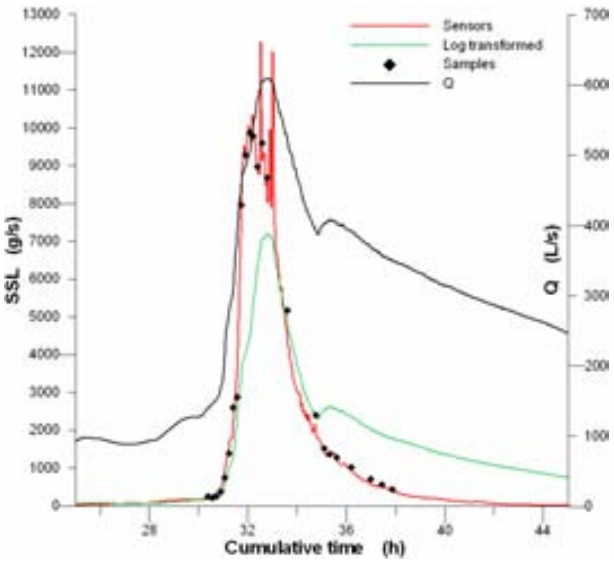

Figure 4.30: Comparison of sediment load by sensor readings and a sediment rating curve.

Table 4.14: Mean and standard deviation for residuals.

SRC option	Sediment rating curve	n	Mean of residuals	Std. dev. of residuals
1 curve hydrograph	$SSL = SSL_i \times dt$	24	0.001	0.659
1 curve rising limb	$SSL_r = SSL_i \times dt$	11	-0.011	0.228
1 curve falling limb	$SSL_f = SSL_i \times dt$	13	-0.008	0.298

regression on logarithmic transformed data underestimates the sediment transport in the rising limb of the hydrograph and overestimates in the last segment of the curve, this is due to the high values of water discharge, which results in a large difference between the curve for sensors calibrations and sediment rating curves. By applying the smearing correction (Duan, 1983) the retransformation bias is solved.

Confidence intervals Confidence intervals were assessed through Monte Carlo procedure, which consists in this specific case of a code named *sedcurve* described previously. Confidence interval assessment was done only for the load estimate without decomposing the hydrograph in two segments. The mean $\overline{x}$, standard deviation s of residuals (shown in Table. 4.14), the constant a, and exponent b of the power function were used to run *sedcurve*.

Two approaches to assess the confidence intervals were studied (for the remaining 26 events presented in the next sections, only the second approach is applied). The first case was done by assuming that CR010301 is the only event being studied (isolated) and have samples and for which it is needed to estimate an confidence interval, with *sedcurve* it is simulated the distribution function of residuals of this event, where the variation can be only due to the degree of scattering of data points (samples) in regard to the fit line. In Fig. 4.31 is shown a scheme of inputs and outputs of *sedcurve*.

With the first case the confidence interval is defined between 137.5 Mg and 159.4 Mg (with 90% of certainty), the difference between both limits is 16%.

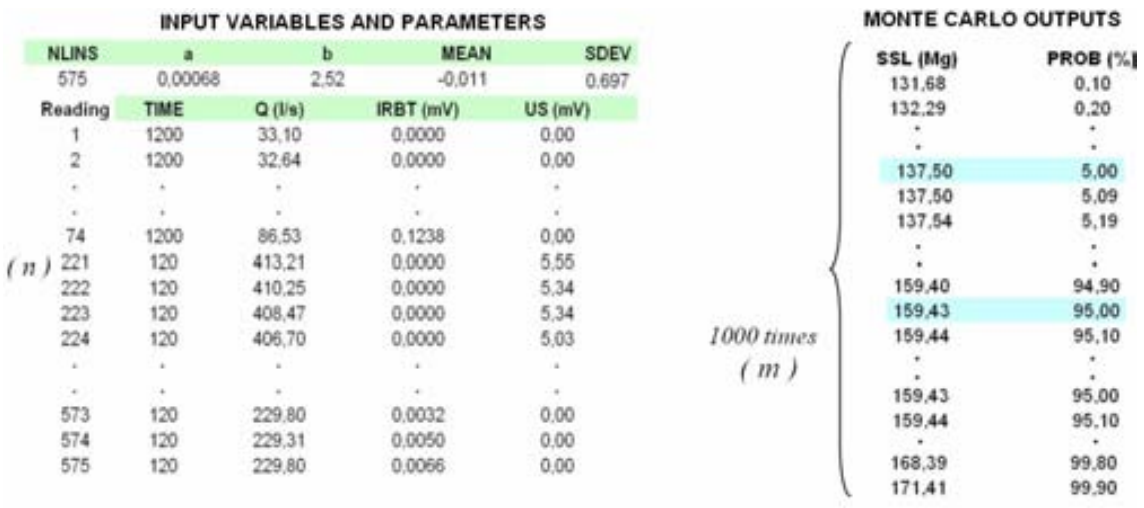

Figure 4.31: Scheme of inputs and outputs to run *sedcuesq*.

Table 4.15: Summary of SSL (Mg) estimations for event CR010301.

Method	**Lower bound**	**Average**	**Upper bound**	**Error** ±%
Sensors	90.0	92.0	93.7	2.0
MC annual SRC	15.0	92.2	662.7	351.2
MC seasonal SRC	14.2	80.1	524.2	318.1

The second case, consists of analysing the event CR010301 assuming this event as a member of a set of rainstorm events. The uncertainty associated to the total load estimate for a set of events has two origins, the uncertainty due to the events and uncertainty due to the samples within each event. The confidence interval for annual sediment rating curve for the same level of certainty was defined between 15 Mg and 662 Mg, which represents a difference of 351% between both bounds, the median is 80 Mg. On the other hand, as this event falls within the seasonal category of "rest of the events" its confidence interval was defined from 14 Mg to 524 Mg which represents a difference of 318% between both bounds. In Fig. 4.32 it is shown the confidence intervals for annual and seasonal sediment rating curves, where the range of seasonal rating curve is narrow especially on the upper right of the plot.

A summary of sediment load estimates for CR010301 obtained using sensor calibrations and sediment rating curves are shown in Table 4.15. The confidence interval for the estimate by sensor calibrations is much narrower (2%) than the interval defined for rating curves, which is extremely spread (> 300%), however the estimations found by sensors is within the confidence interval obtained for rating curves.

On the other hand, the seasonal 90% confidence interval is narrower than the annual interval, and also both of its limits decreased slightly at the lower bound; however, large decreases occurred at the upper bound. The sediment load simulations in *sedcurve* are log normally distributed, therefore in the linear scale are positively skewed.

Results obtained by logarithmic retransformation of SRC ("conventional" approach) has shown that the average estimate is greater than the estimate obtained through sensor calibrations,

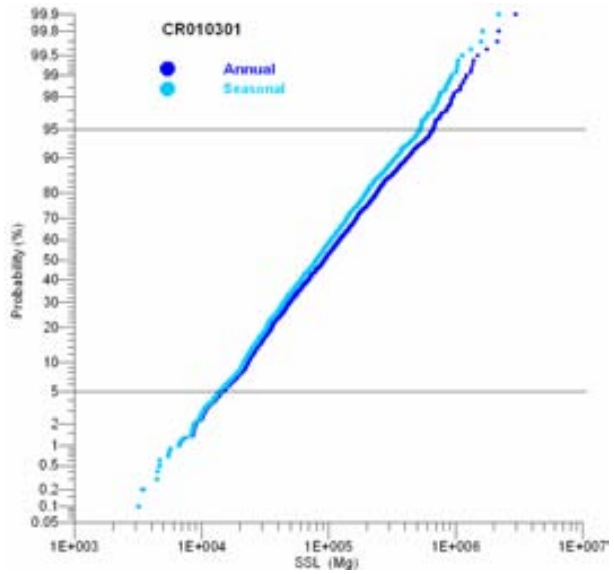

Figure 4.32: Confidence intervals from Monte Carlo simulations.

however, these discrete load estimations are within the confidence interval defined using Monte Carlo simulation, which was done by modelling the distribution function of sediment load obtained by the "conventional" rating curve.

Within the rating curve, splitting the hydrograph and defining a rating curve for each limb is better than having one rating curve for the entire hydrograph, this was possible, because of a good distribution of samples along the hydrograph.

4.5.1.2 CR220196

No samples were collected during this event, which occurred between the 22nd and 24th of January 1996. Only readings from infrared turbidity sensor were available (Fig. 4.33a). However the sediment concentration values obtained by using the reference calibration (from event CR010301) were very low (less than 1 g/L). Infrared sensor readings does not seem to be incorrect, therefore, alternative calibrations of infrared sensor were explored. For discharges higher than 8000 L/s, infrared sensor calibrations of two adjacent events, such as CR070697 and CR111196 were used. By doing so, the concentrations have increased up to 14 g/L, the new curve is shown in Fig. 4.33b. The concentrations given by CR070697 were higher than the ones found using calibrations of CR111196.

Confidence intervals were defined by considering the sediment load obtained from CR070697 as the upper limit, and the sediment load obtained from CR111196 as the lower limit. It was not possible to run *sederror* because the infrared sensor readings for this event were not reliable, and also because there were no readings from ultrasound sensor.

In Table 4.16, a summary of sediment load estimations obtained by sensor calibrations and sediment rating curves are shown. Load estimates by annual and seasonal sediment rating curves were calculated using the power function whose parameters are presented in Table 4.8. In Table 4.16 can be seen that confidence interval for sensors, is way below and outside the confidence interval

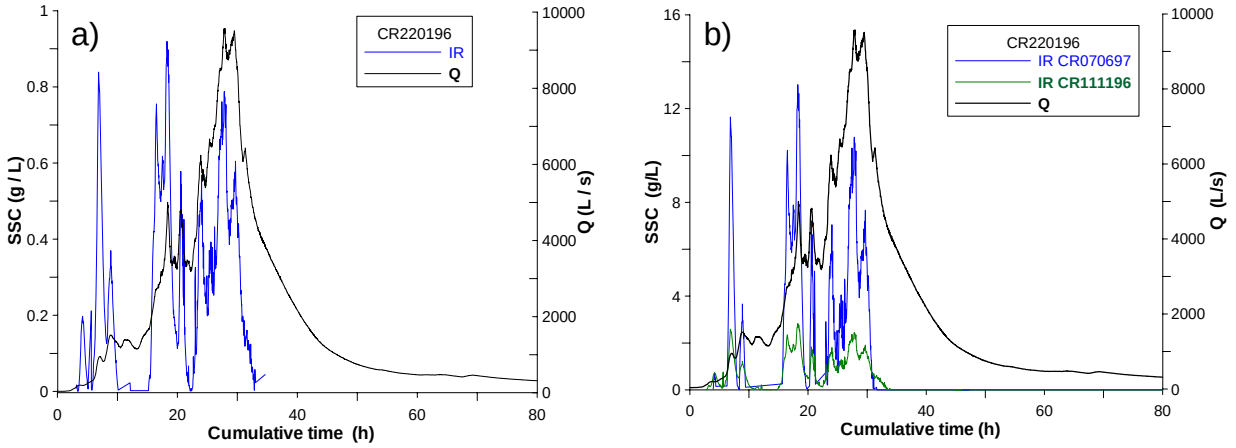

Figure 4.33: Suspended sediment concentrations for CR220196 by sensor calibrations: (a) reference calibration, (b) calibration for adjacent events.

defined for annual or seasonal sediment rating curves, and it is much narrover than the interval for rating curves. In Table 4.16 MC stands for Monte Carlos simulation.

Table 4.16: Summary of SSL (Mg) estimations for event CR220196.

Method	**Lower bound**	**Average**	**Upper bound**	**Error** $\pm\%$
Sensors	455.0	976.5	1498.0	53.4
MC annual SRC	3409.0	20573.0	149640.0	355.4
MC seasonal SRC	3006.0	16602.0	109860.0	321.8

4.5.1.3 CR220496

During this event 12 samples were collected, nevertheless, the majority of these samples are on the falling limb of the hydrograph, and only 2 samples are located before the peak of water discharge (Fig. 4.34a). By using these samples a infrared sensor calibration was defined, the resulting sediment concentration curve is shown in Fig. 4.34b. The calibration curve is reliable ($r^2 = 0.92$).

The confidence interval for the estimated sediment load values through calibrations of sensors was assessed by means of *sederror*.

On the other hand, the confidence interval of the median defined by rating curves (done by *sedcurve*) includes the interval defined for sensors. The confidence interval for sensors is narrower than for rating curves which are highly spread ($> 300\%$). The mean load estimate by sensor calibrations is 4 times lesser than the median obtained by SRC.

A summary of sediment load estimations by the means of both methods are presented in Table 4.17.

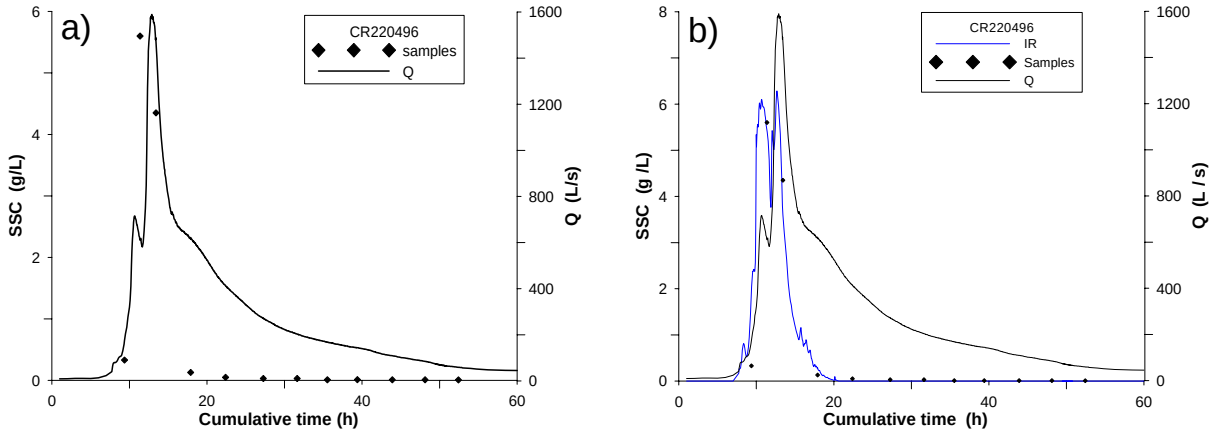

Figure 4.34: Suspended sediment concentrations for CR220496 by calibrations of sensors.

Table 4.17: Summary of SSL (Mg) estimations for event CR220496.

Method	**Lower bound**	**Average**	**Upper bound**	**Error** ±%
Sensors	79.0	87.0	83.0	4.8
MC annual SRC	57.0	357.6	2516.0	343.8
MC seasonal SRC	53.0	304.0	1953.0	312.0

4.5.1.4 CR141096

Sediment concentration for this event was estimated by using the reference calibrations for both sensors. The collected samples (18) are shown in Fig. 4.35a, these samples are scattered around concentration curves defined from sensors, and are closer to US sensor curve than to IR curve. Between hours 4.6 and 4.9, (Fig. 4.35a), the ultrasound sensor was clogged (providing unreliable readings), therefore, concentrations for that section of the curve were pruned, instead a few linear interpolations between the extreme data points of the gap were performed, and interpolations between samples also were done. The resulting new concentration curves used to estimate the load for this event are shown in Fig. 4.35b.

The confidence interval for the mean estimate by sensors was defined based on Fig. 4.35b, it was not possible to run *sederror*, because there were no reliable continuous sensor readings; therefore, as the lower bound of the confidence interval it was considered the curve obtained by: sample interpolations, infrared sensor calibration and some segments obtained by ultrasound sensor calibration. In Fig. 4.35 the lower bound is labeled as "IR + interpolations"; on the other hand, as the upper bound was considered the curve labeled as "IR + US + interpolation", which is the same as lower bound but concentrations between hour 5 - 6 are considered as reliables, which in the former were not.

With regard to sediment rating curves, the confidence intervals were performed using *sedcurve* and it was much wider than the one defined for sensor readings, the mean estimate by sensors is 3 times than the median defined by SRC. The confidence interval for sensors is included in the one defined for SRC. In Table 4.18 a summary of sediment estimations given by both methods are presented.

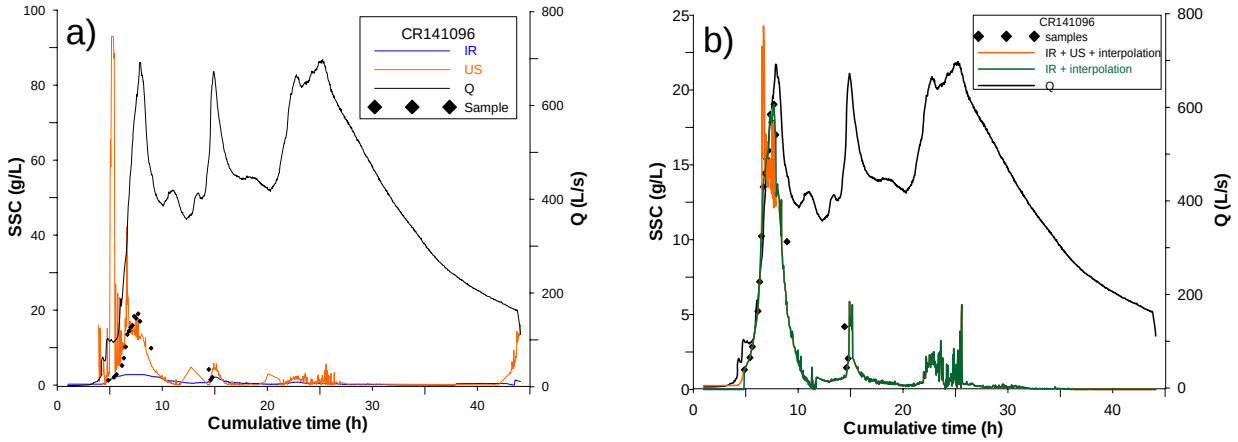

Figure 4.35: Suspended sediment concentrations for CR141096 by calibrations of sensors.

Table 4.18: Summary of SSL (Mg) estimations for event CR141096.

Method	**Lower bound**	**Average**	**Upper bound**	**Error** ±%
Sensors	93.0	98.0	103.0	5.1
MC annual SRC	49.7	307.0	2217.0	353.0
MC seasonal SRC	46.6	264.0	1737.0	320.2

4.5.1.5 CR111196

During this event 15 samples were collected and they are distributed along the hydrograph Fig. 4.36a. Reference calibration for both sensors were applied, and results are shown in Fig. 4.36a. These calibrations have seemingly given reliable readings, nevertheless, concentrations given by calibration of infrared sensor are low, an additional issue is that fot both sensors at hour 28 the sediment concentration starts to increase again while water discharge is decreasing, this might be due to a clogging occurring to ultrasound sensor. These unreliable segments of the curves were not considered for load estimations.

In addition, it was obtained a calibration for ultrasound sensor (for the event being studied) and its concentrations (on Fig. 4.36b labeled as US CR111196), which were above the concentration curve defined by using the reference calibration.

The confidence interval limits for sediment load obtained by sensor calibrations were defined by considering the ultrasound calibration curve obtained from reference calibration as the upper limit, and the ultra sound curves for the event being studied as the lower bound, both curves are shown in Fig. 4.36b.

Regarding to sediment rating curves, its confidence intervals were defined by modelling the distribution function of sediment load obtained from these rating curves by Monte Carlo procedure (*sedcurve*) and they were wider than the confidence interval defined for sensor calibrations. The confidence interval defined for rating curves includes the interval defined for sensors.

A summary of sediment load estimations are displayed in Table 4.19. The median SSL estimate

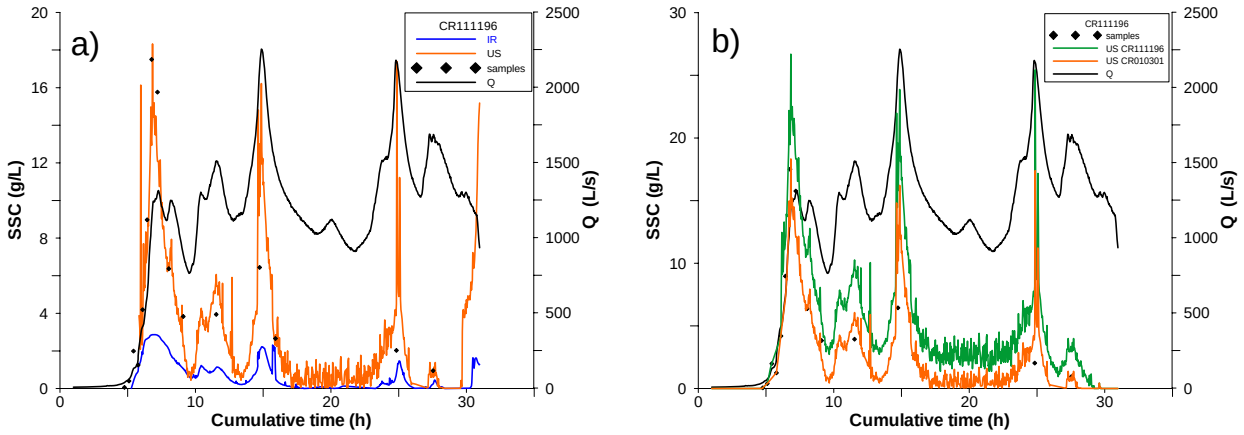

Figure 4.36: Suspended sediment concentrations for CR111196 by calibrations of sensors.

by SRC are 3 times greater than the mean defined for sensors. For rating curves the value of the medians are skewed towards the lower bounds, this happens because the simulations performed with *sedcurve* follow a log normal distribution.

Table 4.19: Summary of SSL (Mg) estimations for event CR111196.

Method	**Lower bound**	**Average**	**Upper bound**	**Error** ±%
Sensors	321.0	501.0	644.0	32.2
MC annual SRC	242.0	1526.0	10966.0	351.4
MC seasonal SRC	221.7	1276.0	8335.0	317.0

4.5.1.6 CR040697

During this episode 24 samples were collected, and they are mostly concentrated at the beginning of the event. Although IR and US sensors readings are reliable, their calibrations curves are highly separated from each other, as it is shown in Fig. (4.37a). IR was able to measure concentration only up to ≈ 5 g/L, when it got saturated, on the other, hand US sensor seemingly performed well. On the falling limb of the hydrograph both curves obtained by sensor calibrations should have coincided if they were correct, however they are not.

In an experiment conducted at Cal Rodó on the 27th of May 2007, using particles of diverse size, it was found that for the same concentration, IR has given high readings (mV) for fine material and low reading for coarse material, whereas the US sensor showed the opposite behaviour (Soler *et al.*, Submitted). Considering the size of this flood episode (large), the IR values were much lower than the one given by US, because of the ability of sensors to interpret sediments of same size. Therefore, for high flood episodes (over 43 Mg of sediment per event (percentile 80)) IR sensor can be used usually up to ≈ 7 g/L, however for higher concentrations the recalibrated US sensors (for coarse material) need to be used.

In order to determine if the sensor calibrations at the event scale (CR040697) which are shown in Fig. (4.37a) are truly correct, the newly developed calibration for US sensor was applied, assuming

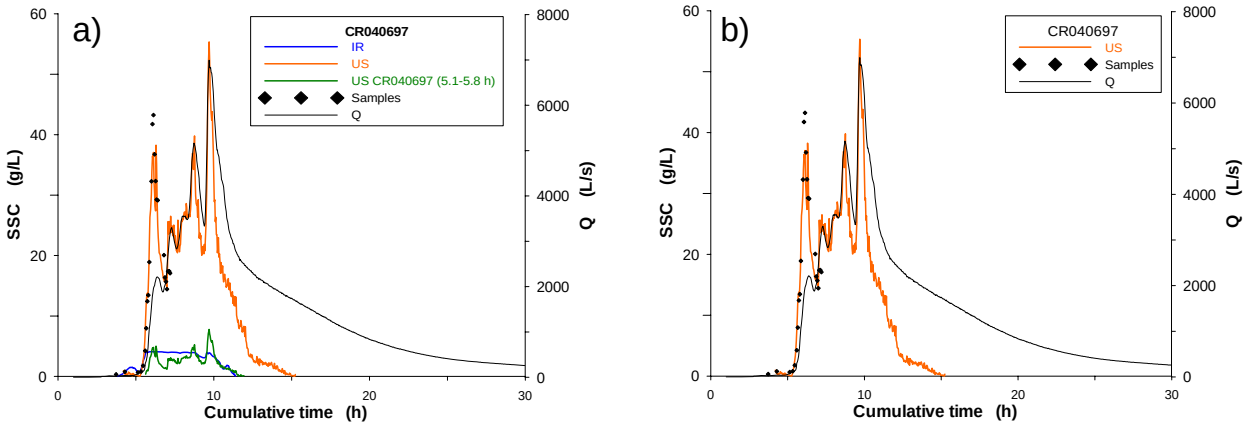

Figure 4.37: Suspended sediment concentrations for CR040697 by calibrations of sensors.

that the previous calibration was done for fine sediments. A coarsening of transported material occurs with increasing discharge (Hejduk *et al.*, 2006) thus for large runoff episodes a different calibration is advised.

The new linear regression (US sensor) had as constant $a = 0.832$ and slope $b = -6.25$ ($r^2 = 0.99$, residuals had $\overline{x} = 0$ and $s = 1.84$) the new calibration for US sensor is similar to the previous calibration for US sensor where $a = 0.805$ and b = -6.806 ($r^2 = 0.99$, residuals had $\overline{x} = 0.37$ and $s = 4.38$). As no significant differences were found, it was used the previous calibration to perform load estimates in order to obtain wider confidence interval (because of higher s).

The sediment load was estimated using US concentrations as it is shown in Fig. (4.37b) and IR concentrations between 4 and 5 (Fig. 4.37a) were also included.

The confidence interval of the mean SSL estimate was obtained through *sederror* and it was defined between 2015 Mg and 2078 Mg (90% confidence level), the difference between both bounds is 3.2%, this value is extremely low; this difference was rounded up to 5% in order to define the upper and lower limits of the confidence interval.

On the other hand, estimations performed by the means of rating curves have shown that the confidence intervals are very broad compared to sensors, and it includes the confidence interval defined for sensors. The mean SSL estimated for annual and seasonal SRC are 11 and 8 times greater respectively than the load obtained by sensor calibrations. In Table 4.20 a summary of sediment load estimations obtained through both methods are given.

Table 4.20: Summary of SSL (Mg) estimations for event CR040697.

Method	**Lower bound**	**Average**	**Upper bound**	**Error** ±%
Sensors	1944.0	2046.0	2148.0	5.0
MC annual SRC	653.0	3514.0	24330.0	336.9
MC seasonal SRC	473.0	2868.0	18107.0	307.0

4.5.1.7 CR051197

During this flood episode 19 samples were collected, and they are spanned almost along the whole hydrograph (Fig. 4.38a). Sediment concentration values obtained by using reference calibrations for both sensors are shown in Fig. 4.38a, clearly, the curve of IR are more reliable unlike the concentration given by US calibration. US sensor was clogged many times during this flood episode. Sediment load estimations were done using IR's concentration curve which is shown in Fig. 4.38b, in spite of the low concentrations they seem to be consistent with water discharge values.

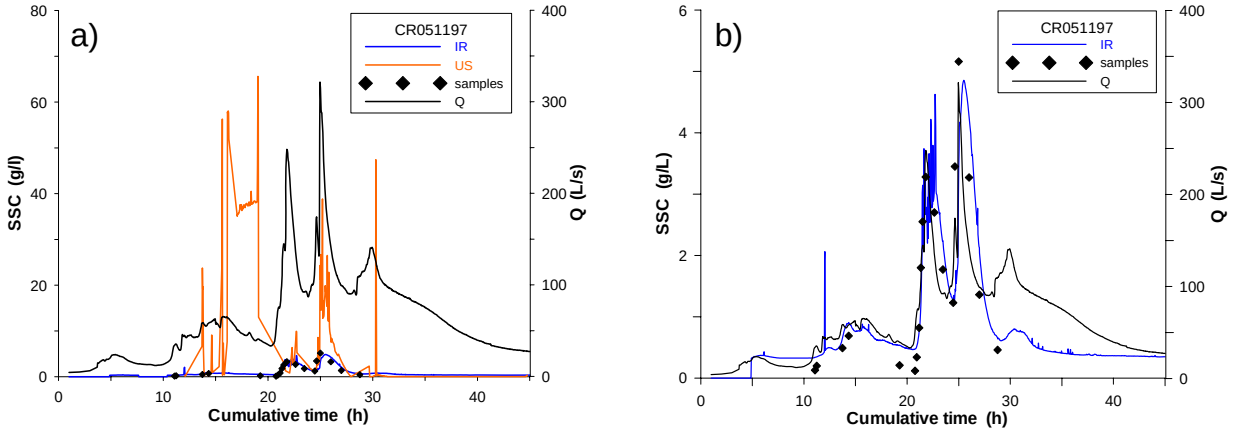

Figure 4.38: Suspended sediment concentrations for CR051197 by calibrations of sensors.

Confidence interval of SSL values defined for sensors was assessed through *sederror* this have a difference of 5% between its lower and upper bounds.

On the other hand, load estimates obtained through the process of modelling the power function of SSL by *sedcurve* has given a much wider confidence interval, and its median is skewed towards the lower limit. A summary of load transport for this event is presented in Table 4.21.

Table 4.21: Summary of SSL (Mg) estimations for event CR051197

Method	**Lower bound**	**Average**	**Upper bound**	**Error** ±%
Sensors	13.3	14.1	14.7	5.0
MC annual SRC	2.3	14.2	99.1	340.8
MC seasonal SRC	2.2	12.7	81.0	310.2

4.5.1.8 CR171297

During this event 12 discrete samples were collected, however, unfortunately they are not distributed along the entire hydrograph, on the contrary all of them were collected at the beginning of the flood episode; this fact illustrates clearly the importance of having a good representativeness of samples drawn at specific intervals in order to assure that they are spanned along the entire hydrograph. Several curves of sediment concentration were obtained (Fig. 4.39a) using calibrations for IR and US sensor using the samples for this event. These were: the reference calibration (CR010301) for

IR sensor, the calibration from CR111197 of IR sensor, US calibration from CR040697 (Q > 2000 L/s); all of them were applied to IR readings of event being studied.

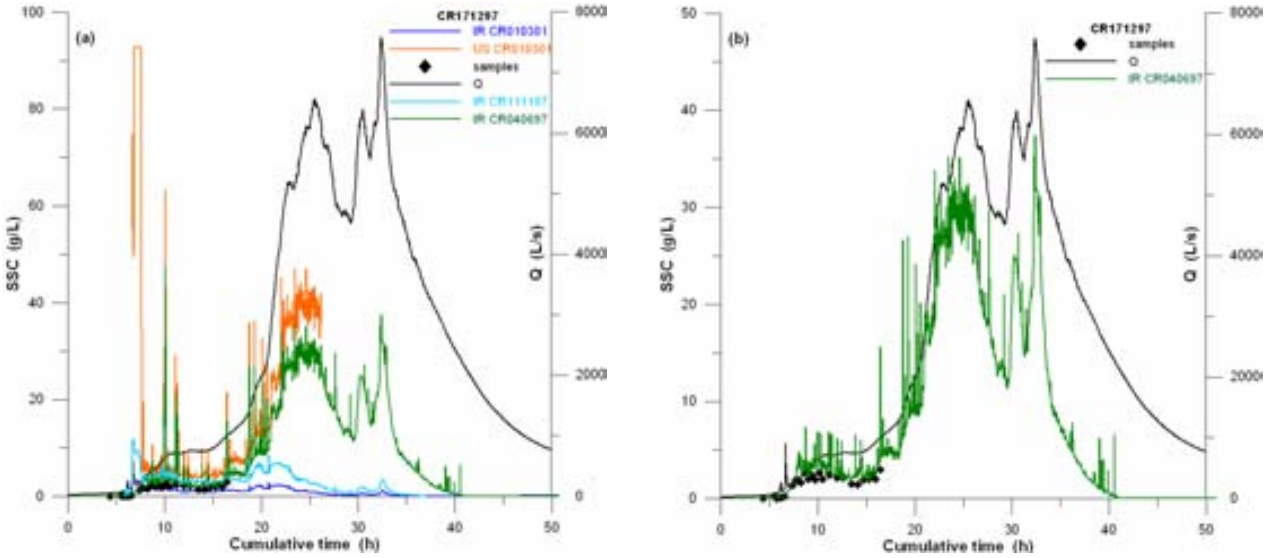

Figure 4.39: Suspended sediment concentrations for CR171297 by calibrations of sensors

Results indicate that concentrations obtained by IR calibrations are very low considering the high water discharge values. The only curve that seems trustworthy is the one generated from US calibration (for water discharge values higher than 2000 L/s) of CR040697 and applying it to IR readings for CR171297, however, some segments, where the IR sensor was clogged were not included to perform load estimations. The curve used to estimate the sediment transport during this episode is shown in Fig. 4.39b.

Given the fact that calibrations of US sensor are different from the event being studied, it was not possible to run *sederror* to assess the confidence intervals, instead an arbitrary cautious 5% was established to calculate the limits of the confidence interval.

A summary of sediment load estimations are presented in Table 4.22, the confidence interval for sediment rating curves are far higher than the one defined for sensors, load estimations obtained through sensor calibrations are within the range defined for rating curves.

Table 4.22: Summary of SSL (Mg) estimations for event CR171297.

Method	**Lower bound**	**Average**	**Upper bound**	**Error** ±%
Sensors	6111.0	6433.0	6755.0	5.0
MC annual SRC	2474.0	15290.0	108736.0	347.5
MC seasonal SRC	2184.0	12454.0	80162.0	313.1

4.5.1.9 CR070599

During this event 6 samples were collected and all of them are on the rising limb of the hydrograph (Fig. 4.40a). By applying the reference calibration (CR010301) to IR sensor readings, the sediment concentration estimates are very low, despite that the IR sensor does not seem saturated, it did

sometimes got clogged, from this calibration some reliable segments were identified such as: between hours 0 - 11 and from hour 15.2 on; the gap in between, was calculated by linear interpolations of consecutive samples as it is shown in Fig. 4.40a.

Two possibilities were explored in order to closely estimate the sediment load, the first alternative is shown in Fig. 4.40a, which consisted of excluding the sample with the highest value; the second alternative consisted of including all samples to perform calibrations as it is shown in Fig. 4.40b.

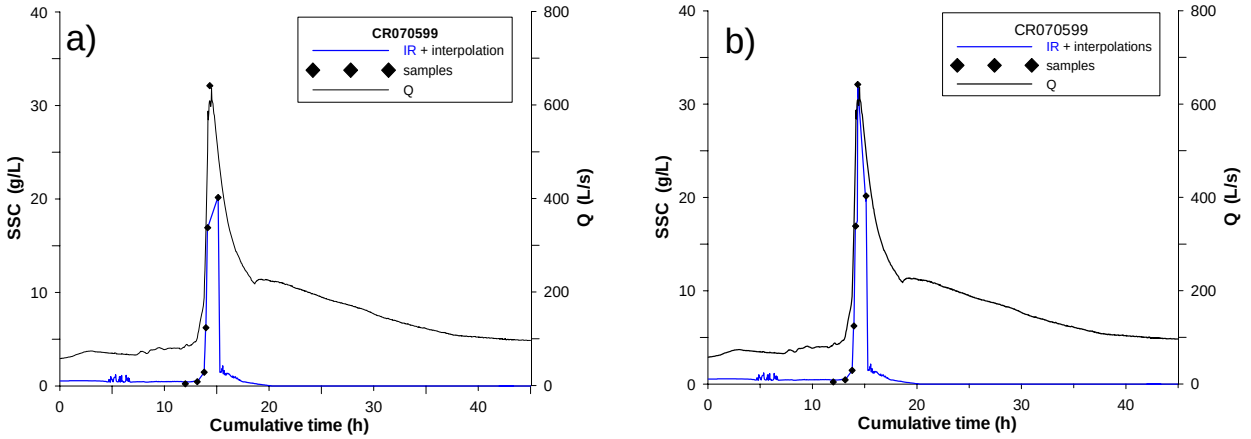

Figure 4.40: Suspended sediment concentrations for CR070599 by calibrations of sensors.

By the means of IR sensor calibration and interpolations, it was estimated an average suspended sediment load of 57 Mg and its confidence is slightly wide (10.5%).

On the other hand, the rating curves have a wider confidence intervals than the one defined for IR sensor. The limits defined for SSL estimate by sensors are within the confidence interval defined for rating curves.

A summary of sediment load results by the means sensor calibration and sediment rating curves is presented in Table 4.23.

Table 4.23: Summary of SSL (Mg) estimations for event CR070599.

Method	**Lower bound**	**Average**	**Upper bound**	**Error** ±%
Sensors	51.0	57.0	63.0	10.5
MC annual SRC	12.5	76.7	545.6	347.0
MC seasonal SRC	12.0	67.0	437.2	317.2

4.5.1.10 CR280899

During this event 5 samples were collected, 2 of them have very high concentration values ≈ 96.5 g/L, which make an over-steepened segment in the curve and the remainder 3 samples were collected in the falling limb of the hydrograph (Fig. 4.41). The gap between both subsets of samples is large, because of this, it was performed individual (separate) sensor calibrations using each subset of samples.

The calibration that gave reliable concentrations was the one performed using samples collected at the decreasing part of the hydrograph, and this calibration was applied to US readings, nevertheless it was not able to fit the entire event, but at least, it has allowed to define concentrations between hour 3.2 to 5.7. For the remainder section of the hydrograph (between hours 0 and 3.2) concentrations were acquired from linear interpolations.

Three linear interpolations were performed between 96.5 g/L (hour 1.3) and 22.5 g/L (hour 3.2), and between between 96.5 g/L and 96.4 g/L (≈ hour 1 and 1.2), the third interpolation was done between 0 and 96.5 g/L. In Fig. 4.41a the interpolated cuve is labeled as "interpolation (a,b,c)+US calibration". Concentrations obtained from these interpolations were considered as valid (first alternative).

According to Fig. 4.41a, concentrations higher than 96.5 g/L might be true, therefore a second alternative has been developed by extending the length of the two data points (samples) (Fig. 4.41a) until they intersect at 112 g/L (hour 1.25) and for the remainder part of the hydrograph, the concentrations obtained through the first alternative was used as it is shown in Fig. 4.41b.

Both alternatives were considered as the lower and upper limits of the confidence interval for the estimate obtained from calibration of sensors.

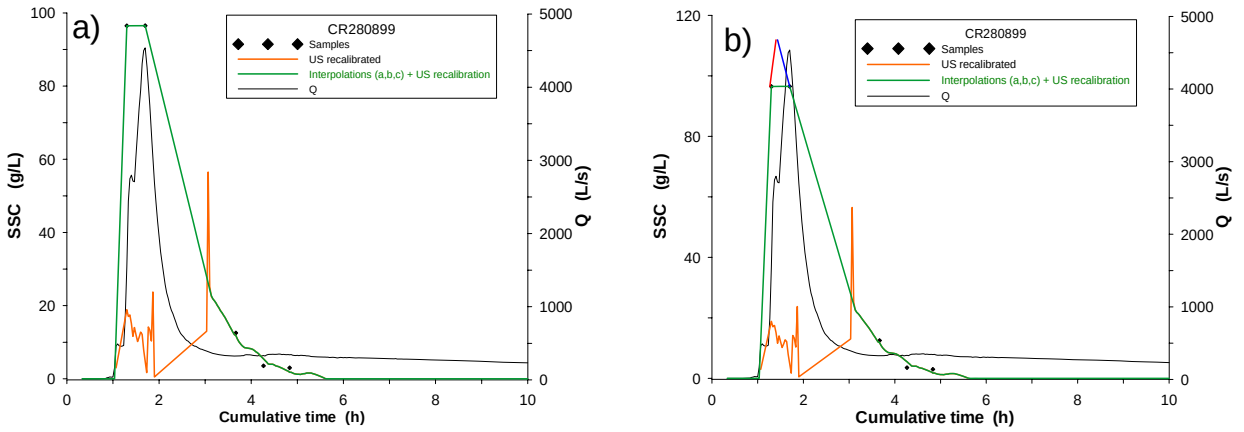

Figure 4.41: Suspended sediment concentrations for CR280899 by calibrations of sensors.

The average amount of sediment estimated through sensors was 1023.0 Mg, however its confidence intervals were very narrow (2%); on the other hand, the SSL estimates through sediment rating curves were very high; being 2 times and 3 times for annual and seasonal rating curves respectively. Their confidence intervals are wider than the confidence interval assessed for sensors with a difference of more than 300% between its limits. A summary of sediment load estimates and its confidence intervals are shown in Table 4.24.

Table 4.24: Summary of SSL (Mg) estimations for event CR280899.

Method	**Lower bound**	**Average**	**Upper bound**	**Error** ±%
Sensors	1002.7	1023.0	1044.2	2.0
MC annual SRC	49.5	302.0	2185.4	353.6
MC seasonal SRC	297.1	907.0	3095.0	154.2

4.5.1.11 CR140999

No samples were collected during this flood episode. By applying the reference calibrations to readings from both sensors, the concentration curves shown in Fig. 4.40a were obtained, apparently IR sensor was not saturated nor clogged, however the concentrations are extremely low, in regard to US sensor it was clogged several times throughoutt the episode, nevertheless during the peaks of water discharge it functioned well.

Although IR sensor readings seemingly are correct, another calibration was applied to them in order to verify it. A IR calibration for CR220496 was applied to IR readings of the event being studied, which is shown in Fig. 4.40b. Concentrations obtained by using the reference calibration for US sensor and linear interpolations between gaps, the IR calibration belonging to CR220496 and applying it to IR readings of CR140999 were considered as the upper and lower bounds of the confidence interval for this event (Fig. 4.40b).

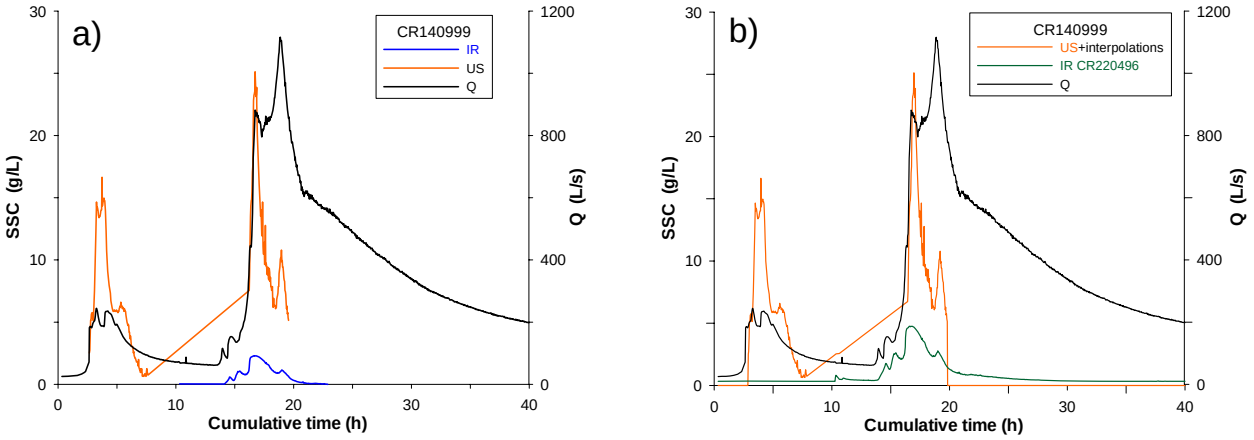

Figure 4.42: Suspended sediment concentrations for CR140999 by calibrations of sensors.

The amount of sediment load estimated by the means of sensors calibrations and interpolations was 108 Mg, and its 90% confidence interval is between 61 and 156 Mg, which is narrow if it is compared with confidence intervals defined for annual and seasonal sediment rating curves. The average sediment estimate by annual SRC is 2 times the estimate by sensors, and the estimate by seasonal SRC is 3 fold higher. The confidence interval defined for sensors is within the range defined for rating curve. A summary of load estimations is shown in Table 4.25.

Table 4.25: Summary of SSL (Mg) estimations for event CR140999.

Method	**Lower bound**	**Average**	**Upper bound**	**Error** ±%
Sensors	61.0	108.0	156.0	44.0
MC annual SRC	43.7	269.0	1863.0	338.2
MC seasonal SRC	518.0	1630.0	5265.0	145.6

4.5.1.12 CR190999

During this event no samples were collected, which are crucial to determine whether the concentrations obtained from sensor calibrations are suitable or not. In Fig. 4.43a the concentration curves obtained using the reference calibration for IR and US sensors are shown. US sensor was clogged prior to hour 4.3, shortly afterwards it has given reliable concentrations until hour 8.3. In regard to IR sensor, it seemingly functioned well throughout the episode except at around hour 8 when sediment concentrations dropped.

The amount of sediment transport, was assessed by linear interpolation between reliable segments of IR sensor and US sensor as it is shown in Fig. 4.43b.

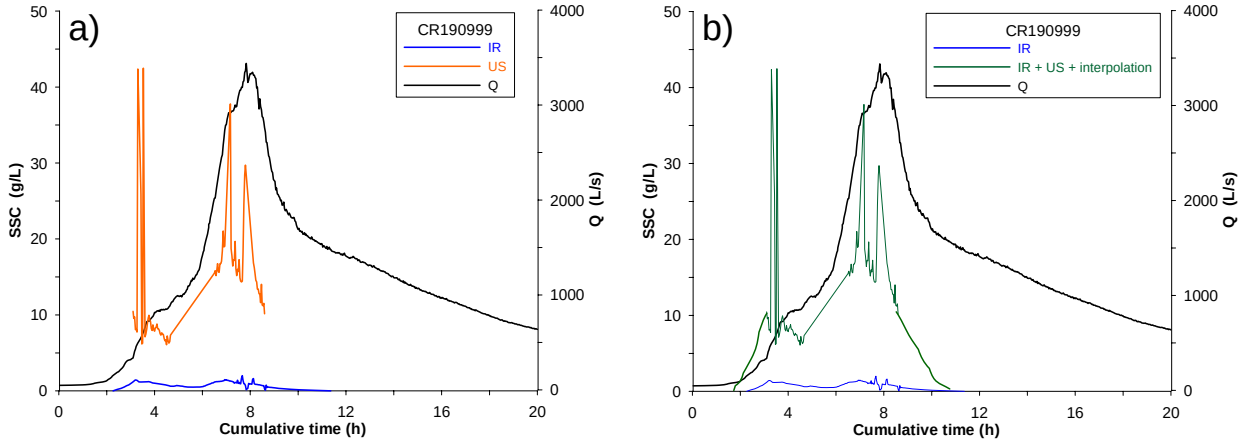

Figure 4.43: Suspended sediment concentrations for CR190999 by calibrations of sensors.

In Table 4.26, a summary of the assessed suspended sediment load carried out during this event is presented. Due to the fact that some interpolations between reliable segments of sensor calibrations was done (Fig. 4.43a), *sederror* was not run to estimate the confidence intervals. The confidence interval was estimated by considering an arbitrary error of 5% above and below the average load. Confidence intervals for sediment rating curves were assessed by *sedcurve* and it presented a wide interval, especially for annual rating curve. The confidence interval estimated for sensors is included in the interval defined for rating curves.

Table 4.26: Summary of SSL (Mg) estimations for event CR190999.

Method	**Lower bound**	**Average**	**Upper bound**	**Error** ±%
Sensors	607.0	638.5	670.4	5.0
MC annual SRC	241.6	1535.0	11048.0	352.0
MC seasonal SRC	1579.0	4833.0	16145.0	150.7

4.5.1.13 CR121199

During this episode of sediment transport 5 samples were collected. By applying the reference calibrations to sensor readings the curves shown in Fig. 4.44a were obtained. US sensor was not

able to collect reliable readings, and IR sensor operated well. There seems to be an incongruence between the very low concentration and high discharge, therefore, another calibration for IR sensor (CR040697) was performed using high discharges ($> 2000 L/s$), by doing so the IR sensor concentrations have increased considerably, and the samples are located around the new curve Fig. 4.44a. In addition, interpolations between samples and a conservative concentration found on the new curve were done. In Fig. 4.44b the curves which were considered as the lower and upper bounds of the confidence interval are shown.

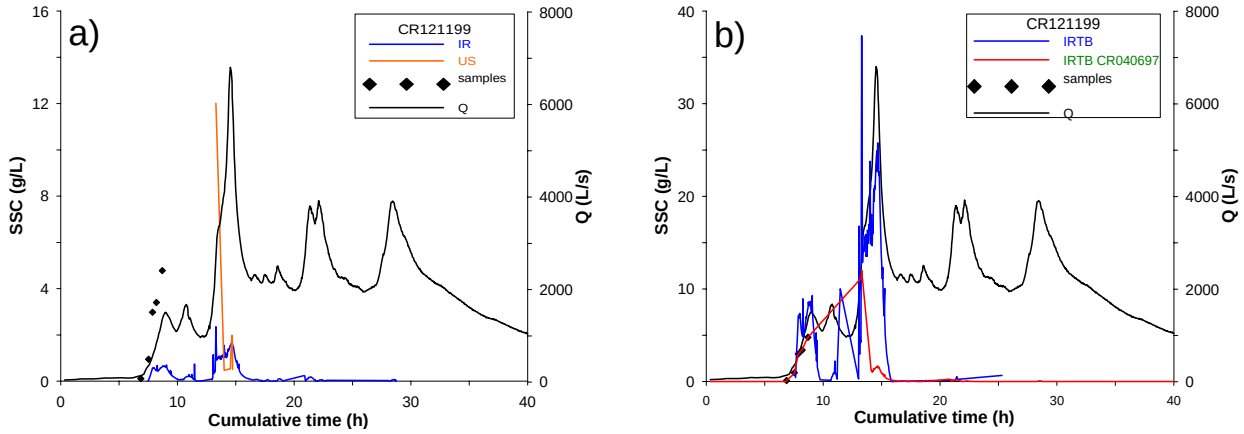

Figure 4.44: Suspended sediment concentrations for CR121199 by calibrations of sensors.

The amount of sediment load estimated from sensors, was 474.5 Mg ± 39%, this confidence interval is narrower than the one estimated for sediment rating curves, which presented a median of 6,223 Mg for annual (13-fold) and 5,117 Mg for seasonal (11-fold), and its confidence interval is more than 300%. A summary of sediment load estimates for this event are presented in Table 4.27.

Table 4.27: Summary of SSL (Mg) estimations for event CR121199.

Method	**Lower bound**	**Average**	**Upper bound**	**Error** ±%
Sensors	286.0	474.5	663.0	39.0
MC annual SRC	1016.0	6223.0	43577.0	342.0
MC seasonal SRC	911.9	5117.0	32707.0	310.7

4.5.1.14 CR280900

During this event 16 samples were collected, and they are well distributed along the hydrograph (Fig. 4.45a). By applying the reference calibrations to IR and US sensor readings the curves shown in Fig. 4.45a were obtained. IR sensor was saturated for concentrations higher than 6 g/L as it was expected, and US sensor performed well and its peak of concentration coincides with peak of water discharge. Two alternatives to estimate sediment load were possible, the first is taking the IR sensor concentrations, excluding the segment where it was saturated, and taking US concentration instead. The second alternative, is taking IR as in the first alternative and for the segment where it was saturated performing linear interpolations between consecutive samples (Fig. 4.45b). These two alternatives were used as the limits of the confidence interval.

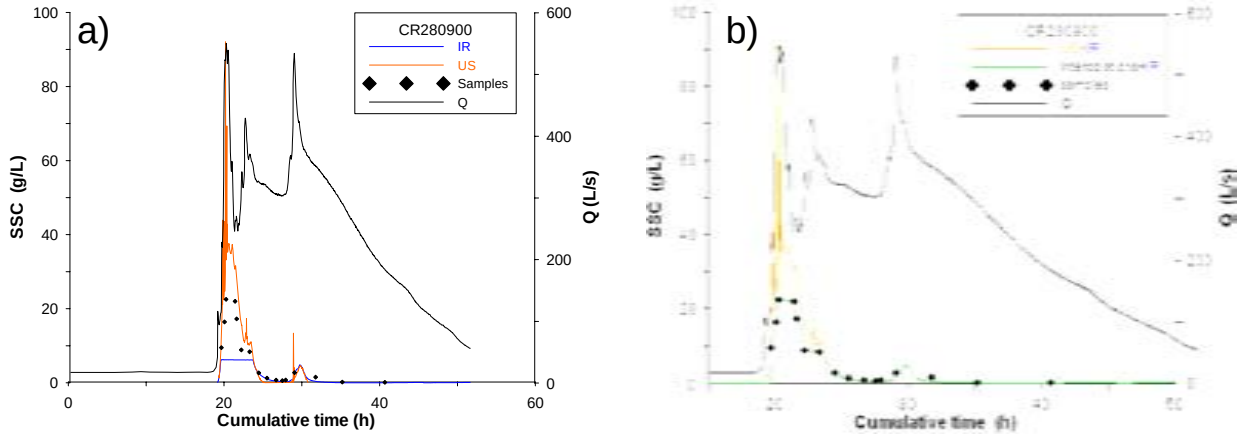

Figure 4.45: Suspended sediment concentrations for CR280900 by calibrations of sensors.

A summary of suspended sediment load estimations by both methods is presented in Table 4.28, the confidence interval defined for sensor falls within the confidence interval defined for sediment rating curves.

Table 4.28: Summary of SSL (Mg) estimations for event CR280900.

Method	**Lower bound**	**Average**	**Upper bound**	**Error** ±%
Sensors	97.0	124.0	151.0	21.8
MC annual SRC	16.2	104.0	747.1	351.4
MC seasonal SRC	15.4	91.0	592.0	317.0

4.5.1.15 CR231100

No sediment samples were available for this event. By applying the reference calibration of each of the sensor, the sediment concentration curves shown in Fig. 4.46a were obtained. IR sensor worked well, but was saturated for concentrations higher than 6 g/L; on the other hand, US sensor started working well, however it stopped sending reliable readings after hour ≈ 10.

In order to estimate the amount of sediment load transported during this event it was used concentrations given by IR sensor and performing two linear interpolations by extending the lines until their intersection, as it is shown in Fig. 4.46b. The confidence interval of the estimation computed through sensor calibration was done assuming 5% of variability. It was not possible to run *sederror* (no continuous sensor readings were available) and no other alternatives to estimate concentration were possible.

In regard to sediment rating curves, the confidence interval estimated by *sedcurve* was wider than for sensors and it includes the confidence interval assessed for sensors. A summary of sediment estimates for this event is presented in Table 4.29.

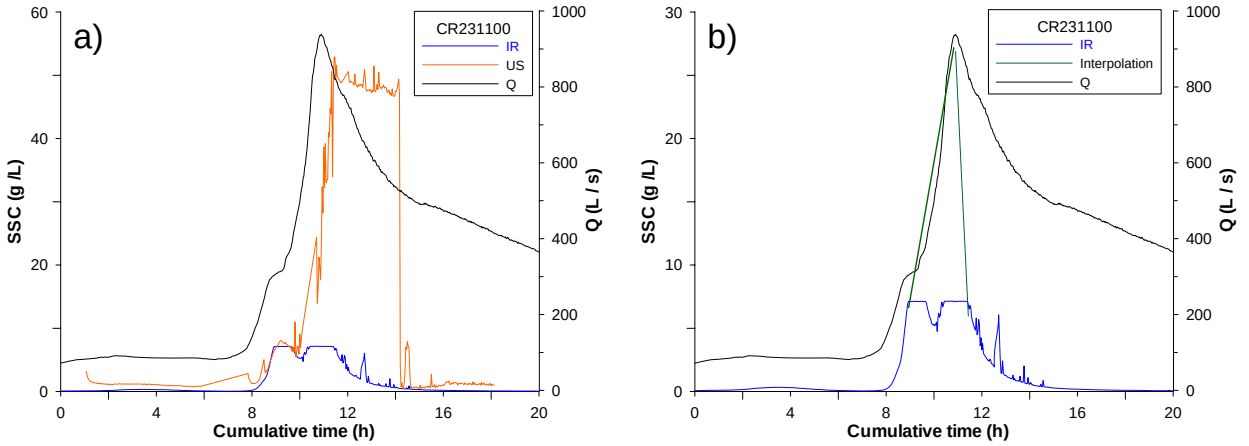

Figure 4.46: Suspended sediment concentrations for CR231100 by calibrations of sensors.

Table 4.29: Summary of SSL (Mg) estimations for event CR231100.

Method	**Lower bound**	**Average**	**Upper bound**	**Error** ±%
Sensors	101.3	106.6	112.0	5.0
MC annual SRC	33.9	182.0	1281.0	342.6
MC seasonal SRC	27.0	157.0	592.1	317.0

4.5.1.16 CR231200

During this flood episode no samples were collected. By applying the reference calibration to IR sensor readings it was obtained the curve shown in Fig. 4.47a, US sensor did not return reliable readings. IR sensor was saturated at around 6 g/L, hence for the missing segment (saturation) concentrations were obtained by drawing out the peak of concentrations until their intersections as it is shown in Fig. 4.47a. However, the maximun concentration obtained by doing so is ≈ 10 g/L, which is very low considering the high discharge values. Therefore, calibration done for event CR040697 for discharges higher than 2000 L/s was used, the new curve obtained is shown in Fig. 4.47b. Both curves were considered as the lower and upper bounds of the confidence interval.

The amount of sediment load transported during this event estimated by the means of sensors and, then performing linear interpolations was 1017.6 Mg, and its confidence interval is wide considering the relatively narrow intervals defined for previous episodes. On the other hand, the confidence interval defined for sediment rating curves are larger than for sensors ($> 300\%$).

The median estimate by annual sediment rating curve is 2.5 times higher than the mean estimated by sensor readings, and by seasonal rating curve is ≈ 2 times higher. A summary of sediment load estimations for this event is presented in Table 4.30.

4.5.1.17 CR180801

During the flood episode only five samples were collected, and they were not enough to obtain reliable calibrations at event scale. Hence the reference calibration of sensors were used, however

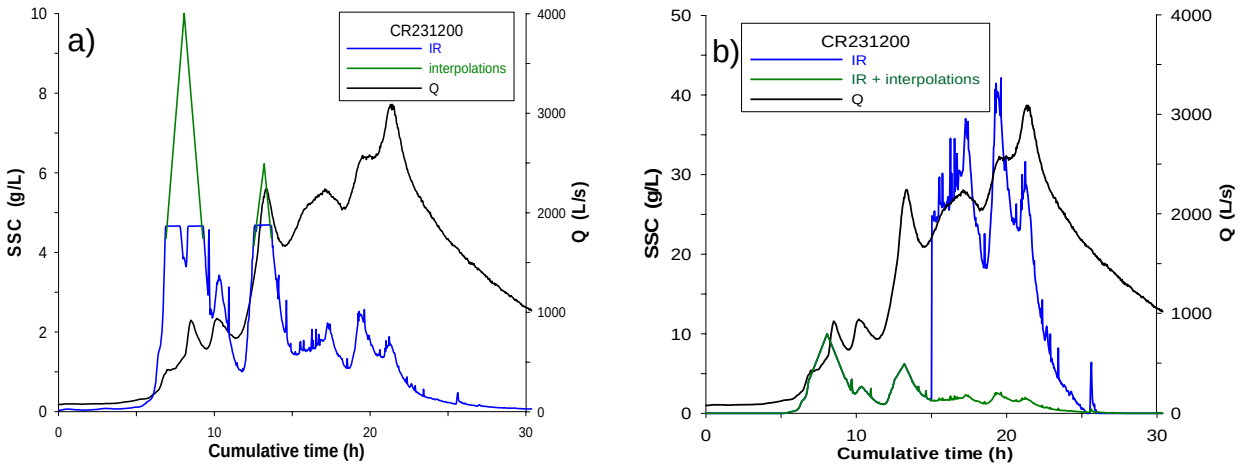

Figure 4.47: Suspended sediment concentrations for CR231200 by calibrations of sensors.

Table 4.30: Summary of SSL (Mg) estimations for event CR231200

Method	**Lower bound**	**Average**	**Upper bound**	**Error** ±%
Sensors	246.5	1017.1	1787.6	75.0
MC annual SRC	406.2	2470.0	17226.0	340.5
MC seasonal SRC	366.3	2044.0	12991.0	308.0

these did not perform well either, as it is shown in Fig. 4.48a.

In order to estimate sediment load two options were explored. The first, consisted of performing linear interpolations between: IR (left side on the plot) - US - interpolation between samples (the maximum concentration for this particular case was 103 g/L) - US - interpolation between lower values obtained with US (right side), and IR (left side) as it is shown in Fig. 4.48b.

The second alternative also shown in Fig. 4.48b, was based on the analyses of the distribution of samples on the plot. There are three samples ≈ 80 g/L, which indicate that indeed the sediment concentration was higher than ≈ 80 g/L. Additionally, in the plot for IR sensor there is a *valley* at around hour 11.2, which confirms that concentration was high at that moment (the IR sensor gives low values when oversaturated), but unfortunately, its peak is unknown. Therefore to solve this problem, the sediment concentration dataset the sub-catchment *Cal Isard* at that point in time was used as checklist, the sediment concentration in *Cal Isard* was ≈ 148 g/L; therefore, an inference has been made that at least such amount passed through *Cal Rodó*, under such assumption two interpolations were made.

During this event which had the shortest duration (15.77 h) among the events studied, the amount of sediment transported were: according to first alternative 221.3 Mg, and according to the second alternative 267.8 Mg. These two values were considered as the bounds of the confidence interval. The bounds estimated are 9.5% below and above the average value. The maximum concentration for the first alternative was 98 g/L and for the second the maximum concentration was 148 g/L. Most of the sediment for both alternatives, have been transported between hours 10.2 and 15.7 after the flood event had started.

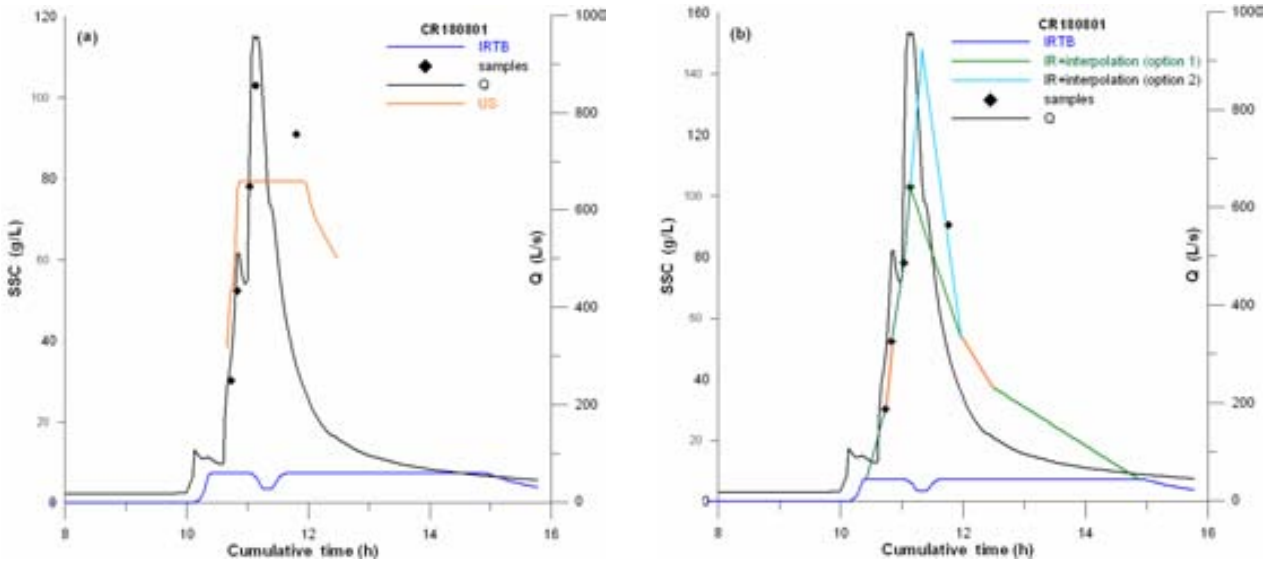

Figure 4.48: Suspended sediment concentrations for CR180801 by calibrations of sensors.

On the other hand, sediment estimates by rating curves differed significantly from each other; through annual SRC the estimated median was 17.6 Mg and by seasonal SRC was 109 Mg; their confidence intervals are far wider than the confidence interval defined for sensors.

A summary of sediment load estimates by the means of both methods studied is presented in Table 4.31.

Table 4.31: Summary of SSL (Mg) estimations for event CR180801.

Method	**Lower bound**	**Average**	**Upper bound**	**Error** ±%
Sensors	221.3	244.6	267.9	9.5
MC annual SRC	2.8	17.6	124.6	346.0
MC seasonal SRC	34.1	109.0	355.7	147.0

4.5.1.18 CR201001

The number of samples available for this event were 9, their distribution along the hydrograph coincide with peak of water discharge. Although the number of samples is not large, they are enough to make close estimation of sediment transport. At the beginning of the episode, ultrasound and infrared sensors worked correctly (Fig. 4.49a), however, at hour 42 US sensor got clogged and IR was saturated.

In order to assess the sediment load, it was used the IR reference calibration for IR and linear interpolations between consecutives samples (Fig. 4.49b). The confidence interval was estimated considering the variability of the SSL estimate (182 Mg) as an arbitrary 5%. On the other hand, load estimations performed by annual SRC was 1.3 times the estimated by sensor calibrations and 1.6 times with seasonal SRC, their confidence interval are much wider than the estimated for sensors.

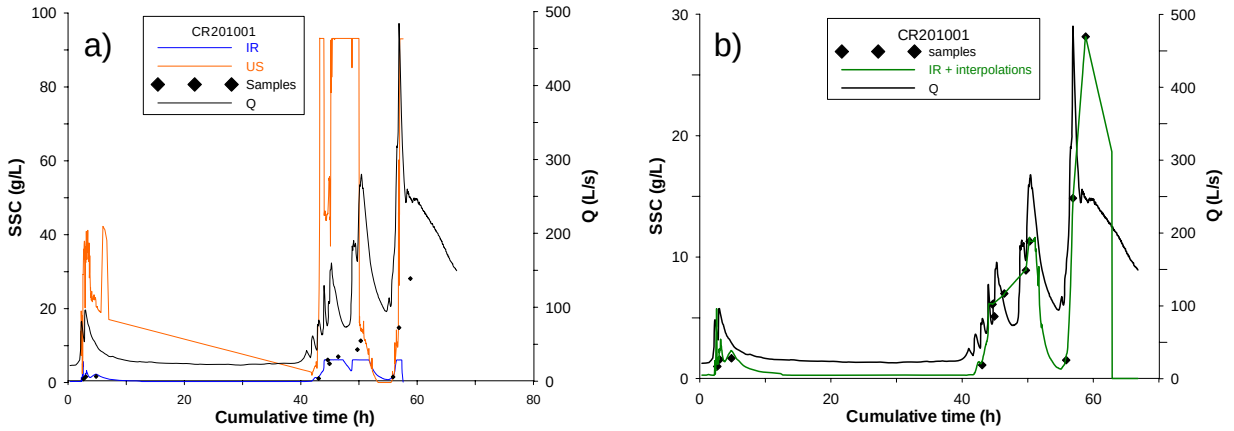

Figure 4.49: Suspended sediment concentrations for CR201001 by calibrations of sensors.

A summary of sediment load estimations are given in Table 4.32.

Table 4.32: Summary of SSL (Mg) estimations for event CR201001.

Method	**Lower bound**	**Average**	**Upper bound**	**Error** ±%
Sensors	164.0	173.0	182.0	5.0
MC annual SRC	6.9	42.0	296.0	344.5
MC seasonal SRC	6.6	37.0	237.8	312.4

4.5.1.19 CR070402

During this event 5 samples were collected, unfortunately all of them are located on the falling limb of the hydrograph (Fig. 4.50a). Using these samples sensor calibrations were performed, however the concentration for US sensor are high (> 70 g/L), hence the reference calibration was applied to sensor readings, and which has given concentrations less than 50 g/L for ultrasound sensor, the latter seems more reasonable considering the values of water discharge. IR sensor calibrations were not much different from each other.

In order to estimate the suspended sediment load carried out during this event two alternatives were identified. These are shown in Fig. 4.50b. The first, consists of taking the IR sensor calibration as reliable up to hour 37 and after hour 42. Between hours 37 and 38, US sensor calibration values were considered reliable; for the last section the IR sensor calibration values (left side of IRTB on Fig. 4.50b) were taken as reliable. The second alternative is taking the as valid the US sensor calibration between hours 37 and 42, and also the left and right side of IR sensor (on Fig. 4.50b labeled as option 2).

The amount of suspended sediment transport according to the first option was 505.3 Mg, and through the second alternative was estimated 529.3 Mg. These two values were considered as the limits of the confidence interval, where the average sediment load is 517.2 Mg. These bounds are 2.3% above and 2.3% below the average. The maximum concentration was 12 g/L for alternative one, and 27 g/L for alternative two.

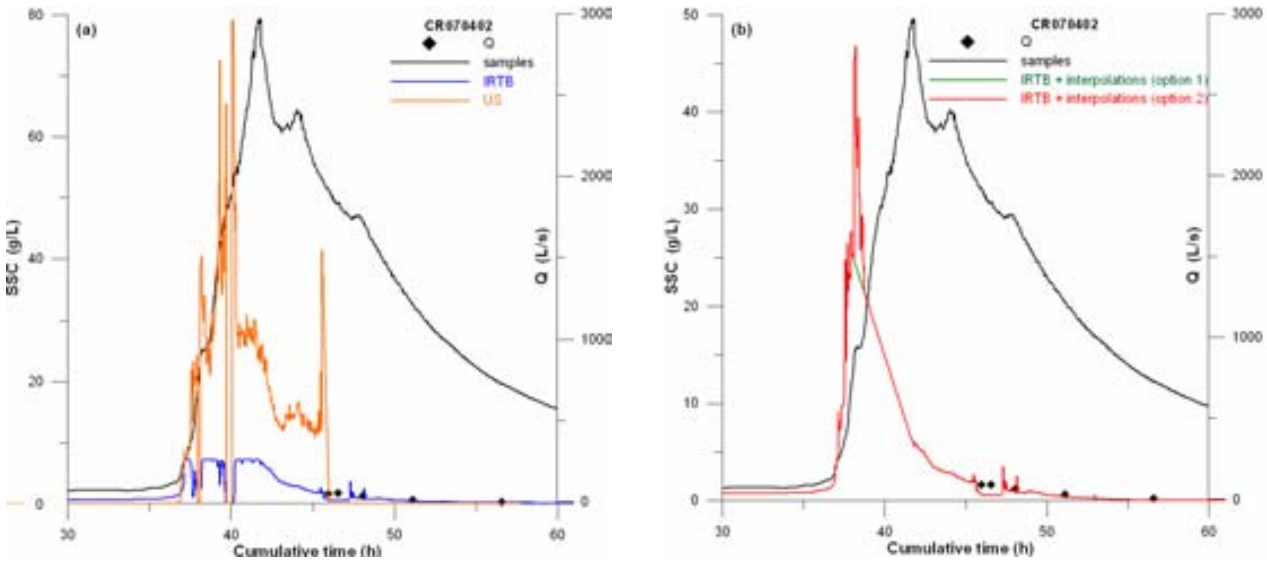

Figure 4.50: Suspended sediment concentrations for CR070402 by calibrations of sensors.

Sediment load estimated using the annual sediment rating curve was 14,279 Mg, and by the means of seasonal rating curve was 10,806 Mg; these values are much higher than the estimated by sensors (17 times with annual SRC). The confidence intervals also were wider than for sensors.

A summary of suspended sediment load estimates for this event are provided in Table 4.33.

Table 4.33: Summary of SSL (Mg) estimations for event CR070402.

Method	**Lower bound**	**Average**	**Upper bound**	**Error** ±%
Sensors	505.3	517.2	529.2	2.3
MC annual SRC	321.3	1983.0	14279.0	351.3
MC seasonal SRC	292.4	1652.0	10806.0	318.4

4.5.1.20 CR100402

During this event, 8 samples were collected. By applying the reference calibrations to sensor readings it was obtained the curves shown in Fig. 4.50a. Concentrations using the IR sensor calibration fit closely to the pattern of samples. On the other hand, concentrations obtained using the ultrasound sensor calibration presented high values. The most reliable concentration curve is the one performed for IR sensor, this was taken as the correct curve and it is shown in Fig. 4.50b.

Confidence interval of the sediment load estimate through sensors was obtained considering an arbitrary 5% variability. In regard to sediment rating curves, median load estimates for annual SRC was 38 times the estimate for sensors, and for seasonal SRC was 32 times larger, also the interval defined for SRC is above and outside the interval estimated for sensors.

A summary of load estimates and confidence intervals for both techniques studied are presented in Table 4.34.

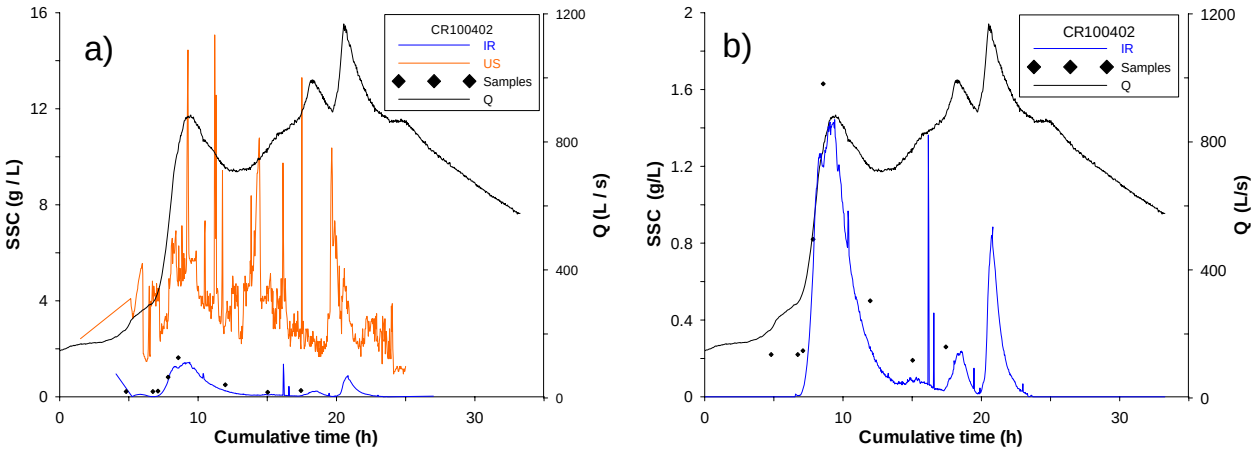

Figure 4.51: Suspended sediment concentrations for CR100402 by calibrations of sensors.

Table 4.34: Summary of SSL (Mg) estimations for event CR100402.

Method	**Lower bound**	**Average**	**Upper bound**	**Error** ±%
Sensors	16.2	17.0	18.0	5.0
MC annual SRC	107.4	653.0	4664.0	348.0
MC seasonal SRC	99.4	555.4	3599.0	315.1

4.5.1.21 CR091002

Nine samples were collected during this event, and they do not have a good spanning along the hydrograph. However, calibration using these samples and the reference calibrations for both sensors were obtained but none of them were reliable. The problem is that sensor readings were not reliable (Fig. 4.52). Ultrasound sensor got clogged early during the flood event and infrared sensor also stopped sending signals to datalogger.

Table 4.35: Summary of SSL (Mg) estimations for event CR091002.

Method	**Lower bound**	**Average**	**Upper bound**	**Error** ±%
MC annual SRC	76.1	481.0	3494.0	355.3
MC seasonal SRC	71.1	411.0	2714.0	321.5

In order to assess the sediment load transported during this flood, it was used the estimates given by Monte Carlo simulations of the distribution function of load given by rating curves. A summary of load estimates and its confidence intervals are given in Table 4.35.

4.5.1.22 CR280203

During this episode 15 samples were collected, and with them calibrations for both sensors were developed. In addition, reference calibrations were applied to sensors readings. In Fig. 4.53a it is shown the distribution of samples along the hydrograph, their pattern coincide with the pattern of

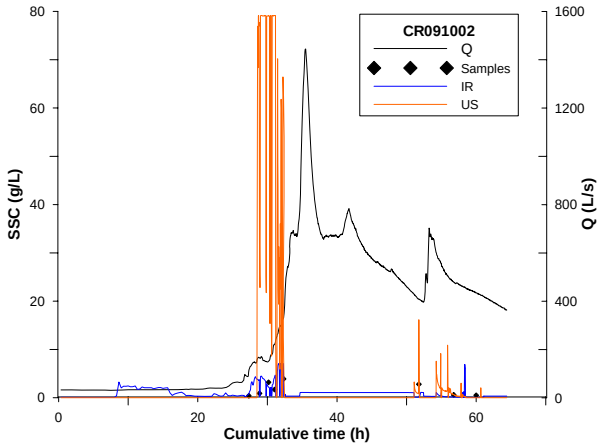

Figure 4.52: Suspended sediment concentrations for CR091002 by calibrations of sensors.

water discharge. With these samples sensor calibrations were performed as illustrated in Fig. 4.53a, which are not much different that the ones obtained while applying the reference calibrations.

Ultrasound sensor was clogged after hour 70 and the remainder segments gave high concentrations, which do not coincide with the pattern of samples. Therefore, the sediment load values were obtained by using concentrations given by IR sensor except the segment when it got saturated (between hours 72 to 74), for which, linear interpolations between samples were applied (Fig. 4.53b).

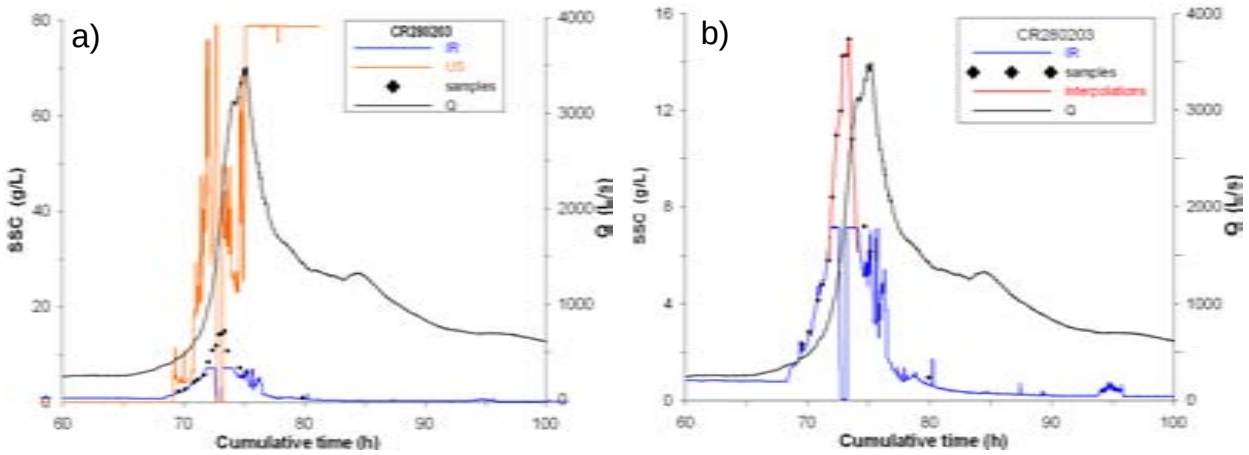

Figure 4.53: Suspended sediment concentrations for CR280203 by calibrations of sensors.

By the mean of IR sensor calibration and linear interpolations of samples, it was estimated a sediment load of 392.7 Mg, and its confidence interval was estimated by considering a 5% of variability. It was not possible to run *sederror* because no continuous sensor readings were available.

Sediment load estimates by means of annual and seasonal sediment rating curves, were 2,283 Mg and 1,906 Mg respectively, and its confidence intervals are much wider than the interval defined for sensors.

A summary of sediment load estimates for this event is presented in Table 4.36.

Table 4.36: Summary of SSL (Mg) estimations for event CR280203.

Method	Lower bound	Average	Upper bound	Error ±%
Sensors	373.1	392.7	412.3	5.0
MC annual SRC	382.3	2283.0	15680.0	335.0
MC seasonal SRC	347.5	1906.0	11905.0	303.2

4.5.1.23 CR311003

During this event 23 samples were collected, and they are well distributed along the hydrograph. Using these samples, calibrations for both sensors were performed, their curves are shown in Fig. 4.54a. Ultrasound sensor was clogged at least 4 times during the flood event (hours ≈ 2, 7, 11 and 20 on), on the other hand, infrared sensor performed well most of the time, except when it got saturated between hours ≈ 7 to 10.

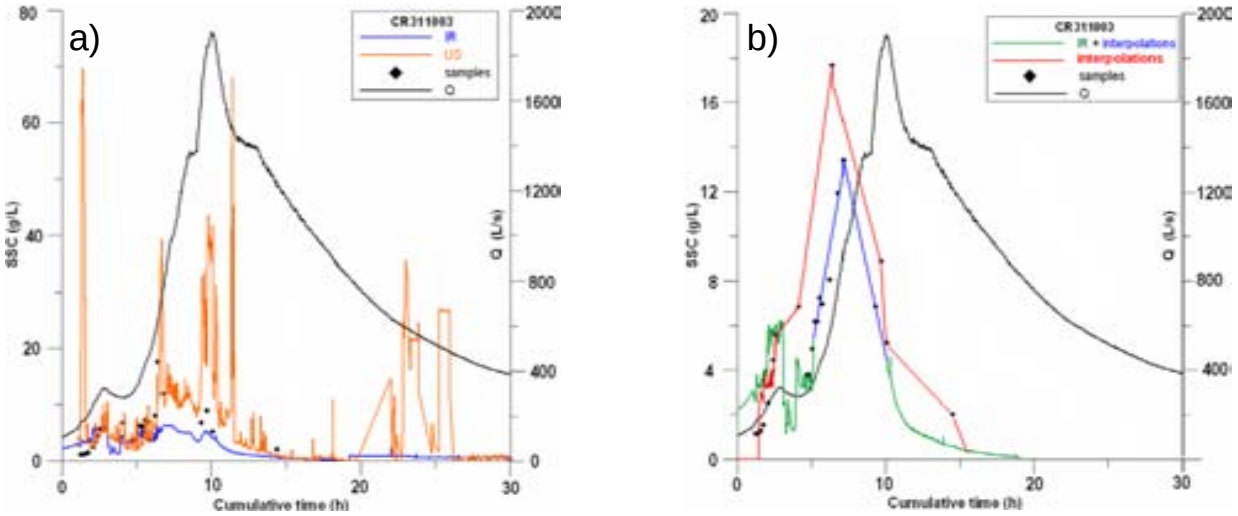

Figure 4.54: Suspended sediment concentrations for CR311003 by calibrations of sensors.

In order to estimate the sediment load by means of sensor readings, two alternatives were analysed. First, according to the pattern of samples the curve which closely estimates concentrations, is the calibration for infrared sensor, for the first alternative these concentrations were chosen, and for the time when it got saturated linear interpolations between consecutives samples were performed (on Fig. 4.54b labeled as "IR + interpolations"). The second alternative, consisted of selecting concentrations given by the calibration of ultrasound sensor between hours 2 and 3, and linear interpolations between samples (on Fig. 4.54b labeled as "interpolations").

This event had a duration of ≈ 60 hours, it transported an average 313.4 Mg of suspended sediment. Through the first alternative it has been estimated 256.4 Mg, and it was considered as the lower bound of the confidence interval. With the second alternative, it was estimated 370.4 Mg, which was considered as the upper bound of confidence interval. The bounds are 18% above and below the average.

In regard to sediment rating curves, annual SRC has given load estimates 3 times higher than the

Table 4.37: Summary of SSL (Mg) estimations for event CR311003.

Method	Lower bound	Average	Upper bound	Error ±%
Sensors	256.4	313.4	370.4	18.2
MC annual SRC	153.7	977.0	7058.0	353.3
MC seasonal SRC	142.0	824.0	5420.6	320.3

load estimated by sensors, and by seasonal SRC was 2.6 times. Confidence intervals for rating curves were assessed by Monte Carlo simulation and these were very wide, and they included the interval estimate for sensors.

A summary of sediment load estimates and its confidence intervals by the means of both techniques are presented in Table 4.37.

4.5.1.24 CR041203

For this event no samples were available. Aplying the reference calibrations of both sensors, it was obtained the concentration curves shown in Fig. 4.55a, considering the water discharge values, the sediment concentrations values are low. Infrared sensor performed well, until hour 18, and ultrasound sensor calibration curve is reliable between hours 7 and 21.

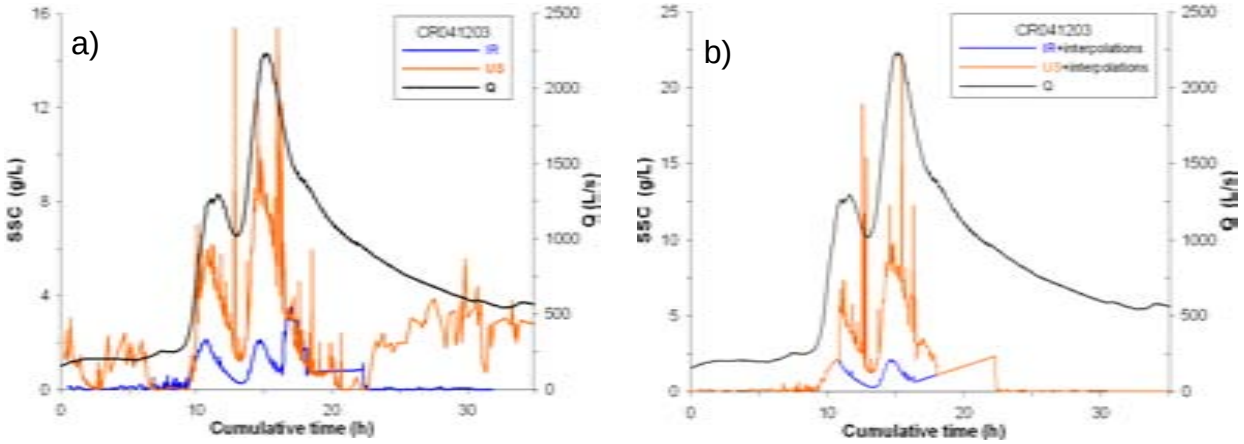

Figure 4.55: Suspended sediment concentrations for CR041203 by calibrations of sensors.

Sediment load was estimated by using the two curves presented on Fig. 4.55b, two alternatives were possible, as the lower bound of the confidence interval it was used the curves labeled as "IR + interpolation", and as the upper bound was used the curve labeled as "US + interpolations".

Table 4.38: Summary of SSL (Mg) estimations for event CR041203.

Method	Lower bound	Average	Upper bound	Error ±%
Sensors	80.0	152.0	224.0	47.4
MC annual SRC	191.4	1210.0	8396.0	339.0
MC seasonal SRC	176.1	839.6	6434.0	372.7

Through sensor calibrations and interpolations it was estimated 152 Mg, and its confidence interval was 47% above and below the average value. Load estimates by rating curves are 8 and 5.5 times larger than the estimated by sensors. The upper segment of the confidence interval defined for sensors are within the interval defined for sediment rating curves. A summary of load estimates and confidence intervals are given in Table 4.38.

4.5.1.25 CR310304

No samples were collected during this event, and no sensor readings were reliable. Despite the infrared sensor sent signals readings these were not reliable, apparently the sensor was clogged during almost the entire event, except during a few minutes at around hour 15, but these were not enough to draw a concentration curve. Therefore, only sediment rating curves were performed to make load estimations, these are presented in Table 4.39, similar to the events studied so far, the confidence intervals are higher than 300%.

Table 4.39: Summary of SSL (Mg) estimations for event CR310304.

Method	**Lower bound**	**Average**	**Upper bound**	**Error** ±%
MC annual SRC	135.0	838.0	6052.0	353.0
MC seasonal SRC	124.0	704.0	4642.0	321.0

4.5.1.26 CR050804

Fifteen samples were collected during this flood episode. Using these samples sensor calibrations were performed (Fig. 4.56a), concentrations given by ultrasound sensor calibration were reliable between hours 1 - 1.8, and after hour 2.2 no reliable readings for this sensors were available. In regard to infrared sensor readings, these were saturated early during the episode and performed well after hour 4.2. In Fig. 4.56a two sets of samples can be observed, one set is characterized by high concentrations, and they are located in between the US and IR curves.

In order to calculate the sediment transport during this event, two alternatives were identified. The first is considering the US concentration curve as reliable, and for the segments where concentration data were missing, it was performed linear interpolations between reliable data points, in Fig. 4.56b is labeled as "IR + US + interpolations". The second alternative consists of ignoring the US curve instead IR curve, is chosen and linear interpolations between samples are performed, this curve is shown in Fig. 4.56b and labeled as "IR + interpolations".

Through the first alternative it was estimated 541.9 Mg, and by the second alternative 602.8 Mg. These two estimations were considered as the bounds of the confidence interval.

Table 4.40: Summary of SSL (Mg) estimations for event CR050804.

Method	**Lower bound**	**Average**	**Upper bound**	**Error** ±%
Sensors	542.0	572.3	876.0	5.3
MC annual SRC	89.0	540.0	3743.0	338.0
MC seasonal SRC	609.6	1846.0	6172.2	150.7

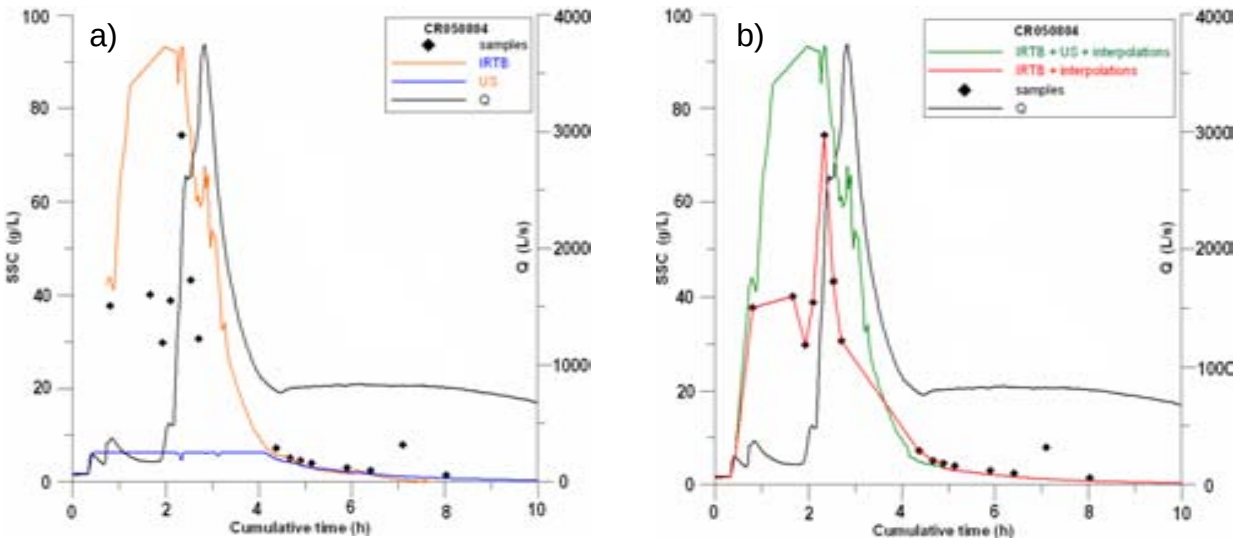

Figure 4.56: Suspended sediment concentrations for CR050804 by calibrations of sensors.

On the other hand, sediment load estimations through rating curves were close to the load estimate by sensors especially the estimate by the annual rating curve, the estimate by seasonal sediment rating curve was ≈ 3 times the estimate by sensors, their confidence intervals are wider than for sensors, however, it includes the interval defined for sensors.

A summary of sediment load estimates and its confidence intervals are given in Table 4.40.

4.5.1.27 CR141005

During this event 15 samples were collected, although 10 of these samples are located on the falling limb of the hydrograph, and they present concentrations less than 5 g/L; the remainder 5 samples have concentrations higher than 25 g/L. By applying the reference calibrations and performing separate calibrations using samples for this event, it was not found significant differences between both curves.

The reference calibration curves are shown in Fig. 4.57a, both sensors started to send reliable information after hour 2, and their concentrations are similar to the ones obtained by sampling. Therefore, in order to assess the sediment load transport, it was considered as valid the last segment (after hour 3) of infrared sensor calibration and for ultrasound sensor, between hours 2.6 and 3, for the rest of the time linear interpolations between samples were performed (Fig. 4.57b).

Table 4.41: Summary of SSL (Mg) estimations for event CR141005.

Method	**Lower bound**	**Average**	**Upper bound**	**Error** ±%
Sensors	990.0	1,042.0	1,094.0	5.0
MC annual SRC	461.0	2,812.0	20,779.0	361.3
MC seasonal SRC	415.0	2,319.0	15,566.0	326.0

On the other hand, sediment load estimated by annual and seasonal rating curves are 2.7 and 2.2

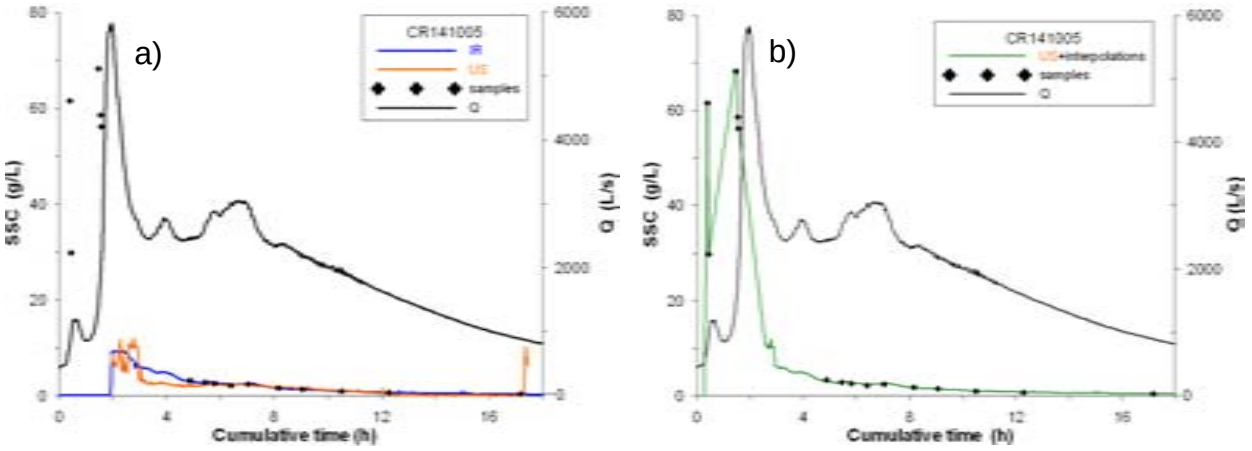

Figure 4.57: Suspended sediment concentrations for CR141005 by calibrations of sensors.

times larger than the estimate by sensors respectively.

A summary of these estimates are presented in Table 4.41. The confidence interval for the load estimate by sensors and interpolations, was estimated by considering an arbitrary variability of 5%, *sederror* was not used because continuous sensor readings were unavailable.

4.5.2 Suspended sediment yield and confidence intervals for the whole period

There are some considerations that need to be addressed before estimating the total sediment yield (for the 10 years period). The quality of sediment load estimations are accurate, if sediment concentration is calculated based on a very good spanning of samples along the entire hydrograph, it this is not possible, at least during the peak of water discharge they must be guaranteed, which can give a hint of the true pattern of suspended sediment concentration. However, collecting too many samples may not be always the ideal if it is looked from the economic point of view, because this might not be efficient while allocating resources of a project, therefore, defining an adequate sampling frequency is crucial in order to not lose the quality of the sediment load estimations.

Below, the sediment yield and its 90% confidence interval for each method (sensor calibrations and sediment rating curves) is described, summarized, compared and discussed.

4.5.2.1 Sensors

The total average suspended sediment yield (SSY) estimated by calibrations of sensors and linear interpolations between discrete samples, for the studied period (1996 - 2005) was assessed by summing the sediment load obtained for every event (SSL_j), which can be expressed as in Eq. 4.26, where j represents a given event and goes from 1 to 27.

$$SSY = \sum_{j=1}^{n=27} SSL_j \tag{4.26}$$

The confidence interval of the average SSY (j) for the whole period, was assessed by assuming that the errors of sediment load estimates at event scale and for the set of events are normally distributed. Therefore for this type of distribution, the load error with 90% of confidence can be estimated through Eq. 4.27, where e_{90} is the difference between the average suspended sediment load and the limits of the confidence interval with a 90% of confidence level expressed in Mg. This means that with a 1.64 standard deviation, 90% of sediment estimates will be found within this range; and σ is the standard deviation, which is unknown.

$$e_{90} = \pm 1.64\sigma \tag{4.27}$$

The confidence interval of the average suspended sediment load estimate for the whole period was estimated, first by calculating the σ_j and σ_j^2 for each flood episode, and second by calculating the variance for the whole period σ_{total}^2 by averaging the σ_j^2 (27 events). This error propagation can be mathematically expressed as in Eq. 4.28.

$$\sigma_{total}^2 = \frac{1}{n}\sum_{j=1}^{n=27}\sigma_j^2 \tag{4.28}$$

By means of sensor calibrations, the average amount of suspended sediment transported during the 27 biggest flood episodes was 17,353 Mg. The total error (e_{90}) was 1,042 Mg with 90% of confidence. The confidence interval for the whole period, lies between 16,311 Mg and 18,395 Mg which represents 6% above and below the average estimate.

A summary of errors e_{90}, standard deviation σ_j, variance σ_j^2, σ_{total}^2 and confidence intervals for individual events, and for the entire period studied is summarized in Table 4.42.

4.5.2.2 Sediment rating curves

Sediment load obtained by sediment rating curves are very different from the estimates from sensors and interpolations for the same event, and for the entire period. Estimations obtained by the traditional sediment rating curve (without bias correction), has shown that sediment load estimates are overestimated for large events and underestimated for small events in most of the cases (Table 4.43). However, after applying the smearing correction (Duan, 1983) these estimates are much higher than the estimates obtained by sensor calibrations. This fact is well documented in the literature and the studied events have similar outcome patterns.

The main problem while using sediment rating curves is the definition of the confidence intervals for the average load estimate, that is why Monte Carlo approaches were used to assess the confidence intervals; however, the confidence intervals assessed by Monte Carlo simulations of the distribution function of sediment load (at the annual scale and without distinguishing differences between samples among events and samples within each event) presented a very wide range.

The load estimate by Monte Carlo simulation of the distribution function of the total SSL was 103,441 Mg, and its confidence interval with 90% of confidence was between 49,107 Mg and 254,803

Table 4.42: Confidence interval for SSL estimate by calibration of sensors (90% confidence).

Name of the event	Average (Mg)	Lower bound (Mg)	Upper (Mg)	Difference ± %	Error ± Mg	σ	σ^2
CR220196	976.5	455.0	1,498.0	53.4	521.5	317.0	101,116.2
CR220496	83.0	79.0	87.0	4.8	4.0	2.4	5.9
CR141096	98.0	93.0	103.0	5.1	5.0	3.0	9.3
CR111196	501.0	321.0	644.0	32.2	161.5	98.2	9,638.6
CR040697	2,046.5	1,944.0	2148.0	5.0	102.0	62.0	3,844.8
CR051197	14.1	13.3	14.7	5.0	0.7	0.4	0.2
CR171297	6,433.0	6,111.0	6,755.0	5.0	322.0	196.0	38,316.0
CR070599	57.0	51.0	63.0	10.5	6.0	3.6	13.3
CR280899	1023.4	1002.7	1044.2	2.0	20.8	12.6	159.1
CR140999	108.0	61.0	156.0	44.0	47.5	28.9	833.8
CR190999	638.5	606.6	670.4	5.0	31.9	19.4	376.1
CR121199	474.5	286.0	663.0	39.7	188.5	114.9	13,130.8
CR280900	124.0	97.0	151.0	21.8	27.0	16.4	269.0
CR231100	106.6	101.3	111.9	5.0	5.3	3.2	10.4
CR231200	1,017.1	246.5	1,787.6	75.8	770.6	468.4	219,428.1
CR010301	92.0	90.0	93.7	2.0	1.9	1.1	1.3
CR180801	244.6	221.3	267.9	9.5	23.3	14.2	200.6
CR201001	173.0	164.0	182.0	5.2	9.0	5.5	29.9
CR070402	517.2	505.3	529.2	2.3	12.0	7.3	52.8
CR100402	17.0	16.2	17.9	5.0	0.9	0.5	0.3
CR280203	392.7	373.1	412.3	5.0	19.6	11.9	142.0
CR311003	313.4	256.4	370.4	18.2	57.0	34.8	1,200.7
CR041203	152.0	80.0	224.0	47.4	72.0	43.9	1,915.7
CR050804	709.0	541.9	876.0	23.6	167.1	101.6	10,312.4
CR141005	1,042.0	990.0	1,094.0	5.0	52.0	31.6	999.3
Summary	17,353.6	17,353.0	17,554.2	1.2	200.6	121.9	14,866.5

Mg, indicating a difference of 102,848 Mg between both limits. The difference between the lower and upper bounds of the confidence interval at the event scale in all the cases, are higher than 330%, however this difference is smaller (99%) for the whole period (Table 4.44). The estimates obtained by Monte Carlo simulations are log-normally distributed, which made the median being strongly asymmetric and is it skewed towards the lower limit of the confidence interval.

In Table 4.44 a summary of the confidence intervals for annual rating curves at event scale and whole period is given.

On the other hand, sediment load estimated by performing a Monte Carlo simulation of the distribution function of load obtained by seasonal rating curves was 88,302 Mg, and its confidence interval with 90% of confidence lies between 49,099 Mg and 197,038 Mg, indicating a difference of 73,969 Mg between both limits.

The difference between the lower and upper bounds of the confidence intervals at the event scale in all the cases are higher than at least 140%, however this difference is smaller (84%) for the entire period.

Table 4.43: Suspended sediment load transported by the 27 biggest flood episodes.

Event name	Duration (h)	SSL (Mg)			
				Conventional	
		First raw SSL approach	Sensors and interpolations	annual SRC [a]	aeasonal SRC [b]
CR220196	144.2	1,026.9	976.5	12,862.0	10,506.0
CR220496	198.0	281.3	83.0	220.4	128.3
CR141096	44.1	315.1	98.0	190.0	165.5
CR111196	30.9	551.9	501.0	933.5	790.7
CR040697	104.4	2,494.3	2,046.5	2,128.3	1,762.4
CR051197	83.9	49.2	14.1	8.8	8.0
CR171297	89.5	4,534.7	6,433.0	9,417.1	7,723.0
CR070599	80.4	106.8	57.0	47.4	42.3
CR280899	44.2	278.1	1023.0	194.3	482.0
CR140999	84.9	151.9	108.0	167.8	843.0
CR190999	102.1	518.6	638.5	3,883.0	2,527.6
CR121199	4.4	1,138.2	474.5	971.4	798.0
CR280900	51.6	348.7	124.0	64.1	56.6
CR231100	31.7	385.3	106.5	111.6	97.2
CR231200	30.4	1,833.5	1,017.1	1,534.8	1,287.1
CR010301	46.3	89.9	92.0	57.3	50.4
CR180801	15.7	264.8	244.6	11.1	57.0
CR201001	66.8	62.4	173.0	26.0	23.2
CR070402	71.1	1,308.2	517.2	1,226.6	1,030.8
CR100402	33.3	132.0	17.0	405.1	348.2
CR091002	64.4	133.5	-	297.0	256.7
CR280203	117.3	483.0	392.7	1,407.8	1,188.8
CR311003	313.4	563.1	313.4	600.2	512.9
CR041203	24.8	144.0	152.0	746.7	636.0
CR310304	38.1	62.4	-	516.5	440.4
CR050804	24.5	737.9	709.0	338.6	968.0
CR141005	25.3	1,785.9	1,042.0	1,774.0	1,479.1

[a] *Without smearing correction factor (m = 2.51)*

[b] *Without smearing correction factor (for summer m = 2.22 and for autumn, winter and spring m = 2.33)*

The distribution of sediment load derived from Monte Carlo simulations are log-normally distributed, therefore the median is also asymmetric and strongly skewed towards the lower bound of the confidence interval.

In Table 4.45, a summary of the confidence intervals for seasonal rating curves at event scale and the whole period obtained by Monte Carlo simulation are presented.

Table 4.44: Bounds for SSL using annual SRC (90% confidence).

Name of the event	SSL average (Mg)	Lower bound (Mg)	Upper bound (Mg)	Difference (± %)	Error (± Mg)
CR220196	20573.0	3409.0	149640.0	355.4	73115.5
CR220496	357.6	57.0	2516.0	343.8	1229.5
CR141096	307.0	49.7	2217.0	353.8	1083.0
CR111196	1526.0	242.0	10966.0	351.4	5362.0
CR040697	3514.0	653.0	24330.0	336.9	11838.5
CR051197	14.2	2.3	99.1	340.8	48.4
CR171297	15290.0	2474.0	108736.0	347.5	53131.0
CR070599	76.7	12.5	545.6	347.5	266.6
CR280899	302.0	49.4	2185.4	353.6	1068.0
CR140999	269.0	43.7	1863.0	338.2	909.7
CR190999	1535.0	241.6	11048.0	352.0	5403.2
CR121199	6223.0	1016.0	43577.0	342.0	21280.5
CR280900	104.0	747.1	747.1	351.4	365.5
CR231100	182.0	33.9	1281.0	342.6	623.6
CR231200	2470.0	406.2	17226.0	340.5	8409.9
CR010301	92.2	15.0	662.7	351.2	323.9
CR180801	17.6	2.8	124.6	346.0	60.9
CR201001	42.0	6.9	296.3	344.5	144.7
CR070402	1983.0	321.0	14279.0	351.9	6978.9
CR100402	653.0	107.4	4664.0	348.9	2278.3
CR091002	481.0	76.1	3494.0	355.3	1709.0
CR280203	2283.0	382.3	15680.0	335.0	7648.9
CR311003	977.0	153.7	7058.0	353.3	3452.2
CR041203	1210.0	191.4	8396.0	339.0	4102.3
CR310304	838.0	135.0	6052.0	353.0	2958.5
CR050804	540.0	89.0	3743.0	338.3	1827.0
CR141005	2812.0	461.0	20779.0	361.3	10159.0
Summary	103,441.0	49,107.0	254,803.0	99.4	102,848.0

4.5.2.3 Comparison of techniques

Sediment load obtained by calibrations of sensors and sediment rating curves presented large differences (Tables 4.44 and 4.45), not only in the average estimate, but also on the magnitude of their confidence intervals. Clearly, sediment rating curves overestimated the sediment load in most of events. The median of sediment load obtained by annual rating curve is higher in 21 events than the values obtained from sensor calibrations. Three episodes presented higher sediment load values obtained from sensor calibrations than the values obtained from rating curves, this happened to events with low load transport. The average estimate for the whole period by annual rating curve is 6 times the estimate by sensors.

A comparison of load estimates from both techniques is illustrated in Table 4.46. There are 2 events out of 27 events which do not have load estimates by sensors because samples were unavailable, therefore only load calculated from rating curves are given.

Table 4.45: Bounds for SSL using seasonal SRC (90% confidence).

Name of the event	SSL average (Mg)	Lower bound (Mg)	Upper bound (Mg)	Difference (± %)	Error (± Mg)
CR220196	16,602.0	3,006.0	10,9860.0	321.8	53,427.0
CR220496	304.0	53.0	1,953.0	312.5	950.0
CR141096	264.0	46.6	1,737.0	320.2	845.2
CR111196	1,276.0	221.7	8,335.0	317.0	4,056.7
CR040697	2,868.0	473.0	18,107.0	307.4	8,817.0
CR051197	12.7	2.2	81.0	310.2	39.4
CR171297	12,454.0	2,184.0	80,162.0	313.1	38,989.0
CR070599	67.0	12.0	473.2	317.1	212.6
CR280899	907.0	297.1	3,095.0	154.2	1,399.0
CR140999	1,630.0	518.0	5265.0	145.6	2,373.5
CR190999	4,833.0	1,579.3	16,145.0	150.7	7,282.0
CR121199	5,117.0	911.9	32,707.0	310.7	15,897.6
CR280900	91.0	15.4	592.1	316.9	288.4
CR231100	157.0	27.0	1,003.0	310.8	488.0
CR231200	2,044.0	366.3	12,991.0	308.8	6,312.4
CR010301	80.1	14.2	524.2	318.4	255.0
CR180801	109.0	34.1	355.7	147.5	160.8
CR201001	37.0	6.6	237.8	312.4	155.6
CR070402	1,652.0	292.4	10,806.0	318.2	5,256.8
CR100402	555.4	99.4	3,599.0	315.1	1,749.8
CR091002	411.0	71.1	2,714.0	321.5	1,321.5
CR280203	1,906.0	347.5	11,905.0	303.2	5,778.8
CR311003	824.0	142.0	5,420.6	320.3	2,639.3
CR041203	839.6	176.1	6,434.0	372.7	3,129.0
CR310304	704.0	124.0	4,642.0	320.9	2,259.0
CR050804	1,846.0	609.6	6,172.2	150.7	2,781.3
CR141005	2,319.0	415.0	15,566.0	326.0	7,575.5
Summary	88,302.0	49,099.0	197,038.0	83.8	73,969.5

Similarly, suspended sediment load obtained by seasonal sediment rating curve is higher than the estimate by sensor in 23 episodes. Nevertheless, these estimates are slightly lower than the values obtained by annual sediment rating curve except for 2 episodes, where seasonal estimates are higher than the estimates on the annual basis. The average load estimate by seasonal rating curve is 5.1 times the estimate by sensors.

A summary of the differences between sediment load by seasonal sediment rating curve and sensor calibrations is illustrated in Table 4.46.

In regard to confidence intervals, annual sediment rating curves presented wider ($> 300\%$) confidence intervals than the intervals defined for load estimates by sensor calibrations ($< 76\%$). The confidence interval defined for sediment rating curve (Monte Carlo simulation) included the confidence interval defined for sensors calibrations, except for 4 episodes (CR220196, CR231200, CR100402, CR310304), where confidence intervals for estimates by sensors calibration are totally outside the interval defined for annual rating curve, and for 1 episode (CR041203) the upper bound

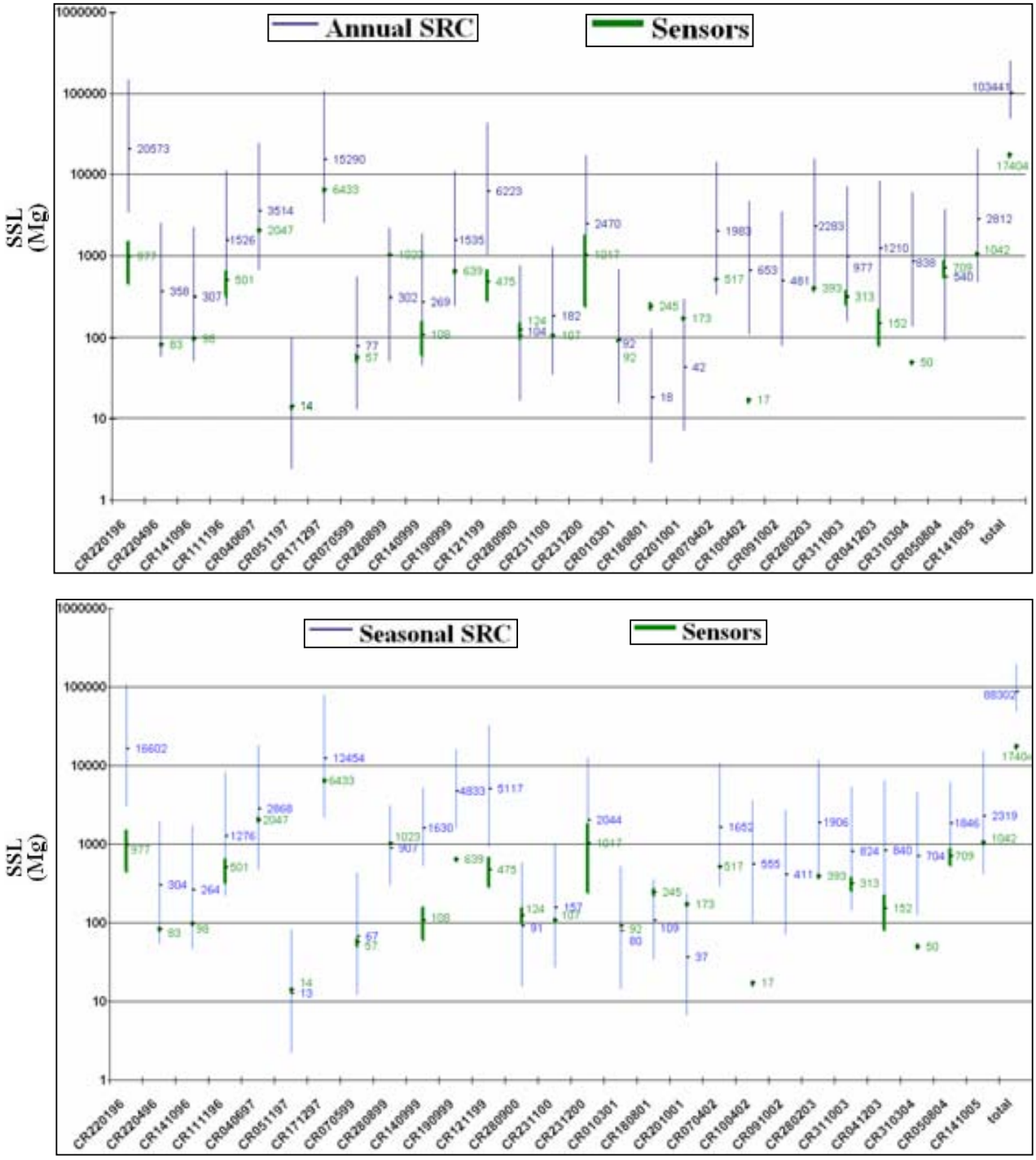

Figure 4.58: Comparison of the confidence intervals of suspended sediment load obtained by sensor calibrations, and annual (a) and (b) seasonal sediment ratings curves, at event scale and whole period.

Table 4.46: Comparison of SSL values obtained by sensors calibration and annual SRC.

Event name	Annual SRC	Seasonal SRC	Sensor	Ratio Annual SRC/sensor	Ratio Seasonal SRC/sensor
CR220196	20573	16602.0	976.5	21.1	17.0
CR220496	357.6	304.0	83.0	4.3	3.7
CR141096	307.0	264.0	98.0	3.1	2.7
CR111196	1526.0	1276.0	501.0	3.0	2.5
CR040697	3514.0	2868.0	2046.5	1.7	1.4
CR051197	14.2	12.7	14.1	1.0	0.9
CR171297	15290.0	12454.0	6433.0	2.4	1.9
CR070599	76.7	67.0	57.0	1.3	1.2
CR280899	302.0	907.0	1023.0	0.3	0.9
CR140999	269.0	1630.0	108.0	2.5	15.1
CR190999	1535.0	4833.0	638.5	2.4	7.6
CR121199	6223.0	5117.0	474.5	13.1	10.8
CR280900	104.0	91.0	124.0	0.8	0.7
CR231100	182.0	157.0	106.6	1.7	1.5
CR231200	2470.0	2044.0	1017.1	2.4	2.0
CR010301	92.2	80.1	92.0	1.0	0.9
CR180801	17.6	109.0	244.6	0.1	0.4
CR201001	42.0	37.0	173.0	0.2	0.2
CR070402	1983.0	1652.0	517.2	3.8	3.2
CR100402	653.0	555.4	17.0	38.4	32.7
CR091002	481.0	411.0	-	-	-
CR280203	2283.0	1906.0	392.7	5.8	4.9
CR311003	977.0	824.0	313.4	3.1	2.6
CR041203	1210.0	839.0	152.0	8.0	5.5
CR310304	838.0	704.0	-	-	-
CR050804	540.0	1846.0	572.3	0.9	3.2
CR141005	2812.0	2319.0	1042.0	2.7	2.2
summary	103,441.0	88,302.0	17,217.0	6.0	5.1

of confidence interval for sensors was included in the interval for annual rating curve.

Finally, the confidence interval of annual sediment rating curve defined for the whole period investigated, is higher and outside the interval defined for sensors. An illustration of confidence intervals of the estimates defined by annual sediment rating curve is presented in Fig. 4.58a.

Similarly, the confidence intervals defined for seasonal rating curves are higher than the interval defined by sensors, except for 6 events (CR2201096, CR140999, CR121199, CR190999, CR100402 and CR310304) and for 1 event (CR231200) its upper limit fell within the confidence interval for seasonal rating curve. An illustration of confidence intervals of estimates defined by seasonal rating curve is presented in Fig. 4.58b.

Two episodes (CR220196 and CR171297) have contributed largely to the total sediment yield in both, annual and seasonal rating curves, these are shown in Tables 4.44 and 4.45. While removing the biggest sediment contributor (CR220196) the total sediment yield decreased by 30% (from 103,441 Mg to 73,416) for annual rating curve, and it decreased by 27% (from 88,302 Mg to 64,458 Mg) for seasonal rating curve. The reduction while removing two of the biggest episodes were 52% and 44% for annual and seasonal rating curves respectively.

The difference between the total load from rating curve and load values by sensors after removing the two biggest events gets smaller. For instance by removing CR220196, the ratios are 4.4 and 4.0 for annual and seasonal rating curves respectevily; while removing both episodes, the ratios are 4.9 and 4.8 for annual and seasonal rating curves respectively. The confidence intervals are also narrower than considering the whole set of episodes. Nevertheless, the estimates by sensors are still below and outside the estimates by rating curves.

4.5.2.4 Sediment Rating Curves by splitting hydrographs

In an attempt to analyse the large differences between sediment loads obtained by sediment rating curves and calibration of sensors, separate rating curves for each limb of the hydrograph were developed.

First, a test using samples from event CR010301 was conducted in order to determine if developing separate rating curves for each segment of the hydrograph improved the sediment load estimates, results have shown that estimations are improved. Therefore, it was assumed that this might be also valid for the remainder episodes as well. Individual SRC were obtained for each limb of the hydrograph for each event, splitting the hydrograph is backed up by an ANOVA test of residuals (null hypothesis: one SRC is equal than having two SRC's). ANOVA results have shown that, for all events developing one SRC for each limb of hydrograph improved SSL estimates. In Table 4.47 are shown the constant and exponent of SRC's, r^2 and other statistical parameters of ANOVA ($\alpha = 0.05$) tests for each event.

Table 4.47: Statistical parameters of SRC's by splitting hydrographs.

Event	Whole hydrograph			Rising limb			Falling limb			$F_{0.05}$	p
	a	b	r^2	a	b	r^2	a	b	r^2		
CR220496	7.10^{-7}	3.08	0.82	6.10^{-4}	2.28	0.82	3.10^{-5}	2.22	0.85	70.0	< 0.01
CR141096	8.10^{-3}	1.77	0.69	7.10^{-3}	2.25	0.98	6.8	0.93	0.26	16.0	0.02
CR111196	1.10^{-2}	1.87	0.86	8.10^{-4}	2.43	0.97	150.0	0.47	0.49	25.8	< 0.01
CR040697	2.10^{-2}	1.94	0.97	8.10^{-3}	2.10	0.99	30.9	0.92	0.75	52.0	< 0.01
CR051197	3.10^{-4}	2.74	0.92	4.10^{-4}	2.73	0.94	7.10^{-8}	4.53	5.05	0.17	< 0.01
CR171297	3.10^{-4}	2.34	0.90	-	-	-	-	-	-	-	-
CR070599	6.10^{-6}	3.40	0.99	-	-	-	-	-	-	-	-
CR280899	4.10^{-3}	2.27	0.90	-	-	-	-	-	-	-	-
CR121199	3.10^{-5}	2.72	0.96	-	-	-	-	-	-	-	-
CR280900	4.10^{-3}	2.12	0.13	1.46	1.43	0.91	1.10^{-10}	4.96	0.54	35.5	< 0.01
CR010301	7.10^{-4}	2.52	0.75	3.10^{-4}	2.72	0.74	4.10^{-13}	5.96	0.74	118.5	< 0.01
CR201001	1.10^{-2}	2.24	0.78	-	-	-	-	-	-	-	-
CR070402	7.10^{-5}	1.85	0.98	-	-	-	-	-	-	-	-
CR100402	9.10^{-3}	1.60	0.53	4.10^{-5}	2.54	0.80	9.10^{-3}	1.60	0.59	5.1	0.03
CR091002	6.10^{-1}	1.13	0.21	-	-	-	-	-	-	-	-
CR280203	1.10^{-2}	1.57	0.70	-	-	-	-	-	-	-	-
CR311003	1.10^{-1}	1.61	0.77	2.10^{-2}	1.92	0.86	8.10^{-7}	3.07	0.99	13.6	< 0.01
CR050804	1.10^{1}	0.98	0.27	23.2	1.08	0.95	2.10^{28}	-8.53	0.17	89.0	< 0.01
CR141005	6.10^{5}	-0.26	0.40	6.4	1.29	0.67	4.10^{-6}	2.68	0.94	478	< 0.01

For this analysis only 19 events were included, because the remainder 8 events do not have samples

on both segments of the hydrograph. For each event, 3 SRC's were developed: one for the entire hydrograph (episode), one for the rising limb, and another for the decreasing limb of the hydrograph.

Also 3 SRC's for the whole set of events (19) were developed, using 262 samples. Many events only had samples on the rising limb of the hydrograph. The parameters of these rating curves are illustrated in Table 4.48.

Table 4.48: SRC parameters by splitting the hydrograph.

					Residuals	
SRC	a	b	r^2	n	Std. dev.	Mean
Whole hydrograph	0.0154	1.863	0.65	262	1.53	0.00
Rising limb	0.0113	1.978	0.78	178	1.12	0.00
Decreasing limb	0.0007	2.172	0.65	84	1.61	0.00

Nevertheless, the main purpose is to find relationships that can be applied for events without samples. Therefore in order to define whether the rating curves presented in Table 4.48, are or are not suitable for events without samples, it is necessary to perform error analyses. Therefore, residuals were computed in order to determine the degree of variability between events and the variability of samples within each event for its rising and decreasing limb of discharge (considering the relationship shown in Eq. 4.20.

The error analyses was done by an ANOVA test for each section of the hydrograph, results of this test have shown that splitting the hydrograph into two sections reduces the degree of variability ($p < 0.001$). Therefore, the constant and exponent defined for each segment of the hydrograph are suitable to be used for events without samples.

In order to assess the uncertainty of sediment load, the confidence intervals were obtained by Monte Carlo simulation (by runnng *sedcuesq*), the inputs used are presented in Table 4.49, where s_j is the standard deviation of residuals (in ln scale) between events and s_i is the standard deviation of residuals (in ln scale) of samples within each event; the constant a and exponent b were obtained from the rating curves. The algorithm *sedcuesq* was run 1000 times for each limb of the hydrograph, in it was included the errors due to events and errors among samples within events.

Table 4.49: Data inputs to run *sedcuesq*.

Nlins	s Q (%)	Rising limb				Decreasing limb			
		a	b	s_j	s_i	a	b	s_j	s_i
n	10	0.0113	1.978	1.012	0.485	0.000699	2.172	1.646	0.272

In Table 4.53 results are shown, where the average sediment load obtained by splitting the hydrograph and performing a Monte Carlo simulation was 97,718 Mg, and the limits of the confidence intervals were 106% above and below the average estimate; however, the confidence interval is slightly wider than the range defined without splitting the hydrograph; yet the average decreased.

Results by removing two of the biggest episodes (CR220196 and CR171297) have reduced the average load estimates, these were 57,512 Mg and 38,392 Mg respectively, and the wideness of their confidence intervals were reduced to 78.6% and 62.5% respectively, the average estimate is closer to the lower bound rather than to the upper bound (log normal distribution).

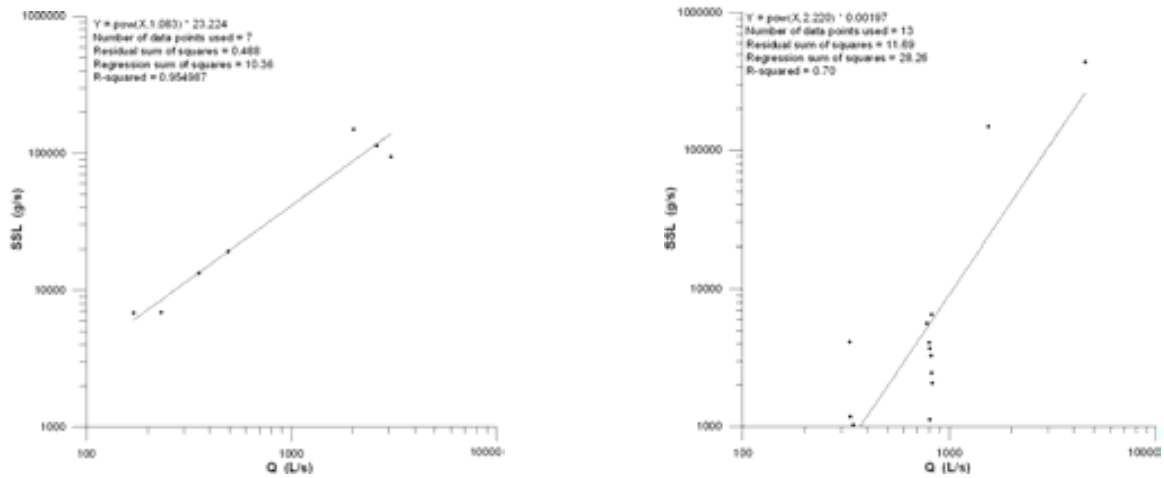

Figure 4.59: Summer SRC: rising limb (left) and decreasing limb (right).

In addition, seasonal analyses were done, following a similar procedure described for the annual rating curve. Among the total events (19) with samples, only 3 fell within summer and the remainder belong to the category "rest of the seasons". For this analysis 4 subsets were obtained, such as: summer-rising limb, summer-falling limb, rest of seasons - rising limb, and rest of seasons - falling limb of the hydrograph. In Figs. 4.59 and 4.60 plots of these 4 subsets are illustrated, and the constant, exponent of rating curves for each subset are shown in Table 4.50. For the subset summer-rising limb only 7 samples were available, the SRC's exponent is near 1 which means that load transport is not influenced by discharge. r^2 for all subsets are high.

Table 4.50: Seasonal SRC parameters by splitting the hydrograph.

SRC	a	b	r^2	n
Decreasing summer	0.00197	2.221	0.71	13
Decreasing rest	0.00069	2.149	0.66	71
Rising summer	23.2200	1.083	0.95	7
Rising rest	0.0102	2.002	78	170

Residuals were computed for each subset in order to determine the degree of variability between events within seasons, and variability of samples within each event for its rising and decreasing discharge. This analyses was done by an ANOVA test for each subset, results of this test have shown that developing 4 equations, one for each subset are suitable ($p < 0.001$). A summary of variances and standard deviations (among events and within events) are illustrated in Table 4.51. Splitting the whole set of samples into four subsets reduces the degree of variability ($p < 0.001$).

Table 4.51: Variances and standard deviation for seasons and limb of hydrograph.

SRC's limb	season	s^2 total	s^2 samples	s^2 event	s total	s samples	s event
Decreasing	Rest of seasons	2.547	0.074	2.473	1.596	0.271	1.573
	Summer	0.974	0.072	0.969	0.987	0.268	0.984
Rising	Rest of seasons	1.277	0.243	1.034	1.130	0.493	1.017
	Summer	1.112	0.078	1.034	1.055	0.279	1.017

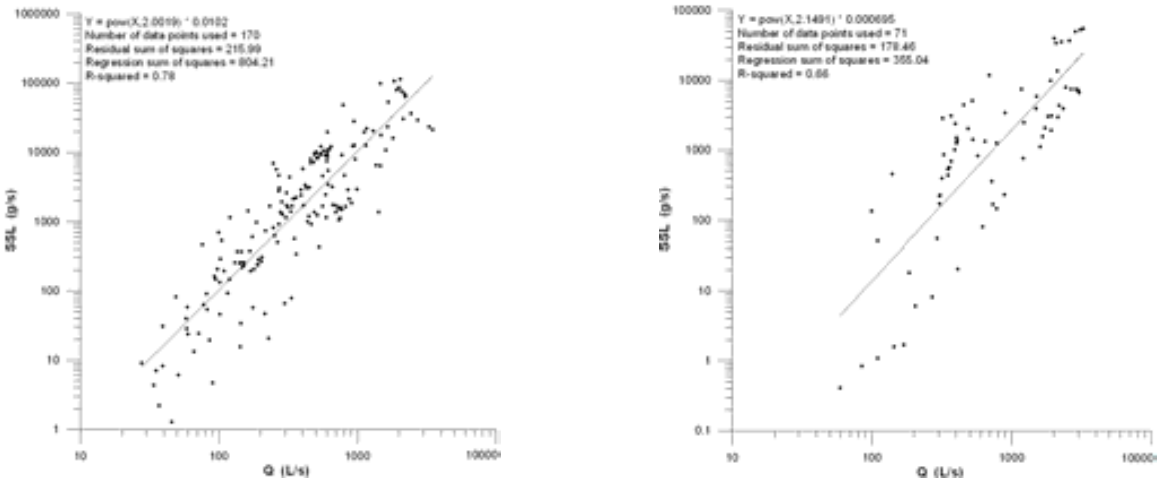

Figure 4.60: Rest of season SRC: rising limb (left) and decreasing limb (right).

The input data used to run *sedcuesq*, in order to obtain the limits of the confidence interval are shown in Table 4.52, where the standard deviations of seasonal variability and rising and decreasing variability were taken into account.

Table 4.52: Data inputs for *sedcuesq*.

Nlins	s Q (%)	Rising limb				Decreasing limb			
		a	b	s_j	s_i	a	b	s_j	s_i
Summer n	10	23.220	1.083	1.017	0.279	0.00197	2.221	0.984	0.268
Rest n	10	0.010	2.002	1.017	0.493	0.000695	2.149	1.573	0.271

Sediment loads obtained based on season and section of hydrograph are presented in Table 4.53. The average load was 87,645 Mg, and the width of its confidence interval was 84.4% above and below the average value, these estimates were smaller than the estimates on the annual basis. Removing two of the biggest episodes the width of the intervals are smaller than for the whole set of episodes.

4.5.2.5 Comparison of techniques

Sediment load obtained by taking into account the rising and falling limb of the hydrograph, and without distinguishing errors among events and errors within events are smaller than the load obtained from one rating curve for the entire hydrograph. Nevertheless, despite of the slight improvement (reduction) in sediment load values, these are still much larger than the estimates obtained by sensors.

The ratio of sediment load value obtained by rating curve to values from sensors illustrates the magnitude of these differences, for most of the episodes the rating curve estimate is larger than for the sensors, especially for CR220196, CR121199, CR100402 and CR280203 which ratios are 22.0, 11.9, 30.7 and 14.6 respectively. Clearly, sediment rating curve overestimated largely the sediment load for big episodes, and it underestimated for small episodes, no sediment exhaustion effects were found except for CR100402 due to a previous episode.

Table 4.53: Comparison of SSL values obtained by sensor calibrations and splitted SRC.

Event name	Annual SRC	Seasonal SRC	Sensor	Ratio Annual SRC/sensor	Ratio Seasonal SRC/sensor
CR220196	21528.3	21657.0	976.5	22.0	22.1
CR220496	217.4	191.7	83	2.6	2.3
CR141096	204	181.6	98	2.0	1.8
CR111196	1284.9	1156.5	501	2.5	2.3
CR040697	2926.2	2566.9	2046.5	1.4	1.2
CR051197	6	5.2	14.1	0.4	0.3
CR171297	16228.9	15062.3	6433	2.5	2.3
CR070599	116.9	31.3	57	2.0	0.5
CR280899	307	622.3	1023	0.3	0.6
CR140999	163.5	4214.5	108	1.5	39.0
CR190999	1245.3	3332.5	638.5	1.9	5.2
CR121199	5643.8	5066.2	474.5	11.8	10.6
CR280900	52.1	45.5	124	0.4	0.3
CR231100	88.2	84.5	106.6	0.8	0.8
CR231200	2168.8	2136.9	1017.1	2.1	2.1
CR010301	15.3	13.1	92	0.2	
CR180801	11.1	57.6	244.6	0.04	0.2
CR201001	20.7	18.3	173	0.12	0.1
CR070402	1623.7	1473.6	517.2	3.1	
CR100402	521.5	459.4	17	30.6	27.0
CR091002	326.9	293.8			
CR280203	5750.6	1773.3	392.7	14.6	4.5
CR311003	729.6	657.5	313.4	2.3	2.0
CR041203	850.7	840.0	152	5.5	5.5
CR310304	602.9	602.6			
CR050804	460.1	1128.0	572.3	0.8	1.9
CR141005	2599.9	2338.0	1042	2.4	2.2
summary	97,718.1	87,645.0	17,217	5.6	5.0
all - 1	72,853.0	57,512.0	16,288	4.5	3.5
all - 2	34,012	38,392.0	9,855	3.4	3.8

A comparison of load estimates between sensors and the estimates obtained by annual rating curve considering both segments of the hydrograph is illustrated in Table 4.53, and graphically are illustrated in Fig. 4.61.

In Table 4.53, it can be seen that the sediment load for each episode follows the same pattern than the estimates obtained on the annual basis but are slightly smaller.

A correlation between sediment load assessed by sensor calibrations, and the difference between load obtained by seasonal SRC (split hydrograph) and sensor calibrations was done. The correlation coefficient was 0.401, which indicates a significant relation ($p < 0.042$, $\alpha = 0.05$). This means that the smaller the episode, smaller is the difference between the estimates by each of the methods. However, by removing the three of the biggest events (CR220196, CR171297 and CR121199) no correlation was found ($r = 0.294, p < 0.175$), which means there is a large influence of these 3 episodes in the correlation found previously.

In addition, a likely existence of correlations between the difference (sediment load) between values obtained by sensor calibration and sediment rating curve (split hydrograph), peak of discharge, and

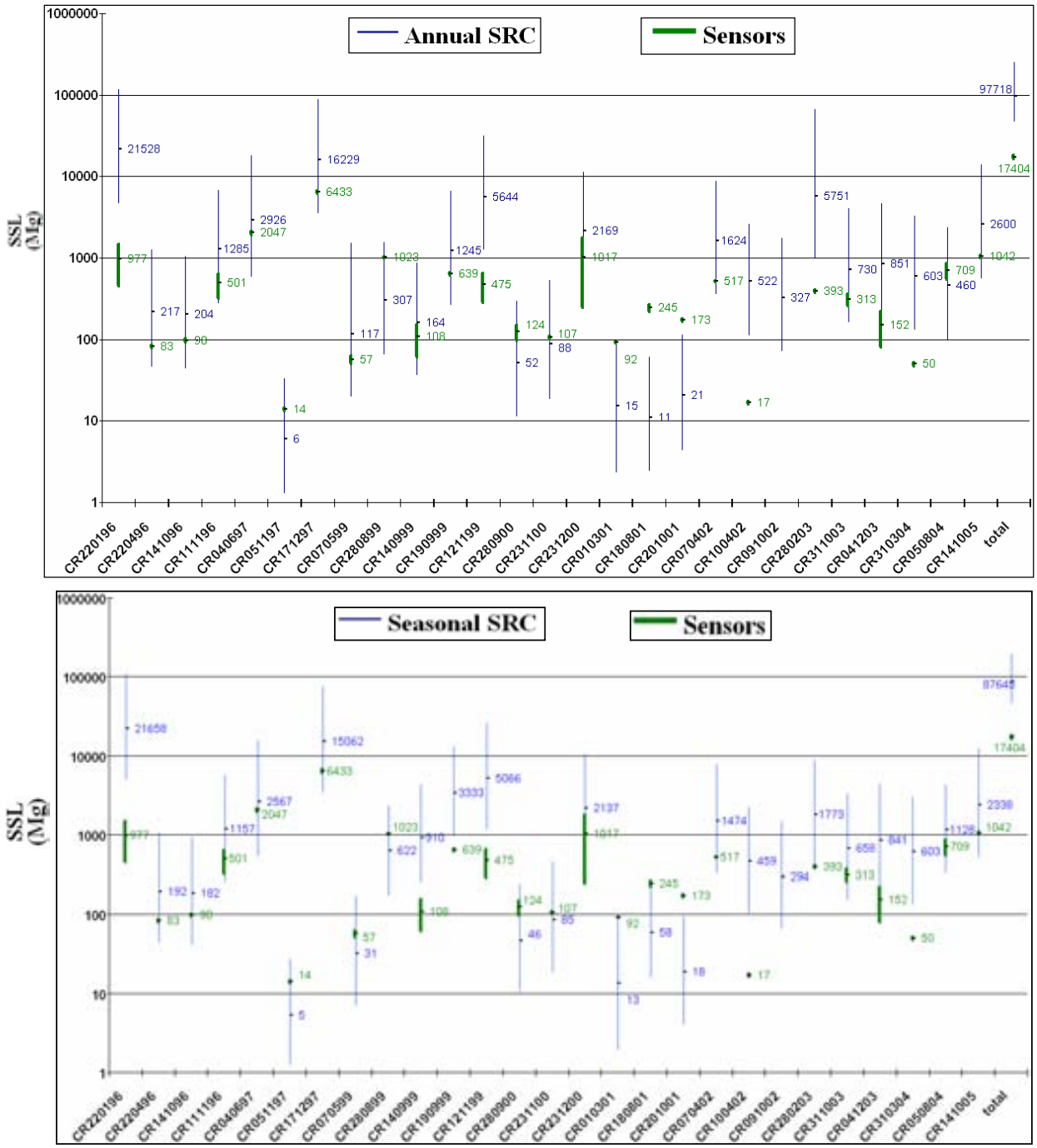

Figure 4.61: Comparison of confidence intervals for the average suspended sediment load estimates obtained by the means of sensors and two sediment ratings curves, at event scale and whole period.

the day of the year when a given flood occured, were tested. Results have shown that there is a correlation ($r = 0.618, p < 0.001$) with peak of discharge, which makes the model valid although it is not strong; and no correlation with day of the year was found (r = -0.174, p = 0.396).

In order to determine whether there is a correlation or not, between variance and sediment load and peak of discharge and total discharge, a correlation test was performed. Results have determined

Table 4.54: Correlation between Q and variance of rest of seasons subset.

SRC	peak of Q		total Q	
	r	p	r	p
Rising limb	0.14	0.568	0.15	0.533
Decreasing limb	0.029	0.911	0.051	0.84

that the variance of load is not related to peak of discharge and total discharge. In Table 4.54 a summary of these correlations are presented. For summer subset as only few samples (7) were available a correlation test was not done.

None of the Monte Carlo simulation of the distribution function of SSL and its error, were able to reduce the uncertainty in the confidence interval of the average estimate. It was tested splitting the data in a seasonal and annual basis, falling and decreasing limbs of the hydrograph, and the variability between events and variability of samples within each event. The lack of a representative coverage of samples along the hydrograph might be the cause of such a large differences found between sediment load assessed by sensors and Monte Carlo simulations.

Table 4.55: SRC parameters by high frequency sampling.

					Residuals	
SRC	a	b	r^2	n	Std. dev.	Mean
Whole hydrograph	0.00617	1.650	0.40	613	3.124	0.000
Rising limb	0.01810	1.800	0.80	294	1.350	0.000
Decreasing limb	0.00117	1.649	0.40	317	3.281	0.000

4.5.3 Testing uncertainty results

Since the samples during most of the events studied did not have a good distribution along the hydrograph it remains unclear, whether this non-uniform spanning of samples has to do with the large uncertainty defined for the confidence intervals. In order to clear out this hypothesis, a simulation of sampling strategy was tested.

In order to ascertain that sampling strategy (distribution on hydrograph) does not have influence on the large differences between both methods, a few episodes with the best quality of sediment concentration curves were selected (10 events), in order to acquire equal time samples (virtual samples) derived from the aforementioned curves, the sampling frequency was 1 hour. None of these event ocurred within summer, hence further analysis was done, on the annual basis only.

Table 4.56: Inputs for *sedcuesq* high frequency sampling.

Nlins	s Q (%)	Rising limb				Decreasing limb			
		a	b	s_j	s_i	a	b	s_j	s_i
n	10	0.0181	1.800	0.975	0.933	0.00117	1.649	3.066	1.168

Using the new "virtual samples" means that the longer the event, the more relevant is for the construction of a sediment rating curve.

The whole set of samples from the 10 episodes was 613, with these samples 613 instantaneous sediment load values were calculated, which later were used to develop three sediment rating curves: for the entire hydrograph, rising limb and falling limb.

In Table 4.55 a summary of the statistics is presented. In order to determine whether the variability is reduced or not, ANOVA tests were done and it gave significant ($p < 0.001$). Therefore, a sediment rating curve was defined for each limb of the hydrograph. Similarly, the total variance was divided in the variance between events, and variance of samples within each event, these along with other parameters are presented in Table 4.56, Monte Carlo simulation was performed using *sedcuesq*.

Results have shown that the confidence intervals defined for sensors, are within the confidence interval defined for sediment rating curves. The average sediment yield for sensors was 10,400 Mg and its confidence intervals with 90% of confidence was between 10,057 and 10,742 Mg, the uncertainty is relatively small.

On the other hand, for rating curves the average was 11,952 Mg and its confidence interval at same level of probability has ranged from 4,597 and 74,103 Mg, the uncertainty involved is high and presents a log distribution; however, the averages from both methods are very similar.

Table 4.57: Inputs for *sedcuesq* high frequency sampling and total variability.

Nlins	s Q (%)	Rising limb				Decreasing limb			
		a	b	s_j	s_i	a	b	s_j	s_i
n	10	0.0181	1.800	0.000	1.350	0.00117	1.649	0.000	3.281

These results confirm that a good spanning of samples along the hydrograph, and splitting the total variability of residuals in the variability between events, and variability of samples within each event, highly influences the reliability of sediment rating curves.

In order to demonstrate the latter, a Monte Carlo simulation was performed, this time considering the total variability (one error term) shown in Table 4.57, results have shown that confidence intervals for sediment rating curves are above and outside the confidence intervals defined for sensors. A comparison of both analysis are illustrated in Fig. 4.62.

4.6 Sediment load and sediment yield from hydrological variables

Hydrological variables such as precipitation, rainfall intensity, runoff, peak of discharge, kinetic energy and sediment concentration are continuously or nearly continuously measured at the study area, and these might be used to predicted sediment load (at event scale) and by summation sediment yield can be computed. A list of such variables is provided in Table 4.58 for the set of studied events.

4.6.1 Bivariate correlations

Correlations between pairs of variables illustrated in Table 4.58 were performed (25 events), in order to test, if there is any significant relationship between suspended sediment load (from sensor calibration and linear interpolations of samples) and one or more variables from Table 4.58. Keeping

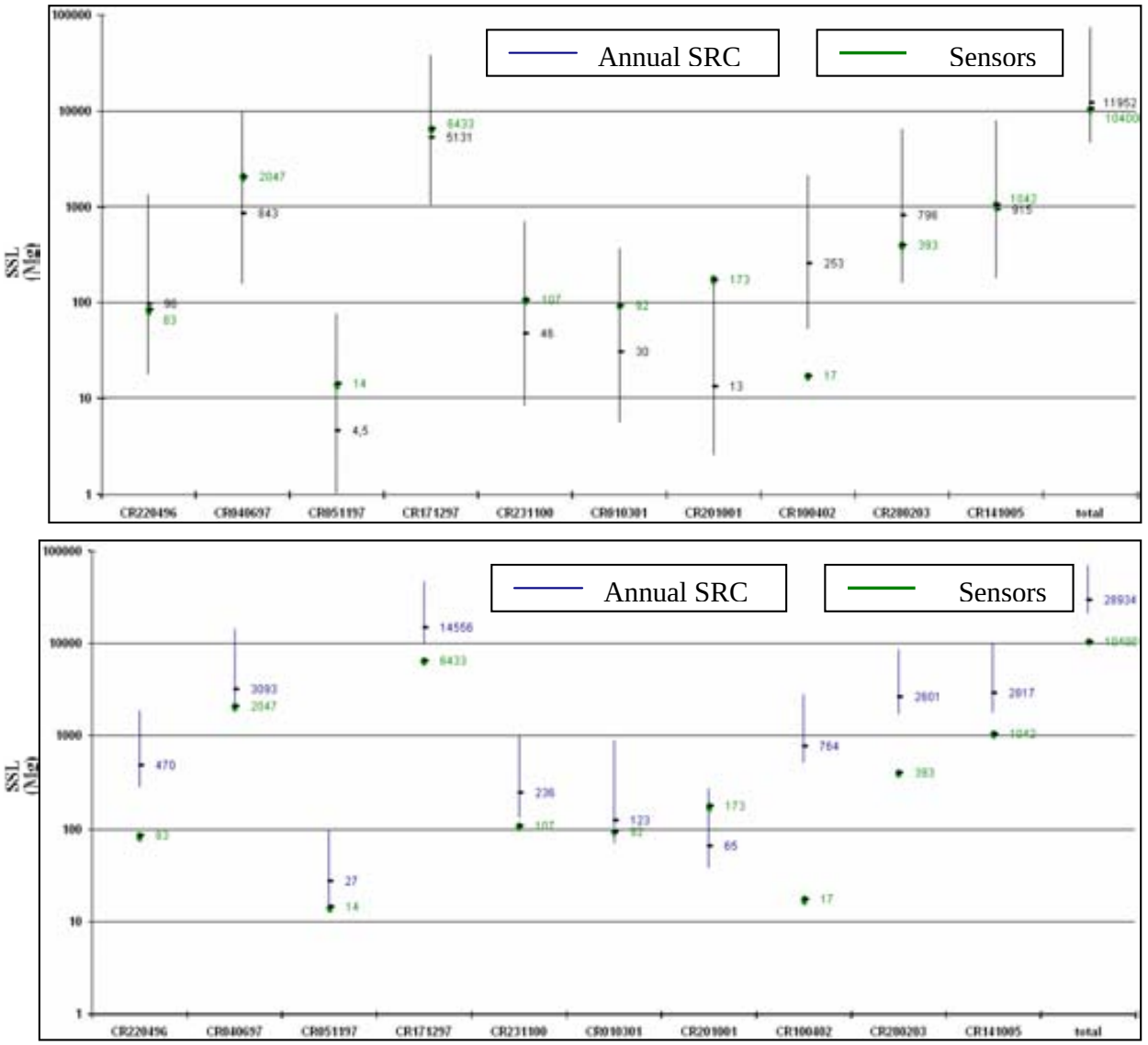

Figure 4.62: Confidence interval for events with high reliable SSC: (above) std. deviation of events and samples within events; (below) total std. deviation.

in mind that correlation coefficient assumes that the relationship is linear. Analyses were done at the annual and seasonal basis (summer and rest of seasons).

4.6.1.1 Annual

Pearson correlation coefficients were calculated in $SPSS^{©}$ v.13. Coefficients were determined by using the input data in the arithmetic scale. A summary of the results is shown in Table 4.59a, bold values indicate a significant correlation ($p < 0.05$). Significant correlation was found between suspended sediment load and the following variables: peak of discharge, runoff, total kinetic energy and total precipitation. Pearson correlation assumes that both variables are normally distributed. Given that the two variables with the highest correlation coefficient (runoff and precipitation)

Table 4.58: Hydrological variables measured at Cal Rodó station.

Event	total pp (mm)	peak Q (L/s)	runoff (mm)	intensity pp (mm/h)	total kinetic E (J/m^2)	max kinetic E (J/m^2/h)	max SSC (g/L)	total SSL (Mg)
CR220196	157.6	9574.3	146.9	16.9	2135.6	384.2	7.9	976.5
CR220496	51.5	1589.4	16.4	21.9	975.9	516.4	6.3	83.0
CR141096	74.7	697.8	14.0	16.9	1393.8	382.8	30.5	98.0
CR111196	90.9	2253.4	27.7	14.5	1675.2	319.5	22.5	501.0
CR040697	105.0	6994.1	37.6	65.6	2396.9	1823.0	53.0	2046.5
CR051197	51.9	321.5	2.9	29.4	894.6	727.2	9.1	14.1
CR171297	135.1	7588.9	113.8	16.9	2440.5	382.8	47.6	6433.0
CR070599	30.1	636.4	8.3	30.0	604.7	743.2	26.1	57.0
CR280899	47.5	4536.9	6.7	88.0	1245.6	2542.3	104.2	1023.4
CR140999	57.1	1115.8	14.3	26.8	1115.2	654.4	25.1	108.0
CR190999	54.7	3438.6	32.2	12.1	1057.0	257.4	47.1	638.5
CR121199	29.9	6804.0	11.5	26.7	2612.4	2612.4	24.5	474.5
CR280900	63.4	550.6	7.2	32.0	1335.5	802.4	57.5	124.0
CR231100	42.3	939.0	8.6	9.6	734.6	196.4	28.0	106.6
CR231200	89.4	3089.0	34.1	12.0	1577.2	255.8	25.1	1067.8
CR010301	41.9	610.4	6.1	9.6	746.4	196.4	20.0	92.0
CR180801	36.5	957.9	1.0	57.8	946.7	1577.8	121.0	244.6
CR201001	51.6	484.0	4.7	29.6	997.6	731.8	28.1	173.0
CR070402	58.6	2967.5	34.5	16.9	1099.8	383.8	27.7	517.2
CR100402	53.9	1168.5	19.2	12.0	938.8	256.8	1.4	17.0
CR280203	69.5	3491.5	39.2	9.6	1186.6	196.3	14.5	392.7
CR311003	44.9	1905.7	20.5	9.5	758.8	196.3	15.4	313.4
CR041203	54.6	2233.5	22.1	7.2	908.2	139.3	14.0	152.0
CR050804	55.5	3750.0	11.2	65.5	1347.0	1819.1	43.9	709.0
CR141005	59.9	5834.4	25.0	39.6	1304.0	1022.7	68.3	1042.0

are well correlated (r=0.90), total precipitation was chosen as predictor, because is more readily available. Therefore, a linear regression was obtained between sediment load (dependent) and precipitation (predictor), the algebraic expression is illustrated in Eq. 4.29, the r^2 of the regression was 0.63, the F test value of ANOVA was 14.9 and $p < 0.05$, in addition the significance test of the regression coefficients have shown that they are significant, as illustrated in Table 4.60a.

When applying Eq. 4.29 to data presented in Table 4.58, a number of the predicted sediment load values were negative, as result residuals were also negative. The predicted sediment load values are misleading, therefore, in order to verify the validity of Pearson's correlation coefficients a Spearman's rank correlation test was used. Spearman's rank correlation test does not require any assumptions about data distribution unlike Pearson's correlation. The correlation coefficients calculated with this test are presented in Table 4.59b, where peak of discharge and total kinetic energy present the highest Spearman's rank correlation values, but these two variables are also well correlated (r=0.68).

The predicted negative values obtained by using Eq. 4.29, can be atributed to the non-linear relationships between variables, thus the input data set was tranformed into logarithmic scale, then Pearson's correlation coefficients were calculated using the transformed data. Results are illustrated in Table 4.61, and they show that peak of discharge and total kinetic energy are indeed better predictors of sediment load as it has been indicated by Spearman's rank correlation. As both predictors are well correlated (r=0.71), peak of discharge was chosen as predictor of sediment load. As a consequence, a new linear regression was obtained, which is shown in Eq. 4.30, the r^2

Table 4.59: Correlations coefficients between suspended sediment load and other hydrological variables in the arithmetic scale and all events (annual): (a) Pearson correlation, (b) Spearman's rank correlation.

(a) Pearson

	intensity pp	max kinetic E	max SSC	peak Q	runoff	total kinetic E	total pp	total SSL
intensity pp	1.00	**0.85**	**0.74**	0.20	-0.23	0.17	-0.11	0.09
max kinetic E		1.00	0.59	0.34	-0.24	0.40	-0.22	0.06
max SSC			1.00	0.12	-0.17	0.08	-0.12	0.21
peak Q				1.00	**0.75**	**0.82**	**0.66**	**0.61**
runoff					1.00	0.58	**0.90**	**0.63**
total kinetic E						1.00	**0.66**	**0.62**
total pp							1.00	**0.63**
total SSL								1.00

(b) Spearman

	intensity pp	max kinetic E	max SSC	peak Q	runoff	total kinetic E	total pp	total SSL
intensity pp	1.00	**0.95**	**0.62**	0.08	-0.36	0.30	-0.03	0.21
max kinetic E		1.00	0.54	0.17	-0.35	0.38	-0.13	0.22
max SSC			1.00	0.14	-0.19	0.28	0.07	0.48
peak Q				1.00	**0.72**	**0.68**	0.45	**0.84**
runoff					1.00	0.50	**0.73**	0.59
total kinetic E						1.00	**0.68**	**0.71**
total pp							1.00	0.54
total SSL								1.00

was 0.71, the F test value of ANOVA was 54.9 and $p < 0.05$, in addition the significance test of the regression coefficients have shown that they are significant, as illustrated in Table 4.60b.

By applying Eq. 4.30 to data given in Table 4.58 (peak of discharge and total kinetic energy) the estimated sediment yield from the 25 events was 11,703 Mg, which is 32% less than the estimated from the calibration of sensors and interpolations. This is approximately 3.49 Mg $ha^{-1}yr^{-1}$, calculated by using the catchment's area (4.2 km^2), duration (10 years) and considering that the 25 events represents about 80% of the sediment produced in the catchment.

$$SSL = -996.62 + 26.32pp \tag{4.29}$$

$$SSL = 10^{-1.60} \times Q^{1.22} \tag{4.30}$$

4.6.1.2 Seasonal

Data set from Table 4.58 were split into summer episodes and episodes occurred during the rest of seasons, correlation and regression analysis were made only for the rest of the seasons, since there are not enough events for summer (only 5).

Table 4.60: Regression coefficients including all events (annual): (a) arithmetic scale, (b) logarithmic scale.

(a) arithmetic scale					
	Unstandardized Coeffic.		Standard. Coeffic.	t	Sig.
	B	Std. Error	Beta		
Constant	-996.6	484.0		-2.06	0.051
total pp (mm)	26.32	6.82	0.62	3.86	0.001
(b) logarithmic scale					
Constant	-1.60	0.55		-2.91	0.008
peak Q (L/s)	1.22	0.17	0.84	7.41	**0.000**

Table 4.61: Pearson correlations coefficients between suspended sediment load and other hydrological variables in the logarithmic scale and all events (annual).

	intensity pp	max kinetic E	max SSC	peak Q	runoff	total kinetic E	total pp	total SSL
intensity pp	1.00	**0.95**	0.55	0.10	-0.39	0.25	-0.11	0.20
max kinetic E		1.00	0.50	0.17	-0.38	0.37	-0.21	0.21
max SSC			1.00	0.17	-0.24	0.20	-0.06	0.55
peak Q				1.00	**0.72**	**0.71**	0.48	**0.84**
runoff					1.00	0.53	**0.74**	0.57
total kinetic E						1.00	**0.65**	**0.69**
total pp							1.00	0.54
total SSL								1.00

First, Pearson's correlation coefficients were calculated between the pair of variables of all events except summer, as illustrated in Table 4.58, a significant correlation ($p < 0.05$) of sediment load and runoff and total precipitation was found, 0.65 and 0.64 respectively. Since both are highly correlated ($r = 0.89$), precipitation was chosen as predictor. Then a regression was developed using these variables, which is represented in Eq. 4.31 where r^2 was 0.41, $F = 12.4$, $p < 0.05$, a significance test of regression coefficients were also performed and it is shown in Table 4.63, the test suggest that the coefficients are suitable. Furthermore, when this equation was applied to the rest of the seasons data sub-set, a number of the predicted sediment load values were also negative as in the annual basis.

To verify this incosistency, a Spearman's rank correlation test was performed, the results of this test are summarized in Table 4.62b, where the highest coefficients exist between sediment load, and peak of discharge ($r = 0.83$) and runoff ($r = 0.77$). Thus, the input dataset was transformed into the logarithmic scale, then a Pearson's correlation coefficient was calculated again, results are shown in Table 4.62a, and they show that peak of discharge and runoff have the highest coefficients, as these two likely predictors are well correlated, peak of discharge has been selected.

Finally, a regression was developed using as predictor peak of discharge, and as dependent variable sediment load; the outcome relationship is illustrated by Eq. 4.32, where r^2 was 0.69, F was 40.7 for a $p < 0.05$, in addition a test of regression coefficients shown in Table 4.63 was performed and

which has shown that coefficients are suitable to perform sediment load calculations (coefficients are significantly different from zero).

Table 4.62: Correlations coefficients between suspended sediment load and other hydrological variables in the logarithmic scale and seasonal basis (rest): (a) Pearson correlation, (b) Spearman's rank correlation.

(a) Pearson

	intensity pp	max kinetic E	max SSC	peak Q	runoff	total kinetic E	total pp	total SSL
intensity pp	1.00	**0.92**	0.41	0.06	-0.16	0.35	0.05	0.14
max kinetic E		1.00	0.37	0.16	-0.18	0.47	-0.11	0.16
max SSC			1.00	0.16	0.01	0.30	0.10	0.57
peak Q				1.00	**0.86**	**0.73**	0.52	**0.83**
runoff					1.00	**0.60**	**0.75**	**0.76**
total kinetic E						1.00	**0.65**	**0.73**
total pp							1.00	**0.62**
total SSL								1.00

(b) Spearman

	intensity pp	max kinetic E	max SSC	peak Q	runoff	total kinetic E	total pp	total SSL
intensity pp	1.00	**0.96**	0.52	-0.03	-0.18	0.33	0.09	0.11
max kinetic E		1.00	0.45	0.07	-0.18	0.39	-0.01	0.13
max SSC			1.00	0.06	-0.01	0.31	0.21	0.44
peak Q				1.00	**0.89**	**0.69**	0.54	**0.83**
runoff					1.00	0.57	**0.73**	**0.77**
total kinetic E						1.00	**0.68**	**0.73**
total pp							1.00	**0.63**
total SSL								1.00

$$SSL = -1134.3 + 27.54pp \quad (4.31)$$

$$SSL = 10^{-1.61} \times Q^{1.22} \quad (4.32)$$

By applying Eq. 4.32 (where its components variables are in logarithmic scale) to sub-data of rest of seasons (excluding summer events) given in Table 4.58 (peak of discharge and runoff) the estimated sediment yield from the 20 events was 9,423 Mg, which is 35% less than the estimated from the integration of sensors and discrete sampling for the same sub-set of events (20). This is approximately 3.34 Mg $ha^{-1}yr^{-1}$, calculated by using the catchment's area (4.2 km^2), duration (10 years) and considering that the 20 events represents about 67% of the sediment produced in the catchment during rest of the seasons.

Table 4.63: Regression coefficients including all events except summer (rest): (a) arithmetic scale, (b) logarithmic scale.

(a) arithmetic scale					
	Unstandardized Coeffic.		Standard. Coeffic.	t	Sig.
	B	Std. Error	Beta		
Constant	-1134.3	587.3		-1.93	0.069
total pp (mm)	27.54	7.81	0.64	3.53	0.02
(b) logarithmic scale					
Constant	-1.61	0.63		-2.54	0.02
peak Q (L/s)	1.22	0.19	0.83	6.38	**0.00**

4.7 Discussion

4.7.1 Instruments and sampling strategy

Having an appropriate sampling program is crucial in order to track sediment transport at diverse temporal resolutions. Sampling program should guarantee that samples are collected, before, during, and after the peak of water discharge. As Julien (1998) indicates, sediment rating curves method is most reliable when: (1) the recording period is long, (2) sufficient data at high flows are available, and (3) the sediment rating curve shows considerable scatter of the plotted points of discharge and concentration data. In this study the first criteria is accomplished fairly well, since the recording period is relatively long (10 years); however, samples at high discharge were not available for most of the episodes, the difficulties of collecting samples at high frequency was acute especially during flash flood, which is common in mediterranean mountain catchments; regarding the last criteria the rating curves showed high scattering, both at annual and seasonal scales.

In the light of the large differences between "observed" (calibration of sensors and interpolations) and the predicted by sediment rating curves, which were 6 and 5 times larger for annual and seasonal rating curves respectively, an analysis using "virtual" samples obtained every 1 h, has indicated that the averages between "observed" and predicted are similar (difference ≈3%), therefore a lack of a good spanning of samples throughout the hydrograph was critical, and it has hampered a reliable assessment of sediment transport through Monte Carlo simulation using sediment rating curves. It is recognized that setting a sampling program should be a priority if accuracy is aimed.

Malfunction or saturation of IR and US sensors ocurred during a number of events. Ultrasound sensor readings were not reliable in a wide range of sediment concentrations during many flood events, certain degree of malfunction, missreading, or missing readings was observed in 15 (56%) out of 27 episodes. Episodes, where ultrasound sensor failed included the biggest episode (CR171297), other events were CR141096, CR111196, CR051197, CR171297, CR280899, CR140999, CR190999, CR231100, CR180801, CR201001 , CR070402, CR121199, CR280203, CR311003, CR041203, given the large capacity range of concentration it would have provided valuable data.

On the other hand, infrared turbidity sensor was less prone to failure, although not less important, in 6 flood episodes (22% out of 27 events) infrared sensor suffered some degree of failure (CR200101, CR180801, CR051197, CR121199, CR231100, CR231200), however in this case it is also related to

saturation process, which occurs at ≈ 6 g/L.

In a few events (e.g. CR171297, CR100402) where sensors functioned well, the tails of the concentration curve from infrared and ultrasound sensors do not coincide, pressumably because those rare events were sand-dominated, and the used calibrations was set by using silt/clay fraction, which is predominant in the catchment. It was demonstrated that sensor calibrations performed with different particle sizes, ($< 63\mu$m and $63 < d < 250$ μm) showed, that in the presence of sand, the infrared sensor underestimates the sediment transport, whereas the ultrasonic sensor tends to overestimate it, this was learned after those rare flood events have occured. Therefore, a calibration of ultrasound sensor for heavy loaded episodes, which carries significant proportion of sand-sized material was developed, and it will be used from now on for large floods (Soler *et al.*, Submitted).

The peak of sediment discharge in all the studied events was reached before the peak of water discharge, moreover there is an sediment exhaustion effect thus, when there is still discharge there is less available sediment to be transported, although in some events samples were still collected even when water was almost clear.

Sediment load estimates assessed by sediment rating curves are probably overestimated due to the fact that, sampling was made aiming to calibrate the sensors and not necessarily aiming to obtain a good representativeness of sediment concentration. Suspended sediment concentration was analysed or determined only for samples which had noticeable amounts of sediments, whereas, many samples obtained in clear water were desestimated. This means that "virtual samples" are needed to cover all the flow conditions if sediment rating curves are going to be used.

4.7.2 Sediment rating curves

Sediment rating curves (annual and seasonal) overestimated the sediment load for most events. Monte Carlo simulation has revealed the magnitude of error at both temporal (event and annual/seasonal) resolutions. The errors at event scale are larger than for long term time frame, which were > 300 and 99% respectively in the case of annual rating curves, this is because, at a larger temporal scale, small and large events tend to compensate each other.

Most of the sediment transport occurred during a few number of episodes. Thus, considering the sensors during five episodes (CR040697, CR171297, CR280899, CR231200, CR141005) 67% of the total sediment during the whole period studied was transported, especially one episode (CR171297) had great effect on the total estimates supplying with 37%; on the other hand, sediment estimates by sediment rating curve, also has shown that a very few episodes (CR040697, CR171297, CR121199, CR231200, CR141005) transported 29% of the total, and one episode (CR171299) had transported 37% out of the total. There is no clear evidence of temporal variation of sediment transport, considering that the study area remained undisturbed during at least the last 30 years.

Only marginal improvements were achieved by developing sediment rating curves based on seasonal and limb of hydrograph, the degree of uncertainty is still large, however is better than the annual. In Cal Rodó a high short-term variability of discharge and suspended sediment load is evident, therefore, annual sediment rating curves is ineffective.

4.7.3 Uncertainty

Uncertainty when calculating sediment load by using sediment rating curves is large, because the non-linear regression does not fully capture the natural variability (random error is not zero).

The sources of uncertainty associated to each method can be grouped in two main sources, the first is the quality of the regression model fit to samples, and the second, is related to data used for derivation of regression models (samples, discharge, hydrological variables) whether or not they are representative of the characteristics of the study area.

The confidence intervals assessed to describe the uncertainty surrounding the suspended load estimates by both methods were: $\pm 6\%$ for sensors, and $> 300\%$ for sediment rating curves, at 90% of confidence level. Widening the confidence interval increases the confidence of load estimate but also makes necessary more cautioness while making decisions.

4.7.4 Sediment load and hydrological variables

Some hydrological variables such as precipitation and peak of discharge are easier to obtain, therefore, correlation between sediment load and a number of hydrological variables were done. However, consistency of the regression coefficients were needed to be verified, because for example Pearson's correlation assumes that input data are normally distributed and this is not accomplished by hydrological variables such as discharge and sediment concentration. After verifying against Spearman's rank correlation, it was found that peak of discharge and total kinetic energy are better predictors of suspended sediment transport, which can be used as a first assessment of sediment load.

4.8 Conclusions

Suspended sediment load estimates obtained by calibration of turbidity sensors and sediment rating curves had a difference of half an order of magnitude, under sound statistically-based procedures.

The reason for this difference was an inadequate spanning of samples during the whole episode, representativeness is fundamental in order to identify and prune data points from the sedigraph regardless of the method used. The sampling design relied on the use of sensors, so "virtual samples" are needed if sediment rating curves are to going to be applied.

Automated sampling is a useful technique but should be checked often during flood episodes in order to withdraw the bottles and avoid missing samples, and allow collection of samples during the whole episode, especially during high flows.

Sediment transport in mountainous catchments are dominated by infrequent large events, and the rating curves fail to estimate accurately the sediment yield because of the extreme episodic events.

Within sediment rating curve methods tested, it is more accurate defining an individual rating curves for the increasing and decreasing limbs of hydrograph.

The confidence interval of the suspended sediment estimate is much narrower for sensors than the

interval defined for sediment rating curves at the same level of confidence. This is a consequence of the very high variability of suspended sediment concentration.

The large difference of sediment transport between episodes and probably and the few episodes from where the parameters used with Monte Carlo procedure were taken have made the confidence interval for sediment rating curve very wide; however, the confidence intervals still provide a clear insight of the amount of suspended sediment load transported, despite the fact that when it is extremely wide its usefulness might be compromised.

Stochastic methods of estimating sediment transport provides a quantification of the uncertainty and are useful to compare to results obtained from deterministic methods which rely on a data-based approach. Nevertheless, it should be kept in mind that a model is as good as its ability to represent the reality.

Peak of discharge might be used as predictor of suspended sediment load in small catchments at the event scale, but, the results need to be compared with results obtained by other techniques and taken cautiously.

The selection of the technique used to perform sediment load estimations will vary according to the budget to conduct the research, and on the needs of controlling precision and accuracy. If the accuracy is needed regardless of its cost a good sampling program should be guaranteed.

In summary, a better understanding of the spatial and temporal dynamics of natural environmental processes is needed, and this can not be isolated from decision making processes. In decision making processes commonly, it is assumed that the quality of data pertaining to a certain set of data is good and enough, however, going a step further, sometimes depending on the technique, methods and quality of input data conclusions will vary and as results this will affect the management decisions; therefore, it is needed to insight into the source of information and provide useful information for decisions such as risk assessment and land use.

Results of studies at the catchment scale should not be transferred to larger scales before a uncertainty assessment is made and if the characteristics (land use, topography, soil type, etc.) are similar might be considered extrapolation. As river basin management choices involves complexity and uncertainty of trade-offs of resources these type of assessment is extremely necessary and can help to the long term sustainability.

Chapter 5

SEDIMENT YIELD IN THE UPPER LLOBREGAT BASIN BY CATCHMENT APPROACHES

5.1 Introduction

Sediment yield prediction at the river basin scale is still a challenge despite of the important progress achieved, because of the complexity involving the geomorphology, land cover and land use, climatic, geology and lithology of basin. However, there is an increasing need on determining the amount of sediment delivered downslope, especially the sediment reaching reservoirs, because it reduces its storage capacity. At the worldwide scale, it is estimated that the annual loss in storage capacity due to sediment infilling is around 0.5-1%, but values as high as 4-5% for individual reservoirs (WCD, 2000) or up to 4-10% for reservoirs built for agricultural irrigation has been reported (Heinemann, 1981).

Several approaches to estimate sediment yield at the basin scale exist, such as, the physics-based ones, for example SHETRAN (Ewen *et al.*, 2000), however their application is limited because of the large data requirements and limited understanding of the complex processes and interactions between the different characteristics occurring within a basin (Merritt *et al.*, 2003); the second type, is the empirical approach where it belongs the well-known (R)USLE (Wischmeier & Smith, 1978; Renard *et al.*, 1997), although it is less computationally demanding still requires a relatively high input data resolution, and it does not account for gully and bank erosion nor for mass movements, while these type of processess can be important suppliers of sediment (Poesen *et al.*, 2003); the third approach, is comprised by statistical methods, where the sediment yield is predicted by relating the annual sediment yield to catchment properties, such as drainage area, topography, climate and vegetation characteristics (Onstad, 1984; Verstraeten & Poesen, 2001), the most popular is the regression between sediment yield and the area of the basin; within this category can also be included the semi-quantitative or scoring methods, such as the Factoring Scoring Model (FSM) (Verstraeten *et al.*, 2003) and the Pacific Southwest Inter-Agency Committee (PSIAC, 1968). In this Chapter it is dealt with the third approach.

The advantages of the statistical approach is that the required input data are relatively easy to obtain and its simplicity of use; however, to develope these equations a large quantities of data are

required, but once the relationship is defined, it is easy to apply to a basin in the same region where the equation was developed for. For example, although, the FSM and PSIAC require calibration for application to new areas the advantage over other regressions models is that the focus is not only on one factor, instead, it integrates the most relevant factors in one score, and also provide insight into which factors are likely to be the most responsible for sediment yield (de Vente *et al.*, 2006). This approach can be particularly effective as a first assessment tool, or whenever other methods are not available or not suitable for a specific basin. The main drawbacks are that the statistical models are site specific, thus the regression formulas obtained for a given geographical location can not be applied as such in other locations before calibrating and adapting to local conditions.

An additional issue within the third approach, and related to the sediment yield - area relationship is that, it is often assumed that sediment yield decreases with increasing drainage area, following a power function which can be explained by the theory of sediment sources and sinks (Walling, 1983), because with increasing area the proportion of sediment depositional areas (e.g. flat areas and gentle slopes) increase, and they will not normally contribute to sediment yield (Verstraeten *et al.*, 2003); however, such a negative relation between sediment yield and drainage area is not always the case, positive relationship was reported, for example (Dedkov & Gusarov, 2006; de Vente *et al.*, 2006; Birkinshaw, 2006) found that where channel erosion is dominant or the sediment is supplied solely from bank erosion (no hillslpe erosion) the relationship is positive. Therefore, both an inverse and direct relationships are possible, depending on the principal source of sediment, on rainfall spatial distribution and on land use distribution (Birkinshaw, 2006).

The sediment yield - area relationship, is a realistic and reliable alternative method for sediment yield estimation, suitable for basins with a reservoir at the outlet. A regression using dataset from 60 Spanish reservoirs was developed by Avendaño *et al.* (1997), but the regression explained only 17% of the observed variability in sediment yield, thus in an attempt to explain the remaining variability in sediment yield was made by Verstraeten *et al.* (2003) by using a quantitative and a semiqualitative approach (FSM) for selected 22 basins. In addition, de Vente & Poesen (2005) calibrated the PSIAC model (for the Pacific Southwest, US) to the Spanish conditions.

The reliability of the sediment yield estimated by these statistical models, can be evaluated by comparing to sediment yield obtained from site specific bathymetry surveys after adjusting it for the trap efficiency of the reservoir. The uncertainty of bathymetry results should be considered while comparing to results derived from statistical soil erosion models.

5.2 Objectives

The purposes of this Chapter are to:

- provide a brief review of bathymetry surveys and sediment yield from calculations from these surveys.
- estimate the sediment yield in the Upper Llobregat Basin, by using a statistical and two semi-quantitative approaches, and compare the outcomes with results from a bathymetry survey of La Baells Reservoir.
- and assess the uncertainty of the sediment yield obtained from a bathymetry survey conducted by CEDEX (2002) at the La Baells Reservoir.

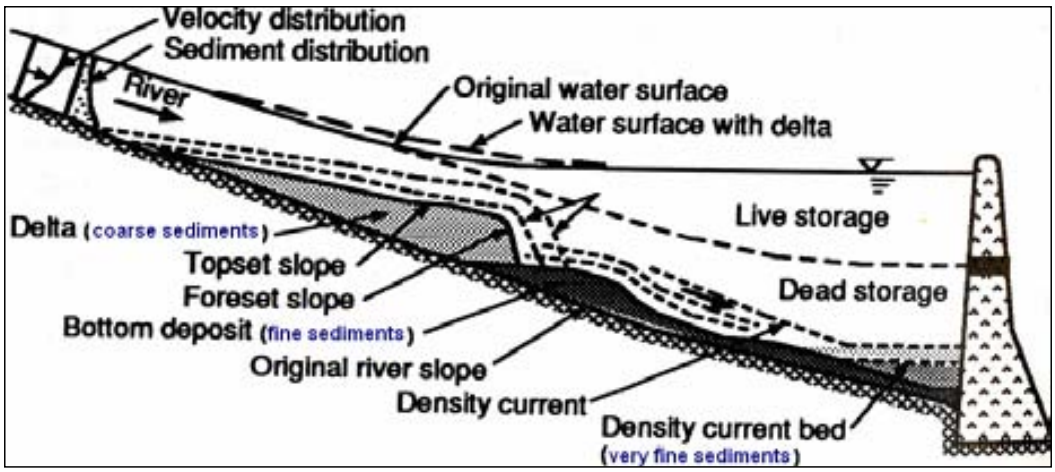

Figure 5.1: Typical reservoir sedimentation pattern.
Source: Frenette and Julien (1986a), after Julien (1998).

5.3 Review of sediment yield from reservoir surveys

Two basic strategies for measuring sediment yield (not predicting, which models do) are: (1) by determining the volume of sediment deposited in reservoirs, and (2) monitoring continuosly the fluvial sediment discharge. Reservoir surveys are generally more accurate, because reservoirs collect sediment from all events since their construction, therefore, there are no missed events (Morris *et al.*, 2007), as might occur at measuring stations in a river.

Bathymetry is the underwater equivalent of hypsometry, which is the measurement of land elevation in relation to sea level. Bathymetry survey of reservoirs are neccesary to determine the sediment deposited in the reservoir after its contruction, with infilling sediment the storage capacity is reduced over time. Reservoirs built below drainage basins with low rates of erosion do not suffer appreciable damage, because of sediment accumulation, but in areas where erosion rates are relatively higher serious deposition occurs (Vanoni, 1975). Reservoir survey can be generally performed at intervals of about 5 to 20 years, but this can vary substantially depending on budgetary constraints, rate of storage depletion, the type and importance of the uses threatened by sediment accumulation and management requirements (Morris *et al.*, 2007).

Reservoir sedimentation is a complex process and depends on the river regime, flood frequencies, reservoir geometry and operation, flocculation potential, sediment consolidation, density currents, and possible land use changes over the life expectancy of the reservoir (Julien, 1998). Sediment deposition in the reservoir is a function of sediment size and water velocity; typically, the larger-sized sediments, deposits in the upper portion of the reservoir, where water velocities decrease rapidly, and finer-sized sediment (e.g. silt) move further into the reservoir or pass through the reservoir entirely. Fig. 5.1 illustrates the typical reservoir sedimentation pattern.

Reservoir sedimentation surveys have advantages over river measurements (e.g. sediment rating curves) because they can provide a meaningful estimate of sediment yield averaged over a period of several years (Walling, 1988), and they include bedload and provide direct measurements of sediment yield instead of indirect estimates (Strand & Pemberton, 1987). The most important factors that determine the volume of deposited sediment are: (a) the trap efficiency and (b) the

density of the deposited material (Yang, 1996), and among these two the trap efficiency can be considered as the most informative descriptor of a reservoir (Heinemann, 1981).

A common method to conduct bathymetry surveys uses a combination of Geographic Positioning System (GPS) and acoustic depth sounding technologies, both connected to a portable computer that records the resulting x, y and z coordinate data into a file that can be processed subsequently to draw a contour map (Morris *et al.*, 2007).

The bathymetry survey process, typically is conducted in two phases: estimation of the quantity, and characterization of the deposited sediment, for which appropriate sampling protocols are followed.

Sedimentation rates worldwide are variable. Crowder (1987) in the U.S. estimated at 0.22% per year the storage loss. Reservoir storage loss estimates for different regions of the world and worldwide compiled by White (2001) and cited by Morris *et al.* (2007) are summarized in Table 5.1.

Table 5.1: Worldwide rates of reservoir sedimentation.

Region	Inventoried large dams	Storage (km^2)	Annual storage loss by sedimentation (%)
China	22,000	510	2.3
Asia excluding China	7,230	861	0.3-1.0
North America	7,205	1,845	0.2
Europe	5,497	1,083	0.17-0.2
South and Central America	1,498	1,039	0.1
North Africa	280	188	0.08-1.5
Sub-Sahara Africa	966	575	0.23
Middle East	895	224	1.5
Worldwide	45,571	6,325	0.5-1.0

Source: Adapted by Morris (2007) from White (2001).

The trap efficiency of a reservoir is the portion of the total sediment delivered to the reservoir that is retained in the reservoir (Mitchell & Bubenzer, 1980). It conveys information on what happens to most of the sediment coming into the reservoir and is indicative of the reservoir's useful life (Heinemann, 1981). Julien (1998) defines the useful life of a reservoir as the expected time at which the reservoir will be completely filled with sediments, and indicates that the data required to estimate the life expectancy are: the storage capacity, the mean annual incoming total sediment discharge in weight per year, the sediment size distribution, the trap efficiency (TE) of the reservoir and the dry specific weight of sediment deposits.

In large reservoirs, possibly those with 12.3 hm^3 or more of storage capacity, it may be assumed that the TE will be $\approx 100\%$, however in small dry reservoir, most of the time most of the inflowing sediment may be transported through the pool (Vanoni, 1975). In a bathymetry survey conducted by CEDEX (2002) in La Baells Reservoir it was reported a trap efficiency of 99%, and annual storage loss of 0.19% which is within the range defined for Europe by White (2001) cited by Morris (2007).

Important factors influencing the TE are the sediment characteristics, the retention (storage) time, and the flow dynamics of the reservoir (Bube & Trimble, 1986). All of these are related to the

sedimentation process, thus, parameters controlling this process are important to determine the amount of sediment deposited. The particle size size distribution has to do with the settling velocity, coarse material will have a higher settling velocity, on the other hand, fine material will need long retention times. The retention time is related to the characteristics of the inflow hydrograph and the geometric characteristics of the reservoir, including storage capacity, shape and outlet typology (Verstraeten & Poesen, 2000).

In addition, it should be also considered that the use of sediment density data into sediment yield and erosion rates presents a conversion from volumetric to gravimetric measures. Vanoni (1975) suggests that to estimate the storage loss in reservoirs it is necessary to convert the weight values into volume, but suggests that this is an inexact procedure, because the volume of a given weight of sediment, when deposited in a reservoir varies with the proportions of sand, silt, and clay-size materials, the depth of the deposit, the mineralogical and chemical characteristics of the clay sediments and water, and variations of the pool level that might expose the deposits to alternate wetting and drying. Therefore it would be better first analyse the specific gravity, dry bulk density and moisture content of the deposits because it can affect the accuracy of calculations (Butcher *et al.*, 1993).

The sediment accumulated over a known period of time can be used to obtain the average annual sediment yield, by relating drainage area and sediment yield from reservoir survey, this type of relationship is a common procedure to estimate the sediment yield and is widely accepted (ICOLD, 1989) and used worldwide (White *et al.*, 1996; Verstraeten & Poesen, 2001). Nonetheless, careful consideration of the TE should be paid, because reservoir deposition and sediment yield are not synonymous (Mitchell & Bubenzer, 1980).

The procedure to develop sediment yield and drainage area relationships, consists of measuring specific sediment rates at other reservoirs in the region and plotting them against drainage area, to develop a regional relationship; however, it is essential that the reservoirs all occupy basins having geologic and land use conditions similar to the site under investigation (Morris, 1997), moreover not all reservoirs in a general geographic area are similar, therefore it may not work in these cases.

An apparent weakness of the yield - area relationship, is that it gives only an annual average of the sediment yield and not its temporal evolution. However, if frequent hydrographic surveying of the reservoir is permitted (e.g. every 5 years) then sediment yield can be computed in finer time scales. Alternatively, this method can be combined with hydrological models as well as sediment discharge measurements in upstream locations to reconstruct the temporal evolution of reservoir sedimentation (Zarris & Koutsoyiannis, 2002).

Several studies relating sediment yield to basin area exist such as the one conducted by Strand and Pemberton (1987) using 28 reservoirs in the semi-arid climate of Southwestern USA consisting of basin areas of 1 to 100000 km^2; in Spain, Avendaño et al. (1997) developed a relationship using data from 60 reservoirs, with basin areas raging from 30 to 16,952 km^2, and distributed all over Spain in various climatic, geomorphologic and geologic characteristics.

5.4 Methodology

5.4.0.1 Estimation of the uncertainty of sediment yield from reservoir survey

In the report of bathymetry results given by CEDEX (2002), there is no mention of the variation of sediment yield, nonetheless, it provides reports of the degree of precision of instruments, such as the error of GPS. It is important to define the degree of uncertainty involved in the sediment yield derived from bathymetry surveys, so fair comparison with predictions of sediment yield obtained by other models can be performed.

The confidence interval of sediment yield was assessed by including relevant error sources, namely, (1) topography and bathymetry, (2) bulk density, and (3) trap efficiency. First, the magnitude of error for each of these sources was assessed, and then these sources were combined in order to estimate the error associated to the sediment yield value reported by CEDEX (2002) by using a error propagation formula as shown in Eq. 5.1.

In Eq. 5.1 S_{DS}^2, S_V^2, S_D^2 and S_{TE}^2 are the variances of the deposited sediment (DS), variance of the topography and bathymetry (V), variance of bulk density (D), and variance of trap efficiency (TE) respectively; D^2, V^2 and TE^2 are the squares of the mean values of bulk density, volume and trap efficiency respectively.

$$S_{DS}^2 = S_V^2 \times D^2 \times TE^2 + S_D^2 \times V^2 \times TE^2 + S_{TE}^2 \times D^2 \times V^2 \tag{5.1}$$

5.4.1 Sediment yield from a regression sediment yield - drainage area

Sediment yield for the Upper Llobregat basin was estimated by using a power regression given by (Avendaño *et al.*, 1997). Avendaño *et al.* (1997) developed several relationships between sediment yield (SY) and drainage area (A), they used 60 bathymetry results distributed throughout Spain and obtained Eq. 5.2, nonetheless, the regression explained only 17% of the variability on sediment yield, thus, in order to improve the fit of data they grouped the set of reservoirs in three categories according to their specific sediment yield. Group 1, consisted of 20 catchments and specific sediment yield <1.5 Mg $ha^{-1}yr^{-1}$; group 2 was comprised of 33 basins with an intermediate specific sediment yield between 1.5 and 10.0 Mg $ha^{-1}yr^{-1}$; and group 3 was comprised of 7 basins with yields >10.0 Mg $ha^{-1}yr^{-1}$. Table 5.2 shows the regressions developed for each group, where SY is given in Mg yr^{-1}, and A in km^2.

Table 5.2: Relationships between sediment yield and drainage area.

Group	SSY (Mg $ha^{-1}yr^{-1}$)	Equation SY (Mg yr^{-1}), A (km^2)	R^2	n
1	<1.50	$SY = 617A^{0.67}$	0.77	20
2	1.50 - 10.0	$SY = 202A^{1.07}$	0.92	33
3	>10.0	$SY = 3137A^{0.87}$	0.91	7

Source: Avendaño et al. (1997)

The equation developed for group 2, was one of the equations used to estimate the sediment yield

in the Upper Llobregat Basin, since the r^2 is the highest and n is the largest; in addition Avendaño *et al.* (1997) indicates that it can be regarded as representative of the average situation in Spain.

$$SSY = 4139 \times A^{-0.43} \tag{5.2}$$

5.4.2 Factorial Scoring Model

Empirical relations relating sediment yield to basin properties such as area, rainfall and runoff is a common practice (Verstraeten & Poesen, 2001; Walling, 1983). As the regression developed (from 60 reservoirs) (Eq. 5.2) by Avendaño *et al.* (1997) between sediment yield and area, where, area alone explained little of the variation on sediment yield, Verstraeten *et al.* (2003) added to the existing regression a few additional basin properties. Verstraeten *et al.* (2003), presented a Factorial Scoring Model (FSM) to explain part of the remaining variation of Eq. 5.2 by using sedimentation rates of 22 out of the 60 reservoirs studies by Avendaño *et al.* (1997). In a subsequent study, de Vente & Poesen (2005) developed additional regressions using data all of the 60 reservoirs, but the regressions did not improve the explaination of variation in sediment yield, thus FSM is the one that explain most of the variation on sediment yield.

Factorial Scoring Model (Verstraeten *et al.*, 2003) predicts the annual specific sediment yield of a basin (>100 km^2) based on a nonlinear equation involving the catchment area and five weighted additional factors: topography, vegetation cover, gullies, lithology and slope. Verstraeten *et al.* (2003) identified the general geomorphic setting of the basin, the presence or absence of ephemeral, permanent and bank gullies in the immediate vicinity (5 km) of the reservoir or main river channels, the presence of highly erodible substrates like marls, and the vegetation cover in the surroundings of the reservoir.

The model given by Verstraeten *et al.* (2003) is represented by Eq. 5.3, where I is the total scoring index (product of scores of each factor), this equation is based on 19 out of 60 reservoirs, data of 3 reservoirs were left out because of their strong influence on FSM.

$$SSY = 4139 \times A^{-0.43} + 4.55 \times I + 211 \tag{5.3}$$

Sediment yield for the Upper Llobregat basin was calculated by Eq. 5.3, the scoring of the five factors was performed following the description given in Table 5.2. The method consists of scoring each of the five factors, with a score of 1,2 and 3 for low, moderate and high sediment yields respectively. Then, the index I is calculated by multiplying the score given to each factor, the index can vary between 1 and 243 (if all fators are assigned a score of 3).

- To define the score of the topography factor, it was used a topographical map of the study area, and a geological map at scale 1:25000 (IGN, 1987). It was given a score of 3, since the topography in the vicinity (<5 km) of the reservoir and main streams present steep slopes and the relief within the 5 km is more than 500 m.
- The score for gullies factor was set to 2, within the 5 km a few bank and/or ephemeral gullies can be observed especially in the upslope areas.

Factor	Score	Description
Topography (T)	1	Very gentle slopes near reservoir and main rivers; elevation differences < 200 m within 5 km.
	2	Moderate slopes near reservoir and main rivers, elevation difference between 200 and 500 m within 5 km.
	3	Very steep slopes near reservoir; elevation difference > 500 m within 5 km.
Gullies (G)	1	Bank and ephemeral gullies are rare.
	2	A few bank and/or ephemeral gullies can be observed.
	3	Many bank and/or ephemeral gullies can be observed.
Vegetation cover (V)	1	Contact cover of the soil is very good (> 75% of the soil is protected).
	2	Moderate contact cover (25 - 75 % of the soil is protected).
	3	Little contact cover (< 25% of the soil surface is covered).
Lithology (L)	1	Dominant limestone, sandstone (low weathering degree).
	2	Dominant neogene sedimentary deposit (gravels, etc.).
	3	Strongly weathered (loose) material and marls.
Catchment shape (S)	1	Elongated catchment shape with one main river channel draining to the reservoir.
	2	Catchment shape in between elongated shape and (semi-circular catchment shape).
	3	(Semi) circular catchment shape with many rivers and draining into the reservoir and/or with much direct runoff from hill-slopes to the reservoir.

Figure 5.2: Description of the scores for each of the five factors used with FSM. Source: Verstraeten et al. (2003).

- The vegetation cover factor was given a score 1, since most of the area is forested with a well-developed understory.
- Lithology factor was given a score of 2, because of the presence of marls and strongly weathered materials.
- Finally the basin shape was given a factor 2, because of its semicircular-elongated shape, and relatively low drainage density runoff concentration can be considered moderate.

The product of the scores given to each factor is 36, which was replaced in Eq. 5.3 in order to calculate the sediment yield.

5.4.3 Pacific Southwest Inter-Agency Committee

The PSIAC Model (Pacific Southwest Inter-Agency Committee, 1968) is a parametric and index model which was developed for basins in the western USA greater than 25 km^2. Conceptually it is similar to FSM, but it is different from it, in the sense that it does not combine the drainage area within the factors.

In the PSIAC model nine factors are used, namely: surface geology, soil, climate, runoff, topography, ground cover (land cover), land use, upland erosion, and river erosion and sediment transport. In Table 5.3 the scores and main characteristics of each factor are described. Not all the nine prediction factors are independent of one another, but considers the yield contribution from all types of erosion sources. The highest weight are given to actual signs of erosion (e.g. gullies, landslides), then the

scores of the nine factors are summed in order to calculate an index, which is related to a sediment yield class.

Since the PSIAC model was developed for the western part of the USA, de Vente & Poesen (2005) calibrated and evaluated the model performance for the Spanish conditions, by using the same dataset used to develop FSM. The model calibrated for the Pacific Southwest, and the one calibrated for the Spanish conditions are represented by Eq. 5.4 and Eq. 5.5 respectively.

Sediment yield for the Upper Llobregat basin was estimated by Eq. 5.5, the PSIAC is computed by summing the scores given to each of the nine factors. Scores were obtained from Table 5.3.

$$SSY = 48.59 \times e^{0.036 \times PSIACIndex} \quad (5.4)$$

$$SSY = 35.74 \times e^{0.031 \times PSIACIndex} \quad (5.5)$$

- The surface geology factor was given a score of 5 (moderate), since moderately weathered materials of the neogene deposits exist.
- Soil factor was assigned a score of 5, since the basin can be considered as having medium textured soil, although very fine texture can exist in localized areas.
- Climate factor was set to a score of 5, since the basin is characterized by storms of moderate duration and intensity (mean annual precipitation $\approx$ 900 mm).
- Runoff factor was assigned a score of 5, since peak flows can be considered moderate.
- Topography factor was given a score of 10, because half of the basin has slopes >45%.
- Ground cover factor was set to a score of -10, because there is a good soil protection by understory because about 66% of the basin is forest and 33% grassland.
- Land use factor was also given a score of -10, because of the ausence of agriculture practice and low-intensity grazing.
- Upland erosion factor was assigned a score of 10, since a few rill and gully erosion areas are evident.
- Finally for the channel and sediment transport factor a score of 10 was given, since occasional bank erosion occurs.

The sum of the scores given to each factor was 35, which was pluged in Eq. 5.5 in order to calculate the sediment yield.

Sediment yield levels	A. Surface geology	B. Soils	C. Climate	D. Runoff	E. Topography	F. Ground cover	G. Land use	H. Upland erosion	I. Channel erosion and sediment transport
	(0)*	(0)	(0)	(0)	(0)	(-10)	(-10)	(0)	(0)
Low	a. Massive hard formations.	a. High percentage of rock fragments.	a. Humid climate with low-intensity rainfall.	a. Low peak flows per unit area.	a. Gentle upland slopes (<5%).	a. Area completely protected by vegetation, rock fragments, litter.	a. No cultivation.	a. No apparent signs of erosion.	a. Wide shallow channels with flat gradients, short flow duration.
		b. Aggregated clays.	b. Precipitation in form of snow.	b. Low volume of runoff per unit area.	b. Extensive alluvial plains.	Litle opportunity for rainfall to reach erodible material.	b. No recent road construction.		b. Channels in massive rock, large boulders or well-vegetated.
		c. High in organic matter.	c. Arid climate; low-intensity storms.	c. Rare runoff events.			c. Low-intensity grazing.		c. Artificially controlled channels.
			d. Arid climate; rare convective storms.						
	(5)	(5)	(5)	(5)	(10)	(10)	(10)	(10)	(10)
Moderate	a. Rock of medium hardness.	a. Medium textured soil.	a. Storms of moderate duration and intensity.	a. Moderate peak flows.	a. Moderate upland slopes (<20%)	Covering not exceeding 40%	a. Less than 25% cultivated.	a. About 25% of the area characterized by rill and gully or landslide erosion.	a. Moderate flow depths, medium flow duration with occasionally eroding banks or beds.
	b. Moderately weathered.	b. Occasional rock fragments.	b. Infrequent convective storms.	b. Moderate volume of flow per unit area.	b. Moderate fan or floodplain development.	a. Noticeable litter.	b. 50% or less recently logged.	b. Wind erosion with deposition in stream channels.	
	c. Moderately fractured.	c. Caliche layers.				b. If trees present, understory not well developed.	c. Less than 50% intensively grazed.		
							d. Ordinary road and other construction.		
	(10)	(10)	(10)	(10)	(10)	(10)	(10)	(25)	(25)
High	a. Marine shales and related mudstones and silt-stones.	a. Fine textured, easily dispersed; saline-alkaline; high shrinkage-swell.	a. Storms of several days'duration with short periods of intense rainfall.	a. High peak flow per unit area.	a. Steep upland slopes (>30%).	Ground cover does not exceed 20%.	a. More than 50% cultivated.	a. More than 50% of the area characterized by rill and gully or landslide erosion.	a. Banks eroding continuosly or at frequent intervals with large depths and long flow duration.
		b. Single grain silts and fine sands.	b. Frequent intese convective storms.	b. Large volume of flow per unit area.	High relief; litle or no floodplain development.	a: Vegetation sparse; little or not litter.	b. Almost all area intensively grazed.		
			c. Freeze-thaw.			b. No rock in surface soil.	c. Entire area recently burned.		

** Weighting factors in parentheses.*

The total score is the sum of individual scores.

Total score	Estimated sediment yield ranges (Mg/km2/yr)
> 100	> 1830
75 - 100	610 - 1830
50 - 75	300 - 610
25 - 50	120- 300
0 - 25	< 120

Figure 5.3: Description of the scores for each of the nine factors used with PSIAC. Source: PSIAC (1968) after Morris (1997).

5.5 Results

5.5.1 Sediment yield from reservoir survey

5.5.1.1 Mean sediment yield

The sediment yield or delivered to La Baells Reservoir from the entire drainage area and reported by CEDEX (2002) was 4.32 Mg $ha^{-1}yr^{-1}$, however this value was calculated using as drainage area of 532 km^2, after adjusting to 504 km^2 which is the area value used throughout this thesis the sediment yield is 4.54 Mg $ha^{-1}yr^{-1}$. These values were calculated by multiplying the sediment weight times the bulk density, then, this is adjusted by trap efficiency, drainage area and years since construction. Table 5.3 summarizes relevant data of the reservoir.

Table 5.3: Summary of the relevant data of La Baells Reservoir.

Description	Value
Initial volume (construction finished in 1967)	115.00 hm^3
Volume in 2002	109.43 hm^3
Reservoir's surface (2002)	3.67 km^2
Reservoir's height	102 m
Years of explotation	25
Drainage area	532 km^2
Mean annual loss capacity	0.19%
Expected useful life	>100
Bulk sediment density	1021.00 kg/m^3
Trap efficiency	99 %
Sediment yield	4.32 Mg $ha^{-1}yr^{-1}$

Source: adapted from CEDEX (2002).

The estimated sediment yield (4.54 Mg $ha^{-1}yr^{-1}$) is used as benchmark against, which the results estimated through other models or methods are compared. Reservoir surveys are generally seen as producing more reliable results than alternatives procedures, since reservoir sedimentation data provide direct measurements instead of indirect estimates (Pemberton & Strand, 1987), but as in any other measurement error analysis are important to consider.

5.5.1.2 Error sources

Topography and bathymetry The error due to topography and bathymetry, was calculated by using the vertical error of the GPS reported by CEDEX (2002) which was ± 2 cm (0.02 m), and the area of the reservoir which is 36,700 m^2. The product of these two parameters is 734 m^3, this represents roughly 0.013% of the volume of deposited sediment (Table 5.3), but its contribution to the error associated to sediment yield might be considerable, since it is mulplied by other variables such as bulk density and trap efficiency.

Bulk density The mean bulk density of the deposited sediment and reported by Avendaño *et al.* (1997) was 1,021 kg m^{-3}, in order to estimate the error associate to it, it was considered an error

of 5% for profile bulk density measurements suggested by Allen *et al.* (1993) and related to error in the use of instruments, errors associated to sampling was considered negligible; therefore, the error linked to the mean bulk density value was 51.1 Mg $ha^{-1}yr^{-1}$.

Trap efficiency Trap efficiency is the ratio of the sediment mass deposited within the reservoir to the mass of sediment entering a reservoir. The trap efficiency was estimated at $\approx$ 99% by CEDEX (2002) by applying Brow's curve, which relates the ratio of the capacity of the reservoir and drainage area to trap efficiency.

Brown's curve is shown in Fig. 5.4 and it is represented by Eq. 5.6, where C is the reservoir storage capacity expressed in m^3, W is the drainage area expressed in km^2 and D values range from 0.046 to 1, which is dependent on the characteristics of a reservoir; however, Brune (1953) cited by Verstraeten & Poesen (2000) noted that C/W ratio could have different TE's values if their drainage areas produced different runoff volumes, due to other hydrological characteristics. To overcome this problem Brune (1953) quoted by Verstraeten & Poesen (2000) used a capacity-annual inflow ratio (C/I), this curve is shown in Fig. 5.5.

The confidence interval of TE derived from Brown's curve 5.4 and using a ratio C/W of 228,000 m^3km^{-2} (ratio of 115 hm^3 to 504 km^2) would be somewhere between 95% and 100%. On the other hand, the TE confidence interval using Brune's curve (5.5) estimated by using a capacity-inflow ratio of 0.54 (ratio of 115 hm^3 to 212 hm^3) lies between 93% and 100% (mean 96.5%). Since the intervals are very similar, it was used the range derived from Brune's curve since it uses the annual discharge inflow, therefore, assuming a Normal distribution of TE and with 90% confidence the error range of 7% is adjusted to the Normal curve by dividing it by 1.64 (90% confidence), which means that the error is 2.1% in each tail of the Normal distribution curve, this error is used in the error propagation error formula.

$$TE = 100 \times [1 - \frac{1}{1 + 0.0021 \times D \times \frac{C}{W}}] \tag{5.6}$$

5.5.1.3 Confidence interval

The magnitude of error associated to sediment yield was calculated by Eq. 5.1 and using data given in Table 5.4. With 90% confidence the lower and upper bounds of the confidence interval of sediment yield are 4.29 Mg $ha^{-1}yr^{-1}$ and 4.79 Mg $ha^{-1}yr^{-1}$ respectively.

Table 5.4: Data used in the error propagation formula.

Description	Mean	Std.dev.	Variance
Topography and bathymetry (m^3)	5570000	734	538756
Bulk density of deposited sediment (kg m^{-3})	1021	51.1	2611.21
Trap efficiency (%)	0.965	0.021	0.000441

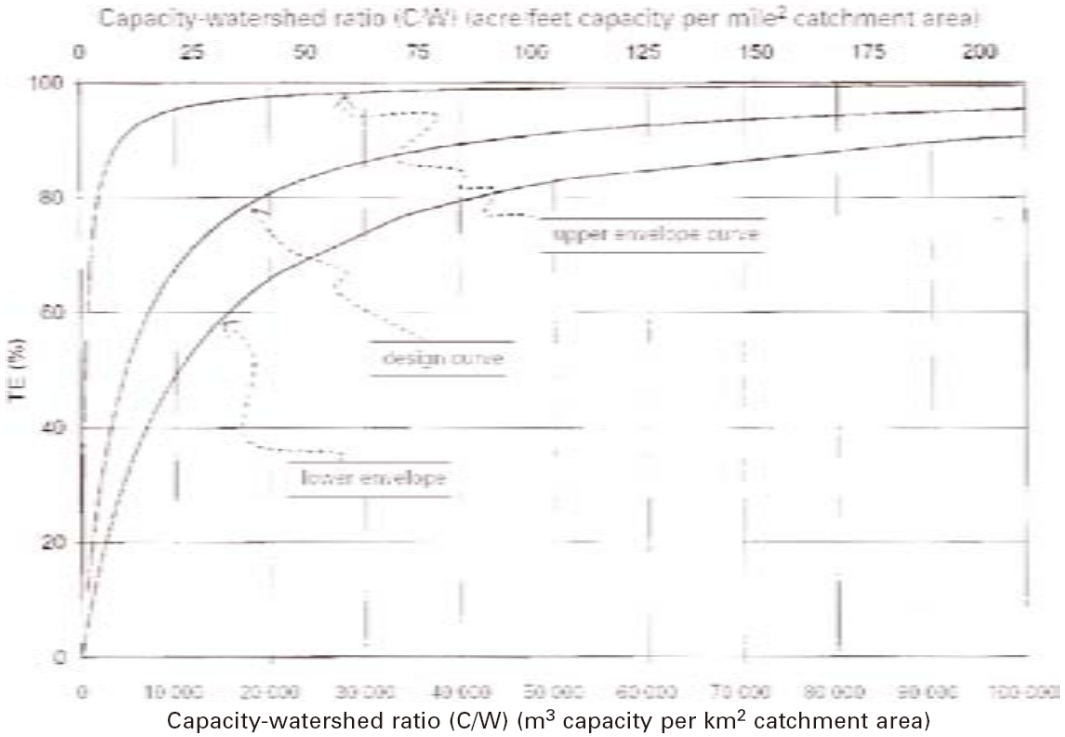

Figure 5.4: Trap efficiency related to capacity/watershed ratio. Source: Brown, C.B.(1943) Proceedings of the American Society of Civil Engineers. Cited by Verstraeten (2000).

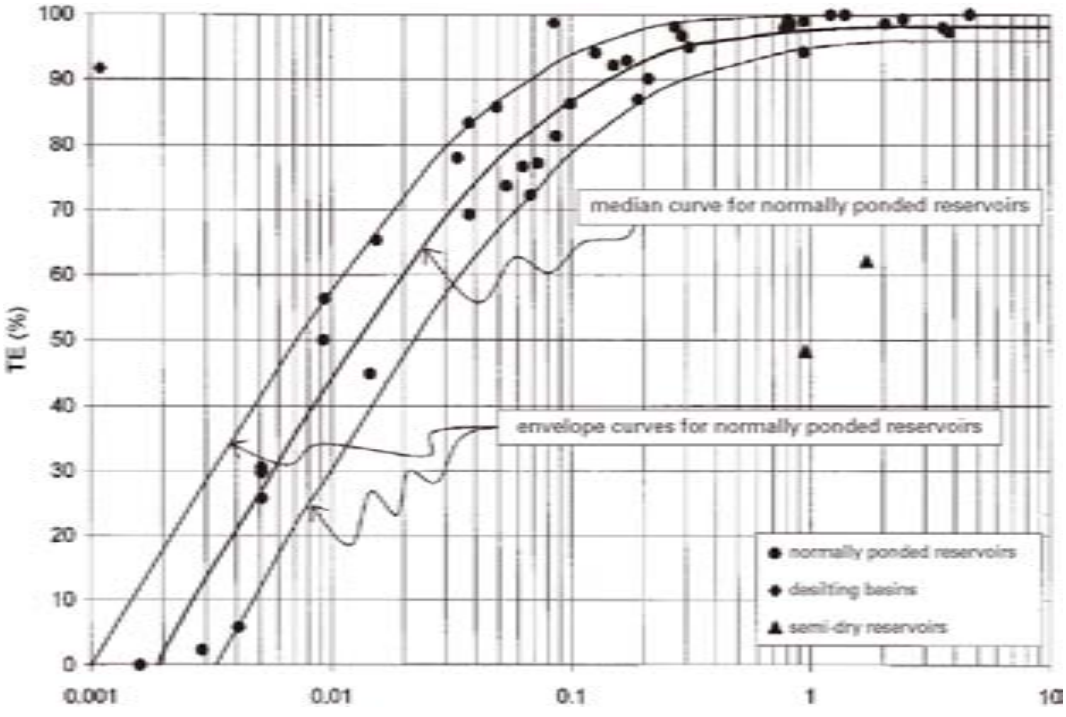

Figure 5.5: Trap efficiency related to capacity/annual inflow ratio. Source: Modified by Verstraeten (2000) from Brown, C.B.(1943), Transactions of the American Geophysical Union. Cited by Verstraeten (2000).

5.5.2 Sediment yield from a regression sediment yield - area

The amount of sediment yield estimated by equation developed for group two presented in Table 5.2 was 3.12 Mg $ha^{-1}yr^{-1}$, which is 31% less than the sediment yield obtained by bathymetry survey (4.54 Mg $ha^{-1}yr^{-1}$ (CEDEX, 2002); however, it is within the interval of sediment yield given for Spanish reservoirs by Avendaño *et al.* (1997) which is between 0.84 and 27.03 Mg $ha^{-1}yr^{-1}$, nevertheless it is 30% less than the average yield (4.44 Mg $ha^{-1}yr^{-1}$) given by the same author. Similarly, the estimated sediment yield is 26% less than the average yield calculated by Avendaño *et al.* (1997) for river basins in the Ebro River (4.23 Mg $ha^{-1}yr^{-1}$), which are also located in the northern Spain.

By using Eq. 5.2, the sediment yield was 2.85 Mg $ha^{-1}yr^{-1}$, which is 37% less than the yield calculated from bathymetry survey. Eq. 5.2 was developed by using dataset from 60 reservoirs, and had a low coefficient of determination ($r^2 = 0.17$), the underestimation is larger than when using the equation developed for group two showed in Table 5.2.

Sediment yield estimated by Eq. 5.2 and second equation from Table 5.2 are fairly similar, the difference between the both is that the relationship: sediment yield-area, is negative in the former and positive in the latter. Given that in the the study area, bank erosion is not the dominant type of erosion, although it exists in some areas, thus, the sediment yield estimated by Eq. 5.2 is probably closer to the real sediment yield.

5.5.3 Factorial Scoring Model

Sediment yield estimated by Eq.5.3 was 6.59 Mg $ha^{-1}yr^{-1}$. A closer examination of the sediment yield values for each component of Eq. 5.3 indicates that the area component (developed by Avendaño *et al.* (1997)) contributes with 2.85 Mg $ha^{-1}yr^{-1}$, and the second component added by Verstraeten *et al.* (2003) provides 3.74 Mg $ha^{-1}yr^{-1}$ by using an total scoring index of 36.

5.5.4 Pacific Southwest Inter-Agency Committee

The sediment yield obtained by Eq. 5.5 was 1.06 Mg $ha^{-1}yr^{-1}$, using a total score of 35. The estimated yield is 77% less than the sediment calculated from bathymetry survey, and 66% less than the yield estimated by FSM.

5.6 Discussion

Sediment yield from bathymetry survey is very important benchmark, because it is used to evaluate the perfromance of FSM and PSIAC, nonetheless an exhaustive uncertainty assessment using measurement dataset would have been recommendable, here only three relevant error sources were included. The confidence interval of sediment yield is relatively narrow, by including additional error sources the interval might be wider.

Regarding the FSM and PSIAC models, they present some difficulties while assigning a specified score to factors, especially in large basins with large topographical variation. In FSM it is assumed

an independence between factors and all factors have the same weight. FSM models was developed by adding additional factors to the regression developed using 60 reservoirs, which had a low r^2;therefore, the variability on sediment yield is mostly explained by the additional scores to which values are assigned. If additional factors were added, so the equation for group 2 would have improved estimations.

For a neighboring river basin with similar topographic and geologic characteristics (Reservoir Sant Pons), although of smaller area, to the Upper Llobregat Basin (Reservoir La Baells) the reported annual loss of storage capacity was 0.94% (Avendaño *et al.*, 1997).

5.7 Conclusions

Factorial Scoring Model, Pacific Southwest Interagency Committee and a regression between sediment yield and basin area were used to estimate the sediment yield in the Upper Llobregat basin. PSIAC and the regression sediment yield - area underestimated the sediment yield, although, the magnitude of underestimation is smaller for the sediment yield - area regression, on the other hand, FSM overestimates the sediment yield.

Despite the under or overestimation, and the subjectivity involved while using these models, the results obtained can be still be considered useful as an initial assessment of the amount of sediment delivered to the outlet of the basin.

Chapter 6

SOIL EROSION WITH GIS BASED RUSLE AND ASSESSMENT OF SEDIMENT YIELD IN THE UPPER LLOBREGAT BASIN

6.1 Introduction

Erosion models provide one way of quantifying soil erosion rates. These models have represented soil erosion dynamics at different levels of complexity and at different spatial and temporal scales. Commonly, the study area is divided into a series of basic small units, and erosion values are calculated for each unit based on the topological structure defined for the catchment, then are used to determine the amount of soil actually entering and leaving the individual units (McDonnell, 1998). Data from these small units are extrapolated to river basin scale applying a sediment delivery ratio, in this process uncertainty is involved and need to be addressed when these models are used to support management practices.

The Revised Universal Soil Loss Equation (RUSLE) is an empirical erosion model designed to predict the longtime average annual soil loss carried by runoff from specific field slopes in specified cropping and management systems, as well as from rangelands (Renard *et al.*, 1997). RUSLE has evolved from USLE (Universal Soil Loss Equation) which is an empirical model developed by (Wischmeier & Smith, 1978) to predict long-term average annual soil loss from agricultural fields and it has been utilised for over 30 years; however, it has been critised for its unability to estimate gully erosion, because, it only allows prediction of soil loss caused by sheet (inter-rill) and rill erosion. RUSLE is a significant improvement over the widely used USLE, such as prediction of soil erosion in hillslopes but it has not been yet tested extensively against field data.

While it is likely that application of more complex models than RUSLE might provide more accurate estimates of soil erosion for specific sites (plot, hillslopes scales), for example of process-based models such as WEPP (Water Erosion Prediction Project) (Laflen *et al.*, 1997) and EUROSEM (European Soil Erosion Model) (Morgan *et al.*, 1998), these are too data and computationally intensive in many circunstances (Kinell, 2007) making them difficult to use on a regional scale. For example

USDA Agricultural Research Service (ARS) indicates that, while the WEPP model is superior for cropland, rangeland, and forest applications, it requires considerably more data and expertise than RUSLE in its application and interpretation (Jones *et al.*, 1995).

RUSLE and its predecessor USLE have as their main drawback the unability to predict deposition, sediment yields from complex shaped hillslope profiles, sediment size information, or temporal and spatial distributions of erosion (Nearing & Nicks, 1998). The advantages of RUSLE are the flexibility to adapt to other climates rather than only temperates, it is an empirical based model rather than a strict mathematical model, and has been widely used as the leading tool for the prediction of erosion and conservation planning in the USA and elsewhere. It enables prediction of an average annual rate of soil erosion for a site of interest for any number of scenarios involving cropping systems, management techniques, and erosion control practices (Angima *et al.*, 2003). Erosion rates of ungauged catchments can also be predicted using RUSLE by using knowledge of the catchment characteristics and local hydro-climatic conditions (Garde & Kathyari, 1990).

Larsen & MacDonald (2007) indicate that RUSLE is more successful in predicting sediment yields from groups of hillslopes than predicting sediment yields from individual hillslopes. In spite of some drawbacks, improvement in soil erosion prediction within RUSLE has come along with GIS technology development, which has allowed better estimations of the factors involved, and continues to be the primary soil erosion prediction tool in use, until other erosion simulation models are developed for the general user (Jones, 2001) and for river basin scale.

Indeed, GIS software which has become an useful tool in watershed analysis, because it provides a mean of handling, integrating and visualising digital spatial data at many scales; however, as with all tools, limitations and problems can be asociated to the current state of the technology (McDonnell, 1998), the outcomes need to be compared with field observations.

RUSLE empirically represents the infiltration, overland flow, particle detachment or sediment transport, despite the fact it does not explicitly model them (Renard *et al.*, 1997). It computes the average annual erosion expected on hillslopes by multiplying several factors together by the means of the Eq. 6.1:

$$A = R \times K \times LS \times C \times P \tag{6.1}$$

Where:

A is the computed spatial average soil loss and temporal average soil loss per unit of area, expressed in the units selected for K-factor and for the period selected for R-factor. A in the SI generally is expressed as Mg $ha^{-1}yr^{-1}$. R is the rainfall-runoff erosivity factor in MJ mm $ha^{-1}h^{-1}$; K is the soil erodibility factor in Mg h $MJ^{-1}mm^{-1}$; L is the slope length factor; S is the slope steepness factor; C is the land cover and management factor; and P is the conservation support-practices factor. The L, S, C, and P factors are dimensionless.

RUSLE is a powerful tool and it can be used to calculate soil loss, but it does not account for all the dynamic hydrologic and soil loss processes that occur within a watershed (Cox & Madramootoo, 1998). It provides an estimate of potential soil loss only from slope segments, where erosion is occurring and does not account for sediment delivery and deposition, therefore, delivery ratio functions need to be used to determine the amount of sediment delivered down slope (Renard *et al.*, 1997).

For many parts of the world, the advent of improved and inexpensive Digital Elevation Models (DEM) generation through softcopy photogrammetry and interference SAR (Synthetic Aperture Radar), along with land cover mapping using remotely sensed imagery, have allowed to carry out soil erosion estimates. For example, in mountain areas in Europe, attempts to quantify the soil erosion and sediment yield exists such as the adaptation of RUSLE model (cartographic maps of soil erosion) in the French Pyrenees (Le Lauragais) which allowed to identify areas highly affected by erosion (Morschel & Fox, 2004), due to its simplicity it was also used to calculate average soil erosion rates in the Austrian alpes (Klaghofer *et al.*, 2002).

For this study, three primary GIS data layers were used to develop the RUSLE factors. These were:

- the DEM, with a pixel resolution of 20 m by 20 m, or 0.4 ha grid cell resolution. DEM which is a three-dimensional raster representation of the topography;
- soil type coverage and
- land use coverage.

The DEM was used to derive the slope length (L) and slope steepness (S) factors in the model. The soil type coverage was required to derive the soil erodibility (K) factor and the land-use coverage was required to develop the crop management (C) and conservation practice (P) factors. The rainfall erosivity (R) factor was developed from data collected for over a decade in 8 weather stations.

The use of GIS in soil erosion allows the spatial distribution and integration of information. IDRISI Kilimanjaro software (Eastman, 2003) includes RUSLE module, and it works integrating the five factors in the form of rasters to estimate the amount of eroded soil in the river basin. It allows the identification of high risk areas and define intervention scenarios. The soil erosion in the Upper Llobregat basin was estimated through RUSLE module, for each RUSLE's factors a raster was developed, to do so, input information was based on field work, statitiscal analyses of dataset and review of published data.

The spatial influence of each factor on erosion rates varies according to local biological, climatic, geologic, geomorphology and human influence; therefore, the spatial resolution of input data plays a key role on the accuracy of soil loss estimates.

Sediment Delivery Ratio (SDR) is defined as the ratio of sediment delivered at a location in the streams system to the gross erosion from the drainage area above that point, this ratio varies widely with size of area, steepness, density of drainage network, and many other factors (Elliot, 1995b). In order to estimate the sediment yield at the Upper Llobregat basin a SDR was calculated and multiplied to the average soil erosion in the river basin (gross soil loss).

The obtained sediment yield is compared with sediment yield estimated from a reservoir sedimentation survey conducted during 2001 by the *Centro de Estudios y Experimentacin de Obras Públicas*, and other estimates by using semi-quantitative methods. Results of reservoir bathymetry provides benchmark information for evaluating the degree to which RUSLE's results are similar.

In addition, sensitivity and uncertainty analysis of each factor on soil loss was assessed, the relief complexity of the study area makes the density and location of point observations have strong variability in extrapolation processes. It is important to consider that the micro- to meso-scale variations of climatic features and soil properties increase with increasing topographic complexity of the landscape (Christakos, 1992).

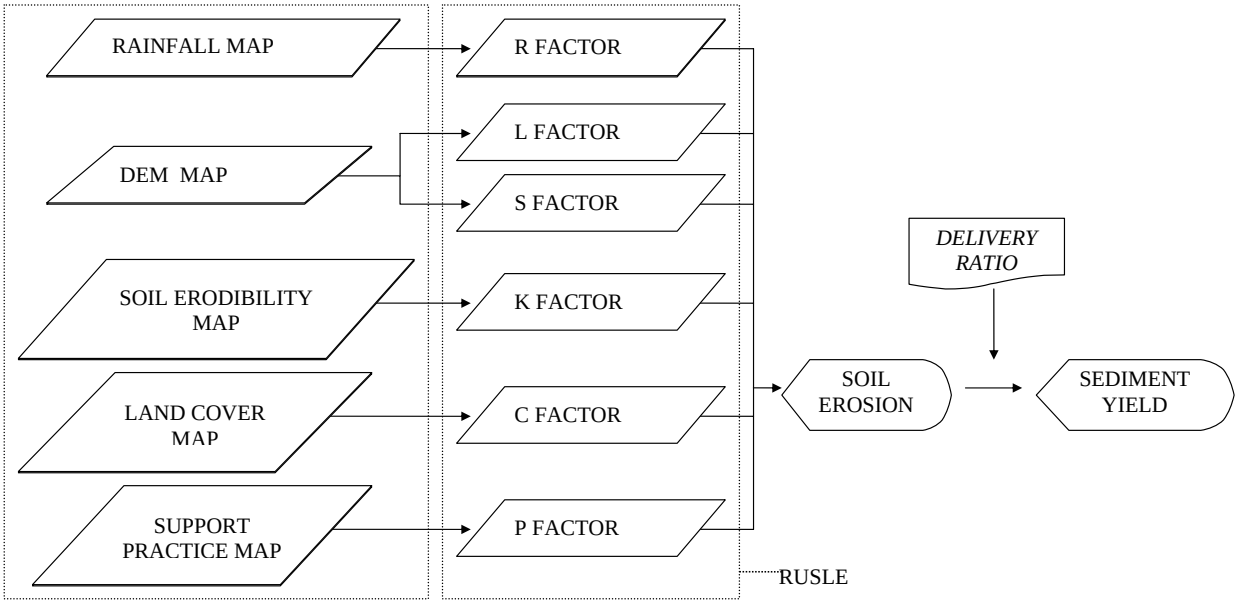

Figure 6.1: Scheme of RUSLE's input factors and sediment delivery ratio.

6.2 Objectives

The aims of this Chapter are to:

- evaluate the applicability of RUSLE in the Upper Llobregat basin.
- to assess the magnitude of uncertainties in soil erosion and sediment yield values at the Upper Llobregat basin.

6.3 Materials and methods

6.3.1 Rainfall-runoff erosivity factor

R factor is one of the most important factors to estimate soil loss. In its calculation only the characteristics of precipitation are involved. Precipitation is any form of solid (hail, snow) or liquid (rain, drizzle) water that falls from the atmosphere to the earth's surface. It is formed from water vapor in the atmosphere by condensation of some water vapor in the air into liquid or solid water (Elliot, 1995a). Precipitation is a natural phenomenon that humans can do very litle to control (Ward & Trimble, 2004). It defines the type of vegetation in the spatial and temporal scales, type of farming systems, and it is the meteorological characteristic which has the greatest impact on sediment movement (Ichikawa, 2005). The term rainfall is characterized by water droplets of size 0.5 - 6 mm, the drops larger than 6 mm tend to break into drops of smaller sizes during their fall (Mishra & Singh, 2003).

Rainfall dominantly causes interrill erosion (Parsons, 2006; Heathcot, 2002), whilst rill and gully erosion are driven by hydraulic processes related to shear of the water flow at the soil-water interface

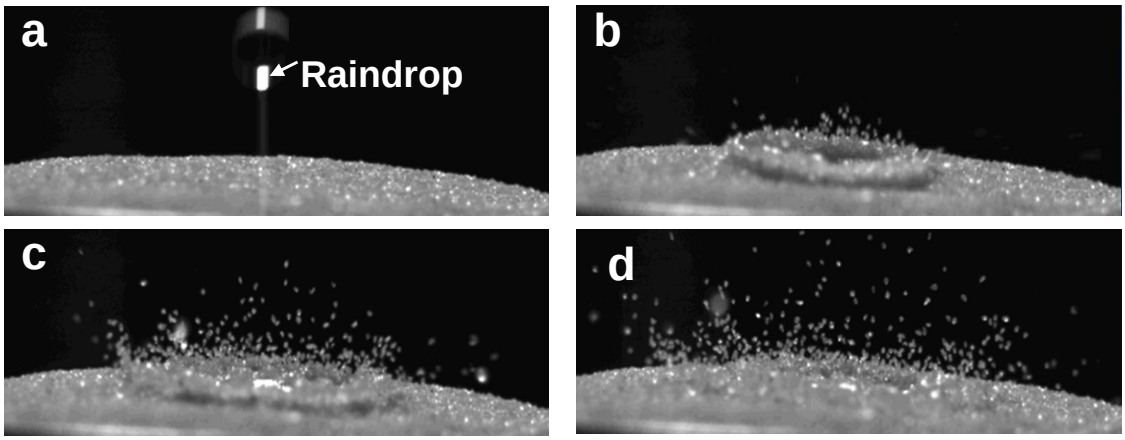

Figure 6.2: Process of soil particle detachment: (a) falling raindrop, (b) raindrop impact, (c) and (d) soil particle detachment. Source: Kinell (2007).

(Grissinger, 1996). Rills are channels small enough to be removed by ploughing, in other words are continuous channels of narrow width and shallow depth (Heathcot, 2002), gullies by contrast, are not (Parsons, 2006). Interrill erosion occurs when soil between rills is detached by impacting raindrops and is transported to rills by overland flow (Heathcot, 2002).

Rainfall erosivity is the ability of rainfall to detach and transport soil particles (Elliot, 1995a). The rate of detachment is a function of the rainfall energy at the soil surface, so that where vegetation intercepts most of the energy of the rainfall, or a layer of surface water exists, most of the energy of the falling rain will be dissipated (Parsons, 2006).

It has been identified four detachment and transport systems (Kinell, 2006): (1) raindrop detachment with transport by raindrop splash (commonly known as splash erosion), (2) raindrop detachment with transport by raindrop-induced flow transport (where each drop impat causes soil particles to saltate underwater), (3) raindrop detachment with transport by flow (when loose particles travel with the flow without the aid of raindrop impact), and (4) flow detachment with transport by flow (rill erosion is dominated by this type) (Kinell, 2006). For instance in some more or less natural land units in a Mediterranean area (South Italy) the mean sediment transport by splash and by overland flow measured over a period of three months, was reported to be about the same order of magnitude (Van Asch, 1983).

Fig. 6.2 illustrates the detachment and transport of soil particles associated with splash erosion, which includes the raindrop impact on soil surface and soil particle detachment.

To assess the rainfall erosivity, the important parameters include the amount of precipitation (depth), intensity (temporal distribution of depth), type of precipitation, kinetic energy and the distribution and velocity of raindrops (Mikos *et al.*, 2006). These parameters indicate how much and how hard a specific rainstorm has fallen in a specific area. The rate at which rain occurs is denoted by rainfall intensity, which is classified as light if it is less than or equal to 2.5 mm/h, moderate if it is between 2.5 and 7.5 mm/h, and heavy if it is greater than 7.5 mm/h (Mishra & Singh, 2003).

An average annual value of rainfall erosivity is determined from historical weather records, and it is the average annual sum of the erosivity of individual storms. For a given rainfall amount,

the rainfall intensity and time duration are inversely related, the greater the rainfall intensity, the lesser will be the time duration and vice versa (Mishra & Singh, 2003). The erosivity of an individual storm is computed as the product of the storm's total energy E (storm kinetic energy), which is closely related to the amount of water, and the storm's maximum 30-minute intensity I_{30}. The maximum 30-minute intensity is a better measure of the intensity effect than either average intensity or peak intensity (Foster, 2004).

The energy of a given storm depends upon all the intensities at which the rain occurred, and the amount of precipitation that is associated with each particular value of intensity (Lee, 2003). From the relationship between the amount and intensity of rainfall can be developed erosivity maps and its distribution percentage . As far it concerns to the type of relationship between E and I_{30} it has been discussed by researchers, for example Wischmeier and Smith (1958) sugested a logarithmic function to use within USLE, but some others such as Kinell (1980) have suggested a exponential relationship. The use of logarithmic or power equations implies that there is no upper limit to kinetic energy (Van Dijk, 2002), nevertheless other researchers have suggested that a maximum value does exist (Kinnell, 1980; Brown and Foster, 1986). Wischmeier and Smith (1978) acknowledged this phenomenon and adaptated their original equation, and it was considered that the kinetic energy contents remain constant at 28.3 J m^2 mm^{-1} for rainfall exceeding 76 mm h^{-1}, therefore, for RUSLE the EI is assumed to be linear, and the parameter's of individual storm values are directly additive (Renard *et al.*, 1997). The correlation between erosion and rainfall intensity occurs not only because of rainfall energy, but also because during a rainfall episode variation in salt dilution in the soil solution enhancing defloculation and dispersion (Imeson & Verstraten, 1981).

The R factor in RUSLE indicates that when factors other than rainfall are held constant, soil losses from cultivated fields are directly proportional to the multiplication of the total storm energy (E) times the maximum 30-min intensity (I30). The R factor in MJ mm $ha^{-1}h^{-1}$ was calculated from Eq. 6.2 (Wischmeier and Smith, 1978).

$$R = \frac{1}{n}\sum_{j=1}^{n}[\sum_{k=1}^{m}(EI_{30})_k] \tag{6.2}$$

Where EI30 is the rainfall erosivity index for storm k, m is the number of storms in an n year period. The total storm kinetic energy E_k (MJ ha^{-1}) was obtained by Eq. 3, where p_k and i_k are, the rainfall depth (mm) and rainfall intensity (mm h^{-1}) for rainfall periods in which intensity was considered constant, and it was calculated by using Eq. 6.3 (McGregor *et al.*, 1995; Foster, 2004).

$$E_k = p_k \times 0.29 \times [1 - 0.72exp^{-0.082i_k}] \tag{6.3}$$

R factor does not account the water supplies from: snow melting, the water from irrigation nor the rainfall on frozen soil (López-Vicente *et al.*, 2007).

The R factor for the weather stations shown in Table 6.1 were computed in two stages, because of diverse temporal resolution of rainfall series. First, R factor values were computed for the stations (Vallcebre) where sub-hourly rainfall dataset was available, and a few relationships between R factor and amount of rainfall were developed. Second, the established relationships were extrapolated to stations having coarse temporal resolution of rainfall data.

Figure 6.3: Rain gauge in Vallcebre catchments.

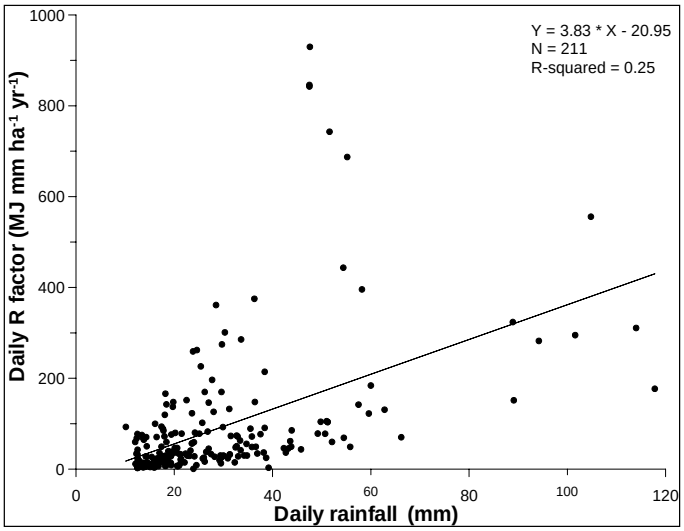

Figure 6.4: R factor annual basis.

6.3.1.1 R Factor for Vallcebre

For Vallcebre catchment the long-term average annual R factor values were calculated according to Eq. 6.2. This equation is given by the sum of individual erosion index (EI) values and which are obtained by multiplying the energy of a storm by its maximum 30 minute intensity. Data were collected in a weather station located in the Vallcebre catchment Fig. 6.3. Rainfall dataset between 1994 and 2005 were used. The calculation has involved the analysis of the hyetograph of every rainfall event, rains of less than 12.5 mm and separated from other rains by more than 6 hours were not included in the computations unless the maximum 15 minute intensity exceeded 12.5 mm as indicated by Foster (2004). It was demonstrated that light rains are usually too small for practical significance and that, collectively, they have little effect on the distribution of the annual EI or erosion (Renard *et al.*, 1997).

The total number of rainfall events (rainy days) having depth $\geq$ 12.5 mm and ocurred between 1994 and 2005 were 211. These rain storms were divided into two groups according to the season

when they ocurred: summer and the rest (all seasons but summer). In Vallcebre, rainy seasons typically are autumn and spring; however, during summer short intense convective storms may provide significant rainfall amounts (Latron *et al.*, 2003).

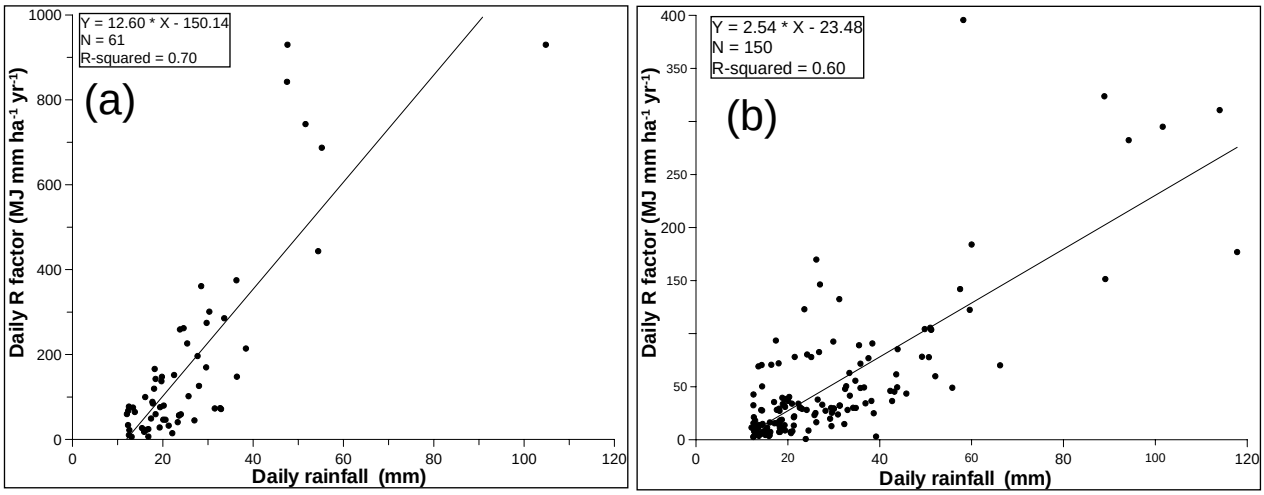

Figure 6.5: Linear regression between daily rainfall and R factor for Vallcebre catchment: (a) summer, (b) rest of the seasons.

Due tot he resolution of the available rainfall dataset from the remaining 7 stations was daily -not at event scale-, the rainfall dataset from Vallcebre were transformed into daily resolution. Here, day is undertood as the 24 hour period counted from 8:00 am until 8:00 am of the next calendar-day, thus, there were events where part of them were computed in two different days.

For each rainfall episode, first, the kinetic energy was determined by using Eq. 6.3. Second, the rainfall intensity in 30 minutes (I_{30}) was determined. To help to identify the segment with the maximum rainfall depth in a given rainfall event, a cumulative plot between time and rainfall depth was done, and the segment with the highest slope was selected and summed their corresponding rainfall depths (I_{30}).

The kinetic energy and rainfall intensity (I_{30}) data for all rainfall daily episodes were placed in a worksheet in order to calculate the daily R factor factor. In the next step, two linear regressions between the computed daily R factor values and their corresponding rainfall depth was performed. The development of two regressions is backed up by an ANOVA analysis, which outcomes showed that the degree of variability is reduced by using separate regressions for summer (61 out of 211) and rest of the seasons (150 out of 211), the statistics of this analysis were: F = 310.4, p $<$ 0.05 and α=0.05.

The two equations are presented in Eq. 6.4 and 6.5 for summer and rest respectively, and where P is the daily rainfall depth expressed in mm.

In Fig. 6.5a and 6.5b the scattered plots for summer and rest of the seasons respectively, between daily R factor and daily rainfall are shown. The scatter plot for summer shows that the data points of both, daily R factor and rainfall depth have a very high values compared to the rest of the seasons. The coefficient of determinations are $r^2 = 0.70$ and $r^2 = 0.60$ for summer and the rest respectively.

$$R = -150.14 + 12.60 \times P \quad (6.4)$$

$$R = -23.48 + 2.54 \times P \quad (6.5)$$

The obtained regressions developed by using the sub-hourly rainfall dataset from Vallcebre will be used to find the daily R factor values in the weather stations with daily data. A direct extrapolation of R factor values obtained for Vallcebre to a larger basin (Upper Llobregat) would be subjected to large errors, because of the unequal spatial and temporal distribution of rainfall at larger scale.

6.3.1.2 R Factor for the Upper Llobregat basin

Rainfall dataset for the Upper Llobregat basin were available from eigth weather stations, which are illustrated in Fig. 6.6; only four of them are within the perimeter of the basin: Vallcebre, Baga, La Pobla and Figols. The remainder stations are located nearby, namely: Borreda, Berga, Josa and La Molina. The location and altitudes of each of these weather stations are illustrated in Table 6.1.

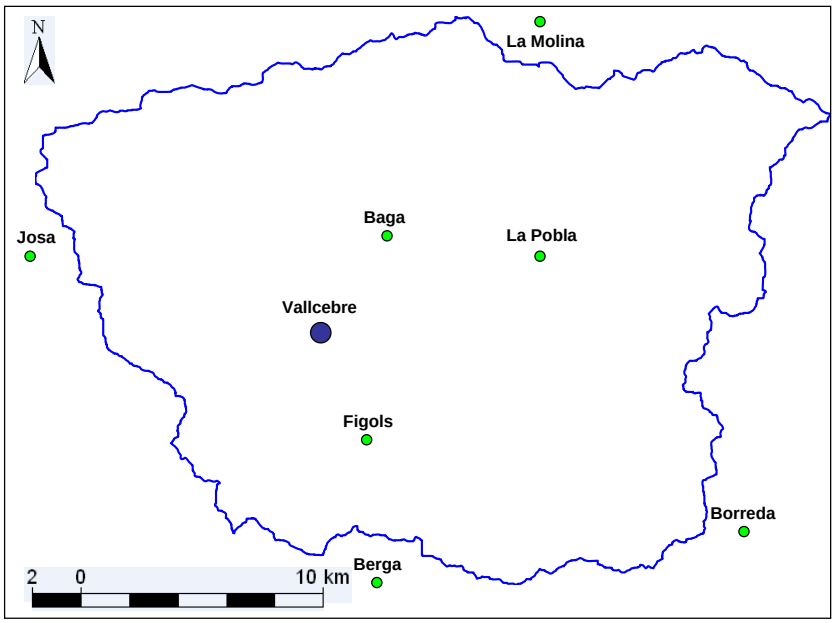

Figure 6.6: Location of weather stations.

In order to estimate the daily R factor for the weather stations having only daily rainfall depth, either of the two linear regressions developed in Section 6.3.1.1 were used, depending on the season when the rainfall event has ocurred (summer or rest of seasons). The available rainfall dataset is comprised by data from 1991 to 2004 for all weather stations, except Josa where data was from 1991 to 2003. The dataset was provided by the Spanish National Meteorological Institute (INM). Only rainfall events having $\geq$ 12.5 mm were included in the analyses.

The outcome daily R factor values were summed up per year and weather station, then, the average annual and standard error of the mean of R factor were calculated. Nonetheless, since the computed annual R factor values were determined using point rainfall data (at the weather stations), a map

Table 6.1: Location of weather stations set up by the Spanish Meteorological Institute (INM).

Weather station	INM code	UTM (x)	UTM (y)	Altitude m a.s.l.
La Molina	585	412463	4687479	1680
Josa Tuixen	632o	381765	4676545	1184
La Pobla	78u	413296	4677011	808
Baga	82	406006	4678709	795
Vallcebre	84i	402375	4673051	1133
Figols	85a	405773	4669858	754
Berga	92c	404520	4662070	664
Borreda	99	421212	4665411	845

Source: Delgado (2006) and INM (2004).

for the R values was obtained by extrapolating (considering the spatial influence of each station) by using the Thiessen Method within IDRISI. The Thiessen Method calculates the size of the land area to which the weather station data is extrapolated, the result is that, each pixel is assigned a R value.

6.3.2 Soil erodibility factor

The erodibility of a soil is an expression of its inherent resistance to detachment and transport by rainfall. It is determined by the cohesive force between the soil particles. Soil erodibility may vary depending on soil characteristics, such as particle distribution, structural stability, organic matter content, nature of clay minerals, chemical constituents, soil structure, slaking and water transmission (Lal, 1988). Other factors, such as the previous cropping activities and/or soil management or the type of bonding that aggregate the soil particles (Millington, 2006; Becher, 1988) can also affect soil susceptibility to erosional processes.

The fact that different soil have different ability to resist detachment is complex, because its estimation relies on many factors as listed above. The agricultural approach USLE and RUSLE (Wischmeier & Smith, 1978; Renard *et al.*, 1997) has played large influence on how the erodibility is estimated, indeed, during the last three decades most of the soil erodibility research has been carried out based on this approach. Applications of RUSLE in areas other than agricultural plots were done, however, this may have led to a simplification of the many variables involved in the calculation of the erodibility factor. In spite of this and as with all models, limitations have been imposed because of simplification and assumptions. Integrating many relevant variables as possible may improve the soil erodibility assessment.

Within RUSLE, soil erodibility factor K, is a quantitative description of the inherent erodibility of a particular soil, and the factor reflects the fact that diferent soils erode at different rates when the other factors that affect erosion are held constant. The K factor represents the average long-term soil loss and it is the soil-profile response to the erosive powers of rainstorms; that is, the soil-erodibility factor is a lumped parameter that represents and integrates the average annual value of the total soil and soil profile reaction to a large number of erosion and hydrologic processes (Renard *et al.*, 1997). These processes can include soil detachment, transport by raindrop impact and surface flow and localized deposition.

For a particular soil, the soil erodibility factor is the rate of erosion in mass per area unit (e.g. kg m^{-2}), per unit of erosivity index from a standard plot. The standard plot used for RUSLE developement is 22.1 m long on a uniform lenghtwise slope of 9% and the recommended minimum plot width is 1.83 m (Wischmeier & Smith, 1978). The plot is tilled up and down slope and maintained in countinuous bare fallow for at least two years. In computing the K factor in the RUSLE, Wischmeier & Smith (1978) found that it could be estimated from silt content, very fine sand content, clay content and organic matter content, as well as the structure of the surface layer and the permeability of the soil profile.

The soil erodibility factor for those cases where, the silt fraction does not exceed 70% can be estimated through an algebraic approximation as shown in Eq. 6.6. This equation or its equivalent nomograph is used in the RUSLE model (Wischmeier & Smith, 1978), in which K is the soil erodibility factor in Mg h $MJ^{-1}mm^{-1}$, A is the percentage of organic matter, B is the soil structure code (Table 6.3), C is the soil profile permeability code (Table 6.2) , and M is the product of the percentages of silt and clay and it is calculated according to Eq. 6.7, the USDA classification of diameter of primary particles classes was used. The permeability classes according to the soil texture can also be assessed by field estimation of the saturated hydraulic conductivity, the approach of (Rawls *et al.*, 1982) is used in the RUSLE model Table 6.2.

$$K = \frac{2.1 \times 10^{-4} \times M^{1.14}(12 - A) + 3.25(B - 2) + 2.5(C - 3)}{100} \times 0.1317 \quad (6.6)$$

$$M = [(silt\% + fine\ sand\%) \times (100 - clay\%)] \quad (6.7)$$

Table 6.2: Permeability classes (C) according to USDA (1983) and Rawls et al. (1982).

Permeability class (code)	Texture USDA 1983	Saturated hydraulic conductivity (mm/h) Rawls et al., 1982
1 (fast and very fast)	Sand	> 60.96
2 (moderate fast)	Loamy sand, sandy loam	20.32 - 60.96
3 (moderate)	Loam, silt loam, silt	5.08- 20.32
4 (moderate slow)	Sandy clay loam, sand clay	1.02 - 2.03
5 (slow)	Silty clay loam, sand clay	1.02 - 2.03
6 (very slow)	Clay, silty clay	< 1.02

6.3.2.1 Sampling units

For this work soil erodibility factor was estimated based on geological units of the study area. This was done under the assumption that the geology of the area influences the parent material that forms the soil and this affects the soil properties, and hence, it is expected differenciate degree of susceptibility to erosive factors. It is known that in the process of soil formation the parent rocks undergo considerable changes manifested in the weathering of the minerals composing them and the formation of new minerals (Vilenskii, 1963), rocks vary in their susceptibility to weathering

Table 6.3: Soil structure classes according to USDA (1983).

Soil structure class (code)	Soil structure USDA 1983
1	Very fine granular and very fine crumb (< 1mm)
2	Fine granular and fine crumb (1-2 mm)
3	Granular and medium crumb (2-5 mm) and coarse granular (5-10 mm)
4	Very coarse granular and very coarse prismatic, columnar, blocky, platy or massive (>10 mm)

according to their chemical composition as well as to their physical properties. As regards the chemical composition of rocks, two constituents are of especial importance, silicic mineral (including quartz) and the earthy carbonates, particulary calcium carbonate (Ramann, 1928). As regards the physical properties, the effects of parental material on it is not very clear, for example (Becher, 1988; Simanton *et al.*, 1980) indicated that variations in measured soil loss seem to be caused by the parent material affecting soil structure, in another study Berndtsson *et al.* (1985) indicated that generally texture and structure depend on the geological origin of materials.

In order to determine the soil erodibility in the Upper Llobregat basin, the factors affecting the K factor values were computed using the nomograph developed by (Wischmeier & Smith, 1978). Each component of the monograph was defined based on a geological map provided by the Catalan Institute of Cartography (ICC, 2002) at scale 1:250,000, and field work to collect data related to texture, structure and organic matter content. A soil erodibility map was developed using Idrisi (Eastman, 2003), Cartalinx 1.2 (CartaLinx Clark Labs, 2001) and Miramon (Pons, 1994). It was of concern only the top soil layer and the primary soil sequence.

A printed version of the geological map at scale 1:250000 was scanned, georeferenced and digitised in Cartalinx 1.2. As for the Upper Llobregat basin the printed version of the geological map presents 27 geological units, it was of interest to group these geological classes in a fewer number according to the type of the major characteristics of the material of each geological unit.

The original 27 units were reclassified into predominant rock types, which seems to have differenciate influence in soil texture; however, during the reclassification process it was encountered that some of the categories defined in the geological map included different type of material in the same category, and the proportion of each type is unknown. This is because geological maps for the study area were developed based on lithostratigraphical units for 1:500,000 map; hence, the range of lithologies and stratigraphies are diverse, and these depending on the scale of the study area, more or less types can be identified. As it is intended to define a baseline or guideline of where to collect soil samples, the general characteristics of each type was considered as the main criteria. Therefore, reclassification was done according to their parent material. The new categories include: (1) metamorphic and igneous rocks, (2) limestone, (3) clays and sandstones, (4) conglomerates and sandstones, (5) marls and sandstones, and (6) superficial deposits. In Table 6.4, it is illustrated the original categories and the reclassified categories.

The original geology units were digitised by means of Cartalinx 1.2, creating a new database, 78 polygons were built. The digitised map was then exported to Idrisi as vector, and the resulting polygons were encoded according to Table 6.4 and using the RECLASS module within Idrisi. Once the new vector map was completed it was converted to raster. Finally, by means of OVERLAY module a product of the new reclassified geology unit map and the topographically delimited map

Table 6.4: Reclassification of surface geology units.

Geological unit (ICC, 1989)	Reclassified categories	Area (km^2)
1) Isometamorphism zones in metapelites: anatexite; 2) lava ; 3) lidites with phosphatic and calcareous nodules; 4) quartzarenite; 5) pelites and sands	(I) Metamorphic and igneous rocks	35.0
1) Lacustrine limestone; 2) bioclastic limestone with rudistes and orbitolines; 3) alveolar limestone; 4) pelite and limestones; 5) non differenciate limestones	(II)Limestone	182.3
1) Clays, lutites, sandstones, gypsum	(III) Clays and sandstones	80.8
1) Sands, conglomerates, marls and lignites; 2) sands and conglomerates; 3) sands and grey marls; 4) sand, marls and limestones; 5) sand, arcosic and conglomerate; 6) massive conglomerates; 7) conglomerates; 8) conglomerate, sand and lutite; sand	(IV)Conglomerates and sandstones	87.1
1) Marls and redish sandy limestones; 2) turbidites and gypsum; 3) dark marls and gypsum; 4) marls	(V) Marls and sandstones	107.8
1) Silt and cobbles (fluvial deposits)	(VI) Superficial deposits	7.3
	Water body	3.7

of the Upper Llobregat basin was made, in order to obtain a new clipped geology map of the basin.

The predominant geological unit is limestone (36%), followed by marls and sandstones (21%), and conglomerates and sandstones (17%), the less common type is superficial deposits (1.4%) (see Table 6.4). The N part of the river basin it is formed by marls and sandstones stretching from W to E all over the Serralada Cadí. In the NE part (nearby Castellar de N'Hug) large areas of limestone exist. In the central part on one hand, (near Vallcebre and Vallcebre itself) can be distinguished areas of clays and sandstones, on the other hand nearby Guardiola de Bergueda, Gosol and around La Baells dam it is formed also by limestones. The SW side (near San Jaume de Frontanyà) and the SE side (above of Castellar del Riu) of the watershed is formed by conglomerates and sandstones. Superficial deposits are found nearby Pedraforca, Sant Jordi de Cercs and the western side between Guardiola de Bergueda and Bagà.

6.3.2.2 Soil sample collection

The purposes for which the samples were collected were: (1) to obtain a representative coverage of each geological unit in order to determine its texture and structure (under the assumption that different rock types have differential effect on these soil properties), (2) to obtain a broad spatial distribution of sampling locations over the study area. Considering the basin limitations with regards to accesibility (e.g. steep slopes) and the large area the large area (504 km^2) a strict method from the statistical point of view was difficult to follow, however, an approximation to it was followed. Accessibility to some areas is difficult, because of the steep slope of most of the basin. As it is of interest to represent the characteristics of the geological units and not to describe a specific sampling site, the criteria followed allowed to attain the objectives of sampling it is intended

to obtain acceptable representativeness at the lowest cost (i.e. minimun travel time).

The sampling plan was designed to collect samples from 3 of the 6 geological units (reclassified categories) listed in Table 6.4. Samples for the categories: (a) limestone, (b) clays and sandstones, were not collected because of the available data from previous surveys such as Rubio (2005); Haro & Fernández (1991); Pérez (1991). Available data, such as texture and organic matter content exist for those areas represented by an (*) in Fig. 6.7. For the rest of the units, considering the material needed for the soil physical property analysis and the expected low variability within each unit, it was decided that for each unit at least 4 samples should be taken (in order to have an estimate of sampling error) at different locations. The total number of soil samples collected were determined according to the area occupied by each type. The total samples were 14, 4 samples were collected for the metamorphic and igneous rocks, 4 samples for conglomerates and sandstones, and 6 samples for the category of marls and sandstones. For the category of superficial deposits no samples were collected because the area occupied by it is not significant (1.4% of the entire watershed), instead results obtained for marls and sandstones were utilized.

A stratified sampling and random criteria were used, the reason for this is to make statements about each geological unit, and to increase the precision of the soil erodibility estimations on the entire watershed. Each geological unit was considered as a stratum and considered as a population. Once the number of samples was determined their location was planned. The reclassified geological map (printed in a see-through material) was overlain on a cartographic and a road maps of same scale for the study area. It was avoided the boundaries of the geological unit polygons because of a likely changing or transition of rock types which can contribute to bias, this was difficult for units with small polygons. Having the three maps overlaid locations close to a road network, along footpaths or any landmark boundary were identified randomly and visually delimited. Then samples were collected along a transect paralel to the road or landmark boundary, from an undisturbed area.

In Table 6.5 a description and UTM of the sampling locations are presented, also in Fig. 6.7 these sampled sites can be visualised within the watershed. Samples were collected on the 1st of April 2008, by 3 people with expertise in working in the study area.

As it of interest only the superficial soil layer samples were collected from the first 15 cm. The vegetation covering the sampling site if there was any was removed using a shovel. Then using a shovel, soil profile was dug up to 15 cm depth. Approximately 1 kg of soil was collected (in case if it is needed to repeat analysis in laboratory). The extracted material was then sorted (large piece of rocks and roots were removed) and placed into a sampling plastic bag correctly identified for physical property analysis, in addition information pertaining to the sampling site was recorded such as the type of vegetation, soil color, parental material and location), also protographs of the samples were taken for future references.

Samples were dried out in an oven at 25 °C, by day 10 all samples had lost moisture content. Then samples were homogenized (to ensure representativeness) and sieved using a 2 mm sieve, the next step was to split the sieved sample in two sets. The first set to be used for texture determination, and the second for organic matter content.

The assumption that different type of geological material origins different texture and structure was verified based on results obtained in laboratoy.

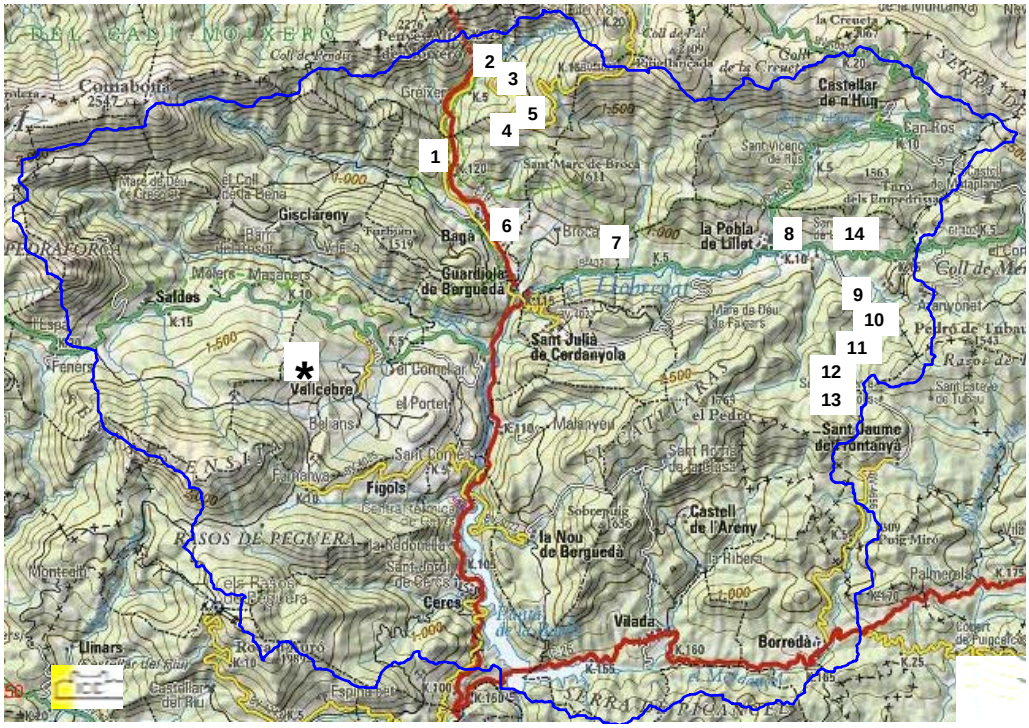

Figure 6.7: Sampling locations based on geological units.

6.3.2.3 Texture

Texture analysis is performed considering that the major features of soil particle are obtained after the destruction or dispersion of soil aggregates into discrete units by chemical, mechanical, or ultrasonic means and the separation of particles according to size limits by sieving and sedimentation (Gee & Bauder, 1986).

The 20 g of each soil sample was placed in a bowl, so as to treat with hydrogen peroxide (35% concentration) and remove (oxidize) any organic matter (Day, 1965). The oxidization process took around 30 days depending on the amount of organic matter content of each sample. Once the OM was removed, $\approx$ 10 g of soil sample was surmerged in 1 L solution of sodium hexametaphospate (35.7 g) and sodium carbonate (7.94 g) in distilled water in order to slake (e.g. to break down the soil aggregates, dissolve the cementing aggents), slaking process can reduce soil infiltration because of the formation of superficial crusts. Then the solution is shaken for 24 h. The next step was to sieve the solution using 1 mm, 500 μm, 250 μm and 50 μm sieve sizes. The solution was sieved by agitating vigorously (using a shaker) until all particles smaller than the sieve openings have a chance to fall through the sieve, particles retained on each sieve were transferred to containers that are suitable for drying. The materials retained on each sieve were oven dried at 40 °C in order to obtain the net weight of each fraction.

a. Sand content (%) was obtained by weighing the dried material retained on the 1 mm, 500 μm, 250 μm and 50 μm. Each mass recorded as coarse, medium, and fine sand in the sample respectively.

b. Silt and clay proportions (%) were determined using the passing soil sample (liquid) through 50

Figure 6.8: Main steps for texture determination.

μm sieve. The distribution size of silt and clay was measured using the laser diffraction technique (Malvern Master Sizer E instrument).

Fig. 6.8 illustrates some of the steps followed to determine the soil texture.

Once the sand, silt and clay fractions of each sample were determined, their textural classes were defined using the USDA classification, which has 12 textural classes. In Appendix 1, the results of the textural class analyses are presented.

Soil texture plays a key role in the K factor value. In general terms, clay soils have a low K value because these soils are resistant to detachment. Sandy soils have low K values because these soils have high infiltration rates and reduced runoff, and because sediment eroded from these soils is not easily transported. Silt loam soils have moderate to high K values because the soil particles are moderately to easily detachable, infiltration is moderate to low producing moderate to high runoff, and the sediment is moderately to easily transported (Lee, 2003; O'Geen *et al.*, 2006). Soils with high percentage of silt and very fine sand are the most erodible because these soils crust readily, producing high runoff rates and quantities, also soil particles are easily detached from these soils and the resulting sediment is easily transported (Lal, 1988; Romero *et al.*, 2007).

In the nomograph proposed by Wischmeier & Smith (1978) are included the main soil features that influence the soil erodibility, however, some of these site specific factors can play a predominant role in some sites, such as the existence of badlands, for example in Vallcebre, processes of freeze-thaw cycles are a dominant factor to cause intense fragmentation of shales, also rainfall and the expansion-contraction of clay can cause the meteorization of shales (Regüés *et al.*, 1995), therefore identifying and sampling these areas are crucial. In surveys conducted by Haro & Fernández (1991);

Pérez (1991) the badlands in Vallcebre were sampled, and their influence is quantified in the K factor for these locations. In Annex 8.4.2 a summary of textural classes is presented.

6.3.2.4 Structure

Soil structure includes the arrangement, size and shape of the major pieces (clods) of the soil profile. Wischmeier & Smith (1978) identify four categories: (a) very fine granular, (b) fine granular, (c) moderately or coarse granular, and (d) blocky, platy or massive structure. Granular types allows an easy movement of water through the soil profile. Soil surface structure degradation influences the Hortonian flow generation, because it leads to a lower infiltration rate, which increases runoff hazards and reduces surface roughness which decreases surface detention (Boardman & Poesen, 2006).

The structure of soil were determined in the field by observing the type and grade of clods and aggregates profiles from the top layer (0-15 cm) and in further detailed analysis of samples, and then classifying them according to the soil structure classes given by USDA (Table 6.3) in order to be used in Eq. 6.13.

6.3.2.5 Permeability

Infiltration is affected by soil properties, and this influences the extent to which soil particles are detached and transported (Elliot, 1995b). An approximation of soil permeability was estimated based upon soil texture and structure, knowing that, these two soil properties do not change on the long-run, specially texture. Percolation test could have been performed in order to determine the soil permeability, however, the laboratory and field methods are expensive considering the size of the study area.

Nielsen *et al.* (1973) indicates that the saturated hydraulic conductivity is dependent upon soil texture and can be significantly affected by the degree of soil structure development. However Becher (1988) argued that the correspondence between values in permeability and saturated hydraulic conductivity or infiltration rate was not clear, but further researches in the USA demonstrated the existence of this relationship (Rawls *et al.*, 1993). Rawls *et al.* (1993) provides a summary data on saturated hydraulic conductivity for each of the major USDA textural classes and points out that soil structure effects can override any differences between texture classes.

For this work hidraulic conductivity classes defined by Rawls & Brakensiek (1989) and USDA (1983) have been used. These values are illustrated in Table 6.2.

Differences in texture and structure over space drives to differences in soil permeability. For instance, in Vallcebre soil developed over the mudstone lithology have a silt-loam texture and are characterized by the rapid decrease of their hydraulic conductivity with depth (Latron *et al.*, 2003). Permeability has to do with runoff pattern, in Vallcebre (sub-basin Can Vila) it was identified three types of runoff events throughout the year, each characterized by a different runoff generation pattern, infiltration excess runoff on low permeability areas was dominant during dry conditions, whereas saturation excess runoff on more permeable soils was dominant during both wetting-up, transition, and wet periods (Latron *et al.*, 2003).

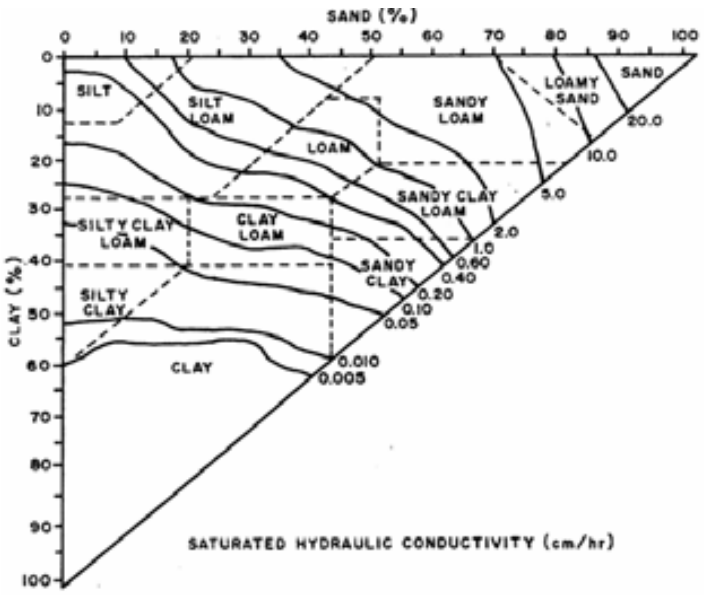

Figure 6.9: Saturated conductivity classified by soil texture. Rawls, et al. 1990.

6.3.2.6 Organic Matter

The organic matter content in the topsoil tends to hold the soil particles together, and reduces erodibility because, it decreases the susceptibility of the soil to detachment and it increases the degree of aggregation and so infiltration, which reduces runoff and thus erosion. Extrapolation of the K factor nomograph beyond the organic matter of 4% is not recommened in RUSLE. Quantifying the role played by organic matter in limiting processes of erosion was a challenge, considering the maximum 4% on the nomograph, which is generally exceeded in a forest environment such as most of the Upper Llobregat basin.

Soil organic matter is defined as those organic materials that accompany soil particles through a 2 mm sieve (Nelson & Sommers, 1982), and it is estimated in function of the total organic carbon (TOC). Lower levels of organic carbon in the soil are generally detrimental to water retention capacity and tend to increase soil compaction, which leads to increases runoff and erosion (EEA, 2008). In soils there are three basic forms of carbon that may be present, they are: (1) elemental C, (2) inorganic C, and (3) organic C. Naturally-occurring organic C forms are derived from the decomposition of plants and animals (Schumacher, 2002).

The basic principle for the quantification of oxidable OM relies on the destruction of organic matter present in the soil. For this study, it was used the rapid dichromate oxidation method or the Walkley-Black procedure. In this procedure, potassium dichromate ($K_2Cr_2O_2$) and concentrated H_2SO_4 were added to between 0.1 g and 0.2 g of ground soil (from second set soil samples). The solution was swirled and allowed to cool (a result of the exothermic reaction when the potassium dichromate and sulfuric acids are mixed) prior to adding water to halt the reaction. The addition of H_3PO_4 to the digestive mix after the sample has cooled has been used to help eliminate interferences from the ferric (Fe^{+3}) iron that may be present in the sample. For the titrimetric quantification an indicator solution is added to the digestate. Phenylalanine was used, the excess $Cr_2O_7^{-2}$ is titrated with ferrous ammonium sulfate $[Fe(NH_4)_2(SO_4)_2 * 6H_2O]$ (Mohr's Salt) until color change occurs

Grinding the soil samples | Soil samples with $K_2Cr_2O_2$ and H_2SO_4 | Titrimetric quantification

Figure 6.10: Main steps for determination of organic matter content.

in the sample from dark violet-green to light green for the phenylalanine.

The Walkley-Black procedure leads to a incomplete oxidation of organic C, and it is particularly poor for digesting elemental C forms, it is accepted that the recovery of organic C using the Walkley-Black procedure is around 77% (Nelson & Sommers, 1982). As a result of the incomplete oxidation and in the absence of a site-specific correction factor, a correction factor of 1.33 is commonly applied to the results to adjust the organic C recovery.

Eq. 6.8 was used to estimate TOC, where V_B and V_M are the recorded volume of $Fe(NH_4)_2(SO_4)_2 * 6H_2O$ spent in the testing and soil Erlenmeyer flasks respectively, N_{Fe} is the normality of ferrous ammonium sulfate (0.5N), F_{Fe} is the corrected normality factor of ferrous ammonium sulfate (0.976) and K is the recovery factor of the reaction (77%). Fig. 6.10 illustrates some of the steps followed to determine the OM content in a soil sample.

$$TOC = (V_B - V_M) \times N_{Fe} \times F_{Fe} \times \frac{12mgC}{4meqC} \times \frac{1}{W_s} \times K \tag{6.8}$$

Finally the organic matter was calculated assuming that approximately 58.8% of soil organic matter is C.

It is believed that grassland soils have higher OM than forest soils (Jenny, 1941), it can vary greatly, for example, most mineral soils in New Zealand have topsoil organic matter levels ranging from approximately 3 to 20% (McLaren & Cameron, 1996). Another factor that may affect the OM content is topography, Jenny (1941) indicates that soils in lowlands have higher OM than soils on upland positions.

6.3.2.7 Determination of K Factor

K Factor values were determined using equations 6.6 and 6.7 (Wischmeier & Smith (1978)). The input information to use those equations are: percent of sand, very fine sand and clay; percent OM; structure of the soil and permeability. Eq. 6.6 was applied to each soil sample for every geological unit. The K Factor value for a specified geological unit was obtained by averaging the K Factor values within that geological unit.

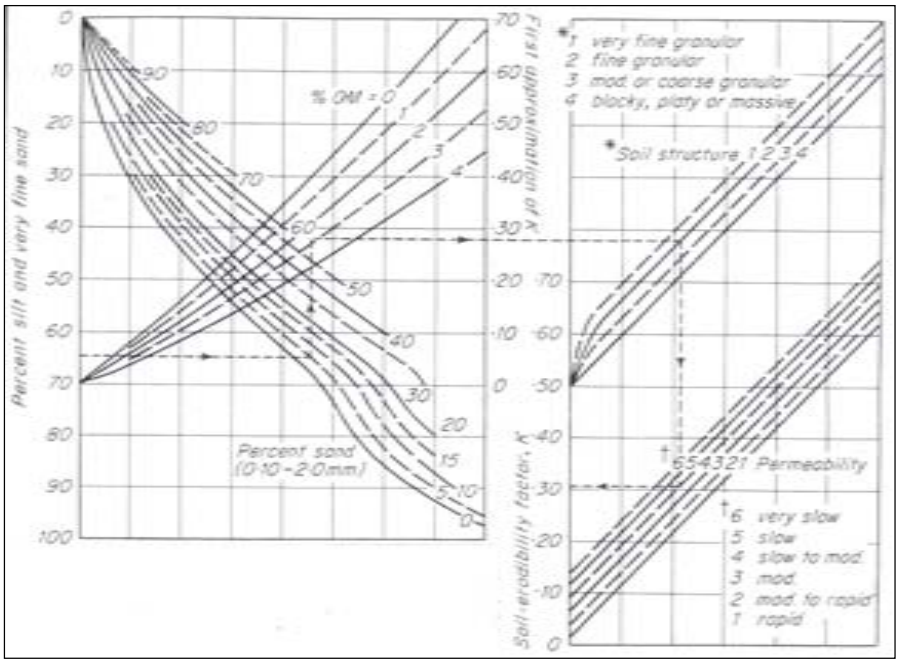

Figure 6.11: The soil erodibility nomograph (Wischmeier and Smith 1978).

In addition, the standard deviation of K factor for each geological unit was computed from the soil sample dataset, so comparison of the magnitude of differences between soil units can be performed.

6.3.3 Slope length and steepness factor

L and S factors are the slope lenght and slope steepness respectively. They represent the topography of the land and their influence on sheet and rill erosion. The L factor is defined as the horizontal distance from the origin of overland flow (usually the top of the ridge) to the point where either the slope gradient decreases to a point where depositon begins, or runoff becomes concentrated in a defined channel (Wischmeier & Smith, 1978; Renard *et al.*, 1997). S factor computes the effect of slope steepness on soil loss. With the incorporation of DEM into GIS, the S factor and L factor are determined and combined to form a single factor known as the topographic factor LS.

The amount of erosion increases as the slope length increases (Wischmeier & Smith, 1978; Renard *et al.*, 1997). On steep slopes, runoff water is more erosive. On convace slopes, with less steep slopes at the foot of the hill, are less erosive than convex slopes (Elliot, 1995b). The Upper Llobregat basin has 97.7% (492.6 ha) of its area having slope gradient $\geqslant$ 9%, 41% of the basin has slope gradient $\geqslant$ 50%, these high slope gradients make the area highly susceptible to erosion.

The L and S factors were calculated together using specialized USLE2d software v.4.1 (Desmet & Govers, 1996; Van Oost *et al.*, 2000). The required inputs are a grid-based DEM and drainage area. Usle2d was designed to calculate the LS-factor to be used with (R)USLE from a grid-based DEM (resolution of 20 m by 20 m), assuming that the flow and the resulting soil loss does not depend on the distance to the divide or upslope border of the field, but on contributing area at a specified point (Desmet & Govers, 1996). Thus USLE2d replaces the slope lenght by the contributing area.

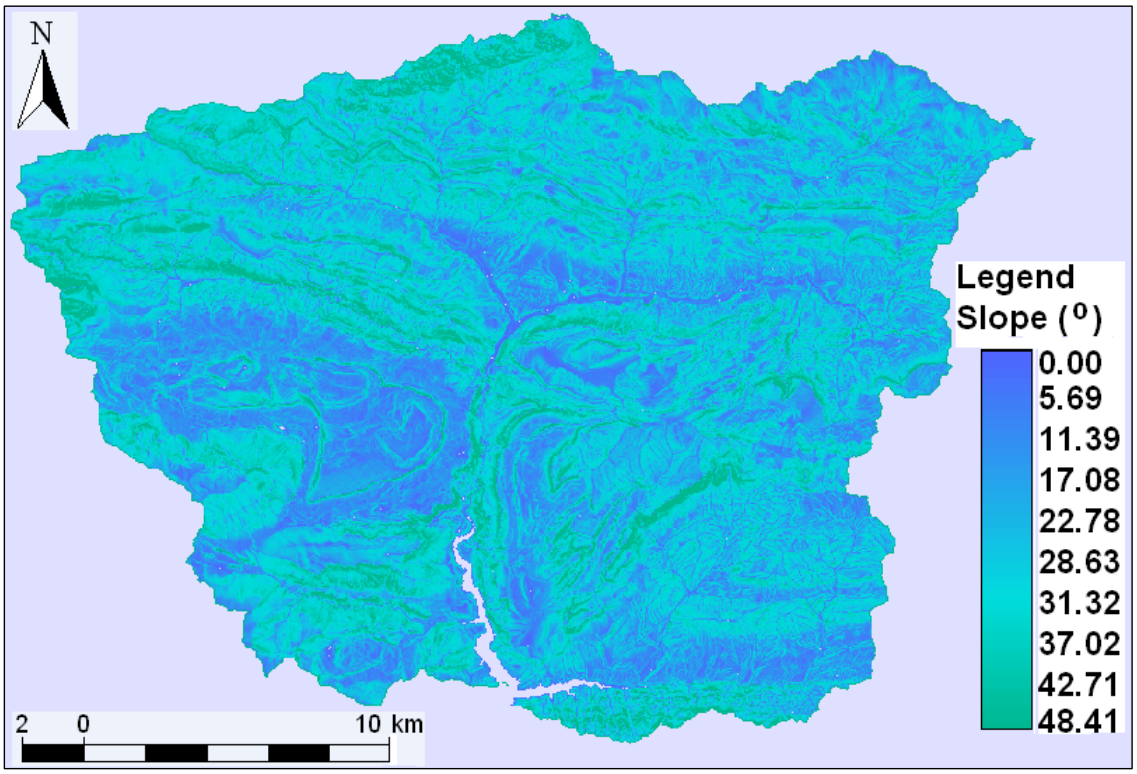

Figure 6.12: Slope distribution.

The USLE2d performs two-dimensional analysis of soil loss of topographically complex landscapes (Van Oost *et al.*, 2000). It is needed to select a routing algorithm and a LS algorithm (provided by the software). The routing algorithms are used to calculate the contributing area and various LS-algorithms. The routing algorithm selected was the multiple flow algorithm (Quinn *et al.*, 1991) and the LS algorithm used was the Nearing (1997) algorithm because, the slopes in the study area are higher than 22%, and for slope length exponent was selected the one given by McCool *et al.* (1989) (rill = interrill). The whole DEM was considered as a single land unit.

In the past, terraces were built for soil conservation and drainage, and they have influence on soil erosion (e.g. decreasing runoff velocity). Given that the DEM's resolution -20m- was not enough to reflect these terraced areas, two instances for LS factor were examined: (a) with terraces, and (b) without terraces.

Terraces are situated where previously were farming areas (mostly below 1700 m a.s.l.). In order to identify and include their effect on soil erosion, a new LS Factor was developed. To do so, areas located below 1700 m a.s.l. were filtered from the DEM, and then, it was overlapped onto a raster of pastures and agricultural areas (extracted from the land cover map). This procedure was done in Idrisi.

The formulae for calculating the computed LS factor are shown in Eq. 6.10 and 6.10:

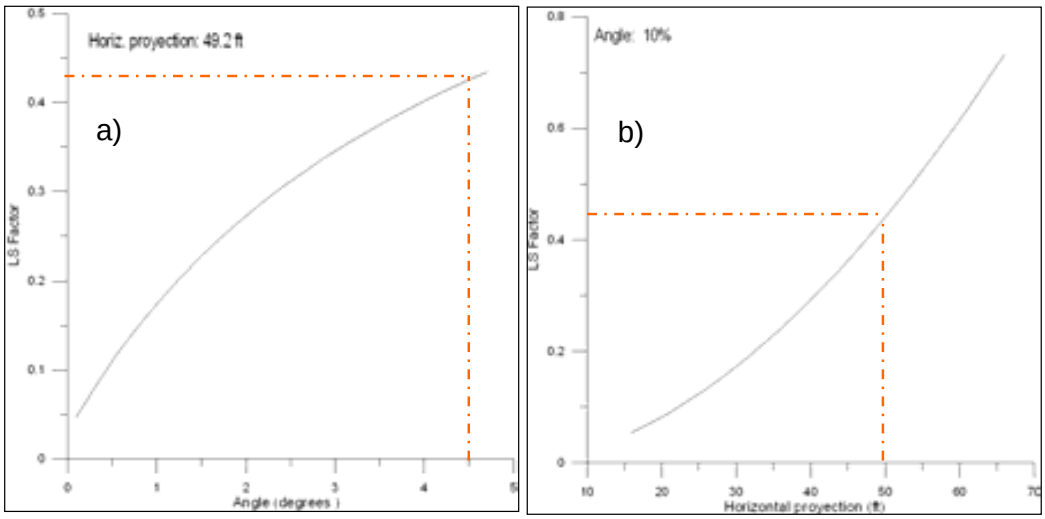

Figure 6.13: LS Factor for pastures and agricultural areas.

$$L = (\frac{\lambda}{72.6})^m \tag{6.9}$$

$$S = 10.8 \times sin\theta + 0.03 \tag{6.10}$$

Where λ is the projection of slope lenght, 72.6 feet (22.1 m) is the unit plot length in feet (Wischmeier & Smith, 1978), m is a variable slope-lenght exponent. The m is defined by Eq. 6.12 (Foster *et al.*, n.d.), where, β is the ratio of rill erosion caused by flow to interril erosion. Values for the ratio β rill to interrill erosion are computed from Eq. 6.12 (McCool *et al.*, 1989).

$$m = \frac{\beta}{(1+\beta)} \tag{6.11}$$

$$\beta = \frac{\frac{sin\theta}{0.0896}}{3.0 \times (sin\theta)^{0.8} + 0.56} \tag{6.12}$$

The slope steepness (S) was calculated using Eq. 6.10 (McCool *et al.*, 1989) which is used for steepness less than 9%.

The θ and λ values were set to 4.5° (10%) and 49.2 ft (15 m) respectively and they were used to numerically and graphycally calculate the new LS values. Fig. 6.13a illustrates the relationship between the θ and LS values holding λ constant at 49.2 ft; likewise, Fig. 6.13b illustrates the same relationship but holding θ constant at 4.5°. From either plots the LS factor values by including terraces is 0.44. This LS value is assigned to terraced areas in the LS raster which does not include terraces.

6.3.4 Land cover and management factor

6.3.4.1 Land cover analysis

C factor is the land cover and management factor. It measures the combined effect of all the interrelated vegetative and management variables. This factor is defined as the ratio of soil loss from land maintained under specified conditions to the corresponding loss from continuous tilled bare fallow. It measures the protection of the soil surface from raindrop impact by vegetative cover. The major effects of vegetation in reducing erosion are: (1) protecting the soil from raindrop impact, (2) reducing surface runoff velocity, (3) holding soil in place, (4) improving soil structure with roots, plant residue, and increased biological activity in the soil, and (5) increasing transpiration rates (Elliot, 1995b). Vegetative cover is the variable controlling erosional activity which is most subject to human manipulation (Trimble, 1990), it changes in time and space, hence predictions of erosion and sediment yield based on vegetation alone is not recommended (Trimble, 1990).

Land cover for the Upper Llobregat basin was defined using a land cover map compiled from aerial photographs taken in 1993, and which was provided by the Center for Ecological Research and Forestry Applications (CREAF) which has a resolution of 20 m. Within the boundaries of the basin, 11 land cover classes were identified, and they are highly scattered (consisted of many small areas); in order to improve the ease of use of the image, some of the similar land uses were reclassed into the same category. The reclassed categories and their areas are shown in Table 6.6. For example the urban high density and the low density urban were combined because it would be difficult to differentiate the influence of the respective land uses on soil erosion. In addition, the highland grassland and brushwood and grassland were reclassed into one land use category (pastures) because of the their likely similar influence on soil erosion.

The areas of the original and reclassed land cover categories are illustrated in Table 6.6, where, open forest occupies the largest proportion (62.6%) and within this category the coniferous type is the largest (46.2%), followed by caducifolious forest (15.3%) and sclerophyllous forest (1.1%). At the intermediate altitudes and the steeper slopes the vegetation is largely forest, mostly *Pinus sylvestris* and some deciduous oak (*Quercus pubescens*), with evergreen oak (*Quercus ilex*) in the warmer locations. Pastures occupy 32.7% of the river basin, large areas are found in northern areas (La Molina, Clot del Moro) and the western side of the La Baells reservoir. The larger the area of grass cover in a river basin, the lesser will be the runoff potential of the river basin and more will be infiltration, it is good because it favors the protection of river basin from erosion for soil conservation purposes (Mishra & Singh, 2003). Agricultural areas only constitutes 1.2% of the area, and they are located nearby urban areas such as, Guardiola de Bergueda, La Pobla de Lillet, Sant Jordi de Cercs and Borreda, below 1350 m a.s.l., most of the gentler slopes are terraced but much of this land is now abandoned and occupied by pastures. Urban areas and water body together represent only 1%, construction sites may become an important source of sediment. In Fig. 6.14 the distribution of these land cover categories is illustrated.

The forest area in the Upper Llobregat basin is about twice the value of forest areas in Europe, which is 37% (EEA, 2006). For several centuries the Pyrenees has been subject to considerable anthrophogenic pressure, the traditional agro-sylvo-pastoral systems of these areas intensified during the 19th century because of increased population density, and the agricultural and industrial revolutions (Taillefumier & Pigay, 2003), however, during the second half of the 20th century these mountain areas have undergone agricultural decline and major changes in agricultural practices and land use (Molinillo *et al.*, 1997). Spontaneous colonization by pine formation, a pioneer stage

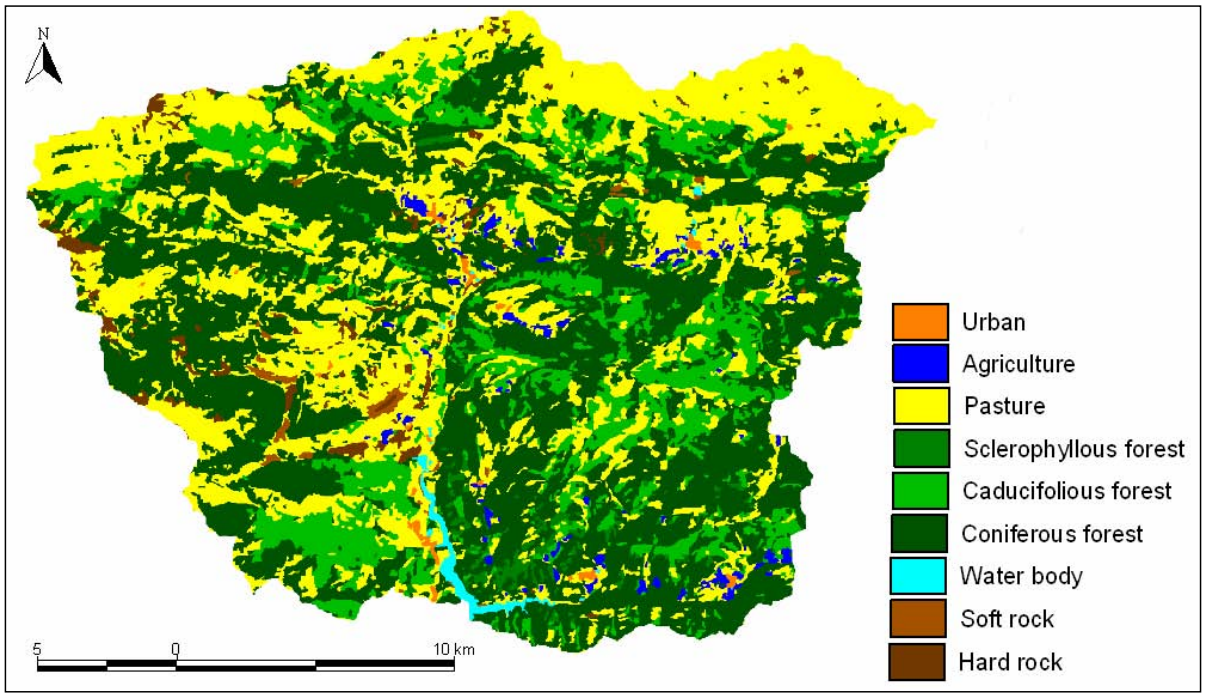

Figure 6.14: Land cover in the Upper Llobregat Basin, 2002.

of forest growth is notorious (Taillefumier & Pigay, 2003).

Subsurface rock fragments were not included, rock fragments are scattered thoughout the watershed and quantifying at the watershed scale is complex. As noted by Van Wesemael *et al.* (2002); Renard *et al.* (1997) rock fragments reduces the infiltration and increase runoff, for sand and loamy-sand textures increases thus soil loss is greater from soils containing cobbles than from soil with coarse gravel.

6.3.4.2 Determination of C Factor

C Factor values were calculated from published sources (Zachar, 1982; Morgan, 1995; Ma, 2001; Raghunath, 2002; Jung *et al.*, 2004; Lee & Lee, 2006; Stumpf & Auerswald, 2006) for the land cover types present in the basin, and these are given in Table 6.7. For most of the land cover types more than one source was identified. In order to assign a C value to each land cover type an average of C value for each category was calculated from existing sources.

To accommodate for the high organic matter, Wischmeier & Smith (1978) recommend multiplying the C factor by 0.7. Here, it was assumed that the C values obtained from literature included already this adjustment.

6.3.5 Conservation or support practice factor

P is the support or land management practice factor. Wischmeier & Smith (1978) define the P factor as the ratio of soil loss with a specific support practice to the corresponding soil loss with up and down cultivation. In RUSLE, this factor is generally applied to disturbed lands and represents how surface and management practices, such as contouring, terracing, strip cropping, sediment basins, grass hedges, silt fences, straw bales, and subsurface drainage are used to reduce soil erosion. The lower the P-value, the more effective the conservation practice is deemed to be at reducing soil erosion. The P factor is the one most subject to error according to Wendt (1998), because of a deficient data base compared to that for other factors in the USLE (Wall *et al.*, 2002).

For this study, P factor value was set to 1, since most of the land cover in the study area is forest ($\approx 66\%$) and agricultural areas is almost negligible ($\approx 1.2\%$). In the past terrracing constituted one of the most common conservation practices, and today crops are often grown on these areas. Nevertheless, the influence of terracing on soil erosion is already included in LS factor.

6.3.6 Soil erosion

The images developed for each of RUSLE's factors were overlaid in IDRISI Kilimanjaro, in order to estimate the average annual soil erosion within the basin. The columns and rows of pixels (resolution 20 m) of each image are internally arranged in a grid matrix representing different characteristics of the basin. Finally, data of interest such as the average annual soil erosion and spatial distribution of erosion can be derived from the outcome image.

6.3.7 Sensitivity and uncertainty analysis of soil erosion

Sensitivity analyses were undertaken for each of the factors involved in RUSLE, in order to see the magnitude of change on soil erosion as one factor (input) at a time changes, and by doing so, tackle the uncertainties involved in soil erosion, and which are reflected in the width of confidence interval. Sensitivity analyses were conducted for both instances, by including or not including terraces. The confidence level at which these analyses were performed was 90%.

6.3.7.1 R factor

In Table 6.8, the R factor values used to estimate lower and upper bounds of the confidence intervals of soil erosion are given.

6.3.7.2 K factor

In Table 6.9, K values used to perform the sensitivity analysis on soil erosion are shown. Error sources of K factor, appart from the associated to soil sampling process and analysis laboratory are the ones due to the assignation of permeability and structure classes, in order to account for this error source on soil erosion, the permeability and structure classes were re-computed by taking the

corresponding values to one class above and one class below for both parameters from the values given in Tables 6.2 and 6.3.

6.3.7.3 C factor

Table 6.8 illustrates the C factor values used to perform a sensitivity analysis on soil erosion.

6.3.7.4 LS factor

The standard deviation of LS image, was derived from the mean square errors images generated by the user-defined filter (3x3) and two neighbor pixel iterations in IDRISI, the assumptions are that the horizontal variability is a surrogate of the point variability.

6.3.7.5 Uncertainty of soil erosion

Finally, the effects of all input factors at once on soil erosion were calculated using the error propagation formula given in Eq. 6.13, by using the mean (X, Y or Z) and variance (σ^2) images of each factor. Variances of R factor for each polygon obtained by Thiessen Method were the squares of standard errors of R at the weather station level (point values). The variances of K and C factors for each geological unit and land cover type respectively were obtained by using standard deviations (Tables 6.13 and 6.10). The variance of LS factor was the average mean square error image derived from iterations using a 3x3 filter in IDRISI.

$$\sigma_A^2 = \sigma_X^2 \times Y^2 \times Z^2 + \sigma_Y^2 \times X^2 \times Z^2 + \sigma_Z^2 \times X^2 \times Y^2 \tag{6.13}$$

6.3.8 Sediment Delivery Ratio

Total soil loss from a watershed is usually significantly greater than the measured sediment yield, the bulk of the sediment is deposited at intermediate locations wherever the entraining runoff waters are insufficient to sustain transport (Vanoni, 1975), deposition occurs where gradients decline downslope, at the base of the slope, in swales, on the flood plain, or in the channel itself (Walling, 1983); therefore, the soil erosion rate estimated by RUSLE need to be adjusted in order to estimate the sediment yield. To do so, it is used a Sediment Delivery Ratio (SDR) defined as the fraction of gross erosion that is transported from a given area in a given time interval. SDR measures the sediment transport efficiency which accounts for the amount of sediment that is transported from the eroding sources to a measurement point (i.e. catchment outlet) compared to the total amount of soil that is detached over the same area above that point (Lu & Sivapalan, 2004).

Mathematically, SDR can be expressed as in Eq. 6.14 where, Y is the average annual sediment yield per unit of area and E is the average annual erosion over that same area (Walling, 1983). SDR is dimensionless scalar. Conversely, Eq. 6.14 can be written as Eq. 6.15, where the unknown variable is Y.

$$SDR = \frac{Y}{E} \quad (6.14)$$

$$Y = E \times SDR \quad (6.15)$$

The percentage sediment delivered from the erosion source to any specified downslope location is affected by the size and texture of erodible material, climate, land use, local environment, and general physiographic position (Vanoni, 1975). Several researches exist showing SDR trends for specific areas. The most popular is the relationship between SDR to the area of the watershed using a power function i.e. (Roehl, 1962), other relationships including morphological features of the watershed exist.

For this study the SDR was estimated as a weighted average of SDR of the ratios obtained by using equations developed by Williams (1977), Roehl (1962), Renfro (1975) and Vanoni (1975).

Drainage area methods are the most commonly used to estimate SDR. It is accepted among researchers that large areas have more chances to trap soil particles; therefore, the amount of soil particles reaching the water channel system is low, thus SDR is low. One of these methods was developed by Renfro (1975); mathematically, expressed as in Eq. 6.16 which relates SDR to the drainage area (A) expressed in km^2.

$$log(SDR) = 1.7935 - 0.14191 logA \quad (6.16)$$

A similar relationship between drainage area and SDR was developed by Vanoni (1975) as it is presented in Eq. 6.17, which was obtained from watersheds throughout the world. where A is the drainage area in square miles.

$$SDR = 0.42 \times A^{-0.125} \quad (6.17)$$

USDA SCS (1979) developed Eq. 6.18, where A is the drainage area in square miles.

$$SDR = 0.51 \times A^{-0.110} \quad (6.18)$$

Williams (1977) developed Eq. 6.19 based on sediment yield data for 15 river basins in Texas, where DA is the drainage area in km^2, ZL is the relief-length ratio in m/km, CN is the long-term average SCS (Soil Conservation Survey) curve number. CN is used to determine how much rainfall infiltrates into soil or an aquifer and how much rainfall becomes surface runoff, a high curve number means high runoff and low infiltration (Zhan & Huang, 2004), the Soil Conservation Service (SCS) now Natural Resources Conservation Service (NRCS) curve-number method is the most common method for predicting storm runoff volume; CN is obtained based on land cover type and infiltration from Tables given by SCS.

$$SDR = 1.366 \times 10^{-11} \times (DA)^{-0.0998} \times (ZL)^{0.3629} \times (CN)^{5.444} \quad (6.19)$$

Roehl (1962) found Eq. 6.20 using data in the South-east Piedmont of the USA. In this equation, D is the sediment delivery percentage, W is the drainage area (square miles), $\frac{L}{R}$ is the dimensionless basin lenght-relief ration (basin measured parallel to the main drainageway divided by elevation difference from drainage divide to outlet), and B is the weighted mean bifurcation ratio, the bifurcation ratio is the ratio of the number of streams of any given order to the number in the next higher order. The $\frac{L}{R}$ was calculated from the ratio of the watershed lenght (18 km) to the elevation difference between the minimum and maximum altitude (627 m and 2540 m respectively) which is 1913 m; bifurcation ratio B was estimated from the ratio of the number of streams of first order to the number of streams in the second order, and so on. The drainage network of the Upper Llobregat basin was achieved by using the RUNOFF and RECLASS modules within IDRISI Kilimanjaro, and finally, the bifurcation ratios were calculated.

$$logD = 4.5 - 0.23 \times log10W - 0.51 \times log\frac{L}{R} - 2.79 \times logB \quad (6.20)$$

6.3.9 Uncertainty of sediment yield

In order to describe the amount of uncertainty associated to the average annual sediment yield, confidence intervals were defined, for both instances: including and not including terraces. Similar to uncertainty assessment of soil erosion, error propagation formula Eq. 6.13 was used, where the inputs to solve the equation are the variances and squares of the mean of soil erosion and sediment delivery ratio. The variance of soil erosion was obtained as described in Section 6.3.7.5, the variance of delivery ratio was obtained by using the standard deviation of results obtained by using the sediment delivery equations (Section 6.3.8).

6.4 Results

6.4.1 Rainfall-runoff erosivity factor

6.4.1.1 Vallcebre

The annual average R factor calculated for Vallcebre using rainfall data collected between 1994 and 2005 was 1461.7 MJ mm ha^{-1} yr^{-1}, and the standard error of the mean 277.1 MJ mm ha^{-1} yr^{-1} (this value is relatively small because of the large sample dataset). The annual R values and rainfall depth year per year are illustrated in Fig. 6.15. R values are $\geq$ 2000 MJ mm ha^{-1} yr^{-1} for 1995, 1996 and 1999. For 1995 the R factor value is proportionaly very large considering the amount of rainfall fallen during that year, three daily rainfall events contributed almost half to the R factor, these events are characterized by high intensity and they ocurred during summer. On the contrary, the R factor value for 1996 is proportionally smaller than the amount of rainfall, during 1996, 37 daily rainfall episodes were recorded (the year with the largest amount of episodes) but they had a relatively low intensity. The lowest R factor and rainfall amount values were computed from year 2000 until 2003.

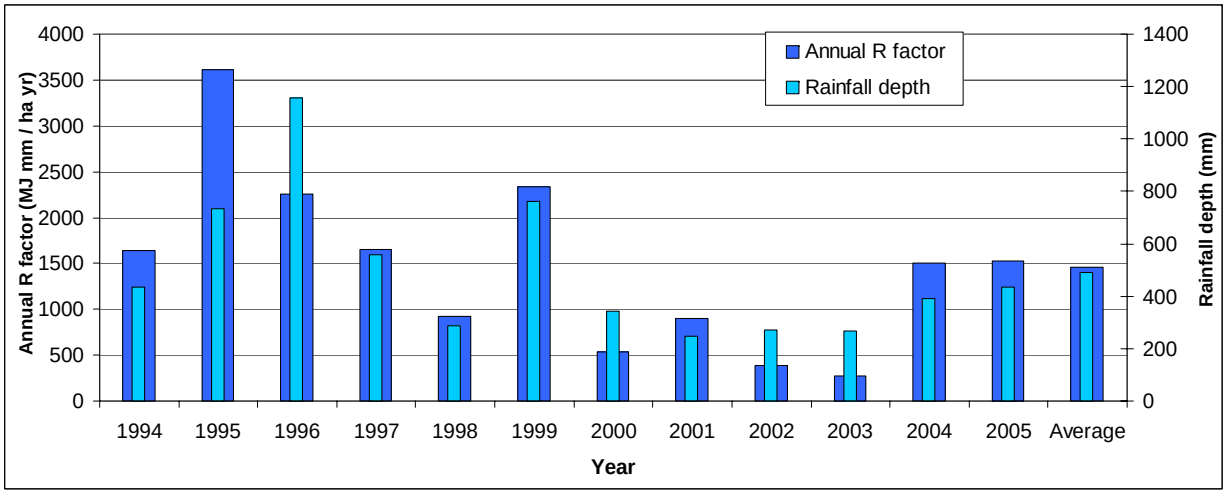

Figure 6.15: Average storm rainfall depth considering rains $\geq$ 12.5 mm for the period studied in Vallcebre.

6.4.1.2 Upper Llobregat Basin

The average annual R factor computed for the Upper Llobregat basin is characterized by a large inter-annual and spatial (inter-weather stations) variation (Fig. 6.16). The average R factor for all weather stations ranged from 1416.8 to 2496.2 MJ mm ha^{-1} yr^{-1} (Table 6.11). The stations with the highest standard error of the mean are Figols and Josa, on the contrary, Vallcebre and Berga present the lowest variability. A clear spatial distribution of the R factor can be observed, there is more rainfall erosivity in the NE and SE of the basin than in the W.

The temporal variation of R factor reveals that in general years with heavy rainy days present a more spread distribution R factor values between weather stations, and on the other hand, years with small and low intensity episodes present a relatively more uniform spatial distribution (Fig. 6.16). For example, during 1999 the R factor values between stations varies largely, where Figols and Borreda (both located in the SE) present the highest values. This is in agreement with the statement that the R factor values vary with amount of rainfall and the individual storm precipitation patterns (Elliot, 1995b).

The average annual R factor for the entire basin is 1960 MJ mm ha^{-1} yr^{-1}, which is 40% higher (1400 MJ mm ha^{-1} yr^{-1}) than the value calculated for a single year (1996) for the NE Spain (Uso & Ramos, 2001).

The R factor values used to estimate the erosion were average values given in Table 6.11. In Fig. 6.17 the R factor image is illustrated, where each Thiessen polygon have a uniform value.

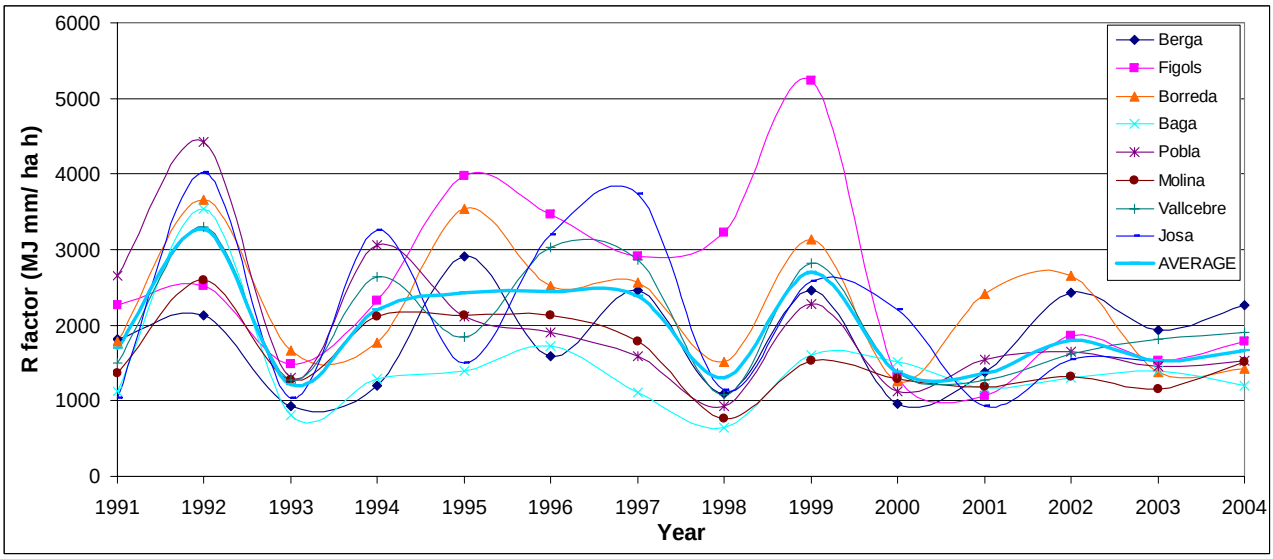

Figure 6.16: Rainfall factor for each weather station and average.

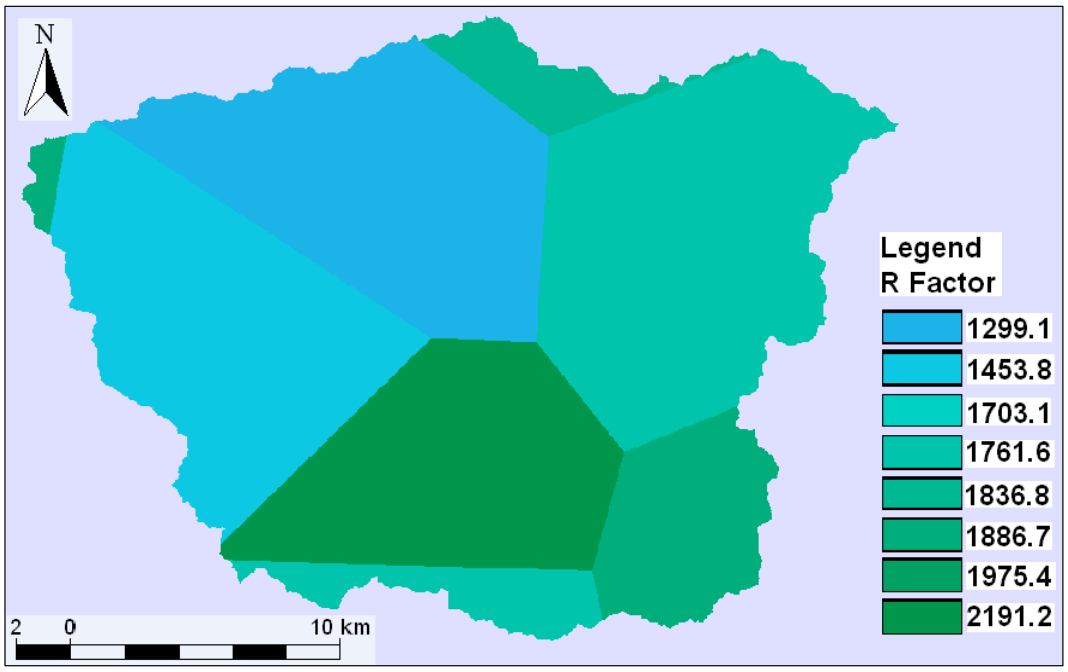

Figure 6.17: R Factor map.

6.4.2 Soil erodibility factor

6.4.2.1 Texture

Soil texture classes determined from Eq. 6.6 were mostly clay (Appendix 1), and the silt content in most of the samples was less than 10%. On the other hand, soil texture derived from previous studies are predominantly clay or clay-loam (Appendix 2) in the majority of samples. Although, sand content makes up more than 60% in the collected samples, the sum of fine sand and silt is $\approx$ 20% in most samples, which increases soil susceptibility to erosion. A summary of soil texture values used in Eq. 6.6 is given in Table 6.12.

6.4.2.2 Structure

The structure of the collected soil samples varied between very fine granular and fine granular with fine cracks (Appendix 1). Samples 2, 3, 4, 5, 6, 8 and 12 were weak, very fine granular, very friable, slightly sticky and plastic, many fine roots were observed. Samples 1, 7, 9, 10, 11 and 14 presented a weak fine granular structure, where spherical and polyhedral clods were common, also many fine roots were observed. On the other hand, soil samples from previous studies (located in Vallcebre and nearby), the structure also varied between fine granular and very fine granular (Pérez, 1991), on the other hand, in Can Vila subcatchment, Rubio (2005) has obtained a bulk density of 1.35 g/cm^3 and porosity 48% which is an indication of granular type structure (Appendix 2).

6.4.2.3 Organic Matter

The OM content for the sampled sites presented high variability. The OM analyses have shown that all samples, except one, presents OM content higher than 4%, the average was 9.2%, the highest was determined in samples 3 (28.8%) and 5 (17.1%), and the lowest in sample 14 (3.7%) (Appendix 1). In the results found in the previous studies (in Can Vila -one of the Vallcebre's subcatchments-) for meadow areas the average was 8.5%, minimum and maximum were 6.2 and 11.4 % respectively, for forested areas the average was 10.1%, the minimum and maximum were 50.6 and 15.3% (Rubio, 2005). Also, for Vallcebre (Can Parisa subcatchment) in areas dominated by badlands the average OM content was 3.0% and the lowest and highest values were 0.9 and 4.7% respectively (Haro & Fernández, 1991). Results obtained by (Pérez, 1991) in Can Vila this time in pasture areas, the average was 9.0 % with minimum and maximum of 1.5 and 42.2 % respectively. These results were used in Eq. 6.13 in order to estimate the K factor for each geological unit. A summary of OM content in soil samples is presented in Appendices 1 and 2.

High OM content in soil samples were expected considering, the large forested areas and decrease of agriculture practice during the last few decades. The high OM content contributes to a decrease in soil erodibility, because of the clear role on the stability of soil agregates (López-Vicente *et al.*, 2007). The organic material binds the particles of soil together, and the loss of soil moisture reduces runoff by making the soil 'thirsty'(Chang *et al.*, 2003).

In order to use the OM values within Eq. 6.6, values higher than 4% were set to 4.0% as suggested by GaSWCC (2000).

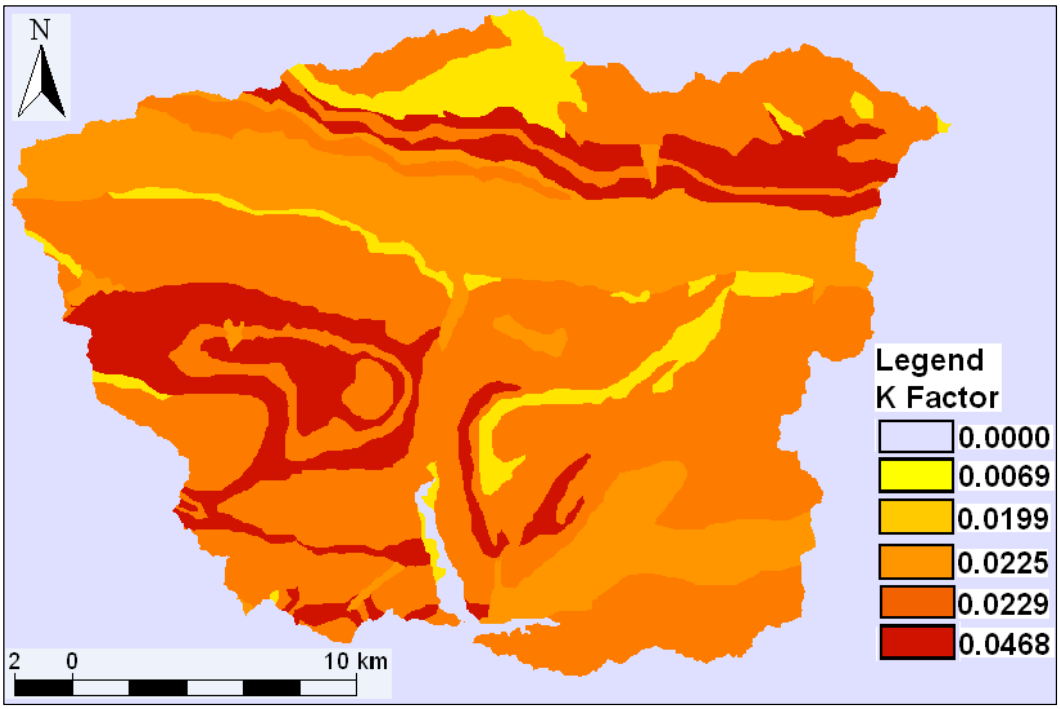

Figure 6.18: K Factor map.

6.4.2.4 K Factor values

The mean soil erodibility for La Baells calculated from Eq. 6.6 was 0.02315 Mg h $MJ^{-1}mm^{-1}$. K values for the defined geological units, varied between 0.0069 Mg h $MJ^{-1}mm^{-1}$ (marls and sandstones) and 0.0468 Mg h $MJ^{-1}mm^{-1}$ (clays and sandstones). These low values reflect the high resistence of soils to rainfall detachment, because most of the soil samples have a fine structure, present clay texture, and high OM content.

In Table 6.13, K values for each geological unit and their standard deviation are illustrated. The K value for superficial deposits was assigned the same values as for marls and sandstones (0.0199), which is one of the lowest K values. In order to determine if there are differences between K values for the five geological units, an ANOVA test (because there are more than two groups) was performed, which was significant ($F = 15.7$, $P<0.05$ and $\alpha=0.05$). The K Factor map and its distribution values is presented in Fig. 6.18.

6.4.3 Slope length and steepness factor

The Upper Llobregat basin is characterized by having high slopes, where more than 50% of the basin presents slopes higher than 40% as illustrated in Fig. 6.12. The northern area and central part of the basin present the highest variability in elevation, and consequently they also have the highest LS values. The majority of the area has LS values less than 75, the range of LS values varied between 0 and 1882. The mean LS value derived from the LS factor image was 29.4.

Figures 6.19a and 6.19b -considering terraces and without considering them respectively-, illustrate

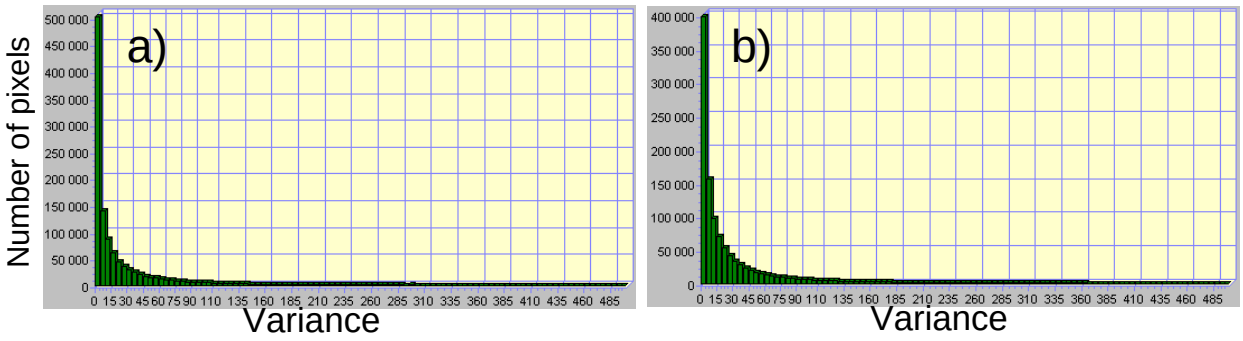

Figure 6.19: Variance distribution of LS factor: (a) not considering terraces, (b) considering terraces.

the frequency of LS values in function of the number of pixels (area). A very few number of pixels present LS values higher than 225, which can have large influence on large soil erosion values. LS values revealed a clear high effect of steepness, where areas of greater slopes having high LS values generally, coincide with backslopes of drainage lines and summits. The LS factor image is presented in Fig. 6.20.

Within the USLE2d software, different algorithms were tested before selecting the: multiple flow algorithm, and the Wischmeier and Smith (1979) algorithm as the Nearing's slope length exponent, which were used to obtain the LS factor image. For comparison purposes, results from these tests were: for example, by using the algorithm flux decomposition and Wischmeier and Smith (1978) algorithm as the Nearing's slope length exponent, the LS factor values varied between 0 and 2018 (very much higher than the obtained from selected algorithms) and the mean was 31; in another test perfomed by using the multiple flow and using as the Nearing's slope length exponent the McCool (1987) algorithm, the LS factor values ranged between 0 and 17493, the mean was 56.2; and finally, in a third test done by using the multiple flow algorithm and as the LS algorithm the one given by Govers (1991) the range was even larger from 0 to 43454 the mean was 115.5. Obviously if soil erosion had been calculated by using these LS values, it would have been extremely high; therefore, it is crucial the process of selecting the appropriate algorithms for the characteristics of the study area, otherwise results might be misleading.

6.4.4 Land cover and management factor

C factor values for each land cover type were obtained by averaging the C factor values given in published sources, as portrayed in Table 6.7. Although most of the basin is occupied by forest and pastures, some scattered soil erosion hotspots, such as road building (nearby urban areas), although temporary may contribute with large amounts of sediment; the existence of bare soft rock outcrops (badlands) may also contribute significantly to sediment delivered downstream, these highly erodible areas were given a C factor value of 1, contrary to bare hard rock, which were set to 0. The soil erosion values are smaller for permanent pastures, rangelands and forest lands, than for agricultural areas Renard *et al.* (1997); Elliot (1995b).

Fig. 6.21 illustrates the C factor values for each land cover type, where, highly erodible areas can be seen, although they are not spatially significant their location near (in some cases) streams, rivers or La Baells reservoir can make them important supplier of sediment reaching the outlet of

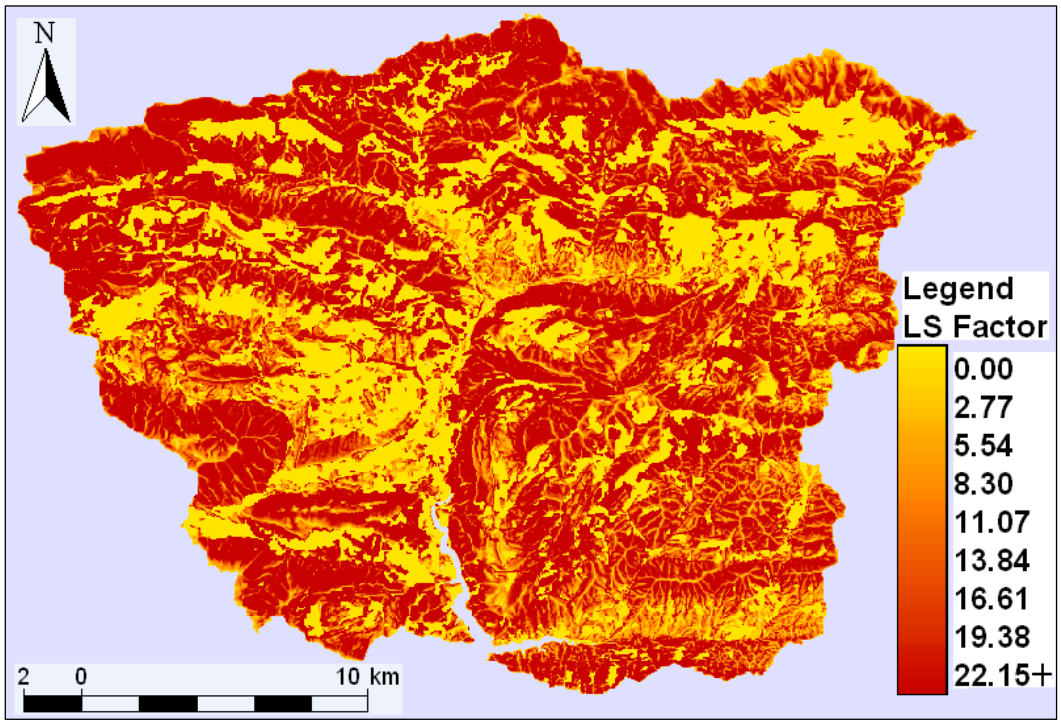

Figure 6.20: LS Factor map.

the basin.

6.4.5 Soil erosion

The average annual soil loss values for the study area was 14.15 Mg $ha^{-1}yr^{-1}$, and it was derived from Fig. 6.23. This value was calculated using the LS factor image which includes terraces and after saturating at 305 $ha^{-1}yr^{-1}$. The pixels of soil erosion image were saturated at 305 $ha^{-1}yr^{-1}$, in order to include only realiable soil erosion values, since the maximum erosion rate measured in a badland area in one of the Vallcebre's subcatchments (Ca l'Isard) was 305 $ha^{-1}yr^{-1}$ (Gallart *et al.*, 2005). It is assumed that within the study area, the badlands areas are the most susceptible and are the biggest suppliers of sediment. The left out values were considered as noise.

The estimated 14.15 Mg $ha^{-1}yr^{-1}$ is the most reliable estimate, since in its calculation, it was considered the role of terraces and noise was excluded, however, it is also important to examine the role of terraces and answer the question, what the soil erosion rate would have been if these agricultural terraces were not included?. The soil erosion, using the LS factor which does not take into account the role of terraces was 24.6 Mg $ha^{-1}yr^{-1}$, which is 74% higher than when terraces were considered -consequently LS factor values were smaller-.

The probability distribution functions of soil erosion -with terraces or without terraces- described by its cumulative distributions are illustrated in Figs. 6.22a and 6.22b respectively. Fig. 6.22a, denotes that 5.6% of the area (pixels) produces ≈50% of soil erosion, and 20% delivers ≈80% of soil erosion; conversely, Fig. 6.22b (terraces are not included), illustrates a more gently distribution function, where 9.5% of the area produces ≈50% of soil erosion, and 20% of the area delivers ≈60%

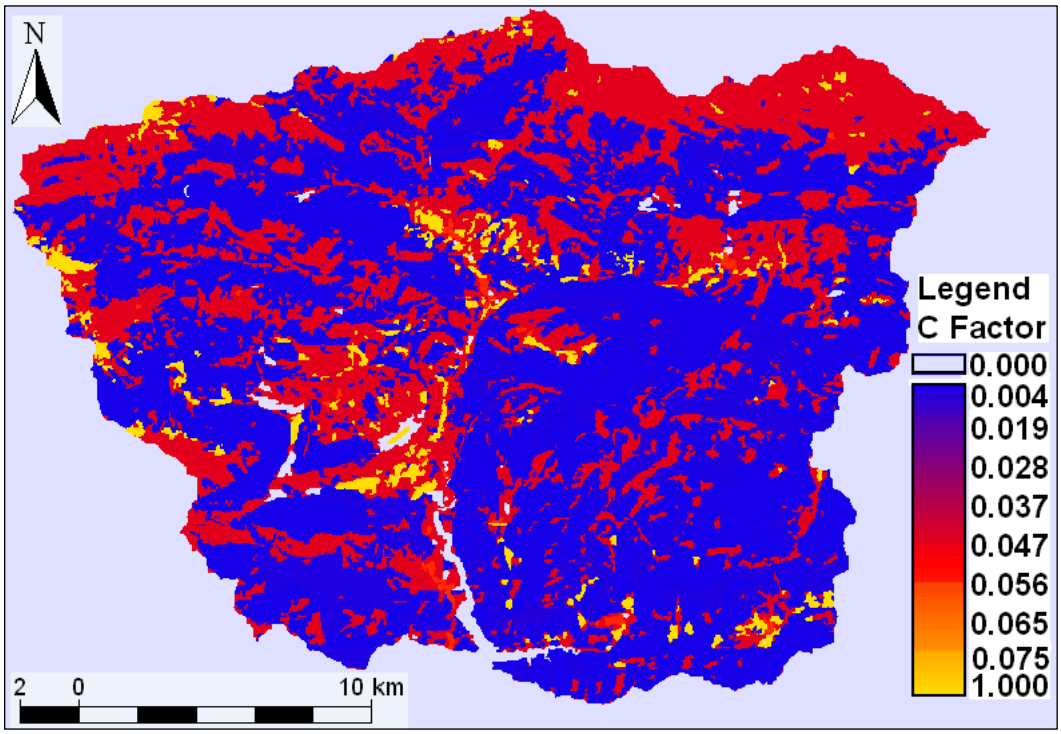

Figure 6.21: C Factor map.

of sediment.

The proportion of left out pixels (during the saturation process at 305 Mg $ha^{-1}yr^{-1}$) in relation to the total number of pixels was 1.7%, pixels having the highest values were checked individually and it was found that they occurr in areas where LS factor values were extremely high, or where the values of R, K and C factors were also. After a cursory look, it was also found that, besides association with steep slopes (high relief), soil erosion rates are extremely high in areas where soft rocks and agriculture are predominant. The results are in agreement with estimations given by Clotet & Gallart (1986) that badland areas on Garumnian clays can supply about a third of sediment production, although this estimation is for a nested catchment, the pattern for the entire Upper Llobregat Basin can be considered to be similar. Table 6.14, illustrates the soil erosion distribution in function of area, before noise was set to 305 Mg $ha^{-1}yr^{-1}$.

The results can be summarized as that eroded soils with negligible to low erosion rate account for 85% of the study area. Moderately erodible soils account for 10% of the total and are dispersed throughout the basin. The most eroded areas account for less than 5% of the total area.

6.4.6 Sensitivity and uncertainty analysis of soil erosion

6.4.6.1 R Factor

The sensitivity of annual average soil erosion to R factor is relatively small, and the 90% confidence interval for the mean soil erosion to R factor varies between 12.4 Mg $ha^{-1}yr^{-1}$ and 15.8 Mg

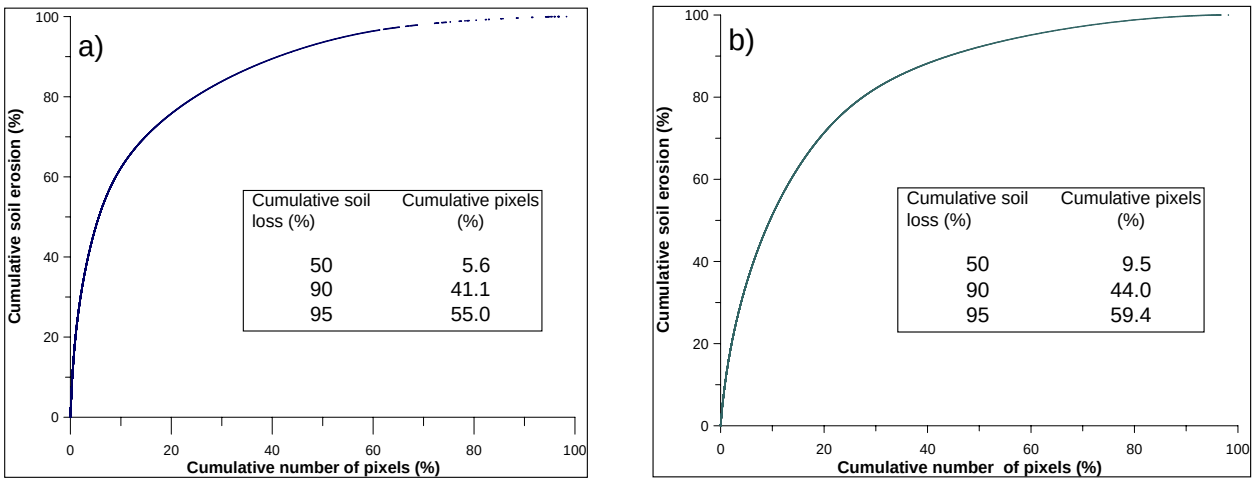

Figure 6.22: Probability distribution function of soil erosion: (a) considering the role of terraces, (b) ignoring terraces.

$ha^{-1}yr^{-1}$ when terraces are included (mean 14.15 Mg $ha^{-1}yr^{-1}$); and between 21.0 Mg $ha^{-1}yr^{-1}$ and 28.1 Mg $ha^{-1}yr^{-1}$ when terraces are not included (mean 24.6 Mg $ha^{-1}yr^{-1}$). Both, confidence intervals are symmetric, and these are shown in Fig. 6.24 and 6.25.

6.4.6.2 K Factor

The sensitivity of soil erosion to K factor is relatively large, for example when terraces are included (in the LS factor) the 90% confidence interval of soil erosion ranges from 8.7% Mg $ha^{-1}yr^{-1}$ to 20.3% Mg $ha^{-1}yr^{-1}$, it is slightly assymetric towards the upper bound in relation to the mean (14.1 Mg $ha^{-1}yr^{-1}$); conversely, when terraces are not included the 90% confidence interval of soil erosion are 20.0% Mg $ha^{-1}yr^{-1}$ and 28.7% Mg $ha^{-1}yr^{-1}$, it is also slightly assymetric but toward the lower bound. Figures 6.24 and 6.25 illustrate both intervals.

6.4.6.3 C Factor

Soil erosion is highly sensivity to C factor, and the 90% confidence interval of soil erosion is very wide. The confidence interval varies between 5.6% Mg $ha^{-1}yr^{-1}$ and 24.6% Mg $ha^{-1}yr^{-1}$ when terraces are included; and between 8.6% Mg $ha^{-1}yr^{-1}$ and 39.5% Mg $ha^{-1}yr^{-1}$ when the role of terraces are not considered, the interval in the latter is very assymetric towards the upper bound. Fig. 6.24 illustrates the confidence interval when terraces are included and Fig. 6.25 when terraces are not considered.

6.4.6.4 LS Factor

The sensitivity of soil erosion to LS factor is large, when terraces are included, the 90% confidence interval of soil erosion is between 6.9% Mg $ha^{-1}yr^{-1}$ and 26.6% Mg $ha^{-1}yr^{-1}$, and it is skewed towards the upper limit; on the other hand, when terraces are not considered, the interval ranges between 19% Mg $ha^{-1}yr^{-1}$ and 29.7% Mg $ha^{-1}yr^{-1}$, and it is nearly symmetric.

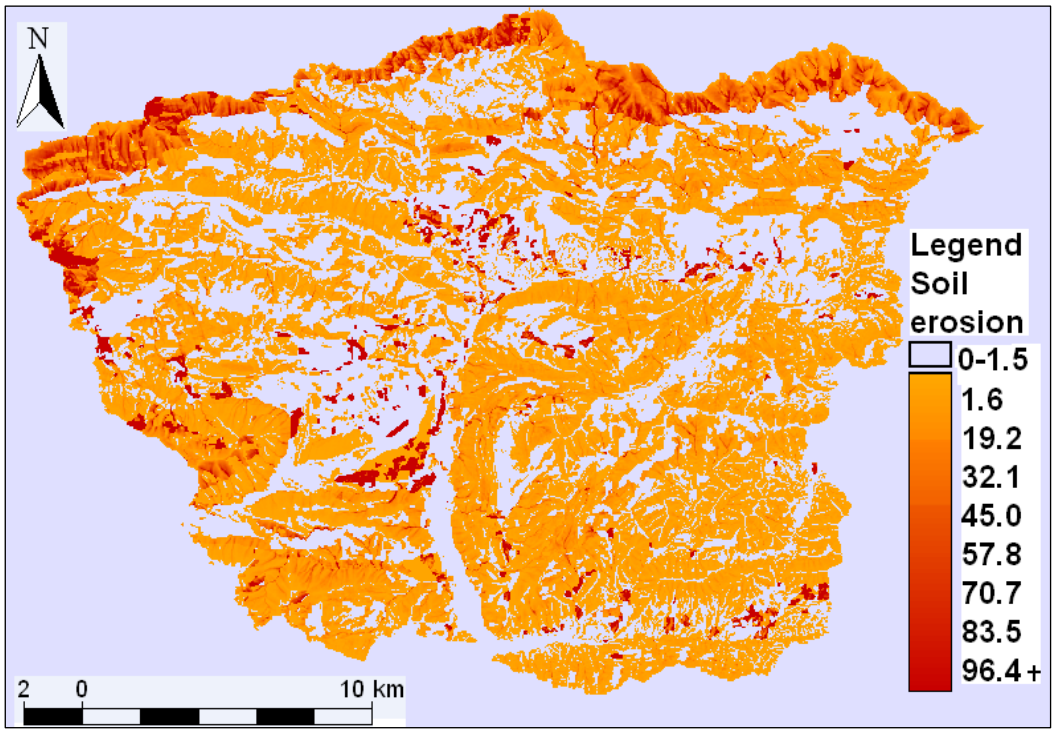

Figure 6.23: Soil erosion map estimated by using RUSLE.

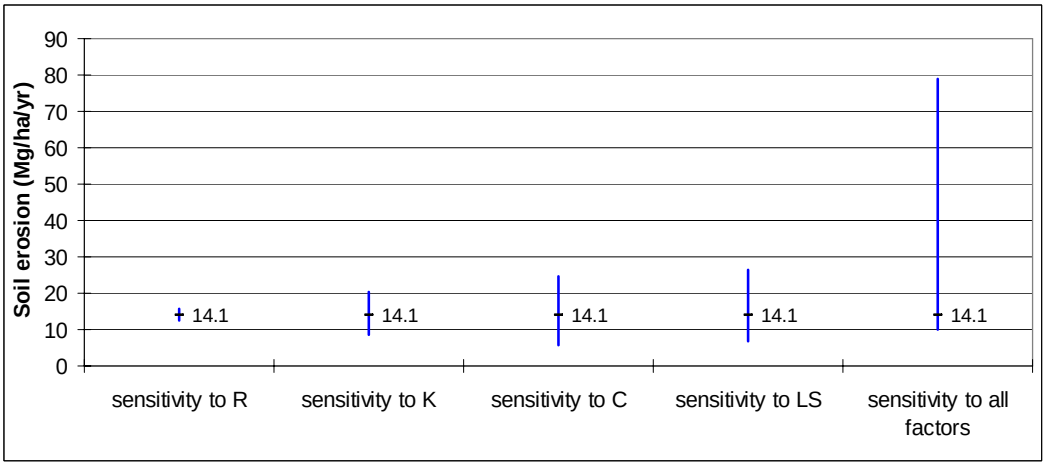

Figure 6.24: Confidence intervals for the sensitivity of soil loss to each factor, considering terraces.

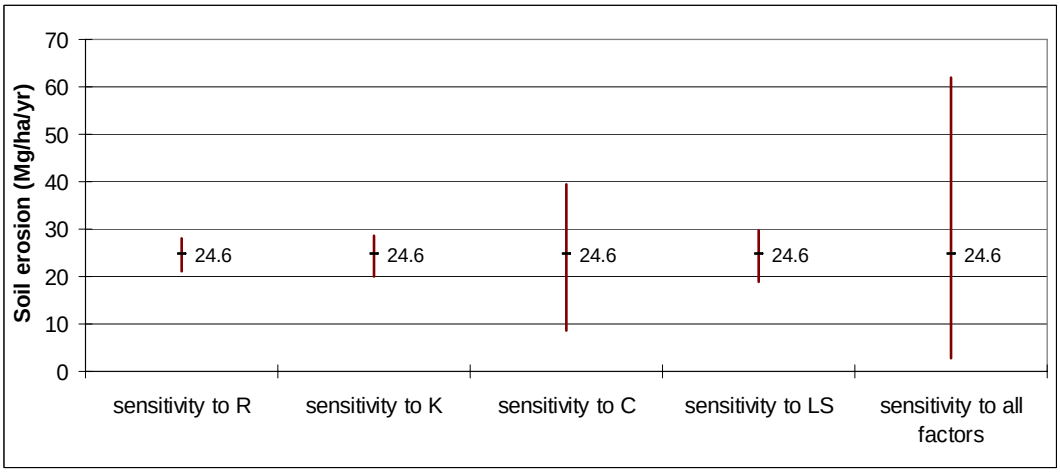

Figure 6.25: Confidence intervals for the sensitivity of soil loss to each factor, without considering terraces.

6.4.6.5 Uncertainty of soil erosion

The outcome 90% confidence interval of soil erosion estimated by Eq. 6.13 had a negative lower bound, because the standard deviation derived by solving Eq. 6.13 was larger (25.8 Mg $ha^{-1}yr^{-1}$) than the average soil erosion (14.1 Mg $ha^{-1}yr^{-1}$); therefore, in order to find out the type of distribution of erosion values, a sample of 1000 soil erosion values obtained by multiplying a set of 1000 random values of each factor was performed, the random values were derived from Monte Carlo simulation based on the mean and standard deviation of each factor.

Then, the probability distribution function of the simulated 1000 soil erosion values were examined, and it adjusted to a Gamma Distribution, finally, the limits of the 90% confidence interval of the mean was derived from a Gamma probability distribution after adjusting the parameters beta and alpha of that distribution using the mean (14.15 Mg $ha^{-1}yr^{-1}$) and standard deviation (25.8 Mg $ha^{-1}yr^{-1}$) (not from the simulated set).

The confidence interval for soil erosion (when the variability of all factors is included) was very wide varying between 9.90 Mg $ha^{-1}yr^{-1}$ and 57.0 Mg $ha^{-1}yr^{-1}$. The interval is asymmetric towards the upper limit, as a consequence of the multiplicative effect of factors.

6.4.7 Sediment Delivery Ratio

The SDR obtained from Eq. 6.20 was 0.235. In that equation the drainage area (W) was 194.7 sq.miles; the ratio length to relief $\frac{L}{R}$ was 9.41, which was calculated from the ratio of basin lenght (18 km) to the elevation difference between the minimum and maximum altitude (627 m and 2540 m respectively) which was 1913 m; bifurcation ratio B was 4.7, and it was estimated from the ratio of the number of streams of first order to the number of streams in the second order, and so on and so forth. In Fig. 6.26, the drainage network of the study area is illustrated, this was done by using the RUNOFF and RECLASS modules within IDRISI Kilimanjaro. The bifurcation ratios were $\frac{204}{37} = 5.5$, $\frac{37}{10} = 3.7$, $\frac{10}{2} = 5$.

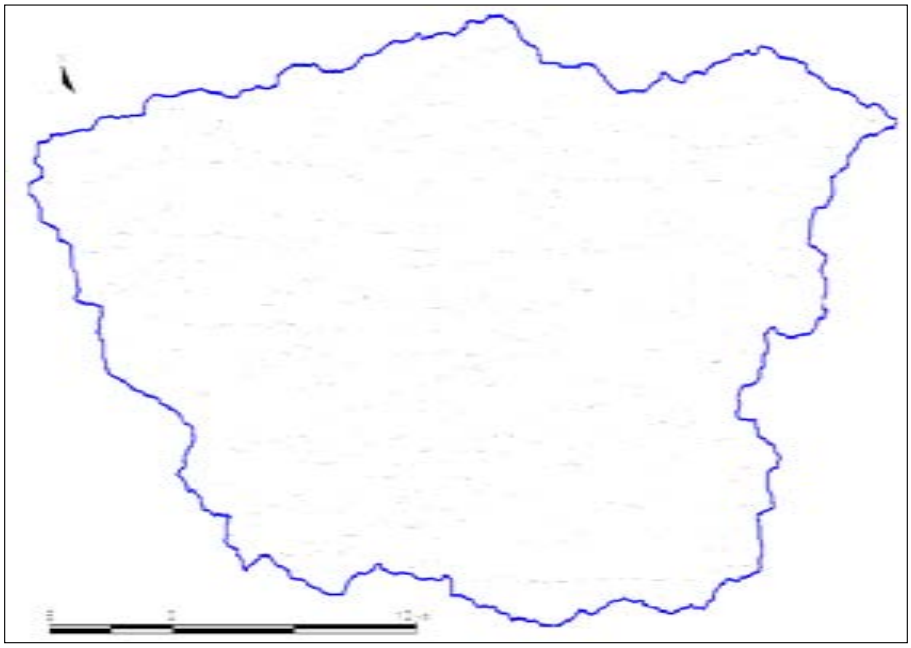

Figure 6.26: Drainage network of the Upper Llobregat Basin.

The SDR calculated from Eq. 6.19 was 0.191, where CN was obtained based on land cover type and infiltration values obtained from Tables given by US Soil Conservation Service. The CN was 60, this was obtained by selecting: the CN corresponding to forest (as it is most of the study area), the hydrological soil group B (soils having moderate infiltration rates when thoroughly wetted and a moderate rate of water transmission) and fair infiltration. The ratio relief-length ZL was obtained from the ratio of 1913 m to 18 km and it was 106.3, and drainage area was 504 km^2.

The SDR obtained from area based methods represented in Eq. 6.17, 6.18, and 6.16 were 0.217, 0.285, and 0.257 respectively.

The average SDR calculated for the study area (0.237) means that $\approx$ 76% of the soil eroded upstream, is deposited before reaching the outlet of the basin. This deposition trend may vary depending on the temporal scale, researches in small basins indicate that huge amount of soil may be translocated during heavy rainfall events, however, sediment loads leaving the basin are comparetevily small (Strauss & Klaghofer, 2004). In this study and for practical purposes the SDR was assumed constant in space and time.

6.4.7.1 Sediment yield

The average annual sediment yield when terraces are included was 3.35 Mg $ha^{-1}yr^{-1}$, which is result of the product between soil erosion and SDR. On the other hand, when terraces were not considered the sediment yield was 5.83 Mg $ha^{-1}yr^{-1}$.

Figure 6.27: Badlands directly connected to streams.

Figure 6.28: Badland formations.

6.4.7.2 Uncertainty of sediment yield

The 90% confidence interval of sediment yield ranged between 0.95 and 13.7 Mg $ha^{-1}yr^{-1}$ when terraces are included, and it varied between 0.61 and 14.9 Mg $ha^{-1}yr^{-1}$ when terraces are dismissed. In Table 6.15 a summary of inputs used to estimate the variance of sediment yield is presented.

The standard deviations derived from the error propagation formula Eq. 6.13 were larger than the mean sediment yield calculated in Section 6.4.7.1, as result the lower bound of the 90% confidence intervals were negative, therefore, a 1000 random samples were obtained based on the mean and standard deviation, then this samples were plotted and examined the type of distribution. Similar to soil erosion, sediment yield also follows a Gamma distribution, thus, the lower and upper limits of the 90% confidence interval were derived from such distribution.

Figure 6.29: Dense gully network in badlands that developed in marls in the study area.

6.5 Discussion

6.5.1 Sediment yield and uncertainties

The estimated sediment yield for the Upper Llobregat basin is relatively low (3.35 Mg $ha^{-1}yr^{-1}$) compared for example to one of the highest reported values obtained in large basins, which is ≈250 Mg $ha^{-1}yr^{-1}$ for the Dali River in China (Walling, 1980 after Mou and Meng, 1980), and it is about three times the assessed by Cerdan *et al.* (2006) (<1 Mg $ha^{-1}yr^{-1}$) for sheet and rill erosion in the western and central Europe, where land cover is forest, grassland and shrubs, and relatively steep slopes; however, the study area presents a few highly erodible areas such as badlands and they are important sediment suppliers.

During the last few decades the land cover and land use in the study area has suffered a sharp shift from being agricultural to forest and pastures, which implies a reduction on erosion rates, for example in the 1950's the erosion rates would have been ≈ 39 Mg $ha^{-1}yr^{-1}$ (more details about this value are provided in Section 7.4.2.2). The performance of the combined RUSLE-SDR has been fairly well, since the estimated average sediment yield is similar to estimations obtained by a bathymetry survey (CEDEX, 2002) of La Baells Reservoir located at the mouth of the basin. The slightly higher value of the estimate from bathymetry survey might obey to the age of reservoir (it was built in 1967) which was 25 years until a bathymetry surveys was conducted, this means that in the early years of the reservoir sediment deposition might have been larger than near year 2002; on the other hand, result obtained from the combined RUSLE-SDR might be smaller, because the land cover used within RUSLE belongs to year 1993, when land cover was already mostly forest and pastures.

The uncertainties related to the average annual sediment yield is large, the lower and upper limits of the 90% confidence interval were 0.95 and 13.7 Mg $ha^{-1}yr^{-1}$ respectively, and it is skewed toward the upper limit.

Although the used sediment delivery formulas are expressed in mathematical form, they do not carry descriptions of the mechanisms that cause the sediment transport and do not identify the separate effects of climate and catchment conditions (Lu *et al.*, 2004), however, a review of the obtained values and variation among them, indicates that it is a close approximation to reality,

since gully erosion is not the dominant form of erosion, therefore, a negative relationship between drainage area and sediment delivery can be accepted. Nevertheless, considering that badlands are well connected to the drainage network, in reality the SDR values are probably higher than 0.235.

In localized small areas, gully erosion may be important source of sediment (not assessed with RUSLE). In other areas of Catalonia gully erosion contribution to total erosion was estimated at 58% (Martínez-Casasnova *et al.*, 2002) and low porcentajes as 26% were assessed for NW Spain (Valcarcel *et al.*, 2003).

6.5.2 Soil erosion and uncertainties

The outcome soil erosion map provides an indication of the hotspots of erosion, and a close examination of the values (e.g. pixel scale) of the RUSLE's factors give an idea of the relative importance of them on soil erosion. Even though land cover is mostly forest and pastures (good soil protection), small highly erodible areas which account for only ≈5% of the basin, have the potential to contribute ≈50% of the total erosion. It was neccessary to examine if the range of soil erosion values of the outcome map were reliable, since some pixels had extremely high values, it was necessary to saturate them to a maximum measured erosion rate (305 Mg $ha^{-1}yr^{-1}$ in badland areas, Gallart *et al.* (2005)).

The confidence interval of soil erosion is large and assymetric Fig. 6.24, as result of the multiplication of several factors of diverse magnitude, nature and different distribution functions. It seems that low values are overcompensated by high values causing the assymetry of the soil erosion confidence interval.

The sensitivity analysis showed that the only RUSLE factor which was estimated through a physical approach (R) was the lowest source for uncertainty. Although the approaches for estimating the uncertainty introduced by the other factors should be considered as tentative, especially the LS factor, where the effect of slope angle and slope length (in USLE2d replaced by contributing area) are combined into a single topographic LS factor, might involve large errors since the study area presents high slopes; the results are consistent with other works where LS and C factors have been reported also as relevant sources of uncertainty (Biesemans *et al.*, 2000; Hartcher & Post, 2005; Falk *et al.*, in press).

The overall uncertainty associated with the RUSLE estimates for soil erosion and sediment yield was large, but similar in range and asymmetry to the estimates obtained by Falk *et al.* (in press) using a Bayesian melding approach in a rather complex 14 km^2 area; it was nevertheless much larger that the uncertainty reported by Biesemans *et al.* (2000) for an uniform agricultural 10 km^2 basin.

When applying the error propagation formula, it is assumed that the input factors are independent of each other, however, this may not be true, some authors indicated that there is considerable interdependence between the factors, for example, rainfall influences the R and C factors and terracing the L and P factors, other interactions, such as the greater significance of slope steepmess in areas of intense rainfall are ignored Morgan (1995), another issue is that in RUSLE runoff is not dealt with explicitly but is incorporated within the R factor (Kinell, 2006; Morgan, 1995).

6.5.2.1 R factor

R factor presents the lowest uncertainty on soil erosion, since the average annual R factor (1960 MJ mm ha^{-1} yr^{-1}) had a relatively low standard error, which has varied between 133.6 and 312.3 MJ mm ha^{-1} yr^{-1} among weather stations. The R factor was derived from a dataset spanning 14 years, with a strong annual variability. Despite the upscaling procedure (linear regressions) used to relate the daily R factor to daily rainfall depth in a station with sub-hour rainfall data to other weather stations which had only daily rainfall depth, the contribution of R factor to soil erosion uncertainty is relatively small.

6.5.2.2 K factor

K factor, a lumped factor has several error sources related to soil texture, organic matter, structure and permeability; among these, only permeability and structure were accounted directly, other likely sources were included through standard deviation; the sensitivity of soil erosion to K factor is large (Fig. 6.24.

The assumption that parental material has direct influence in physical properties of soil was accomplished, since differences between mean K factor values of the considered geological units exist according to an ANOVA test, and considering the fact that K values are obtained based on permeability and structural classes, which are strongly related to texture. Nonetheless, these results are restricted to sampled locations, a specific research including a larger number of samples and locations in order to verify these findings are needed.

Although K factor values between geological units are different, textural classes for samples are homogeneous (mostly clay), this might be due to colluvial deposition. Although it was expected to find clear differences between textural classes for the diverse parental materials, layers of fine colluvium deposited on the surface of a specified type of parental material has likely masked its ability to emerge.

6.5.2.3 C factor

The wide confidence interval of soil erosion as to changes in the values of C factor, can be due the existing bare hard rocks and bare soft rocks, which take values of 0 and 1 respectively, and their concurrence with extreme values of the remainder factors, thus, the uncertainty on soil erosion increases. The role of rock fragments were not considered, which in localized areas may offer significant protection to soil again rainfall erosivity.

6.5.2.4 LS factor

The distribution of LS values is asymmetrical, meaning that a few percent of pixels have high LS values, the lowest values occurred in flat areas which is probably because of the low slope.

6.6 Conclusions

A soil erosion and sediment yield assessment for the current state was conducted in the Upper Llobregat basin, by using the Revised Universal Soil Loss Equation (RUSLE) and sediment delivery ratio. Subhourly and daily rainfall data for the computation of R factor, soil samples to determine the K factor, and a DEM to obtain the LS factor values were available. C factor was derived from published sources. The degree of accuracy of sediment yield predictions were evaluated by comparing results with results from a bathymetry survey. The overall conclusions are given below:

The annual average sediment yield obtained by the combination RUSLE-SDR is fairly consistent with bathymetry results. The sediment yield obtained from a bathymetry survey is within the confidence intervals defined for the combined RUSLE-SDR developed including or not including the role of terraces.

The uncertainties of soil erosion and sediment yield are large, because of the uncertainties related to the input parameters (their standard deviations are proportionally large in relation to their mean values) and the multiplicative nature of RUSLE, resulting in a skewed distribution of soil erosion and sediment yield.

The basin has the potential to be more sensitive primarily to topography and land cover. A local assessment of C factor values are needed to reduce uncertainties in soil erosion assessment and improve the efficiency of RUSLE.

Small highly erodible sources produced half of the sediment, RUSLE allowed to identify these hotspots, which can be used to develop management practices and, thus reduce sediment infilling in the La Baells Reservoir.

Table 6.5: Soil sampling locations.

Sample	Geological unit	UTM		Alt. m.a.s.l.	Location	Land Cover and Rock types
		X	Y			
1	I	405285	4681115	1010	km 3 BV-4024, nearby Rigoreixer	Buxus sempervirens, Pinus sp.. Permutrias
2	III	406775	4683380	1200	km 7 BV-4024, nearby Hospitalet de Roca Sanca	Pinus sp. and Buxus sempervirens. Shales
3	III	406915	4683320	1240	km 7 BV-4024, nearby Hospitalet de Roca Sanca	Pinus sp. and Buxus sempervirens, oak. Shales
4	III	406735	4682920	1280	km 7.5 BV-4024, nearby Hospitalet de Roca Sanca	Pinus sp. and Buxus sempervirens.Shales
5	III	406785	4683070	1255	km 7.5 BV-4024, nearby Hospitalet de Roca Sanca	Pinus sp. and Buxus sempervirens. Shales
6	V	406905	4678762	829	nearby Baga	Pinus sp. Marls
7	V	411080	4677517	865	nearby Camping L'Espelt Moli de Ruitort, B-402	Pinus sp. oak. Marls
8	V	416165	4677842	890	nearby Pobla de Lillet	Pinus sp., Genista scorpio. Marls, salt deposit
9	IV	418455	4675792	990	nearby El Boix	Pinus sp., Buxus sempervirens, oak. Sandstone
10	IV	418450	4675812	995	nearby El Boix	Pinus sp., Buxus sempervirens. Sandstone
11	IV	418290	4673337	990	nearby Santa Eugenia de Solls	Pinus sp., Buxus sempervirens. Sandstones
12	IV	418425	4673287	1020	nearby Santa Eugenia de Solls	Pinus sp., Buxus sempervirens. Sandstones
13	IV	418350	4673317	1010	nearby Santa Eugenia de Solls	Pinus sp., Buxus sempervirens
14	V	416870	4677877	895	nearby Santa Maria de Lillet	Pinus sp. Marls

Table 6.6: Land cover of the Upper Llobregat basin (1993).

Original		Reclassified		
Class	Area (ha)	Class	Area (ha)	%
Civil infraestructure	25.8	Urban	1997.7	0.4
Urban low density	41.6			
Urban high density	130.9			
Herbaceous crop	600.0	Herbaceous crop	600.0	1.2
Pasture	2069.2	Pasture	16456.9	32.7
Brushwood and pasture	14387.7			
Sclerophyllous forest	553.6	Sclerophyllous forest	553.6	1.1
Caducifolious forest	7700.0	Caducifolious forest	7700.0	15.3
Coniferous forest	23224.6	Coniferous forest	23224.6	46.2
Bare soil or rocks	1199.2	Bare soil or rocks	1199.2	2.4
Water body	289.2	Water body	289.2	0.6

Table 6.7: C Factor values derived from published literature.

Land Use	Lee (2006)	Morgan (1995)	Jung et al. (2004)	Zachar (1982)	Ma (2001)	Raghunath (2002)	Stumpf et al. (2006)	Average
Urban	0.002		0.100		0.030	0.050		0.046
Herbaceous	0.300	0.300	0.500	0.600	0.240	0.420	0.230	0.370
Pastures	0.050	0.020	0.080	0.005	0.050		0.004	0.035
Sclerophyllus forest	0.004				0.007			0.006
Deciduous forest	0.004	0.001	0.001		0.009	0.010	0.004	0.005
Coniferous forest	0.004				0.004			0.004
Soft rocks		1.000						1.000
Hard rocks	0.000				0.000	0.000		0.000
Water body	0.000				0.000	0.000		0.000

Table 6.8: R Factor values used for sensitivity analysis.

Weather station	Estimate	stderror	lower 90%	upper 90%
Berga	1827.5	172.3	1545.0	2110.0
Figols	2496.2	312.3	1984.0	3008.3
Borreda	2236.0	217.2	1879.8	2592.3
Baga	1416.8	180.7	1120.5	1713.1
Pobla	1970.7	245.3	1568.4	2373.0
Molina	1582.4	133.6	1363.3	1801.4
Vallcebre	2023.5	201.1	1693.7	2353.2
Josa	2131.5	307.1	1627.8	2635.1

Table 6.9: K Factor values used for sensitivity analysis.

Geological unit	1 class up[a]			1 class down[b]		
	$\bar{x}$	s	$\bar{x} - 1.64s$	$\bar{x}$	s	$\bar{x} + 1.64s$
Limestones	0.020	0.006	0.010	0.028	0.007	0.039
Clays and sandstones	0.039	0.004	0.033	0.054	0.005	0.062
Marls and sandstones	0.014	0.002	0.011	0.024	0.004	0.031
Igneous and metamorphic	0.004	0.000	0.003	0.011	0.000	0.012
Conglomerates and sandstones	0.017	0.023	0.000	0.027	0.021	0.062

[a] 1 class up in permeability and structures classes.
[b] 1 class down in permeability and structures classes.

Table 6.10: C Factor values used for sensitivity analysis.

Land cover	Estimate	stdev	lower 90%	upper 90%
Urban	0.046	0.041	0.0000	0.1133
Herbaceous	0.370	0.141	0.1394	0.6006
Pastures	0.035	0.030	0.0000	0.0844
Sclerophyllus forest	0.006	0.002	0.0020	0.0090
Deciduous forest	0.005	0.004	0.0000	0.0112
Coniferous forest	0.004	0.004	0.0000	0.0103
Water body	0.000	0.000	0.0000	0.0000
Soft rock	1.000	0.044	0.9285	1.0715
Hard rock	0.000	0.000	0.0000	0.0000

Table 6.11: R factor (MJ mm ha^{-1} yr^{-1}) for each weather station.

Year	Weather station							
	Berga	Figols	Borreda	Baga	Pobla	Vallcebre	Molina	Josa
1991	1809.9	2259.2	1785.1	1129.8	2656.7	1367.6	1493.7	1034.4
1992	2135.5	2512.6	3667.5	3544.0	4426.0	2591.7	3304.4	4016.3
1993	924.6	1479.2	1670.2	805.1	1298.0	1279.5	1269.9	1030.7
1994	1200.9	2322.8	1768.4	1293.8	3065.8	2115.3	2647.0	3259.3
1995	2912.7	3967.6	3547.5	1401.4	2115.0	2122.7	1850.5	1500.5
1996	1589.3	3464.2	2523.4	1729.0	1909.8	2131.4	3024.8	3199.7
1997	2463.7	2913.8	2563.6	1106.2	1592.4	1785.6	2871.1	3738.6
1998	1100.3	3232.4	1508.1	651.3	931.4	764.3	1085.1	1138.9
1999	2466.0	5240.2	3137.1	1600.4	2285.4	1524.6	2814.5	2580.7
2000	965.5	1322.0	1260.7	1511.0	1127.8	1297.2	1358.4	2207.1
2001	1375.2	1062.7	2408.7	1171.1	1538.3	1179.3	1278.5	924.0
2002	2437.4	1852.7	2657.0	1303.3	1653.0	1319.6	1616.4	1542.3
2003	1940.8	1536.2	1380.6	1390.3	1462.0	1155.4	1810.4	1536.5
2004	2263.5	1781.0	1426.5	1198.4	1528.0	1518.9	1904.2	
average	1827.5	2496.2	2236.0	1416.8	1970.7	1582.4	2023.5	2131.5
st dev	644.6	1168.5	812.8	676.0	917.8	499.8	752.3	1107.3
st error	172.3	312.3	217.2	180.7	245.3	133.6	201.1	307.1
Area	19.6	86.9	39.5	107.0	125.1	15.9	106.8	3.4

Table 6.12: Soil texture in the Upper Llobregat basin.

Geological unit	Code	Total sand	Fine sand	Silt	Clay	Textural class
Igneous and Metamorphic rocks	I	25.3	13.7	7.8	66.9	Clayey
Limestones[1]	II	33.1	15.0	26.8	40.0	Clayey
Clays and sandstones[2]	III	14.8	7.2	63.4	21.8	Silty loam
Conglomerates and sandstones	IV	29.1	13.3	19.7	51.1	Clayey
Marls and sandstones	V	17.4	13.1	70.3	12.3	Silty loam
Superficial deposits	VI	-	-	-	-	

1. After Pérez (1991); Haro & Fernández (1991).

2. After Rubio (2005)

Table 6.13: K factor values and variation.

Geological unit	K value	Std. deviation
Igneous and metamorphic	0.0069	0.0004
Limestones	0.0225	0.0060
Clays and sandstones	0.0468	0.0037
Conglomerates and sandstones	0.0229	0.0213
Marls and sandstones	0.0199	0.0041
Superficial deposits	0.0199	0.0041

Table 6.14: Distribution of soil erosion in function of area (before saturating at 305 Mg $ha^{-1}yr^{-1}$).

Soil erosion (Mg $ha^{-1}yr^{-1}$)			Area	
Lower limit	Mean	Upper limit	km^2	%
0.0	22.0	44.0	440.3	87.3
44.0	66.0	88.1	37.6	7.5
88.1	110.1	132.1	9.8	1.9
132.1	154.1	176.1	3.9	0.8
176.1	198.1	220.1	1.9	0.4
220.1	242.1	264.2	1.2	0.2
264.2	286.2	308.2	0.8	0.2
308.2	330.2	352.2	0.7	0.1
352.2	374.2	396.2	0.5	0.1
396.2	418.2	440.3	0.5	0.1
440.3	462.3	484.3	0.4	0.1
484.3	15497.0	30509.7	6.6	1.3
			504	100

Table 6.15: Inputs for uncertainty analysis of sediment yield.

		Stdev	Variance	Mean
Terraces	Soil erosion	25.9	670.0	14.1
	SDR	0.036	0.0013	0.237
No terraces	Soil erosion	41.3	1710.0	24.6
	SDR	0.036	0.0013	0.0237

Chapter 7

ASSESSMENT OF THE EFFECTS OF GLOBAL CHANGE ON SEDIMENT YIELD IN THE UPPER LLOBREGAT BASIN

7.1 Introduction

Warming of the climate system in recent decades is unequivocal, although there is uncertainty about the magnitude of future increases, most studies indicate that future warming is very likely (Houghton *et al.*, 2001; Christensen *et al.*, 2007). It is consistently associated with changes in a number of components of the hydrological cycle and hydrological systems (Bates *et al.*, 2008a). Climate change is expected to accelerate (or to intensify) the global hydrological cycle, it manifests itself by increasing the temperature, changing the temporal and spatial distribution of precipitation along the year (Meehl *et al.*, 2005), widespread melting of snow and ice, increasing water vapour, increasing evaporation, changes in soil moisture and runoff, changing the precipitation intensity and extremes (Bates *et al.*, 2008a).

The accelerated hydrological cycle will have indirect effects on land cover and soil characteristics and consequently on soil erosion rates. The cause of these indirect effects are complex to attribute only to temperature or rainfall pattern changes alone, effects of both are combined in many ways. In addition land use changes (LUC) can also be driven by human activities and have its feedback in climate, for instance variations in absorbance and reflectance of radiation because of changes in the surface albedo, and partitioning precipitation into evaporation and runoff.

Although the warming of climate system at the global scale is evident, at the regional or local scales manifestations of climate change remain uncertain (Alcamo *et al.*, 2005; Evans, 2006b), for example precipitation pattern for the Mediterranean areas. These uncertainties in trends of hydrological variables might be explained by limitations in the spatial and temporal coverage of weather and climate monitoring networks (Huntington, 2006). The grid-cell size resolution of the Global Climate Models (GCM) is coarse (typically 300 km), this is useful at the continental or regional scales, however, too coarse to determine local impacts of climate change, for example

Catalonia often is represented with two grid-cells which is a too low resolution to study localized effects and this region has large and complex geography and microclimate. In order to tackle the resolution problem Regional Climate Models (RCM) for Europe were developed such as HIRHAM (Denmark), METNO (Norway) and others who worked in the PRUDENCE Project, the resolution of these RCM's is close to 50 km (López-Moreno *et al.*, 2008). These RCM's allow a better resolution of topography.

For the Mediterranean regions climate change scenarios are not very promising, projecting an intensification of stress conditions during the 21st. century the equilibrium between resources are predicted to be threatened. The stress conditions are predicted to be harsher in these areas because of increase in temperature and reduction of precipitation (EEA, 2004; Giorgi & Lionello, 2007).

The effects of climate change on soil erosion in the headwaters of Llobregat basin (above La Baells Reservoir) will rely upon rainfall and land cover changes. Yet, soil loss assessment at the basin scale is not straightforward, it can be addressed by breaking down the problem by answering questions such as: what are the impacts of climate variability on land cover?, how will the climate variability lead or force human activities (e.g. agriculture) into modifying land cover?, to what extent land cover changes will affect the soil erosion rates?, and what are the potential impacts of predicted rainfall patterns on soil erosion?. These questions can be answered using information obtained in previous chapters and combining them with existing climate predictions.

In this chapter predictions of sediment yield are performed considering most likely scenarios of land cover changes and rainfall patterns, which are most likely to change among the variables used to define the RUSLE model at least at the temporal scale being studied (100 years). Changes to features such as soil texture ocurr, over long geological time spans, while properties such as organic matter and moisture will show a more rapid response (EEA, 2008). Several assumptions of land cover changes and precipitation trends and its impacts on soil erosion are illustrated and discused, using several scenarios, the input data are used within RUSLE model in order to quantify the sediment yield in the river basin in the decades to come.

7.1.1 Objectives

The aim of this Chapter is to provide a quantified statement of sediment yield by the end of the 21st century based on land use and rainfall changing scenarios using RUSLE model.

7.2 Review of anticipated changes

Climate Change on Earth is a fact (Houghton *et al.*, 2001; Christensen *et al.*, 2007; Alexeev, 2007), although geological (millions of years) variations in climate have ocurred, current change has been accelerated within few decades by human activities. A number of Greenhouse Gas (GHG) emission scenarios have been published by the Intergovernmental Panel on Climate Change (IPCC). These are presented in the Special Report Emissions Scenario (SRES), Third Assessment Report (TAR), and Fourth Assessment Report (AR4). These scenarios are the base for GCM's and RCM's, these scenarios are:

- The A1 storyline and scenario family describes a future world of very rapid economic growth,

Table 7.1: Summary of Mediterranean (Region SEM 30N 10W to 48N 40E) averages of temperature and precipitation projections from a set of 21 global models in the MMD (multi-model data) for the A1B scenario. Differences in temperature (°C) and precipitation (%) between 1980-1999 and 2080-2099. Source: Christensen, et al. 2007.

90% Temperature Response (°C)						Precipitation Response (%)					Extreme Seasons (% of years)		
Season	Min	25	50	75	Max	Min	25	50	75	Max	Warm	Wet	Dry
Winter	1.7	2.5	2.6	3.3	4.6	-16	-10	-6	-1	6	93	3	12
Spring	2	3	3.2	3.5	4.5	-24	-17	-16	-8	-2	98	1	31
Summer	2.7	3.7	4.1	5	6.5	-53	-35	-24	-14	-3	100	1	42
Autumn	2.3	2.8	3.3	4	5.2	-29	-15	-12	-9	-2	100	1	21
Annual	2.2	3	3.5	4	5.1	-27	-16	-12	-9	-4	100	0	46

human demography reaches its peak in mid-century and declines thereafter, and introduction of new and more efficient technologies, a substantial reduction in regional differences. Scenario A1 includes three groups, A1F1 which is fossil fuel intensive, A1T is non-fossil fuel intensive and A1B balances all energy sources.

- The B1 scenario describes a convergent world, with the same global population as A1, but with more rapid changes in economic structures toward a service and information economy.
- The B2 scenario describes a world with intermediate population and economic growth, emphasizing local solutions to economic, social, and environmental sustainability.
- The A2 describes a very heterogeneous world with high population growth, slow economic development and slow technological change.

The scenarios for rainfall and land cover are based on review of predictions at the global and regional scales, although increase in temperature is clear predictions for precipitation remains uncertain.

7.2.1 Changes in temperature

Temperature increases for the Mediterranean are widely forecasted for the decades to come. Increases predicted by GCM's are slightly higher than the ones predicted by RCM's.

At the global scale predicted temperature (predictions for the end of 21st. century) increase depending upon emission scenarios is 1.8 °C for B1 scenario and 4 °C for A1F1 (Table 7.2), for the Mediterranean region it is predicted an increase of 3.5 °C (A1B) sharp increases are predicted for summer (4.1 °C) and winter (2.6 °C) (Christensen *et al.*, 2007). Similarly, RCM's (PRUDENCE Project) predict an annual increase of 1.3 °C (similar to A2 scenario), for summer 1.9 °C and winter 1.0 °C (Christensen, 2005).

Based on PRUDENCE Project results and using downscaling techniques, Calbo (2008) for A2 scenario and for the Pyrenees have predicted an annual increase between 0.7 °C and 1.8 °C (2011-2040), and for end of century (2071-2100) seasonal predictions are 2.5 °C - 4.5 °C for winter and 6.5 °C - 7.5 °C for summer. López-Moreno *et al.* (2008) using RCM's indicates increases of 2.8 °C and 4°C for B2 and A2 respectively.

Table 7.2: Projected average surface warming at the end of the 21st century. Source: Christensen, et al. 2007.

	Global (°C)		Mediterranean (°C)	
Scenario	Best estimate	Likely range	Best estimate	Likely range
B1	1.8	1.1 - 2.9		
A1T	2.4	1.4 - 3.8		
B2	2.4	1.4 - 3.8	2.8 (a)	
A1B	2.8	1.7 - 4.4	3.5 (a)	
A2	3.4	2.0 - 5.4	1.3 (b)	2.5 - 4.5 (c)
A1F1	4.0	2.4 - 6.4		

(a) GCM's, (b) RCM's (Prudence Project)

c) Prudence Project (Calbo, 2008).

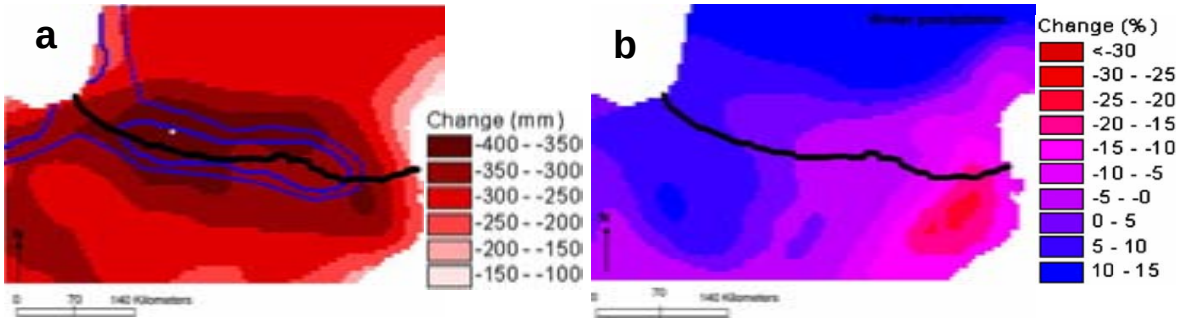

Figure 7.1: Predictions for A2 scenario (control period 1960-1990, future 2070 - 2100). a) predicted decrease in annual climatic water balance, b) predicted winter precipitation. Source: López-Moreno, et al. 2008.

Amid these predictions, increases in temperature and for a transition zone like the Pyrenees this will have a large effect on ecosystems and as a result the landscape will change, such as shifts in vegetation patterns.

7.2.2 Changes in rainfall

Projections for precipitation in Europe are more uncertain than those for temperature, and depend on future, still uncertain, atmospheric circulation patterns, and even more uncertainty is involved at the regional and seasonal scales (EEA, 2008).

Predictions of rainfall for the Mediterranean are diverse and have a strong seasonal variability. A review of recently rainfall changes has indicated an increase of extreme daily rainfall values in spite of decrease in total values (Alpert *et al.*, 2002).

Although for the Mediterranean (including the Pyrenees) rainfall predictions indicate a decrease of it, in some areas of the Pyrenees such as the east side rainfall would increase during winter and autumn (Abanades *et al.*, 2007) and for summer which is predominalty convective is predicted a decrease (Llasat *et al.*, 2008).

Over the last few decades the North Atlantic Oscillation (NAO) has dominated in NE Spain and it expresses itself in a decrease of precipitation during winter (Brunetti *et al.*, 2002; Gallego *et al.*, 2005) especially in north facing areas (Martínez *et al.*, 2007), however the weather in the East Pyrenees was found to be more correlated with Western Mediterranean Oscillation (WeMO) which predicts an increase of rainfall for early winter (January) but strong decrease during late winter (February-March) (López-Bustins, 2007). WeMO is a regional teleconnection developed to improve precipitation predictions in the NE Spain (Llasat *et al.*, 2008).

RCMs for the southern slopes of the Pyrenees (Spanish side) predict a mean decrease in climatic water balance (precipitation minus potentital evapotranspiration) of 244 mm for B2 scenario and slightly higher for A2 (López-Moreno *et al.*, 2008). With regards to precipitation an average decrease of 10% and 15% in the B2 and A2 scenarios respectively is predicted, however these estimates must be considered with caution (López-Moreno *et al.*, 2008). This drying is due to increased anticyclonic circulation that yields increasingly stable conditions and is associated with a northward shift of the Atlantic storm track (Giorgi & Lionello, 2007). These results are in agreement with GCM's predictions which indicate that precipitation is going to decrease by about 12% in annual basis, in summer decrease would be 24%, however for winter small changes (decrease) are predicted (5%), nevertheless it has a low spatial resolution (Christensen *et al.*, 2007). In Table 7.1 available projected temperatures are shown.

On the other hand and based on results from PRUDENCE Project and using downscaling techniques for A2 scenario and for the entire Pyrenees, Calbo (2008) has predicted precipitation increases up to 10% (2011-2040), and for 2071-2100 between -5 and +5 %, and for late of century increases between 5 and 15% for winter , and decreases up to -15% for summer.

Deficiencies in modeling the processes that regulate the local water and energy cycles in Europe also introduce uncertainty, for both the changes in mean conditions and extremes (Christensen *et al.*, 2007) but also not knowing the future emissions of greenhouse gases might add even more uncertainty (EEA, 2008). From MMD results presented in Table 7.1 the magnitude of variability in rainfall decrease is large, the sharpest decrease occurs during summer, the majority of extreme seasons will be warm and dry, wet seasons are almost unexistent.

7.2.3 Review of indirect effects of Climate Change

7.2.3.1 Changes in land cover

Land-cover changes are linked to climate and global change in many complex ways; however, there is no agreement among researchers about changes in land cover. Some argue that increasing content of carbon dioxide in the air has an impact on the amount of biomass produced by various crops via direct carbon dioxide fertilization effects (Stockle *et al.*, 1992), such changes in biomass affect (increase) canopy and ground residue cover. Meanwhile increased CO_2 can also enhance stomatal resistance, reduce transpiration, and lead to a moister soil, which can cause greater run-off and therefore induce erosion (Schulze, 2000), but, in a dry climate this will increase biomass production with similar water balance, the complexity of relations between vegetation type and atmospheric characteristics and the working scale (spatial and temporal) will make uncertainty part of the system.

Predictions for southern Europe indicate that warming will lead to sparser vegetation and therefore

some increase in erosion rates (Kirkby, 2006). Woodland might decrease by decreasing water stocks in the ground due to rise of temperatures and increase of evaporation (MARM, 2006). Warmer climate will influence human activities, for instance it may favour conditions suitable to grow certain agricultural species (e.g. vineyards) and stock breeding in mountain areas, or mountains will be tilled because farmers are forced to do so as lowland areas have become too warm for agriculture practice.

7.2.3.2 Erosion and sedimentation

The IPCC (2008) report indicates that water erosion has increased in many areas of the world, largely as a consequence of anthropogenic land-use change. All studies on soil erosion show that the expected increase in rainfall intensity would lead to greater rates of erosion (Bates *et al.*, 2008b).

As rainfall intensities will increase it will lead to an increase in suspended solids (turbidity) in lakes and reservoirs due to soil erosion (Leemans & Kleidon, 2002). Also rainfall increases generally lead to an increase in runoff and erosion (Kirkby, 2006) and as a consequence causing land degradation and off-site sedimentation (IPCC, 2001). Results indicate that, on average, each 1% increase in average annual precipitation induced between 0.85% and 1.66% change in soil loss (Pruski & Nearing, 2002).

Erosion is projected to increase with increases in precipitation amount and intensity, and to decrease with increases in ground cover an canopy cover (Christensen *et al.*, 2007). Soil erosion is likely to be more affected than runoff by changes in rainfall and cover, and percent of erosion and runoff will likely change more for each percent change in rainfall intensity and amount than to each percent change in either canopy or ground cover. Changes in rainfall amount and intensity will likely have a greater impact on runoff and erosion than simply changes in rainfall amount alone. Changes in ground cover have a much greater impact on both runoff and erosion than changes in canopy cover alone (Nearing *et al.*, 2005). Predictions indicate a decrease on runoff for Mediterranean regions (Bates *et al.*, 2008a). Nearing *et al.* (2005) suggests that there is a significant potential for climate change to increase global soil erosion rates unless offsetting conservation measures are taken.

Predicted high rainfall intensities will increase risk of soil erosion (Bates *et al.*, 2008b). Several researchers have studied erosion under climate change, for instance using the Erosion Productivity Impact Calculator (EPIC) model in the South Downs United Kingdom (simulated sites had 0.68 ha) it was found that a 7% increase in precipitation could result in 26% increase in erosion (Favis-Mortlock & Boardman, 1995); in another study at the Meuse Basin (ca. 33,000 km^2), where simulated increases in R factor (rainfall depth and intensity) lead to 12% and 8% increases for the 21st century compared to the 20th century in sediment yield for the A2 and B1 emission scenarios respectively (Ward *et al.*, 2009). Soil erosion is particularly sensitive to the intensity of individual precipitation events (Pruski & Nearing, 2002) and seasonal changes might have important role for example in Central Europe (Scholz *et al.*, 2008).

The processes linking climate and erosion are nonlinear (Morgan & Quinton, 2001) and are related among others to changes in rainfall depth and intensity, evapotranspiration rates (Nearing *et al.*, 2004).

7.3 Approach

The overall approach was to predict soil erosion rates based on rainfall pattern and temperature predicted changes, and its effects on land cover. The ranges of predictions are extracted from GCM's and RCM's (Tables 7.1 and 7.2). A few scenarios were performed which are based on assumptions, it should be noted that predictions of long-term sediment movement for 10- to 100- year periods is a challenge, and considerable uncertainty still remains in the predictions of long-term sediment movement, which is partly due to the uncertainty of climate (Ichikawa, 2005).

Scenario is understood as a structured account of a possible future, unlike forecasts, scenarios stress irreducible uncertainties that are not controllable by the people making the decisions (Peterson *et al.*, 2003). Scenarios are alternatives and dynamic possible situations which include the uncertainty about the future of a system.

Several independent scenarios for each, R and C factors (in the form of rasters) were performed, then these rasters along with the remaining RUSLE factors were used within the RUSLE/GIS interface. From the modelling point of view, this is a simplified sensitivity analysis.

7.4 Scenarios

7.4.1 Rainfall-runofff erosivity factor

The RUSLE/GIS interface can be used to model various possible weather conditions, for instance by changing the R factor values to simulate the predicted conditions. The greatest impacts on erosion rates are through changes in the kinetic energy of rainfall data at the soil surface (cover), although lesser impacts can occur through changes in gradient (slope) or soil erodibility (Kirkby, 2006).

7.4.1.1 Winter increase and summer decrease in rainfall

The slopes of equations 6.4 and 6.5 indicate that the amount of change of 1 unit R due to change of 1 unit of rainfall depth is greater for summer (12.6) than for the rest of the seasons (2.54). These relationships are the most reliable relations that were possible to obtain from the Vallcebre rainfall dataset (sub-hourly data), which afterwards were applied to the remaining seven weather stations (daily data).

Using the regressions defined from the relationship between the dependent R and independent rainfall depth (Eq. 6.4 and 6.5) for summer and winter respectively, the new Ri factor values were obtained by sustituting the rainfall depth by decreasing it on 10% for summer events and increasing on 5% for events ocurred during winter. By doing so, the new Ri values are smaller than the R values calculated with measured rainfall depth. The predicted R values are smaller because there are more rainy days in summer (73) and a decrease on the depth of them has large influence, compared to increases in winter (18 events) which was not enough to compesate the summer decreases. As summer rainfall depth are much larger than 12.5 mm (erosion power of rainfall) the 10% does not make them less than 12.5 mm. For events ocurred during autumn and spring the rainfall depth were not altered.

Table 7.3: Predicted R values (Mg $ha^{-1}yr^{-1}$) by adjusting rainfall depth (-10% in summer and +5% in winter)

Weather station	Current R	Predicted R	% change
Berga	1827.5	1711.5	-6.3
Figols	2496.2	2216.2	-11.2
Borreda	2236	1970	-11.9
Baga	1416.8	1235.4	-12.8
Pobla	1970.7	1731.9	-12.1
Vallcebre	1582.4	1400	-11.5
Molina	2023.5	1810.8	-10.5
Josa	2131.5	1911.9	-10.3

In Table 7.3 the predicted R values for each weather station are displayed. In all cases R values have decreased, the biggest reductions being at La Molina station.

The average annual soil erosion computed by assuming a 10% decrease in summer rainfall depth and 5% increase in winter was calculated by the overlay module within Idrisi. The only raster which had its numerical values changed was the R; the K, LS, C factors were used as obtained for current conditions (previous chapter).

The average annual soil eroded is 12.2 Mg $ha^{-1}yr^{-1}$ to which after applying the sediment delivery ratio (0.237) gives a sediment yield of 2.89 Mg $ha^{-1}yr^{-1}$. This represents a decrease of 7.4% with regard to 3.12 Mg $ha^{-1}yr^{-1}$ which is the current sediment yield. These results were expected because of the reductions on the intensity of summer rainfalls.

7.4.1.2 Longer summer

A disruption of the present summer (defined meteorologically) conditions due to higher temperatures will likely cause longer summer conditions (lengthen at the beginning and at the end), consequently, an increase of the number of rains of higher intensity, and the extreme rainfall events might also increase their intensity (EEA, 2008). The assumptions for this scenario is that increase in temperature will cause a lengthtening of summer conditions, which means that the average annual R values for that 'season' (longer summer) will present higher values as result of the higher intensity of rainfalls.

The calculation of the additional summer days was done according to the following consecutive steps: (1) calculate the mean daily temperature between 2002 to 2006 for June and September (data measured in Vallcebre), (2) enumerate from 1 to 30 the days of June and from 30 to 1 the ones of September, (3) developed a linear regression between day and temperature, and (4) use the slope of the regression as the ratio of number of day to temperature, in order to calculate the additional summer' days (at the beginning and at the end of the astronomical summer).

The linear regression (Eq. 7.1) between number of day d and temperature T has a slope of 0.20, which is the ratio day to temperature and it indicates that an increase of 1 °C can lead to a lengthen of 5 days to each side of summer. Therefore applying this ratio to the predicted 3.5 °C it can be expected a lengthening of about 17 days at the beginning of summer and 17 days at the end of

Table 7.4: Predicted R factor values for lengthening of summer conditions (Mg $ha^{-1}yr^{-1}$).

Weather station	Current R	Predicted R	% change
Berga	1827.5	2015.3	10.3
Figols	2496.2	2677.8	7.3
Borreda	2236	2350.9	5.1
Baga	1416.8	1544.8	9.0
Pobla	1970.7	2114.6	7.3
Vallcebre	1582.4	1650.1	4.3
Molina	2023.5	2305.8	14.0
Josa	2131.5	2350.3	10.3

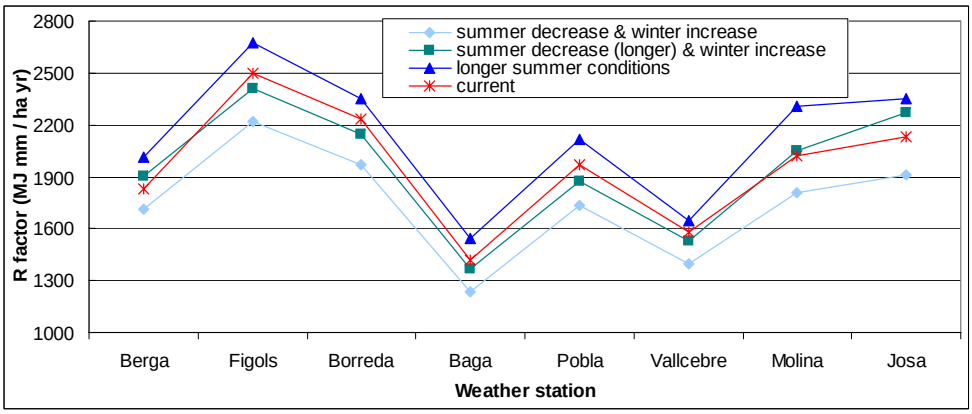

Figure 7.2: R factor values for the two rainfall scenarios compared with current state.

summer. Once the increased number of days during summertime were defined, Eq. 6.4 was applied to them as to any other event ocurred during summer.

For rainfall events falling within the extended summer the average annual R values was computed using Eq. 6.4 and for the remaining events Eq. 6.5 was applied.

$$T = 0.20 \times d + 11.9 \tag{7.1}$$

In Table 7.7 the predicted R values for each weather station are displayed. In all cases R value has increased up to 11.5%.

In this scenario assuming a longer summer, interpreted as increased numerical values of R factor, the average annual soil eroded is 13.8 Mg $ha^{-1}yr^{-1}$ which expressed as sediment yield is 3.27 Mg $ha^{-1}yr^{-1}$. This result represents an increase of 4.8% in sediment yield compared to current yield (3.12 Mg $ha^{-1}yr^{-1}$). A lengthening of the current summer conditions which not only has rainfall events of higher intensity, but also a larger number of them, has resulted increases on sediment yield.

Table 7.5: Predicted R factor values for decrease of rainfall during a longer summer and increase in winter (Mg $ha^{-1}yr^{-1}$).

Weather station	Current R	Predicted R	% change
Berga	1827.5	1901.4	4.0
Figols	2496.2	2407.5	-3.6
Borreda	2236	2145.3	-4.1
Baga	1416.8	1370.3	-3.3
Pobla	1970.7	1876.9	-4.8
Vallcebre	1582.4	1525.6	-3.6
Molina	2023.5	2054.2	1.5
Josa	2131.5	2272.3	6.6

7.4.1.3 Decrease of rainfall during a longer summer and increase in winter

A third assessment of the sediment yield by combining the two previous scenarios (10% rainfall depth decrease during summer and 5% increase in winter, and longer summer) was performed. Again, the only RUSLE factor changing its numerical values was R. Results are shown in Table 7.5.

Under this scenario the average annual soil eroded in the river basin is 13.1 Mg $ha^{-1}yr^{-1}$ which in terms of sediment yield represents 3.10 Mg $ha^{-1}yr^{-1}$. It ocurred a slight decrease of -0.64% compared to current sediment yield. The lengthening of summertime almost compensates the perturbation in rainfall depth (10% decrease in summer and 5% increase in winter).

7.4.2 Land cover and management factor

Predictions of land cover change and its impacts on soil erosion was developed by including spatial and temporal elements. C factor values are conditioned by land cover type and the degree of soil protection they offer against rainfall impact. C factor values can shift from being very low (~ 0) to higher values (~ 1) because of vegetation removal, for instance due to forest fires, land use conversion, alteration in vegetation patterns, etc. Mediterranean species often have different climatic constraints and they will likely respond differently to the climate change. Three scenarios of land cover changes were envisaged which afterwards will be used to predict its impact on soil loss.

7.4.2.1 Increase of forest land

It is likely that the changing temperature and precipitation pattern will produce a strong direct impact on forest land (Kirilenko & Sedjo, 2007). For instance, uphill tree line migration is becoming a global phenomenon, although the magnitude and rate of advancement depend on local topoclimatic conditions (Lloyd, 2005). It appears that pine will benefit substantially by altitudinal advance and increasing abundance in the tree line ecotone, for example in the Swedish Scandes it was reported a rose in the tree line of the Scots pine (*Pinus sylvestris*) by 150-200 m as warmer winters significantly lowered mortality and increased rates of establisment (Kullman, 2007). In

much of continental Europe, it was reported that the majority of forest are now growing faster than in the early 20th century (EEA, 2008).

Currently in the study area *Pinus mugo subsp. uncinata* can be found at altitudes as high as 2,323 m a.s.l. (river basin minimum and maximum altitudes are 627 and 2540 m respectively), within this scenario it is assumed that all existent agricultural and pasture lands below 2,000 m a.s.l. will be transformed into coniferous forest by the end of this century as a consequence of one or both of the following: (a) favorable weather conditions for uphill migration, (b) policies aimed at soil erosion decrease by promoting increase in woodland.

A new C factor raster was obtained by shifting all pasture and agricultural areas below 2,000 m a.s.l. in the 1993 land use map into coniferous forest, and re-assignation of numerical values of C factor was performed. As land cover factor is the only changing factor, the remaining four RUSLE factors were the same as in the previous chapter. The average annual soil loss was computed by overlaying the five rasters within IDRISI.

Results show that the area of coniferous forest has increased from 46.2% to 77.0% under the studied scenario. Pasture above 2000 m will still represent 3% of the basin area (15.1 km^2), small forested areas and bare soil will also exist.

The estimated average annual soil is 9.72 Mg $ha^{-1}yr^{-1}$ or 2.3 Mg $ha^{-1}yr^{-1}$ in terms of sediment yield, there is a decrease of 26.3% in sediment yield as result of shifting pasture and agricultural lands into forest.

7.4.2.2 Shifting from woodland into agriculture as of 1957

In the study area in 1957 (1957 data obtained from Delgado (2009)), grassland constituted 5.7% (28.9 km^2), in 2002 it had increased to 32.7%, similarly agriculture decreased from 23% (115.2 km^2) to 1.2% (6 km^2), forest increased from 55% to 62.6% in the same period. Surprisingly in 1957 bare soil constituted about 26%, mining and logging was important and represented 0.34% of the basin. La Baells reservoir was completed in 1976, previously was mostly occupied by agriculture and shrublands.

Along with a considerable reduction of cultivated land (Garcia-Ruiz *et al.*, 1995), transhumance has practically dissapeared and livestock pressure has diminished Garcia-Ruiz & Lasanta (1990); Molina (2000), mining and logging activities which are recognized drivers of soil erosion have also decreased.

The underlying assumption for this scenario is that by the end of this century land cover in the study area will be reversed to the land cover conditions as of 1957. By devoloping this scenario it is also being assessed the soil erosion in the 1957 if it is assumed that rainfall conditions were similar to the 1991-2004 period. Conditions as of land use in 1957, which is an extreme scenario, if deep environmental and energy crisis happen.

A land cover map of 1957 for La Baells derived from photointerpretation and provided by Delgado (In preparation) was used to obtain the C factor raster. The land cover categories of the aforementioned map and the assigned C values were: dense forest, 0.005; shrubland, 0.005; sparse forest, 0.006; improductive land (bare soil), 1; urban, 0.046; mining and logging, 1; water body, 0; and pastures and crops. As pastures and crops were within the same class it was neccesary to

split them into pastures and crops as both offer different degree of soil protection. The existence of terraces up to 1700 m suggests that areas below 1,700 m a.s.l. were agricultural areas, and above 1700 m land cover was mainly highland pastures. Therefore the C values used for pastures was 0.035 and for crops 0.37. C factor values were obtained from published literature. Once the C factor raster was obtained, the average annual soil loss was computed by overlaying the RUSLE factors R, K, LS, C and P within IDRISI. R, K, LS and P factors remained unchanged.

As expected results show a higher erosion rates, the average annual soil loss is 38.6 Mg $ha^{-1}yr^{-1}$ which expressed as sediment yield is 8.7 Mg $ha^{-1}yr^{-1}$. The obtained sediment yield represents an 180% increase with respect to 3.12 Mg $ha^{-1}yr^{-1}$ which is the sediment yield obtained by using a land cover of year 1993.

7.4.2.3 Ocurrence of forest fires

Introduction Climate change projections indicate an increase of drought frequency and forest fires in the Mediterranean region, specially during summer months (EEA, 2008; Bates *et al.*, 2008b). Causes of forest fire are many such as drought, bonfires, moisture and wind conditions, deforestation, accidents, and lightining (Morgan *et al.*, 2001). In Spain, the main causes are arsons (67%), accidents (24%), and lightning (3%) (MARM, 2009).

Post-fire sediment yield studies show large variable results because of the diverging spatial scale at which they were conducted. In the Catalan Coastal Ranges at the plot scale it was reported after two years of measurement using Gerlach troughs that burned plots produced 8.4 times more sediment than the clear-felled plots and 14.6 times higher than in the woodland (mainly *Quercus ilex*) (Soler *et al.*, 1994). At the river basin scale using RUSLE in the USA for the Cerro Grande fire (occurred in 2000) pre-fire values were 0.45 to 9.22 Mg $ha^{-1}yr^{-1}$ while post-fire erosion rates range from 1.72 to 113.26 Mg $ha^{-1}yr^{-1}$ (increase of 3.7 times) (Miller *et al.*, 2003), also at the basin scale in Southern California was reported 45 Mg $ha^{-1}yr^{-1}$ and 147 Mg $ha^{-1}yr^{-1}$ for pre-fire and post-fire conditions respectively (increase of about 2.3 times) (Drake, 2005).

Forest fires deprive the forest soil of protection from rainfall impact over large areas (González-Bonorino & Osterkamp, 2004), specifically, fire influences erosional processes by reduction or elimination of above-ground biomass, reduction of soil organic matter, and producing hydrophobicity (Miller *et al.*, 2003); however, the degree of its impact on the susceptibility of soil to erosion depends on many factors. Fires generally reduce the organic matter content (Giovannini & Lucchesi, 1983) except when the temperature of the fire is very low (Almendros *et al.*, 1990), heating the soil up above 460 °C causes major disruptions in the physical structure of the soil becoming unsuitable for plant growth and with a great erosion risk (Giovannini, 1994).

Regarding soil hydrophobia when some organic susbstances are leached into the soil produce an increase in soil hydrophobia (Giovannini & Lucchesi, 1983) which can contribute to a decrease of soil infiltration capacity (de Bano, 1971) and consequently increase in runoff. The primary controlling variables of water repellency are the burn severity, percentage of sand and soil moisture (Huffman *et al.*, 2001).

Another critical factor is the timing of a fire, if a storm occurs immediately after the fire, erosion may be severe, but if it occurs after a period of time, the flush of plant growth using the nutrients supplied by the fire may be such that the ground surface is adequately protected from rainsplash and runoff (Evans, 2006a). In quantitative studies soil erosion rates are high immediately after burning

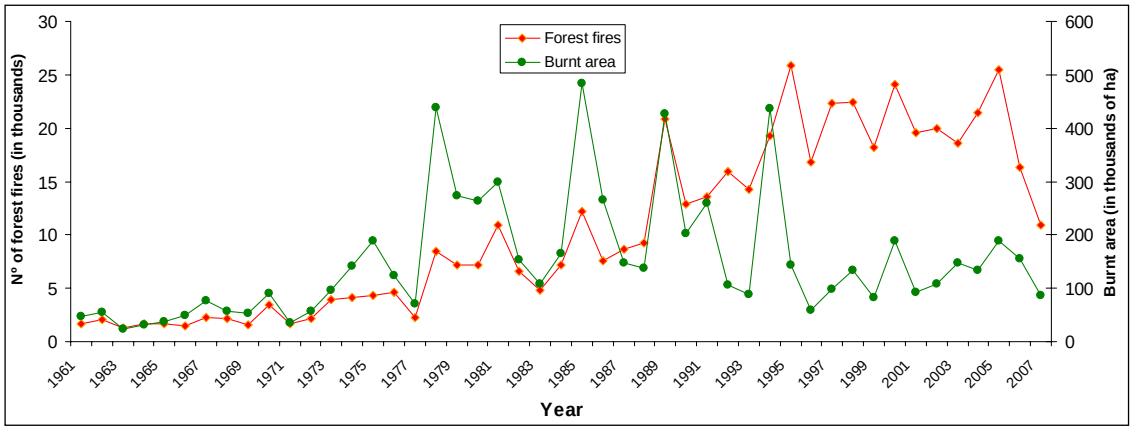

Figure 7.3: Number of forest fires and burnt area in Spain. Source: adapted from (MARM, 2009).

but are reduced greatly after one year (Sala & Rubio, 1994). González-Bonorino & Osterkamp (2004) reported that 3 to 10 years commonly, will suffice to restore protection to the soil and lower soil losses to pre-fire values depending on climate and postburn condition.

Developing scenarios of post-fire sediment yield under predicted changing conditions is neccessary to guide management decisions and assess the potential on-site and off-site impact of soil erosion. The headwaters of the Llobregat basin can be considered moderately prone to forest fire, this might become a concern especially because of increased sediment transport to water streams which can accelerate siltation in La Baells Reservoir. In the study area pine forest occupies the majority of land cover (62.6%), and the ground biomass can encourage the burn severity.

Predicting the ocurrence of forest fires is complex because of the many controlling factors involved and which are not easily and accurately quantifiably, but as mentioned previously it is needed for risk asessment purposes (Morgan *et al.*, 2001).

Forest fires in Spain have increased from about 2,000 (in 1961) to about 11,000 (in 2007) and the burned area has also increased, as illustrated in Fig. 7.3. The annual average of forest fires between 1980 and 2004 was 14,000, this increasing rate is predicted to continue (Moreno, 2005) increase rate is high after 2001. At the local scale and according to the Catalan Ministry of Environment and Housing in the Upper Llobregat area between 1968 and 2008 a total of 288 forest fires have been recorded, only 9% of these were larger than 10 ha, the biggest reported were of 1570 ha (Pobla de Lillet, 1981), 229 ha (Baga, 1984) and 180 ha (Cercs, 1978), however, these are very small areas compared to the size of the river basin (50,400 ha), therefore, forest fires have not been a problem in the study area in the past.

Data and methods RUSLE which is successfully used to estimate average annual field soil loss from agricultural lands is being used on varied land conditions and seems reasonable to apply to burned areas.

The assumptions for forest fire occurrence in La Baells were: first, there will be enough bed fuel susceptible to combustion, the weather is dry under high summer temperatures which increases the hazard and severity of fires, the topography of the land contributes the way a fire is initiated and propagated, southern aspect is more susceptible, because it posseses higher amount of fuel potential

insolation (it has less moisture content) and is more likely to burn. Based on these assumptions fire size spatial distribution within the river basin were identified by examining the aspect and land cover (2002) maps. A few large areas having both south aspect and covered by forest (coniferous, decidious or schlerophyllous) were identified as fire risk areas, then these areas were digitised on pre-fire land cover map, in order to estimate the erosion rates with RUSLE integrated within a GIS.

The degree of soil exposed to rainfall drop varies with time after the burning, at the beginning soil is highly susceptible and after six months it was assumed soil present vegetal protection. Annual soil erosion rates were calculated using the R factor calculated using rainfall events ocurred since the period with the highest fire hazard (15th of July), until six months later when the soil may be expected to be protected by vegetative growth. Soil erodibility and LS factors used were from pre-fire conditions, it is assumed that soil physical properties do not change significantly due to fire, although at the plot scale soil aggregate disruption were observed especially because of the vulnerability of bindings to heat (Cammeraat *et al.*, 2006). P factor value was set to 1 which indicates no post-fire stabilization or remediation practices. It was focused on quantifying the C factor as the main controlling process, for this it was assumed that all vegetation in the post-fire condition was removed and there are no trees fallen or standing, indicating a total bare soil, consequently a uniform C factor value of 1 was applied to the burned areas.

In order to estimate the influence of burned size areas on sediment yield, two scenarios were performed. The first burned patch is located NW of Baga village it has an area of 7 km^2 (1.4% of La Baells). The second scenario comprises three patches which are located at N of Clot de Moro, N of Borreda and near Peguera, the area of the three patches is 11.5 km^2 (2.3% of La Baells). For each scenario a C factor (C_b in Eq. 7.2) raster was obtained.

Once the rasters for each RUSLE factor were defined, annual average of post-fire soil eroded (A_1) was calculated by overlying the rasters within Idrisi, mathematically represented as in Eq. 7.2 where R_m is the rainfall calculated for a period of six months, K, LS and P are soil erodibility, slope steepnees and slope lenght, and support-practice factors respectively. Similarly pre-fire soil eroded was obtained by Eq. 7.3 which is the same as Eq. 6.1 but R_m instead of R, because it is assumed post-fire erosion is acted by the heaviest storm season. However for comparative purposes what matters is the difference of sediment yield between pre-fire and post-fire conditions because R_m is constant in Eq. 7.2 and 7.3.

Finally, comparison of sediment yield (A multiplied by SDR) of the pre-fire and post-fire conditions was made, in order to assess the influence of burned area on increase of sediment yield. All A values exceeding 305 Mg $ha^{-1}yr^{-1}$ (maximum erosion rate reported in a bare soil in the study area) were set to this value.

$$A_1 = R_m \times K \times L \times S \times C_b \times P \tag{7.2}$$

$$A_2 = R_m \times K \times L \times S \times C \times P \tag{7.3}$$

Results As expected, sediment yield was higher for post-fire conditions than for pre-fire conditions as a consequence of increased C-factor value. In Table 7.6 these differences are shown, for the six months studied the burned patch size directly influenced the amount of sediment yield, such as that burning an area equivalent to 1.4% of the basin increases in 36% the sediment yield, and 2.3% of burned area increases in 58% the sediment yield compared to pre-fire conditions.

At the annual scale and considering that the pre-fire soil eroded obtained by using annual R is 13.2 Mg $ha^{-1}yr^{-1}$ which in terms of sediment yield is 3.12 Mg $ha^{-1}yr^{-1}$, and adding the amount of sediment yielded as a direct consequence of burned areas (0.93 and 1.49 Mg $ha^{-1}yr^{-1}$) to 3.12 Mg $ha^{-1}yr^{-1}$ it is obtained the annual potential sediment yield which are 4.05 Mg $ha^{-1}yr^{-1}$ (30% increase) and 4.61 Mg $ha^{-1}yr^{-1}$ (48% increase).

Table 7.6: Sediment yield (SY) and soil erosion (A) rates under different burned size patches.

		post-fire		pre-fire		Increase SY	
Burned	% of La Baells	(Mg $ha^{-1}yr^{-1}$)					
Area (km^2)	(504 km^2)	A	SY	A	SY		(%)
7	1.4	14.8	3.51	10.9	2.58	0.93	30
11.5	2.3	17.2	4.07	10.9	2.58	1.49	48

7.5 Discussion

R factor was computed based on measured data in Vallcebre, based on an established relationship between R factor and daily rainfall, which then was upscaled to compute the R factor at the remaining stations. Furthermore, the R value were assumed uniform for the Thiessen polygons. The error sources involved and which were not evaluated exhaustively are: (a) the calculation of the kinetic energy from rainfall intensity, since rainfall drop size distribution data for the study area was not available, (b) the average annual R values have an error associated to them due to the process of averaging, (c) annual R values also have errors since the daily R values are calculated from a relationship between daily R and daily rainfall data, which best fit had errors. In this study the standard deviation of the average annal R factor for each station was assumed to represent these errors.

Rainfall predictions for the Mediterranean are uncertain, the most likely conditions were evaluated here, such as rainfall depth decreases (10%) during summer and increases (5%) during winter under predicted climate conditions, the overall result of this combination gives a reduction on erosion rates of -7.4% compared to the current rates, this is due to the larger number of summer events whose

Table 7.7: Summary of soil erosion under Global Change scenarios.

	Soil erosion (Mg $ha^{-1}yr^{-1}$)	Change in relation to current values (%)
Changes in R factor		
a) Summer rainfall (-10%) and winter (+5%)	13.3	-6.0
b) Longer summer conditions (+/- 17 days)	14.7	3.9
scenarios a) + b)	14.0	-1.1
Changes in C factor		
Increase in forest area (from 46.2% to 77.0%)	10.3	-27.2
Shifting to agriculture as of 1957	38.6	172.8
Ocurrence of forest fires:		
burned area 1.4%	15.1	6.7
burned area 2.3%	17.6	24.4

rainfall depths were decreased, therefore, their intensities were weakened, and the rainfall depth increase in winter is not enough to compensate for the reductions of summer events.

The ocurrence of a longer summer (larger than the astronomical summer) because of the warming conditions, will increase soil loss in 4.8% compared to the current conditions, as a direct consequence of the increased R factor values for the eight studied weather stations, at the meantime higher R factor values were due to the higher rainfall intensities during summer events. This scenario does not consider changes in land cover factor, which certainly will be affected if changes in rainfall ocurr; however, it is likely that these predicted conditions will reduce the land cover, in that case the estimated -7.4% reduction may not ocurr.

A combined scenario of rainfall reduction during summer and increase during winter, and ocurrence of longer summer, integrated within R factor has caused a slight decrease (-0.64%) in soil loss compared to current conditions.

Land cover changes will certainly impact the magnitude of soil loss, C factor represents the soil protection by vegetation therefore modifying C factor values for the land cover scenarios will give the sensitivity of soil loss to land cover changes.

The predominant land cover type is forest and there is likely that warmer conditions will cause uphill migration of forest, therefore, a scenario was examined by increasing the forestland at the expense of pasture and agricultural areas. The increase of forested areas (from 44.2% to 77%) produces a decrease of 26.3% in soil loss because of lower C factor values for forest than for pastures and agriculture.

In the scenario developed by assuming a conversion of land use into agriculture as of 1957 will increase soil loss in 2.8 times the current yield, as a result of the higher C factor values for agricultural areas than for forest areas; therefore, this results gives insight to what the erosion rates must have been in the 1957, in addition to future predictions.

Predicted warmer conditions and ocurrence of drought periods may trigger ocurrence of forest fires, this a likely scenario since in Spain, during the last few years an accelerated increase of fires was recorded. Thus, an evaluation of the extent to which the size of burned forest patches impacts soil loss shows that small burned patches such as 1.4% and 2.3% can produce significant increases up to 30% and 48% respectively compared to current sediment yield rates.

7.6 Conclusions

The RUSLE model was applied to estimate soil loss in the headwaters of Llobregat basin under several rainfall and land cover scenarios elaborated based on predicted climate conditions. For the Mediterranean region there is agreement about the ocurrence of warming trend, however, prediction on rainfall patterns is still uncertain, although effort to reduce these uncertainties by developing RCM's exist. Three likely scenarios for R factor (rainfall erosivity), and three for C factor (land cover) were performed independently, assuming that the effects of predicted climate conditions on soil erosion will lay predominantly on those two factors. The outcomes were wide-ranging, depending on the R and C factor input values.

Regarding the model, it is very fleixible, since the rasters representing each RUSLE's factors can be assigned new values and then evaluate the degree of changes on soil erosion rates, compuptionally

it is not intensive, the new values should be based on reliable predictions.

The overall global change impact on soil loss and according to most of the examined scenarios shows an increase in erosion rates. Soil loss appears to be more sensitive to land cover management factor than for rainfall-runoff erosivity factor which is independent from human intervention. The land cover management factor can be changed by human activities which adds uncertainty to predicted soil erosion values.

Chapter 8

EVALUATION, CONCLUSIONS AND SUGGESTIONS FOR FURTHER RESEARCH

8.1 Introduction

In this concluding Chapter, first an assessment of the approaches and methods, and quality of data used are provided; next, a summary of main conclusions, and some remarks and suggestions for further research are given.

The problems addressed in this thesis are related to sediment transport at two spatial scales, the effects of Global Change on erosion rates, the role of data resolution and its overall assessment of uncertainties. Reliability of erosion and sediment yield values were developed based on diverse methods and approaches, which were corroborated somehow among them.

Cal Rodó catchment (4.2 km^2) has an event-based stream response, where the uncertainties regarding to the use of sediment rating curves were evaluated. Sediment rating curves are widely used to estimate sediment loads because they are simple and easy to use. Data required to develop a sediment rating curve are: continuous discharge record and discrete suspended sediment concentration, then a relationship between the two is developed in order to calculate sediment load for the whole range of discharges. The relationship is often developed in the logarithmic scale and then back transformed into the arithmetic scale, in this process a bias occurs because the back transformed mean is a geometric and not the arithmetic mean, this fact is well known and documented, and bias corrections factors exist. The problem is that uncertainty of sediment load while using these relationships are rarely provided, particularly in mountain areas with event-based flows.

The Upper Llobregat basin (504 km^2) and neighbouring rangelands are important water supplier, and they can also be sediment supplier, which needs to be assessed to guide management practices. It is of concern the understanding the sediment dynamics in these rangelands with changing environments at the current state and under predicted conditions of Global Change. Studying soil erosion dynamics in these areas are relevant from the applicability and scientific point of views. In this basin an attempt to quantify the sediment yield by using several approaches was performed.

At this large scale, input data was dispersed (climate, soil, topography, land cover and management practices) but were brought together via a GIS framework. Several scenarios of erosion rates were performed, and which can help policy makers.

8.2 Evaluation

8.2.1 Approaches and methods

Throughout this thesis a stochastic or probabilistic approach was followed, as opposed to the deterministic approach, which relies heavily on detailed descriptions of the parts that make up a whole.

In Cal Rodó, assessment of sediment load and sediment yield are subjected to error sources, which might be instrumental (malfunction, drift), sampling, sample processing, and computing errors. While using sediment rating curves these errors were assessed as a whole, and results were compared with estimates obtained from linear interpolation of discrete samples and calibration of an optical infra-red backscattering and ultrasound beam attenuation sediment sensors. Uncertainties of sediment load (event scale) and sediment yield (a set of events) were assessed by simulating the probability distribution function of sediment load by using Monte-Carlo approaches. The role of major events in sediment transport was evaluated and their influence on total uncertainties.

In the Upper Llobregat basin two semiquantitative models and empirical approaches were applied, they do not necessarily require a high data resolution in terms of time and space, as compared to more physically approaches. The two semi-quantitative models were the Factorial Scoring Model and the Pacific Southwest Interagency Committee, which use a scoring system for a given set of basin characteristics and relate them to sediment yield. Also the Revised Universal Soil Loss Equation (RUSLE) was applied in order to evaluate its performance in a forested rangeland with highly complex topography, the outcomes were benchmarked against sediment yield obtained from an existing reservoir bathymetry survey. RUSLE has been widely used at different spatial scales but outcomes generally are not compared with measured values (e.g. bathymetry surveys), and uncertainty assessment of sediment yield estimated by using a combined RUSLE-sediment delivery ratios was done. In this thesis, not only RUSLE performance was evaluated but uncertainty of the outcome sediment yield and insights into erosion rates under Global Change were provided.

In addition, for each of the RUSLE's input factors a sensitivity analysis on soil erosion was performed, this has given an insight into the magnitude of sensitivity of soil erosion to a given change in the input factors. The uncertainty of benchmark data (sediment yield from bathymetry survey) were also assessed, so fair comparison of results can be done.

Because the magnitude of soil erosion is dependent on many factors, which are dynamic the prediction ability of erosion models is limited especially at large areas. Nevertheless, despite their limitations, these models provide some insights into the relevant areas and factors influencing erosion.

8.2.2 Quality of data

In Cal Rodó, suspended sediment concentration was obtained from a dataset of turbidity records (1996-2005), after a scrutiny of the quality of data, regarding the validity of discrete samples and turbidity records, 27 of the biggest (80th percentile) storm episodes were selected. The quality of turbidity records and distribution of samples on the hydrograph in most cases had shortcomings. Discrete samples were mostly collected during the rising limb of the hydrograph, on the other hand, turbidity sensor readings in some cases were incorrect since they became clogged with debris or the sensor's ability to measure concentration was exceeded. Nevertheless, having data obtained with diverse instruments and techniques allowed a cross-checking of the quality of concentration data.

In the Upper Llobregat basin, the quality of the data used as input factors of RUSLE model were varied. Rainfall erosivity factor data is the one with the best quality (low temporal resolution and 14 years record), despite the fact that sub-hourly data was only available from one station, the remaining seven stations had daily rainfall. The distance among weather stations is relatively small (4 to 15 km). The number of soil samples collected for each of the seven geological units of the basin was 4 or more, in cases where information already existed, has allowed to calculate the variance of the mean values (of soil properties), however, it is clear that the number of samples is still low considering the size of the basin. The DEM resolution (20 m) was not enough to reflect terraced areas, therefore, these areas have been accounted for in a separate manner and then integrated into the LS factor image obtained for non-terraced areas. Yet, existing algorithms are not designed to cope with terraced topographies. C factor values were obtained by averaging C factor values from published sources, thus, the error of the mean was calculated, since the study area is forest and pasture, and considering that land cover in recent years has not changed significantly (and intrannual variability is relatively low) the average C factor can be considered a good approximation.

8.2.3 Working scale

At Cal Rodó catchment the climate, soil type, geology, topography, and land cover are much less diverse that at the Upper Llobregat basin. The measured data such as discharge and sediment are fairly known and they have been monitored since the 1990's. Although sediment yielded at this scale has been studied and the knowledge of its dynamics is extensive, the understanding of the mechanisms of how these nested areas are connected to larger areas is not fully understood. According to the findings of this work, the sediment transport is seemingly site specific, the role of sediment deposition-redeposition, and distribution-redistribution along the landscape needs further research.

The estimated sediment yield at Cal Rodó suggests that sediment transport is a time concentrated process since it is produced by a few major pluvial events. Sediment yield at this scale is similar ($\approx$3.49 Mg $ha^{-1}yr^{-1}$) to the one estimated at the Upper Llobregat basin using RUSLE-sediment delivery ratio ($\approx$3.12 Mg $ha^{-1}yr^{-1}$); however, the value in the latter includes only interrill and rill erosion, and the former includes all types of erosion; therefore, this comparison is only to give an insight to the magnitude of erosion at both scales. Seemingly the agradations and degradation processes at both scales are different.

8.2.4 Reservoir sedimentation and sediment yield from river basin

Sediment yield assessment at the outlet of a basin determines the amount of sediment that leaves a basin for over a period of time. It involves erosion processes, sediment deposition and delivery to the mouth of the basin. Sediment yield from a basin can be estimated from sediment deposited in a reservoir after correction of trap efficiency is done. In 2002 the *Centro de Estudios y Experimentación de Obras Públicas* (CEDEX) conducted a bathymetry survey in La Baells Reservoir, which results were used to evaluate the performance of the erosion models studied.

Uncertainty assessment of sediment yield estimated by CEDEX (2002) was done following a stochastic approach, by using the reported measurement error and errors related to bulk density and trap efficiency. The confidence interval of the mean sediment yield (4.54 Mg $ha^{-1}yr^{-1}$) was very narrow (between 4.29 and 4.79 Mg $ha^{-1}yr^{-1}$), this might have been larger if a whole range of error sources were included.

La Baells Reservoir was impounded in 1976, when land cover was still changing mainly from agriculture to forest, until it stabilized in the 1990's, when soil erosion from upstream has seemingly shown a decreasing trend, in the future, sediment yield values will rely on land cover changes due to climate change.

8.2.5 Results

The first stage of this work comprised a short review of soil erosion studies and approaches, it was shown that erosion modelling has gained valuable experience, especially, at the plot and hillslope scales, but some understanding at the basin scale is also significant. Connectivity and integration issues between different spatial and temporal scales remains a challenge.

The second stage of the study served as a basis to characterize the uncertainties of sediment rating curves in a mountain event based streams. The uncertainties of annual and seasonal power rating curves were very wide compared to the ones of reference methods, such as integration of discrete sampling and calibration of turbidity sensors.

Several attempts to fully account for uncertainties were made. First, whilst estimating the confidence interval of sediment yield through Monte Carlo simulation the error term of the regression (rating curve) by considering only one error term (errors due to events and samples within each event) the confidence interval of sediment yield was larger than when splitting the error term in two: errors between episodes, and errors of samples within events. In the second attempt, the F test analysis has shown that errors due to events and samples within events should be considered separately and accounted for separately when Monte Carlo simulations are performed, because the existing few major episodes overshadowed the effects of many small episodes, thus, the errors had to be split.

The third stage of the study involved the use of basin characteristic's approaches to estimate sediment yield. First, a existing relationship between sediment yield and drainage area, and especifically developed for Spanish basins was applied to the Upper Llobregat Basin, the outcome sediment yield was 31% less than the yield estimated from bathymetry survey. Second, two existing semi-quantitative approaches and adjusted to the Spanish conditions were applied, these were the Factorial Scoring Model and Pacific Southwest Interagency Committee, results showed that the former overestimated the sediment yield by a factor of 1.4 and the latter underestimated by a

factor of 4.2 when compared to bathymetry results. The advantage of using these approaches are that the required data is easy to gather and they require less computing time than other methods, and can be useful to have an idea of the erosion rates before other data intensive models are applied.

The fourth stage of the study, consisted of an application of the Revised Universal Soil Loss Equation (RUSLE) to a relatively large basin, characterized of being mostly forest and having high relief, there are many studies of this type, but the uncertainty of outcomes are rarely evaluated. In this study an assessment of uncertainties of soil erosion values was performed, the result is that the distribution of soil erosion values is very assymetric towards the upper limit and it is very wide. In addition, sensitivity analyses of errors in input factors on soil erosion uncertainty was made, soil erosion is most sensitive to slope lenght and slope steepness factor (LS factor) and land cover management factor (C factor). The simplicity of RUSLE model, its black-box characteristic makes it easily applicable, however, from the scientific perspective it has limitations if it is compared with physics-based models.

Furthermore, sediment yield was estimated by multiplying the gross soil erosion estimated with RUSLE by an average sediment delivery ratio, the estimated average sediment yield was 26% less than the value estimated from a bathymetry survey; though the confidence interval of sediment yield was very large.

The fifth stage of this thesis comprised an assessment of the likely effects of Global Change on soil erosion by the end of the 21st century. The two RUSLE's factors that are most likely are going to change their values significantly are the rainfall erosivity and land cover factor (R and C factors respectively). For each of these two factors, a few independent scenarios were studied. First, for rainfall it was considered (a) a decrease of rainfall depth during summer (-10%) and slight increase of it during winter (+5%), the outcome soil erosion was 13.7% less than the current soil erosion estimated by RUSLE, (b) an leghtening of summer conditions (17 days at the beginning and at the end of summer) which meant a change of current rainfall depth, the outcome soil erosion was only 2.4% less than the current estimate, and (c) a combination of the previous two scenarios was made, the outcome soil erosion was 7.4% less than the current value.

Similarly, a few scenarios for land cover factor (C factor) were studied. These were: (a) an increase of forest area from the current 46.2% to 77% (determined by assuming all current grassland areas below 1700 m a.s.l. will become forest), the outcome soil erosion is 26.3% less than the current value estimated by RUSLE, (b) a shift of agricultural areas as of 1957, when agricultural areas were significant, the resulting soil erosion value was an increase of 160% in relation to the current value, and (c) increase of occurrence of forest fires, burning 1.4% and 2.3% of basin's area will represent increases on soil erosion of 4.6% and 21.5% in relation to the current estimate.

8.3 Conclusions

Dynamics and uncertainty assessment of sediment yield at two different scales in the Upper Llobregat Basin have been studied. The approaches and methods used to attain the aims of this study were varied within scales. The following general conclusions can be drawn from the study (detailed conclusions are provided within each Chapter):

8.3.1 Small gauged catchment scale

The uncertainty of the average sediment load was large for events where there were no good spanning of samples on the hydrograph, and when there were no reliable sensor readings for the whole or part of the range of discharge.

A few major events deliver most of the sediment transported during the studied period.

Calibration of infra-red backscattering and ultrasound beam attenuation sensors for a broad range of particle sizes in the study area is necessary, and need to be verified periodically, since they provided faulty readings particularly during large discharge events when mobilisation or re-mobilisation of particle of diverse size occurs.

The confidence intervals of sediment load (event scale) and sediment yield (long-term scale) assessed by Monte Carlo approaches by modelling the distribution function of sediment load obtained from rating curves are 5 and 6 -seasonal and annual respectively- times larger than the intervals obtained from calibration of turbidity sensors. The intervals assessed by Monte Carlo simulations include the intervals estimated from sensor calibrations.

Developing sediment rating curves for events occured during summer and rest of the seasons, and for each limb of the hydrograph, have reduced the wideness of the confidence intervals of sediment load and sediment yield, even though it was not significant.

In event based streams the relationship discharge-suspended sediment concentration is varied (large scattering), therefore, the role of the size of events becomes important when sediment rating curves are developed, since the structure of residuals is modified (high heteroscedasticity for large discharge values).

The use of Monte Carlo approaches to estimate sediment load, allows avoiding the bias correction from the logarithmic to arithmetic scales, since it is based on simulation of large number of sediment load drawn from their deterministic probability distribution function.

A good quality of input data (discrete samples and discharge) in terms of number and distribution along the hydrograph is important to develop reliable sediment rating curves.

Taking into account the whole set of events (annual basis) it was found that peak of discharge and total kinetic energy are good predictors of sediment load. For the rest of seasons dataset, peak of discharge and runoff explain most of the variability in sediment load. Hydrological variables can be used to obtain a first assessment of the magnitude of sediment load and sediment yield before other complex models are used.

8.3.2 Large ungauged river basin scale

8.3.2.1 Sediment yield derived from basin characteristics

Factorial Scoring Model (FSM), Pacific Southwest Interagency Committee (PSIAC) and a regression between sediment yield and basin area were used to estimate the sediment yield in the Upper Llobregat basin. PSIAC and the regression sediment yield - area, underestimated the sediment yield, on the other hand, FSM overestimated the sediment yield.

Despite the under or overestimations, and the subjectivity involved while assigning scores to basin characteristics, FSM and PSIAC can be still be used as reference or as one of the first assessments of sediment yield.

8.3.2.2 Sediment yield by using RUSLE

The variability of rainfall erosivity factor (R factor) presents a large inter-annual and spatial variability, this is due to the unequal distribution of rainfall in the basin (commonly the east receives more rainfall), and because of the high intensity of summer rainy days. The effects of R factor on the uncertainty of soil erosion assessment is narrow, since the standard errors of this factor are relatively small compared to the mean value.

The effects of slope length and steepness factor (LS factor) and land cover management factor (C factor) are the main drivers of the total uncertainty in soil erosion, since their standard deviations are proportionally larger in relation to their mean values.

The spatial distribution of soil erosion seems to be associated with steep slopes and bare soft rocks or agricultural areas. Thus, most of erodible soil account for small localized areas ($\approx$ 5% of the basin), this was expected since the study area is mostly forested.

The distribution of each image factor is assumed to have a normal distribution, but the soil erosion map and sediment yield values follow a Gamma distribution. The distribution instability at the extremes is considerable large and tends to shift the upper bound of the confidence interval to the right. The wide range of the uncertainty associated with the prediction of soil erosion (90% confidence interval) is an indication of the complex relationships among the input factors.

The yield obtained by bathymetry survey (CEDEX, 2002) is similar to the mean and well within the 90% confidence interval defined for the combined RUSLE-sediment delivery ratio.

8.3.2.3 Soil erosion scenarios under Global Change

The RUSLE model was applied to estimate soil loss in the headwaters of Llobregat River under several rainfall and land cover scenarios, which were elaborated based on predicted climate conditions. Three likely scenarios for R factor, and three for C factor were performed independently for the end of 21st century, assuming that, the effects of predicted climate conditions on soil erosion will lay predominantly on those two factors. The outcomes were wide-ranging, depending on the R and C factor input values.

A decrease (10%) in rainfall amount during summer and increase (5%) during winter (according to GCM and RCM's) might reduce the current soil loss by -7.4%, this is due to the larger number of summer events which rainfall depths were decreased, therefore their intensities were weakened, and the rainfall depth increase in winter is not enough to compensate reductions of summer events. On the other hand, ocurrence of a longer summer conditions (larger than the astronomical summer) might increase current soil erosion in 4.8%.

The predominant land cover type is forest and there is evidence that warmer conditions will cause uphill migration of forest; therefore, a scenario was examined by increasing the forestland at the expense of pasture and agricultural areas. The increase of forested areas produced a significant

decrease in soil loss, because of lower C factor values for forest than for pastures and agriculture.

Re-conversion of land cover from the currently forested areas into agriculture (as of 1957) might increase soil erosion in about three times the current erosion rates, as a result of the higher land cover management factor values for agricultural areas than for forested areas. This result also gives insight to what the erosion rates might have been in the 1950's.

Ocurrence of forest fires might increase soil erosion rates, small burned areas increase significantly erosion rates, it was found that 1.4% and 2.3% can produce significant increases up to 30% and 48% respectively compared to current sediment yield rates.

Overall, global change impact on soil loss and according to most of the examined scenarios shows an increase in erosion rates, soil loss appears to be more sensitive to LS and C factors, considering that the latter factor can be directly modified by human activity which adds uncertainty to climate change predictions.

8.4 Suggestions for further research

More research is necessary to better understand soil erosion and sediment yield in the study area, especially verification of confidence intervals of sediment yield and sediment sources.

8.4.1 Cal Rodó

The large uncertainties of sediment load computed from sediment rating curves, both at flood event and set of events, can be validated by ensuring collection of suspended sediment samples that span the entire streamflow, particularly during events having moderate and high water discharges, since they transport most of the sediment. Automatic samplers are great asset, but they have limitations in terms of collected number of samples, flood events lasts from a few hours up to over a day, although the device is preset in function of discharge, during episodes of long duration samples are collected on the rising limb of the hydrograph, so there is the issue of compromising the number of samples between short and long duration events. The recent setting of stage samplers (siphon samplers) may help to address this issue. However, replacement of bottles is required particularly during episodes of long duration. Manual collection of samples can be also helpful during long events.

8.4.2 Upper Llobregat Basin

RUSLE model has allowed identifying the highly erodible surfaces within the basin; these are located in the center of the basin, where badlands are the main sediment sources; high erodible area also exist in the N part of the basin (over 1800 m a.s.l.) where land cover is pasture and erosion might be associated to its patchiness. A future work can be conducting field work in order to verify the extent to which these are important as sediment sources, especially in the Northern area, since exhaustive verification has not be done in these areas. Georeferenced aerial photographs overlaid to the obtained soil erosion map, can be used to check in more detail with smaller grid cell sizes to validate the values predicted by RUSLE. The overall results will provide more insights

into the model performance in those hotspots.

Additional information from badland and other soft rock areas, such as: size, degree of activity can be estimated and used to estimate the sediment yield from these areas. A previous study of sediment production from a badland using the KINEROS2 model (Smith *et al.*, 1995) in Cal Isard exist (Martínez-Carreras *et al.*, 2007), which combined with additional determination of yield from other badlands in the basin can be used to simulate the yield from these areas.

Additional approaches can be used in the Upper Llobregat basin in order to verify the erosion rates or identify other potential sediment sources, such as the sediment budgets, which are mass balances in which the difference between inputs and outputs of sediment must equal any changes in storage. Tracer techniques, such as the 137 Cs Walling & Quine (1991) by collecting soil core samples at subcatchment level, and laboratory measurement of 137 Cs using a standard gamma-spectrometry as described by Murray, et al. 1987, results can be compared with reference values (samples collected at sites without or little disturbance).

Assessment of sediment produced by gully erosion and mass movement should be made, in order to add to the quantity of soil erosion estimated through RUSLE, so total erosion can be determined, which then can be used to determine the sediment delivery ratio by using bathymetry survey results from La Baells Reservoir. This would be useful in order to validate the value of delivery ratio used in this thesis, which was derived by using characteristics of the basin within equations developed for other regions, the value in mention is low considering that highly erosible areas, such as badlands, are well connected to streams.

Bibliography

Abanades, J. C., Cuadrat, J. M., De Castro, M., Fernández, G., Gallastegui, C., Garrote, L., Jiménez, L. M., Juliá, R., Losada, I., Monzón, A., Moreno, J. M., Pérez, J. I., Ruiz, V., Sanz, M. J., & Vallejo, R. 2007. *El Cambio Climático en España. Estado de situación. Documento Resumen.* Tech. rept. Ministry of Rural Affairs and Environment. Madrid.

Abbott, M.B., Bathurst, J.C., Cunge, J.A., O'Connell, P.E., & Rasmussen, J. 1986. An introduction to the European Hydrological System - Système Hydrologique Européen, 'SHE'. 1: history and philosophy of a physically-based, distributed modelling system. *Journal of Hydrology*, **87**, 45–59.

Admiraal, D.A., & Garcia, M. H. 2000. Laboratory measurement of suspended sediment concentration using an Acoustic Concentration Profiler (ACP). *Experiments in fluids*, **28**, 116–127.

Aksoy, H., & Kavvas, M.L. 2005. A review of hillslope and watershed scale erosion and sediment transport models. *Catena*, **64**, 247–271.

Alcamo, J., Grassl, H., Hoff, H., Kabat, P., Lansigan, F., Lawford, R., Lettenmaier, D., Lévêque, C., Meybeck, M., Naiman, R., Pahl-Wostl, C., & V'or'osmarty, C. 2005. *The Global Water System Project: Science Framework and Implementation Activities. ESSP Report No. 3. Earth System Science Partnership.* Tech. rept. Earth System Science Partnership, Stockholm.

Alexeev, V.A. 2007. Some features of Climate Change on Earth and its possible relation to solar-activity variations. *Solar System Research*, **41 (6)**, 527–534.

Allen, R.G., Dickey, G., Wright, J.L., Stone, J.F., & Hunsaker, D.J. 1993. *Workshop ASCE Irrigation and Drainage Division. Management of Irrigation and Drainage Systems: Integrated perspectives.* American Society of Civil Engineers. Chap. Error analysis of bulk density measurements for neutron moisture gauge calibration, pages 1121–1126.

Almendros, G., Gonzales-Vila, F.J., & Martin, F. 1990. Fire-induced transformation of soil organic matter from and oak forest: and experimental approach to the effects of fire on humic substances. *Soil Sciences*, **149**, 158–168.

Alpert, P., Ben-gai, T., Baharad, A., Benjamini, Y., Yekutieli, D., Colacino, M., Diodato, L., Ramis, C., Homar, V., Romero, R., Michaelides, S., & Manes, A. 2002. The paradoxical increase of Mediterranean extreme daily rainfall in spite of decrease in total values. *Geophysical Research Letters*, **29(11)**, 31–1 – 31–4.

Angima, S.D., Stott, D.E, O'Neil, l M.K., Ong, C.K., & Weesies, G.A. 2003. Soil erosion prediction using RUSLE for central Kenyan highland conditions. *Agriculture, Ecosystems and Environment*, **97**, 295–308.

Asselman, N.E.M. 2000. Fitting and interpretation of sediment rating curves. *Hydrology*, **234**, 228–248.

Avendaño, C., Sanz, E., Rayá, C., & Gómez, J.L. 1997. Sediment yield at Spanish reservoirs and its relationship with the drainage basin area. *Pages 863–874 of: Proceedings of the 19th Symposium of Large Dams, Florence. ICOLD (International Committee on Large Dams).*

Ballantine, D.J., Walling, D.E., Collins, A.L., & Leeks, G.J.L. 2008. The phosphorus content of fluvial suspended sediment in three lowland groundwater-dominated catchments. *Journal of Hydrology*, **357(1-2)**, 140–151.

Bates, B., Kundzewicz, Z.W., Wu, S., & Palutikof, J.P. 2008a. *Climate Change and Water.* Tech. rept. IPCC (Intergovernmental Panel on Climate Change), UNEP, Geneva.

Bates, B.C., Kundzewicz, Z.W., Wu, S., & Palutikof, J.P. 2008b. *Climate change and water. Technical Paper of the Intergovernmental Panel on Climate Change.* Tech. rept. IPCC Secretariat, Geneva.

Beasley, D.B., Huggins, L.F., & Monk, E.J. 1980. ANSWERS: A model for watershed planning. *Trans., Am. Soc. Agric. Engrs.*, **23**, 938–944.

Becher, H.H. 1988. *Impact of water and external focerces on soil structure.* Catena suplement 11. Chap. soil erosion and soil structure, pages 15–20.

Bennett, J. P., & Sabol, G. V. 1973. Investigation of sediment transport curves constructed using periodic and aperiodic samples. *Pages B5–1 to B5–12 of: International Association for Hydraulic Research - International Symposium on River Mechanics.*

Berndtsson, R., Hogland, W., & Larsson, M. 1985. *Hydrological Studies in Tunisia.* Chap. Spatial variations of infiltration for a catchment in Northern Tunisia, pages 13–26.

Biesemans, J., Van-Meirvenne, M., & Gabriels, D. 2000. Extending the RUSLE with the Monte Carlo error propagation technique to predict long-term average off-site sediment accumulation. *Journal of Soil and Water Conservation*, **55**, 35–42.

Birkinshaw, S.J.; Bathurst, J.C. 2006. Model study of the relationship between sediment yield and river basin area. *Earth Surface Processes and Landforms*, **31**, 750 – 761.

Black, K. P., & Rosenberg, M. A. 1994. Suspended sand measurements in a turbulent environment: field comparison of optical and pump sampling techniques. *Coastal Engineering*, **24**, 137–150.

Blöschl, G., & Sivapalan, M. 1995. Scale issues in hydrological modelling: A review. *Hydrological Processes*, **9**, 251–290.

Boardman, J., & Favis-Mortlock, D. 1998. *Modelling soil erosion by water.* NATO ASI Series 1: Global Environmental Change, vol. 55. Berlin: Springer.

Boardman, J., & Poesen, J. 2006. *Soil erosion in Europe.* John Wiley and Sons, Ltd. Chap. Soil erosion in Europe: Major processes, causes and consequences, pages 480–487.

Brunetti, M., Maugeri, M., & T., Nanni. 2002. Atmospheric circulation and precipitation in Italy for the last 50 years. *International Journal of Climatology*, **22**, 1455–1471.

Brunsden, D. 1993. *Landscape Sensitivity.* Wiley, Chichester. Chap. Barriers to geomorphological change, pages 7–12.

Bryan, R.B. 1987. Processes and significance of rill development. *Catena supplement*, **8**, 1–15.

Bube, K. P., & Trimble, S. W. 1986. Revision of the Churchill reservoir trap efficiency curves using smoothing splines. *Water Resources Bulletin*, **22**, 305–309.

Butcher, D.P., Labadz, J.C., Potter, A.W.R., & White, A.P. 1993. *Geomorphology and Sedimentology of Lakes and Reservoir*. John Wiley and sons. Chap. Reservoir sedimentation rates in the southern Pennine region, UK, pages 73–92.

Calbo, J. 2008. *Aigua i canvi climatic diagnosi dels impactes previstos a Catalunya*. Chap. Projeccions globals: el cuarto informe de IPCC.

Cammeraat, E. L.H., van de Lockant, A., Rubio, J.L., Andreu, V., & Spanos, I. 2006. Changes in topsoil properties after forest fires studied by thin section analysis. *Geophysical Research Abstracts, European Geosciences Union*, **8**.

Cammeraat, E.L.H. 2004. Scale dependent thresholds in hydrological and erosion response of a semi-arid catchment in Southeast Spain. *Agriculture, Ecosystems and Environment*, **104**, 317–332.

Carreras, J., Carrillo, E., Masalles, R.M., Ninot, J.M., Soriano, I., & Vigo, J. 1994. *Land cover map of Catalonia scale 1:50.000 sheet 255*. Catalan Institute of Cartography, Barcelona.

CartaLinx Clark Labs, Clark University. 2001. *CartaLinx*. USA.

Catalan-Government. 2008. *Database of forest fires since 1968*. Tech. rept. Department of Environment and Housing, Barcelona.

Catari, G. 2007. *Uncertainties behind suspended sediment load estimations in a headwater catchment in the Southern Pyrenees.* Thesis research work, Autonomous University of Barcelona, Barcelona.

CEDEX, Centro de Estudios y Experimentación de Obras Públicas, Centro de Estudios Hidrográficos. 2002. *Reconocimientos sedimentológicos de embalses*. Tech. rept. Ministerio de Fomento.

Cerdan, O., Poesen, J., Govers, G., Saby, N., Le Bissonnais, Y., Gobin, A., Vacca, A., Quinton, J., Auerswald, K., Klik, A., Kwaad, F.F.P.M., & Roxo, M.J. 2006. *Soil erosion in Europe*. John Wiley and Sons, Ltd. Chap. Sheet and rill erosion, pages 501–513.

Chang, T. J., Bayes, T. D., & McKeever, S. 2003. Investigating reservoir sediment and watershed erosion using a geographical information system. *Hydrological processes*, **17**, 979–987.

Chappel, N. A. 2000. Stream discharge measurement - Environmental Science: case study 16. University of Lancaster, Lancaster.

Charlton, R. 2007. *Fundamentals of Fluvial Geomorphology*. London: Taylor and Francis Ltd.

Christakos, G. 1992. *Random field models in Earth Sciences*. Sand Diego: Academic Press Inc.

Christensen, J. H. 2005. *Prediction of regional scenarios and uncertainties for defining european climate change risks and effects, Prudence final report*. Tech. rept. Copenhagen.

Christensen, J.H., Hewitson, B., Busuioc, A., Chen, A., Gao, X., Held, I., Jones, R., Koll, R.K., Kwon, W.T., Laprise, R., Magana, V., Mearns, L., Menendez, C.G., R'ais'anen, J., Rinke, A., Sarr, A., & Whetton, P. 2007. *A: Climate Change 2007. The Physical Science Basis. Contribution*

of Working Group I to the Fourth Assessment Report of the Intergovernmental Panel on Climate Change. Cambridge University Press, Cambridge, United Kingdom and New York, NY, USA. Chap. Regional Climate Projections., pages 849–926.

Clotet, N. 1984. La Conca de la Baells (Alt Llobregat): Els processos geomorfológics actuals responsables del subministrament de sólids i balanc previ de sediments. *Acta Geológica Hispánica*, **19 (3)**, 177–191.

Clotet, N., & Gallart, F. 1986. Sediment yield in a mountainous basin under high mediterranean climate. *Z. Geomorph. N.F.*, **60**, 205–216.

Clotet, N., Gallart, F., & Calvet, J. 1983. Estudio del impacto en la dinámica del medio físico de las explotaciones de lignito a cielo abierto en el valle del torrente de Vallcebre-Alto Llobregat. *Pages 3.19–3.37 of: Actas de la segunda reunión del Grupo Español de Geología Ambiental y Ordenación del Territorio.*

Clotet, N., Gallart, F., & Balasch, J.C. 1988. Medium term erosion rates in a small scarcely vegetated catchment in the Pyrenees. *Geomorphic processes: Catena Supplement 13*, **2**, 37–47.

Conacher, A., & Sala, M. 1998. *Land degradation in Mediterranean environments of the world: nature and extent, casues and solutions.* Wiley, Chichester.

Conner, C. S., & de Visser, A. M. 1992. A laboratory investigation of particle size effects on an optical backscatterance sensor. *Marine Geology.*, **10**, 151–159.

Cox, C., & Madramootoo, C. 1998. Application of geographic information systems in watershed management planning in St. Lucia. *Computers and Electronics in Agriculture*, **20**, 229–250.

Crawford, CG. 1991. Estimation of suspended-sediment rating curves and mean suspended-sediment loads. *Hydrology*, **191**, 331–348.

CREAF. 2002. *Land Cover Map of Catalonia.* Barcelona: CREAF (Centre de Recerca Ecolgica i Aplicacions Forestals), 2002. 1ed.

Crowder, B. M. 1987. The economic cost of reservoir sedimentation: a regional approach to estimating cropland erosion damages. *Soil and Water Conservation*, **42**, 194–197.

Crowder, DW., Demissie, M., & Markus, M. 2007. The accuracy of sediment loads when log-transformation produces nonlinear sediment load-discharge relationships. *Hydrology*, **336**, 250–268.

D&A Instruments, Company. 1991. *Suspended solids & turbidity monitor: instruction manual OBS-1-3.* Logan, UT.

D&A Instruments, Company. 2005. *Suspended solids & turbidity monitor: instruction manual OBS-1-4.* Logan, UT.

Daignieres, M., Gallart, E., Banda, E., & Hirn, A. 1981. Implications of the seismic structure for the orogenic evolution of the Pyrenean Range. *Earth and Planetary Science Letters*, **57**, 88–100.

Day, P.R. 1965. *Methods of soil analysis.* American Society of Agronomy. Chap. Particle fractionation and particle size analysis, pages 545–567.

de Bano, L.F. 1971. The effect of hydrophobic substances on water movement in soil during infiltration. *Soil Sci. Soc. Amer. Proc.*, **35**, 340–343.

de Jong, S.M., Paracchin, M.L., Bertolo, F., Folving, S., Megier, J., & de Roo, P.J. 1999. Regional assessment of soil erosion using the distributed model SEMMED and remotely sensed data. *Catena*, **37**, 291–308.

de Vente, J., & Poesen, J. 2005. Predicting soil erosion and sediment yield at the basin scale. Scale issues and semiquantitative models. *Earth-Science Reviews*, **71**, 95–125.

de Vente, J., Poesen, J., Bazzoffi, P., Van Rompaey, A., & Verstraeten, G. 2006. Predicting catchment sediment yield in Mediterranean environments: the importance of sediment sources and connectivity in Italian drainage basins. *Earth Surface Processes and Landforms*, **31**, 1017–1034.

de Vente, J., Poesen, J., Arabkhedri, M., & Verstraeten, G. 2007. The sediment delivery problem revisited. *Progress in Physical Geography*, **31(2)**, 155–178.

Dedkov, A.P., & Gusarov, A.V. 2006. *Sediment dynamics and the morphology of fluvial systems*. IAHS Publication, vol. 396. Wallingford: IAHS Press. Chap. Suspended sediment yield from continents into the World Ocean: Spatial and temporal changeability, page 311.

Delgado, J.M. 2006. *Análisis de series hidrológicas y climáticas para su aplicació en el estudio de los efectos del cambio de uso del suelo sobre el balance hídrico en la cabecera del Llobregat*. M.Sc. thesis, Autonomous University of Barcelona, Barcelona.

Delgado, J.M. In preparation. *Efecto de la variabilidad climática y de los cambios de uso del suelo sobre el balance hidrológico en la cabecera del Llobregat*. Ph.D. thesis, Autonomous University of Barcelona, Barcelona.

Desmet, P.J.J., & Govers, G. 1996. A GIS procedure for automatically calculating the USLE LS factor on topographically complex landscape units. *Journal of Soil and Water Conservation*, **51**, 427–433.

Douglas, I. 1999. Hydrological investigations of forest disturbance and land cover impacts in South-East Asia: a review. *Phil. Trans.R.Soc. Lond. B.*, **354**, 1725–1738.

Drake, B.E. 2005. *Estimating increased erosion and sediment delivery caused by wildfires*. Tech. rept. University of Texas, Texas.

Duan, N. 1983. Smearing estimate: a non-parametric retransformation method. *American Statistical Society*, **78**, 605–610.

Eastman, J. R. 2003. *IDRISI Kilimanjaro: Guide to GIS and Image Processing*. Clark Labs - Clark University, 950 Main Street Worcester, MA.

EEA, European Environment Agency. 2004. *Impacts of Europe changing climate, an indicator based assessment*. Tech. rept. Office for Official Publications of the European Communities, Luxembourg.

EEA, European Environment Agency. 2006. *Land accounts for Europe 1990 - 2000: Towards intergrated land and ecosystem accounting*. Tech. rept. 11. European Environmental Agency, Copenhagen.

EEA, European Environmental Agency. 2008. *Impacts of Europe's changing climate - 2008 indicator-based assessment*. Tech. rept. European Environmental Agency, Copenhagen.

Elliot, W.J. 1995a. *Precipitation. In: Environmental Hydrology.* Boca Raton, FL: CRC Lewis Publishers. Chap. 2, pages 19–49.

Elliot, W.J. 1995b. *Soil erosion and control practices. In: Environmental Hydrology.* Boca Raton, FL: CRC Lewis Publishers. Chap. 6, pages 177–204.

Ellison, W.D., & Ellison, O.T. 1947. Soil erosion studies - Part VI: Soil detachment by surface flow. *28*, **Agric. Eng.**, 402–408.

Evans, B. 2006a. *Soil Erosion in Europe.* John Wiley and Sons Ltd. Chap. Erosion of Uncultivated Land, pages 623–641.

Evans, R. 2006b. *Soil erosion and sediment redistribution in River Catchments.* CAB International. Chap. Land use, sediment delivery and sediment yield in England and Wales, pages 70–84.

Ewen, J., Parkin, G., & O'Connell, P.E. 2000. SHETRAN: a coupled surface/subsurface modelling system for 3D water flow and sediment and solvent transport in river basins. *ASCE Journal of Hydrologic Engineering*, **5**, 250–258.

Falk, M.G., Denham, R.J., & Mengersen, K.L. in press. Estimating Uncertainty in the Revised Universal Soil Loss Equation via Bayesian Melding. *Journal of Agricultural, Biological and Environmental Statistics.*

FAO. 1997. *Guidelines for mapping and measurement of rainfall induced erosion processes in the Mediterranean coastal areas. Priority actions programme regional activity.* FAO, Split.

Favis-Mortlock, D.T., & Boardman, J. 1995. Nonlinear responses of soil erosion to climate change: a modelling study on the UK South Downs. *Catena*, **25**, 365–387.

Ferguson, RI. 1986. River loads underestimated by rating curves. *Water Resources Research*, **22**, 74–76.

Foster, G.R. 2004. *Revised Universal Soil Loss Equation Version 2. User reference guide.* USDA Natural Resources Conservation Service, Tennessee.

Foster, G.R., Renard, K.G., Yoder, D., McCool, D.K., & Weesies, G. A. *RUSLE Documentation Manual version 1.06, 1997.* USDA ARS.

Francke, T., Batalla, R., Mamede, G., & Mueller, E.N. 2007. Suspended-sediment fluxes at the hillslope and catchment scale during a season of monitoring erosion hot spots in the Isábena catchment (Central Spanish Pyrenees). *Geophysical Research*, **9**.

Gallart, F. 2006. *BASIC syntax to estimate Suspended Sediment Load confidence bounds.* Tech. rept. Institute of Earth Sciences Jaume Almera. CSIC. Spain.

Gallart, F., Llorens, P., Latron, J., & Regües, D. 2002. Hydrological processes and their seasonal controls in a small Mediterranean mountain catchment in the Pyrenees. *Hydrology and Earth System Sciences*, **6 (3)**, 527–537.

Gallart, F., Balasch, J.C., Regüés, D., Soler, M., & Castelltort, X. 2005. *Catchment Dynamics and River Processes: Mediterranean and other Climate Regions.* Elsevier B.V. Chap. Catchment dynamics in a Mediterranean mountain environment: the Vallcebre research basins (Southeastern Pyrenees) II: temporal and spatial dynamics of erosion and stream sediment transport, pages 17–24.

Gallart, F., Llorens P., & Latron, J. 1994. Studying the role of old agricultural terraces on runoff generation in a small Mediterranean mountainous basin. *Journal of Hydrology*, **159**, 291–303.

Gallego, M.C., Garcia, J.A., & Vaquero, J.M. 2005. The NAO signal in daily rainfall series over the Iberian Peninsula. *Climate Research*, **29**, 103–109.

Garcia-Ruiz, J.M., & Lasanta, T. 1990. Land-use changes in the Spanish Pyrenees. *Mountain Research and Development*, **10 (3)**, 267–279.

Garcia-Ruiz, J.M., Lasanta, T., Marti, C., Gonzáles, C., White, S., Ortigosa, L., & Ruiz, P. 1995. Changes in runoff and erosion as a consequence of land-use changes in the Central Spanish Pyrenees. *Phys. Chem. Earth*, **20**(3-4), 301–307.

Garcia-Ruiz, J.M., Lasanta, T., Ruiz-Flano, P., Ortigosa, L., White, S., Gonzáles, C., & Marti, C. 1996. Land-use changes and sustainable development in mountain areas: a case study in the Spanish Pyrenees. *Landscape Ecology*, **1 (5)**, 267–277.

Garde, R.J., & Kathyari, U.C. 1990. Erosion prediction models for large catchments. *Pages 89–102. of: Proceedings of the International Symposium on Water Erosion, Sedimentation, and Resource Conservation.*

GaSWCC, Georgia Soil & Water Conservation Commission. 2000. *Manual for erosion and sediment control in Georgia.* 5th ed. edn. State Soil and Water Conservation Commission, Georgia. Appendix B-2. p.13.

Gee, P.A., & Bauder, J.W. 1986. *Methods of Soil Analysis. Part I.* American Society of Agronomy. Chap. Particle size analysis, pages 383–411.

Geeson, N.A., Brandt C.J., & Thornes, J.B. 2002. *Mediterranean desertification: a mosaic of processes and responses.* London: Wiley: Chichester.

Giorgi, F., & Lionello, P. 2007. Climate change projections for the Mediterranean region. *Global and Planetary Change*, **63**, 90–104.

Giovannini, G. 1994. *Soil erosion as a consequence of forest fires.* Geoforma ediciones. Chap. The effect of fire on soil quality, pages 15–27.

Giovannini, G., & Lucchesi, S. 1983. Effect of fire on hydrophobic and cementing substances of soil aggregates. *Soil Sci.*, **136**, 231–236.

Gippel, C.G. 1995. Potential of turbidity monitoring for measuring the transport of suspended solids in streams. **9**, 83–97.

Gobin, A., Govers, G., & Kirkby, M. 2006. *Soil Erosiion in Europe.* John Wiley and Sons Ltd. Chap. Pan-European Soil Erosion Assessment and Maps, pages 661–674.

González-Bonorino, G., & Osterkamp, W.R. 2004. Applying RUSLE 2.0 on burned-forest lands: an appraisal. *Journal of Soil and Water Conservation*, **59**, 36–42.

Govers, G. 1987. *Rill Erosion: Processes and Significance.* Catena Supplement, vol. 8. Catena Verlag, Cremlingen. Chap. Spatial and temporal variability in rill development processes at the Huldenberg experimental field, pages 35–54.

Grissinger, E.H. 1996. *Soil Erosion, Conservation and Rehabilitation.* Marcel Dekker, New York. Chap. Rill and gully erosion, pages 153–167.

Guardia, R., Raventos J., & Caswell, H. 2000. Spatial growth and population dynamics of a perennial tussock grass (Achnatherum calamagrostis) in a badland area. *British Ecological Society*, **88 (6)**, 950–963.

Harmon, R.S., & Doe, W.W. 2001. *Landscape Erosion and Evolution Modelling*. New York, USA: Kluwer Academic Plenum Publishers.

Haro, S., & Fernández, J.F. 1991. *Caracterización de las propiedades físicas y mecánicas de los suelos de la cuenca de Cal Parisa (Bergueda) afectados por un proceso de erosion hídrica*. M.Phil. thesis, Escuela Superior de Agricultura de Barcelona.

Hartcher, M.G., & Post, D. 2005. Reducing uncertainty in sediment yield through improved representation of land cover: Application to two sub-catchments of the Mae Chaem, Thailand. *Pages 1147–1153 of:* Zerger, A, & Argent, R. (eds), *MODSIM 2005 International Congress on Modelling and Simulation*. Modelling and Simulation Society of Australia and New Zealand.

Hartley, S., & Dingman, S. L. 1993. Effects of climatic variability on winter-spring runoff in New-England River basin. *Physical Geography*, **14**(4), 379–393.

Heathcot, K.A. 2002. *An investigation into the erodibility of earth wall units*. Ph.D. thesis, University of Technology Sydney, Sidney.

Heinemann, H.G. 1981. A new sediment trap efficiency curve for small reservoirs. *Water Resources Bulletin*, **17**, 825–830.

Hejduk, L., Hejduk, A., & Banasik, K. 2006. *Soil erosion and sediment redistribution in river catchments*. CAB International. Chap. Suspended sediment transport during rainfall and snowmelt-rainfall floods in a small lowland catchment, Central Poland., pages 94–100.

Herschy, R.W. 1999. *Uncertainties in Hydrometric Measurements*. John Wiley and Sons. Chap. 13, pages 355–370.

Hewlett, J. D. 1969. *Principles of Forest Hydrology*. Georgia: University of Georgia Press.

Horowitz, A.J. 2003. An evaluation of sediment rating curves for estimating suspended sediment concentrations for subsequent flux calculations. *Hydrological Processes*, **17**, 3387–3409.

Houghton, J.T., Ding, Y., Griggs, D.C., Noguer, M., van der Linden, P.J., Dai, X., Maskell, K., & Johnson, C.A. 2001. *Climate Change 2001: The Scientific Basis.* Cambridge: Cambridge University Press.

Hudson, N.W. 1995. *Soil conservation*. 3rd edn. London: Batsford, Ltd.

Huffman, E.L., MacDonald, L.H., & Stednick, J.D. 2001. Strength and persistence of fire-induced soil hydrophobicity under ponderosa and lodgeple pine, Colorado Front Range. *Hydrol. Proc.*, **15**, 2877–2892.

Huntington, T.G. 2006. Evidence for intensification of the global water cycle: review and synthesis. *Hydrol.*, **319**, 83–95.

Hutchinson, D.E., & Pritchard, H.W. 1976. Resource conservation glossary. *Soil and Water Conservation*, **31(4)**, 1–63.

ICC, Institut Cartogr'afic de Catalunya. 2002. *Geologic Map of Catalonia scale 250000. Catalan Institute of Cartography. Catalan Goverment. Barcelona.*

Ichikawa, Y. 2005. *Current issues and research on sediment movement in the river catchments of Japan. In: Predictions in Ungauged Basins.* IAHS Press. Chap. 8, pages 87–93.

ICOLD, International Commitee on Large Dams. 1989. *Sedimentation Control of Reservoirs.* International Commitee on Large Dams. Bulletin 67.

IGN, National Geographical Institute. 1987. *National Topographic Map.* Ministry of Public Works.

Imeson, A.C., & Verstraten, J.M. 1981. Suspended solids concentrations and river water chemistry. *Earth Surface Processes and Landforms*, **6**, 235–250.

IPCC, Intergovernmental Panel on Climate Change. 2001. *The Scientific Basis: Advancing our Understanding.* Tech. rept. Cambridge University Press, Cambridge.

ISCO, inc. 1986. *Instruction manual model 2700 automatic sampler.*

Jansson, M.B. 1996. Estimating a sediment rating curve of the Reventazon river at Palomo using logged mean loads within discharge classes. *Hydrology*, **183**, 227–282.

Jenny, H. 1941. *Factors of soil formation.* McGraw-Hill. New York.

Jetten, V.G., & Favis-Mortlock, D. 2006. *Soil erosion in Europe.* Wiley and Sons. Chap. Modelling soil erosion in Europe, pages 695–716.

Jones, C. 2001. *Rusle applications on Arizona Rangelands.* University of Arizona College of Agriculture and Life Sciences, Arizona.

Jones, D. S., Kowalski, D.G., & Shaw, R. B. 1995. *Calculating Revised Universal Soil Loss Equation (RUSLE) Estimates on Department of Defense Lands: A Review of RUSLE Factors and U.S. Army Land Condition-Trend Analysis Data Gaps.* Tech. rept. Center for Ecological Management of Military Lands Department of Forest Science, Colorado State University, Colorado.

Julien, P. 1998. *Erosion and Sedimentation.* Cambridge Univ. Press, New York.

Jung, H.C., Jeon, S.W., & Lee, D.K. 2004. *Development of soil water erosion module using GIS and RUSLE AIM Korea team. Tsukuba.*

Kinell, P.I.A. 2006. *Soil erosion and sediment distribution in river catchments.* CAB International. Chap. Runoff and predicting erosion on hillslopes within catchments, pages 170–176.

Kinell, P.I.A. 2007. Runoff dependent erosivity and slope length fators suitable for modelling annual erosion using the Universal Soil Loss Equation. *Hydrological Processes*, **21**, 2681–2689.

Kirilenko, P., & Sedjo, R. 2007. Climate change impacts on forestry. *PNAS*, **104 (50)**, 19697–19702.

Kirkby, M. 2006. *Soil erosion in Europe.* John Wiley and Sons Ltd. Chap. Impacts of environmental changes on soil erosion accross Europe, pages 729–742.

Klaghofer, E., Hintersteiner, K., & Summer, W. 2002. Trends in soil erosion and sediment yield in the alpine basin of the Austrian Danube. *In:* Summer, W., & Walling, D.E. (eds), *Modelling erosion, sediment transport and sediment yield.* Technical Documents in Hydrology, vol. 60IHP-VI, for UNESCO, Paris.

Komar, P.D. 1988. *Flood geomorphology.* London: Wiley. Chap. Sediment transport by floods, pages 97–111.

Kullman, L. 2007. Tree line population monitoring of Pinus sylvestris in the Swedish Scandes, 1973-2005: implications for tree line theory and climate change ecology. *Ecology*, **95**, 41–52.

Laflen, J.J., Elliot, W.J., Flanagan, D.C., Meyer, C.R., & Nearing, M.A. 1997. WEPP predicting water erosion using a process-based model. *Journal of Soil and Water Conservation*, **52**, 96–102.

Lal, R. 1988. *Soil erosion research methods*. Ankeny, Iowa: Soil and Water Conservation Society. Chap. Erodibility and erosivity, pages 141–160.

Lane, L.J., Shirley E.D., & Singh, V.P. 1988. *Modelling geomorfological systems*. John Wiley Publ. Chap. Modelling erosion on hillslopes, pages 287–308.

Larsen, I.J., & MacDonald, L.H. 2007. Predicting postfire sediment yields at the hillslope scale: Testing RUSLE and Disturbed WEPP. *Water Resources Research*, **43**(11), W11412 (1–18).

Lasanta, T., Vicente, S., & Cuadrat, J.M. 2005. Mountain Mediterranean landscape evolution caused by the abandoment of traditional primary activities: a case study of the Central Spanish Pyrenees. *Appl. Geogr.*, **25**, 47–65.

Latron, J. 2003. *Estudio del funcionamiento hidrológico de una cuenca mediterránea de montaña - Vallcebre, Pirineos Catalanes*. Ph.D. thesis, Universitat de Barcelona, Barcelona.

Latron, J., Anderton, S., White, S., Llorens, P., & Gallart, F. 2003. Seasonal characteristics of the hydrological response in a Mediterranean mountain research catchment (Vallcebre, Catalan Pyrenees): field investigations and modelling. *Pages 106–110 of:* Servat, E., Najem, W., Leduc, C., & Shakeel, A. (eds), *Hydrology of Mediterranean and Semiarid Regions*. IAHS, no. 278.

Lee, G.S., & Lee, K.H. 2006. Scaling effect for estimating soil loss in the RUSLE model using remotely sensed geospatial data in Korea. *Hydrol. Earth Syst. Sci. Discuss.*, **3**, 135–157.

Lee, S. 2003. *Soil erosion assessment and its verification using the Universal Soil Loss Equation and Geographic Information System: a case study at Boun, Korea*. Tech. rept. Geoscience Information Center, Korea Institute of Geoscience & Mineral Resources (KIGAM)., Daejeon.

Leemans, R., & Kleidon, A. 2002. *Global desertification: do humans cause deserts?* Dahlem University Press, Berlin. Chap. Regional and global assessment of the dimensions of desertification, pages 215–232.

Letcher, R.A., Jakeman, A.J., Merritt, W.S., McKee, I.J., Eyre, B.D., & Baginska, B. 1999. *Review of techniques to estimate catchment exports*. Tech. rept. Environmental Protection Authority, Sydney, NSW.

Lewis, J. 1996. Turbidity controlled suspended sediment sampling for runoff event load estimation. Pacific Southwest Research Station. *Water Resources USDA*, **32**, 2999 – 2310.

Liam, A. K. 2004. Estimating sediment yield variation in a small forested upland catchment. *Institute of Aquaculture, University of Stirling, Stirling, Scotland.*

Llasat, M.C., Vide, J.M., Lopez, J.A., & Barrera, T. 2008. *Aigua i canvi climatic diagnosi dels impactes previstos a Catalunya*. Chap. Constatacions de caracter meteorologic a Catalunya.

Llorens, P. 1994. Hydrological implications of afforestation in Mediterranean mountainous abandoned lands: findings and questions arisen from the simulation of a small basin water balance. *Pages 75–86 of:* Llorens, P., & Gallart, F. (eds), *Conference on Assessment of Hydrological temporal variability and changes*. CSIC, Barcelona.

Lloyd, A.H. 2005. Ecological histories from Alaskan tree line provide insight into future change. *Ecology*, **86**, 1687–1695.

Loch, R., & Silburn, D.M. 1996. *Sustainable Crop Production in the Sub-trops: an Australian Perspective*. Queensland: Queensland Department of Primary Industries & Fisheries. Chap. Constraints to sustainability-soil erosion, page 376.

López-Bustins, J.A. 2007. *The Western Mediterranean Oscillation and rainfall in the Catalan Countries*. Ph.D. thesis, University of Barcelona, Barcelona.

López-Moreno, J.I., Beniston, M., & Garcia-Ruiz, J.M. 2008. Environmental change and water management in the Pyrenees: Facts and future perspectives for Mediterranean mountains. *Global and Planetary Change*, **61**, 300–312.

López-Vicente, M., Navas, A., & Machín, J. 2007. Identifying erosive periods by using RUSLE factors in mountain fields of the Central Spanish Pyrenees. *Hydrology and Earth System Sciences Discussions*, **4**, 2111–2142.

Lu, H., Moran, C.J., Prosser, I.P., & Sivapalan, M. 2004. *Complexity and Integrated Resources Management, Transactions of the Second Biennial Meeting of the International Environmental Modelling and Software Society*. Vol. 3. Manno: iEMSs. Chap. Modelling sediment delivery ratio based on physical principles, pages 1117–1122.

Lu, H., Moran C. Prosser I., & Sivapalan, M. 2004. *IEMSS 2004 International Congress: Complexity and Integrated Resources Management*. Osnabrueck, Germany: International Environmental Modelling and Software Society. Chap. Modelling sediment delivery ratio based on physical principles, page 600.

Ma, J. 2001 (April). *Combining the USLE and GIS/ArcView for Soil Erosion Estimation in Fall Creek Watershed in Ithaca, New York*. Cornell University website.

MacDonald, D., Crabtree J.R., & Wiesinger, G. 2000. Agricultural abandonment in mountain areas of Europe: Environmental consequences and policy response. *Journal of Environmental Management*, **59**, 47–69.

MARM, Ministerio de Medio Ambiente y Medio Rural y Marino. 2006. *Fourth National Communication to the United Nations Framework Convention on Climate Change*. Tech. rept. Spanish Ministry of the Environment and Rural and Marine Affairs, Madrid.

MARM, Ministerio de Medio Ambiente y Medio Rural y Marino. 2009. *Annual report on forest firest fires in Spain (1961-2007)*. Tech. rept. Spanish Ministry of the Environment and Rural and Marine Affairs, Madrid.

Martínez, M.D., Lana, X., Burgueño, A., & Serra, C. 2007. Spatial and temporal daily rainfall regime in Catalonia Spain) derived from four precipitation indices, 1950-2000. *International journal of climatology*, **27**, 123–138.

Martínez-Carreras, N., Soler, M., Hernandez, E., & Gallart, F. 2007. Simulating badland erosion with KINEROS2 in a small Mediterranean mountain basin (Vallcebre, Eastern Pyrenees). *Catena*, **71**, 145154.

Martínez-Casasnova, J.A., Ramos, M.C., & Ribes-Dasi, M. 2002. Soil erosion caused by extreme rainfall events: mapping and quantification in agricultural plots from very detailed digital elevation models. *Geoderma*, **105**, 125–140.

McCool, D.K., Foster, G.R., Mutchler, C.K., & Meyer, L.D. 1989. Revised slope lenght factor for the Universal Soil Loss Equation. *Transactions of the ASAE*, **32**, 1571–1576.

McDonnell, R. 1998. Applying GIS to catchment-scale soil erosion modelling. *Pages 351–363 of:* Boardman, J., & D.Favis-Mortlock (eds), *Modelling Soil Erosion by Water*. Global Environmental Change, no. 55.

McGregor, K.C., Bingner, R.L., Bowie, A.J., & Foster, G.R. 1995. Erosivity index values for northern Mississippi. *Transactions of the American Society of Agricultural Engineers*, **38(4)**, 1039–1047.

McLaren, & Cameron, R.G. 1996. *Soil Science. Sustainable Production and Environmental Protection (2nd edition)*. Auckland: Oxford University Press.

Meehl, G.A., Washington, W.M., Collins, W.D., Arblaster, J.M., Hu, A., Buja, L.E., Strand, W.G., & Teng, H. 2005. How much more global warming and sea level rise? *Science*, **307**, 1769–1772.

Merritt, W.S., Latcher, R.A., & Jakeman, A.J. 2003. A review of erosion and sediment transport models. *Environmental Modelling & Software*, **18**, 761–799.

Merz, B. 2006. *Hochwasserrisiken: Grenzen und Möglichkeiten der Risikoabschätzung*. Sttutgart: Schweizerbartsche Verlagsbuchhandlung Stuttgart.

Mikos, M., Jost, D., & Petkovsek, G. 2006. Rainfall and ruoff erosivity in the alpine climate of north Slovenia: a comparison of different estimation methods. *Hydrological Sciences*, **51**(1), 115–126.

Miller, J.D., Nyhan, J.W., & Yool, S.R. 2003. Modeling potential erosion due to the Cerro Grande Fire with a GIS-based implementation of the Revised Universal Soil Loss Equation. *International Journal of Wildland Fire*, **12**, 1–16.

Millington, A.C. 2006. Reconnaissance scale soil erosion mapping using a simple geographic information systemin the humid tropics. *Dept. of Geography, University of Reading, Whiteknights, Reading, Berks, UK.*, 64–81. Available online [http://www2.alterra.wur.nl/Internet/webdocs/ilripublicaties/publicaties/Pub40/pub40-h5.pdf]. Last verified: February 8th, 2008.

Mishra, S.K., & Singh, V.P. 2003. *Soil Conservation Service Curve Number (SCS-CN) Methodology*. Vol. 42. Dordrecht: Kluwer Academic Publishers.

Mitchell, J.K., & Bubenzer, G.D. 1980. *Soil loss estimation. In: Soil Erosion*. Wiley & Sons, Chichester, New York. Chap. 2, pages 17–62.

Mobrey, Inc. Emerson Process Management. 2005. *Ultrasonic suspended solids density monitoring and control*.

Molina, D. 2000. *Conservació i degradació de sòls a les àrees de muntanya en procés d'abandonament: La fertilitat del sòl al Parc Natural del Cadí-Moixeró*. Ph.D. thesis, Universitat Autònoma de Barcelona, Barcelona.

Molinillo, M., Lasanta, T., & Garcia-Ruiz, JM. 1997. Managing mountainous degraded landscapes after farmland abandonment in the Central Spanish Pyrenees. *Environmental Management*, **21**, 587–598.

Moreno, J.M. 2005. Land-use change, climate change and fires: are we ready to face the risks? Department for Environment, Food and Rural Affairs. London.

Morgan, P., Hardy, C., Swetnam, T.W., Rollins, M.G., & Long, D.G. 2001. Maping fire regimes accross time and space: understanding coarse and fine-scale fire patterns. *Wildland Fire*, **10**, 329–342.

Morgan, R.P.C. 1986. *Soil erosion and conservation*. Longman Group UK Ltd. Essex.

Morgan, R.P.C. 1995. *Soil Erosion and Conservation*. Addison-Wesley Longman, Edinburgh.

Morgan, R.P.C., & Quinton, J.N. 2001. *Landscape Erosion and Evolution Modelling*. Kluwer Academic/Plenum Publishers: New York. Chap. Erosion Modelling, pages 117–143.

Morgan, R.P.C., Quinton, J.N., Smith, R.E., Govers, G., Poesen, J.W.A., Auerswald, K., Chisci, G., Torri, D., & Styczen, M.E. 1998. The European Soil Erosion Model (EUROSEM): a dynamic approach for predicting sediment transport from fields and small catchments. *Earth Surface Processes and Landforms*, **23**, 527–544.

Morris, G.L., Annandale, G., & Hotchkiss, R. 2007. *Sedimentation engineering: processes, management, modeling, and practice*. American Society of Civil Engineers. Chap. Reservoir sedimentation, pages 579–612.

Morris, G.L.; Fan, J. 1997. *Reservoir Sedimentation Handbook*. McGraw-Hill, New York.

Morschel, J., & Fox, D. 2004. *Une methode de cartographie du risque erosif: application aux collines du Terrefort lauragais*. Tech. rept. Université de Nice.

Muste, M. 2002. Sources of bias errors in flume experiments on suspended-sediment transport. *Hydraulic Research*, **40(6)**, 695–708.

Nearing, A.M., Lane, L.J., & Lopes, V.L. 1994. *Soil Erosion Researh Methods*. CRC Press. Chap. Modeling soil erosion, pages 127–156.

Nearing, M.A., & Nicks, A.D. 1998. Evaluation of the water erosion prediction project (WEPP) model for hillslopes. *Pages 351–363 of:* Boardman, J., & D.Favis-Mortlock (eds), *Modelling Soil Erosion by Water*. Global Environmental Change, vol. 55.

Nearing, M.A., Foster, G.R., Lane, L.J., & Finkner, S.C. 1989. A process based soil erosion model for USDA water erosion prediction project technology. *Trans. Am. Soc. Agric. Engrs.*, **32(5)**, 1587–1593.

Nearing, M.A., Pruski, F.F., & O'Neal, M.R. 2004. Expected climate change impacts on soil erosion rates: A review. *Journal of Soil and Water Conservation*, **59(1)**, 43–50.

Nearing, M.A., Jetten, V., Baffaut, C., Cerdan, O., Couturier, A., Hernández, M., Le Bissonnais, Y., Nichols, M.H., Nunes, J.P., Renschler, C.S. Souchre, V., & Van Oost, K. 2005. Modelling response of soil erosion and runoff to changes in precipitation cover. *Catena*, **61**, 131–154.

Nelson, D. W., & Sommers, L. E. 1982. *Methods of Soil Analysis. Chemical and Microbiological Properties.* Madison, U.S.A.: American Society of Agronomy, Soil Science Society of America. Chap. Total carbon, organic carbon, and organic matter., pages 539–579.

Nielsen, D.R., Biggar, J.W., & Erh, R.T. 1973. Spatial variability of field-measured soil-water properties. *Hilgardia*, **42**, 215–259.

O'Geen, A. T., Elkins, R., & Lewis, D. 2006. *Erodibility of agricultural soils, with examples in Lake and Mendocino counties*. Tech. rept. University of California, Division of Agriculture and Natural Resources, California.

Oms, O., Dinares-Turel, J., Vicens, E., Estrada, E., Vila, B., Galobart, A., & Bravo, A.M. 2007. Integrated stratigraphy from the Vallcebre Basin (southeastern Pyrenees, Spain): New insights on the continental Cretaceous-Tertiary transition in southwest Europe. *Palaeogeography, Palaeoclimatology, Palaeoecology*, **255**, 35–47.

Onstad, C.A. 1984. *Erosion and sediment yield: some methods of measurement and modelling.* GeoBooks, Norwich, England. Chap. Sediment yield modelling., pages 71–89.

Ortigosa, L., & Garcia-Ruiz, J.M. 1995. Geomorphological consequences of afforestation at a basin scale, and example from the Central Pyrenees. *Phys. Chem. Earth*, **20**, 345–349.

Othmer, E. F. Jr., & Berger, B. J. 2002. Future monitoring strategies with lessons learned on collecting representative samples. *Storm Water Program. Office of Water Programs Sacramento State, CA*.

Pardini, G. 1996. *Evoluzione temporale della microtopografia superficiale, della micromorfologia e della structtura in relazione ai processi di meteorizzazione delle marne smectitiche di Vallcebre.* Ph.D. thesis, University of Barcelona, Barcelona.

Parsons, A.J. 2006. Erosion and Sediment Transport by Water on Hillslopes. *Encyclopedia of Hydrological Sciences*.

Parsons, A.J., Wainwright, J., Brazier, R.E., & Powell, D.M. 2006. Is sediment delivery a fallacy? *Earth Surface Processes and Landforms*, **31**, 1325–1328.

Pemberton, E.L., & Strand, R.I. 1987. *Reservoir sedimentation: Design of Small Dams.* U.S. Bureau of Reclamation, Denver, Colorado.

Pérez, J.A. 1991. *Evaluación agrológica de los suelos de la cuenca Cal Parisa (Bergueda).* M.Phil. thesis, Escuela Superior de Agricultura de Barcelona, Barcelona.

Peterson, G.D., Cumming, G.S., & Carpenter, S.R. 2003. Scenario planning: a tool for conservation in an uncertain world. *Conserv. Biol.*, **17(2)**, 358–366.

Phillips, J.M., Webb, B. W., Walling, D. E., & Leeks, G. J. L. 1999. Estimating the suspended sediment loads of rivers in the LOIS estudy area using infrequent samples. *Hydrological Processes*, **13**, 1035–1050.

Planchon, O., Fritsch, E., & Valentin, A. 1987. Rill development in a wet savannah environment. *Catena supplement*, **8**, 55–70.

Poesen, J., & Valentin, C. 2003. Gully erosion and Global Change. *Catena special issue*, **21**, 157–199.

Poesen, J., J., Nachtergaele, G., Verstraeten, & C., Valentin. 2003. Gully erosion and environmental change: importance and research needs. *Catena*, **50 (2-4)**, 91–133.

Pons, X. 1994. *Geographic Information System and Remote Sensing software.* CREAF. Barcelona.

Pruski, F.F., & Nearing, M.A. 2002. Runoff and soil-loss responses to changes simulation study. *Journal of Soil and Water Conservation*, **57**, 7–16.

Quinn, P.F., Beven, K.J., Chevallier, P., & Planchon, O. 1991. The prediction of hillslope flow paths for distributed hydrological modelling using digital terrain models. *Hydrological Processes*, **5(1)**, 59–79.

Raghunath, J. 2002 (September). Potential Erosion Map For Bagmati Basin Using GRASS GIS. *In: Proceedings of the Open source GIS - GRASS users conference 2002*. Department of Civil Engineering, Institute of Engineering, Pulchowk, Kathmandu.

Ramann, E. 1928. *The evolution and classification of soils*. Cambridge W. Heffer and Sons Ltd. England.

Rawls, W.J., & Brakensiek, D.L. 1989. *Unsatured flow in hydrologic modeling. theory and practice*. Kluwer academic publishers. Chap. Estimation of soil water retention and hydraulic properties, pages 275–300.

Rawls, W.J., Brakensiek, D.L., & Saxton, K.E. 1982. Estimation of soil water properties. *Transactions of the American Society of Agricultural Engineers*, **25(5)**, 1316–1320.

Rawls, W.J., Brakenseik, D.L., & Logsdon, S.D. 1993. Predicting saturated hydraulic conductivity utilizing fractal principles. *Soil Sci. Soc. Am.*, **47**, 1193–1197.

Regüés, D., & Gallart, F. 2004. Seasonal patterns of runoff and erosion responses to simulated rainfall in a badland area in mediterranean mountain conditions (Vallcebre, Southeastern Pyrenees). *Earth Surface Processes and Landforms*, **29**, 755–767.

Regüés, D., Pardini, G., & Gallart, F. 1995. Regolith behaviour and physical weathering of clayey mudrock as dependent on seasonal weather conditions in a badland area at Vallcebre, Eastern Pyrenees. *Catena*, **25**, 199–212.

Regüés, D., Guardia, R., & Gallart, F. 2000. Geomorphic agents versus vegetation spreading as causes of badland occurrence in a mediterranean subhumid mountainous area. *Catena*, **40**, 173–187.

Regüés, D., Soler, M., & Gallart, F. 2002. Influencia del tamaño de las partículas sobre la estimación de concentraciones de sedimentos en suspensión mediante turbidímetros de retro-dispersión. *Pages 239–251 of: Estudios recientes (2000-2002) en geomorfología. Patrimonio, montaña y dinámica territorial*. Departamento de Geografía-UVA. Valladolid.

Renard, K.G., Foster, G.R., Weesies, G.A., McCool, D.K., & Yoder, D.C. 1997. *Predicting Soil Erosion by Water: A Guide to Conservation Planning with the Revised Universal Soil Loss Equation (RUSLE)*. Handbook No. 703. US Department of Agriculture, Washington, DC.

Renfro, G.W. 1975. *Present and Prospective Technology for Predicting Sediment Yield and Sources*. Publication ARS-S-40. US Department of Agriculture: Washington, DC. Chap. Use of erosion equations and sediment delivery ratios for predicting sediment yield., pages 33–45.

Roehl, J.E. 1962. Sediment source areas, delivery ratios and influencing morphological factors. *Ass. Sci. Hydrol. Publ.*, **59**, 202–213.

Romero, C., Stroosnijder, L., & Baigorria, A. 2007. Interrill and rill erodibility in the northern Andean Highlands. *Catena*, **70**, 105–113.

Rubio, C. 2005. *Hidrodinámica de los suelos de un área de montaña media mediterránea sometida a cambios de uso y cubierta*. Ph.D. thesis, Universitat Autónoma de Barcelona, Barcelona.

Rustomji, P., & Wilkinson, S. N. 2008. Applying bootstrap resampling to quantify uncertainty in fluvial suspended sediment loads estimated using rating curves. *Water Resour. Res.*, **44**, W09434: 1–12.

Sala, M., & Rubio, J.L. 1994. *Soil erosion as a consequence of forest fires*. Logroño: Geoforma ediciones.

Scholz, G., Quinton, J.N., & Strauss, P. 2008. Soil erosion from sugar beet in Central Europe in response to climate change induced seasonal precipitation variations. *Catena*, **72**, 91–105.

Schulze, R. 2000. Transcending scales of space and time in impact studies of climate and climate change on agrohydrological responses. *Agriculture, Ecosystems and Environment*, **82**, 185–212.

Schumacher, B.A. 2002. *Methods for the determination of total organic carbon (TOC) in soils and sediments*. United States Environmental Protection Agency Environmental Sciences Division National Exposure Research Laboratory, Las Vegas, NV.

Scientific-Campbell. 2002. *Pressure transducer Manual*.

Shen, H.W., & Julien, S.K. 1992. McGraw Hill, New York. Chap. Erosion and sediment transport, pages 12.1–12.61.

Simanton, J.R., Osborn, H.B., & Renard, K.G. 1980. *Application of the USLE to Southwestern rangeland*. Vol. 10. Tucson, AZ: Hydrology and water resources in Arizona and the Southwest.

Sivapalan, M. 2003. Prediction in ungauged basins: a grand challenge for theoretical hydrology. *Hydrol Process*, **17(15)**, 3163–3170.

Smith, R.E., Goodrich, D.C., Woolhiser, D.A., & Unkrich, C.I. 1995. *Computer Models of Watershed Hydrology*. Water resources Publications, Litleton, Colorado. Chap. KINEROS A kinematic runoff and erosion model.

Solé, A., Josa, R., Pardini, G., Aringhieri, R., Plana, F., & Gallart, F. 1992. How mudrock and soil physical properties influence badland formation at Vallcebre (Pre-Pyrenees, Spain). *Catena*, **19**, 208–300.

Soler, M., Sala, M., & Gallart, F. 1994. *Soil erosion as a consequence of forest fires*. Geoforma Ediciones. Chap. Post fire evolution of runoff and erosion during an eighteen month period, pages 149–161.

Soler, M., Latron, J., & Gallart, F. 2005. Analysing flow and suspended sediment dynamics at the event scale in a small Mediterranean mountain basin (Vallcebre, Eastern Pyrenees). *Geophysical Research*, **7**.

Soler, M., Regües, D., & Gallart, F. 2006. Automatic Sampler calibration to estimate the collection capacity of suspended sediment - In: Jister, L.P. and Matgen, P. and Van den Bos and Hoffman, R. (Ed). Uncertainties in the monitoring-conceptualization-modelling sequence of catchment research. pp. 223-226.

Soler, M., Nord, G., Catari, G., & Gallart, F. Submitted. Assessing suspended sediment concentration measurement error in relation to particle size using continuous sensors in a small mountain stream (Vallcebre catchments, Eastern Pyrenees). *Zeitschrift für Geomorphologie*.

Stevens, P. 2005. *Sensor Technologies*. Waterworld Magazine.

Stockle, C.O., Dyke, P.T., Williams, J.R., Jones, C.A., & Rosenberg, N.J. 1992. A method for estimating the direct and climatic effects of rising atmospheric carbon dioxide on growth and yield of crops: Part II. Sensitivity analysis at three sites in the Midwestern USA. *Agricultural Systems*, **38**, 239–256.

Strand, R.I., & Pemberton, E.I. 1987. *Design of Small Dams*. United States Department of the Interior, Bureau of Reclamation. Chap. Reservoir sedimentation, pages 529–564.

Strauss, P., & Klaghofer, E. 2004. Scale considerations for the estimation of processses and effects of soil erosion in Austria. *Chap. Scale considerations for the estimation of processes and effects of soil erosion in Austria, pages 229–238 of:* R., Francaviglia (ed), *Agricultural impacts on Soil Erosion and Soil Biodiversity: Developing Indicators for Policy Analysis*. Rome: Proceedings OECD Expert Meeting.

Stumpf, F., & Auerswald, K. 2006. *Hochaufgelöste Erosionsprognosekarten von Bayern*. Tech. rept. Technische Universität München, München.

Taillefumier, F., & Pigay, H. 2003. Contemporary land use changes in prealpine Mediterranean mountains: a multivariate GIS-based approach applied to two municipalities in the Southern French Prealps. *Catena*, **51**, 267–296.

Thomas, R.B. 1985. Estimating total sediment yield with probability sampling. *Water Resources Research*, **21 (9)**, 1381–1388.

Thomas, R.B. 1989. Constituent loads in small streams: the process and problems of estimating sediment flux. *EOS, Transactions, American Geophysical Union*, **70(43)**, 1105–1106.

Thorne, P.D. 1991. Measuring suspended sediment concentration using acoustic backscatter devices. *Marine Geology*, **98**, 7–16.

Toy, T.J., Foster, G.R., & Renard, K.G. 2002. *Soil Erosion*. New York: John Wiley and Sons, Inc.

Trimble, S.W. 1990. *Vegetation and Erosion, Process and Environments*. London: John Wiley and Sons. Chap. Geomorphic effects of vegetation cover and management: some time and space considerations in prediction of erosion and sediment yield, pages 55–65.

USDA. 1983. *National Soils Handbook No. 430*. United States Department of Agriculture - Soil Conservation Service. Washington, DC.

Uso, A., & Ramos, M.C. 2001. An improved rainfall erosivity index obtained from experimental interrill soil losses in soils with a Mediterranean climate. *Catena*, **43**, 293–305.

Valcarcel, M., Taboada, T., Paz, A., & Dafonte, J. 2003. Ephemeral gully erosion in northwestern Spain. *Catena*, **50**, 199–216.

Van, D.B. 2001. *The Coastal Research Instrumentation Sledge - CRIS*. Tech. rept. University Utrecht, Utrecht.

Van Asch, W.J. 1983. Water erosion on slopes in some land units in a Mediterranean area. *Catena Suplement*, **4**, 129–140.

Van Dijk, A. I. J. M. 2002. *Water and Sediment Dynamics in Bench-terraced Agricultural Steeplands in West Java, Indonesia*. Ph.D. thesis, Vrije Universiteit, Vrije.

Van Oost, K., Govers, G., & Desmet., P. 2000. Evaluating the effects of changes in landscape structure on soil erosion by water and tillage. *Landscape Ecology*, **15**, 577–589.

Van Rompaey, A.J.J., Krasa, J., Dostal, T., & Govers, G. 2003. Modelling sediment supply to rivers and reservoirs in Eastern Europe during and after collectivization period. *Hydrobiologia*, **494**, 169–176.

Van Wesemael, B., Poesen, J., Kosmas, C., Danalatos, N., & Nachtergaele, J. 2002. *Mediterranean desertification: A mosaic of processes and responses*. Chichester: John Wiley and Sons. Chap. The impact of rock fragments on soil degradation and water conservation, pages 131–145.

Vanoni, V.A. 1975. *Sedimentation Engineering, Manual and Report No. 54*. American Society of Civil Engineers, New York.

Verges, J., & Garcia-Senz, J. 2001. *Peri-Tethyan Rift/Wrench Basins and Passive Margins*. Mem. Mus. Natn. Hist. Nat. 186. Chap. Mesozoic evolution and Cainozoic inversion of the Pyrenean Rift, pages 187–212.

Verstraeten, G., & Poesen, J. 2000. Estimating trap efficiency of small reservoirs and ponds: methods and implications for the assessment of sediment yield. *Progr. Phys. Geogr.*, **24(2)**, 219–251.

Verstraeten, G., & Poesen, J. 2001. Factors controlling sediment yield from small intensively cultivated catchments in a temperate humid climate. *Geomorphology*, **40**(1-2), 123–144.

Verstraeten, G., Poesen, J., de Vente, J., & Koninckx, X. 2003. Sediment yield variability in Spain: a quantitative and semiqualitative analysis using reservoir sedimentation rates. *Geomorphology*, **50**(4), 327–348.

Vicente-Serrano, S.M., Lasanta, T., & Romo, M. 2004a. Analysis of spatial and temporal evolution of vegetation cover in the Spanish Central Pyrenees: role of human management. *Environ. Manage.*, **34**, 802–818.

Vicente-Serrano, S.M., Lasanta, T., & Romo, M. 2004b. Analysis of spatial and temporal evolution of vegetation cover in the Spanish central Pyrenees: role of human management. *Environ. Manage.*, **34**, 802–818.

Vilenskii, D.G. 1963. *Soil science*. Jerusalem: The Israel Program for Scientific Translations Ltd.

Wainwright, J. 2006. Degrees of separation: hillslope-channel coupling and the limits of palaeohydrological reconstruction. *Catena*, **66**, 93–106.

Wall, G.J., Coote, D.R., Pringle, E.A., & Shelton, I.J. 2002. *Revised Universal Soil Loss Equation for Application in Canada: A Handbook for Estimating Soil Loss from Water Erosion in Canada.* Research Branch, Agriculture and Agri-Food Canada., Ottawa.

Walling, DE. 1974. Suspended sediment and solute yields from a small catchment prior to urbanisation. *Pages 141–147 of: Fluvial processes in instrumented watersheds.* Institute of British Geographers.

Walling, D.E. 1983. The sediment delivery problem. *Journal of Hydrology*, **65**, 209–237.

Walling, D.E. 1988. Measuring sediment yield from river basin in: Soil Erosion Research Methods. 39–73.

Walling, D.E., & Quine, T.A. 1991. Use of 137 Cs measurements to investigate soil erosion on arable fields in the UK: potential applications and limitations. *Journal of Soil Science*, **42**, 147–165.

Ward, D.A., & Trimble, S. W. 2004. *Environmental Hydrology*. 2nd edn. Washington, D.C.: Lewis Publishers, CRC Press.

Ward, P.J., van Balen, R.T., Verstraeten, G., Renssen, H., & Vandenberghe, J. 2009. The impact of land use and climate change on late Holocene and future suspended sediment yield of the Meuse catchment. *Geomorphology*, **103**, 389–400.

WCD. 2000. *Dams and development. A new framework for decision making.* Tech. rept. World Commission on Dams, Earthscan Publications, London.

Wendt, G.W. 1998. *Guidelines for the use of the Revised Universal Soil Loss Equation (RUSLE) Version 1.06 on Mined Lands, Construction Sites, and Reclaimed Lands.* Joe R. Galetovic Publishing Editor. Chap. P Factor: Support-Practice, pages 6.1–6.25.

White, P., Labadz, J.C., & Butcher, D.P. 1996. *Erosion and sediment yield: Global and regional perspectives. Proceedings of the Exeter Symposium.* IAHS, no. 236. Wallingford: IAHS Publication. Chap. Sediment yield estimates from reservoir studies: an appraisal of variability in the southern Pennines of the UK, pages 163–174.

White, R.E. 2006. *Principles and Practice of Soil Science: the Soil as a Natural Resource.* 4th edn. Blackwell Science, Oxford.

White, S. 2005. Sediment yield prediction and modelling. *Hydrological processes*, **19**(15), 3053–3057.

Williams, GP. 1989. Sediment concentration versus water discharge during single hydrologic events in rivers. *Journal of Hydrology*, **111**, 89–106.

Williams, J.R. 1977. *Erosion and solid matter transport in inland waters.* IAHS. Chap. Sediment delivery ratios determined with sediment and runoff models, pages 168–179.

Willmott, C.J. 1981. On the validation of models. *Phys. Geography*, **2**, 184–194.

Wischmeier, W.H., & Smith, D.D. 1978. *Predicting Rainfall Erosion Losses: A guide to conservation planning.* Vol. 537. Washington, D.C.: U.S.D.A. Agriculture Handbook.

Wren, D., & Kunhle, R. 2005 (December). *Suspended sediment measurement: data needs, uncertainty and technologies.* Tech. rept. 18. U.S.D.A. and Agricultural Research Service, Oxford, Mississipi.

Wren, D. G., Bennett, S., Barkdoll, B., & R., Kuhnle. 2000. *Studies in suspended sediment and turbulence in open channel flows.* Ph.D. thesis, Department of Civil Engineering, University of Mississippi, Mississipi.

Wren, G. D. 2002. *Surrogate techniques for suspended-sediment measurement.* Turbidity and other sediment surrogates workshop, University of Mississipi. National Center for Physical Accoustics, Mississipi.

Yang, C.T. 1996. *Sediment transport: theory and practice.* 2nd edn. McGraw-Hill, New York.

Yang, G., Chen, Z., Yu, F., Wang, Z., Zhao, Y., & Wang, Z. 2007. Sediment rating parameters and their implications: Yantze River, China. *Geomorphology*, **85**, 166–167.

Young, R.A., Onstad, C.A., Bosch, D.D., & Anderson, W.P. 1987. *AGNPS: An agricultural non-point source pollution model: A large water analyses model.* Tech. rept. 35. USDA Cons. Res.

Zachar, D. 1982. *Soil Erosion.* Bratislava: Elsevier Scientific Publishing Company.

Zarris, D.; Lykoudi, E;, & Koutsoyiannis, D. 2002. *Sediment yield estimation from a hydrographic survey: A case study for the Kremasta reservoir basin, Greece.* Tech. rept. National Technical University of Athens, Athens.

Zhan, X., & Huang, M.L. 2004. ArcCN-Runoff: an ArcGIS tool for generating curve number and runoff maps. *Environmental Modelling & Software*, **19**, 875–879.

APPENDICES

1. Texture and K Factor results for each soil sample.

Sample	Depth cm	Total sand %	Fine sand %	Silt %	Clay %	OM %	Textural class	Perm. class	Struct. class	K Factor
1	0-15	25.3	13.7	7.8	66.9	6.1	clay	6	2	0.014
2	0-15	26.7	5.2	4.9	68.4	6.2	clay	6	1	0.007
3	0-15	16.9	15.7	4.6	78.6	28.8	clay	6	1	0.006
4	0-15	29.3	4.0	4.0	66.7	7.2	clay	6	1	0.007
5	0-15	22.1	2.5	8.1	69.8	17.1	clay	6	1	0.007
6	0-15	30.2	7.7	5.4	64.4	6.8	clay	6	1	0.008
7	0-15	22.7	17.2	9.6	67.7	6.1	clay	6	2	0.015
8	0-15	8.9	6.4	7.1	84.0	7.2	clay	6	1	0.007
9	0-15	33.1	11.6	6.4	60.5		clay	6	2	0.016
10	0-15	27.6	11.6	9.0	63.4	8.6	clay	6	2	0.014
11	0-15	29.5	12.6	8.2	62.3	7.7	clay	6	2	0.014
12	0-15	34.1	13.0	4.9	61.0	7.3	clay	6	1	0.009
13	0-15	21.3	17.7	70.2	8.6	3.7	silt loam	3	1	0.061
14	0-15	17.4	13.1	70.3	12.3	7.4	silt loam	3	2	0.056

2. Texture and OM adapted from published sources: (1-24 (Pérez, 1991); 25-32 (Haro, et al., 1991); 33-40 (Rubio, 2005))

#	Depth cm	Total sand %	Fine sand %	Silt %	Clay %	OM %	Textural class	Perm. class	Struct. class	K Factor
1	0-20	23	11.8	15.9	60.9	3.1	clay	6	1	0.013
2	0-8	39.5	21.3	22.2	38.3	6.5	clay loam	4	1	0.017
3	0-2	21	11.9	36.7	42.2	42.2	clay	6	1	0.024
4	0-5	27.4	18.8	15.1	57.5	2.8	clay	6	1	0.016
5	0-50	36.5	22.9	20.6	42.9	2.7	clay	6	1	0.025
6	0-9	30.6	14.4	27.9	41.4	7.2	clay	6	1	0.022
7	0-8	17.1	9.7	20.4	62.4	7.8	clay	6	1	0.012
8	0-5	43.2	24.4	22.3	34.4	7.9	clay loam	5	1	0.023
9	0-35	31	11.4	23.2	45.8	3.9	clay	6	1	0.018
10	0-15	54.6	22.2	13.7	31.6	4.6	sandy clay loam	4	1	0.015
11	0-15	58.7	30.9	20.9	20.4	8.4	sandy clay loam	4	1	0.028
12	0-8	22	9.4	32.2	45.6	1.9	clay	6	2	0.029
13	0-5	39.4	5.6	0	60.5	54	clay	6	2	0.011
14	0-12	24.5	16.3	19.7	55.8	6	clay	6	2	0.020
15	0-5	40.2	22	27.4	32.3	13.1	clay loam	4	2	0.026
16	0-20	46	15.2	14	40	4.1	clay	6	2	0.021
17	0-40	34.4	22.9	20.6	42.9	4.6	clay	6	2	0.026
18	0-12	34.6	21.2	22.04	43.3	6.7	clay	6	2	0.026
19	0-7	42.8	21.7	21.9	35.1	5.8	clay loam	5	2	0.026
20	0-17	32.2	17.8	22.7	44.9	1.5	clay	6	2	0.029
21	0-6	59.4	22.9	14.3	26.3	8	sandy clay loam	4	2	0.022
22	0-4	27.6	16.1	28	44.3	8.8	clay	6	2	0.026
23	0-20	28.9	16	21.5	48	3.9	clay	6	2	0.022
24	0-20	20.1	16.1	34.5	45.4	1.9	clay	6	2	0.033
25	0-10	17.1	8.2	37.8	45.1	1.9	clay	6	1	0.027
26	0-20	29.7	17.4	37.4	32.9	1.8	clay loam	4	1	0.032
27	0-10	33.9	9	25.5	40.8	3.8	clay	6	1	0.019
28	0-15	26.7	15.4	39.2	33.9	0.9	clay loam	4	1	0.034
29	0-7	35.8	11.1	28	36.2	4.7	clay loam	4	1	0.016
30	0-7	39.9	16.5	34.5	25.6	4.7	clay loam	4	1	0.026
31	0-10	39.3	11.6	29.2	31.5	3.5	clay loam	4	1	0.019
32	0-50	28.3	9.4	24.3	46.4	2.5	clay	6	1	0.019
33	0-5	11.3	4.4	67.2	21.5	11.4	silt loam	3	3	0.046
34	5-10	13.9	5.51	65.6	20.4	7.1	silt loam	3	3	0.046
35	0-5	20.3	10.39	61.3	18.4	9.4	silt loam	3	3	0.048
36	5-10	28	9.52	56.9	15.2	6.2	silt loam	3	3	0.046
37	0-5	7.0	2.56	65.1	27.8	15.3	silty clay loam	4	3	0.043
38	5-10	8.0	2.65	63.2	28.8	5.6	silty clay loam	4	3	0.041
39	0-5	21.0	10.79	63.5	15.5	12.4	silt loam	3	3	0.052
40	5-10	23.1	12.99	61.8	15.1	7.2	silt loam	3	3	0.052

3. Distribution of RUSLE's input factors in function of number of pixels.